

657

Volume 17, No. 6

December, 1964

~~SECRET~~
~~SECRET~~
~~SECRET~~

SOVIET ATOMIC ENERGY

АТОМНАЯ ЭНЕРГИЯ
(ATOMNAYA ÉNERGIYA)

TRANSLATED FROM RUSSIAN



CONSULTANTS BUREAU

PLENUM PRESS HANDBOOKS OF HIGH-TEMPERATURE MATERIALS

No. 1 — MATERIALS INDEX

by **Peter T. B. Shaffer** Foreword by **Dr. Henry H. Hausner**

Data on the general, chemical, electrical, mechanical, nuclear, optical, structural, and thermal properties of approximately 520 refractory materials are arranged under each material. Materials discussed fall into the categories of borides, oxides, carbides, nitrides, silicides, mixed carbides, mixed oxides and elements.

All compounds for which information was available are included. The concise listing of property data under each individual refractory compound will greatly facilitate retrieval of both general and specific data on the properties of an individual material.

The work is distinguished by a bibliography of 690 references to the literature on refractory compounds.

782 pages

\$17.50

No. 2 — PROPERTIES INDEX

by **G. V. Samsonov** Foreword by **Dr. Henry H. Hausner**

Revised by the author to include references to investigations as recent as late 1963.

Extensive tabular data is presented to provide a scientific classification of 600 refractory compounds, systematically arranged by the following properties: crystal-chemical, thermal, thermochemical, electrical, magnetic, optical, mechanical, chemical, and refractory properties of borides, carbides, nitrides, silicides, phosphides, and sulfides of metals, as well as nitrides, carbides, and phosphides of boron and silicon and boron-silicon alloys. Invaluable information is also presented on the principal fields of application of refractory compounds in the metallurgical, chemical and machine construction industries, in power generation, and in automation, radio, and electrical engineering. An appendix gives the most up-to-date phase diagrams of systems in which refractory compounds are formed.

The work contains a bibliography of over 1300 references to the literature on refractory compounds, approximately 40% of which are to Soviet literature hitherto comparatively undocumented in the West.

430 pages

Translated from Russian

\$22.50

No. 3 — THERMAL RADIATIVE PROPERTIES

by **W. D. Wood, H. W. Deem, and C. F. Lucks**

A compilation of data on thermal radiative properties originally published in two soft-cover volumes by the Defense Metals Information Center, Battelle Memorial Institute. The importance of the data for all those concerned with radiant heat transfer has prompted republication as a part of this significant reference series.

Thermal radiative data are included for the following materials: titanium and its alloys; stainless steels; iron-, nickel-, and cobalt-base superalloys; refractory metals (chromium, columbium, molybdenum, tantalum, and tungsten) and their alloys; coated materials for elevated-temperature service; ceramics; graphite.

476 pages

\$17.50

Contents on request

 **PLENUM PRESS** 227 W. 17th St., New York, N.Y. 10011

A. I. Alikhanov	A. I. Leipunskii
A. A. Bochvar	M. G. Meshcheryakov
N. A. Dollezhal'	M. D. Millionshchikov
K. E. Erglis	(<i>Editor-in-Chief</i>)
V. S. Fursov	I. I. Novikov
I. N. Golovin	V. B. Shevchenko
V. F. Kalinin	A. P. Vinogradov
N. A. Kolokol'tsov	N. A. Vlasov
(<i>Assistant Editor</i>)	(<i>Assistant Editor</i>)
A. K. Krasin	M. V. Yakutovich
I. F. Kvartskhava	A. P. Zefirov
A. V. Lebedinskii	

SOVIET ATOMIC ENERGY

A translation of АТОМНАЯ ЭНЕРГИЯ

A publication of the Academy of Sciences of the USSR

© 1966 CONSULTANTS BUREAU ENTERPRISES, INC.
227 West 17th Street, New York, N. Y. 10011

Vol. 17, No. 6

December, 1964

CONTENTS

	P A G E	
	ENG.	RUSS.
Some Ways of Development for Water-Moderated Water-Cooled Power Reactors —A. Ya. Kramerov, Yu. V. Markov, S. A. Skvortsov, V. P. Denisov, E. V. Kulikov, Yu. P. Sorokin, V. V. Stekol'nikov, A. A. Khokhlachev, V. P. Tatarnikov, and V. A. Sidorenko	1183	427
The Organic-Cooled Organic-Moderated Nuclear Power Station "Arbus"—K. K. Polushkin, I. Ya. Emel'yanov, P. A. Delens, N. V. Zvonov, Yu. I. Aleksenko, I. I. Grozdov, S. P. Kuznetsov, A. P. Sirotkin, Yu. I. Tokarev, K. P. Lavrovskii, A. M. Brodskii, A. R. Belov, E. V. Borisyuk, V. M. Gryazev, V. D. Tetyukov, D. N. Popov, Yu. I. Koryakin, A. G. Filippov, K. V. Petrochuk, V. D. Khoroshavin, N. P. Savinov, M. N. Meshcheryakov, V. P. Pushkarev, V. A. Suroegin, P. A. Gavrilov, L. N. Podlazov, and I. N. Pogozhkin	1197	439
ТЭС-3 Compact Atomic Power Station—N. M. Sinev, A. K. Krasin, I. F. Bychkov, O. I. Blokhin, D. L. Broder, V. N. Gabrusev, Yu. V. Dudnikov, V. A. Zhil'tsov, M. A. Koptev, A. Ya. Komarov, A. P. Kotov, M. N. Lantsov, G. A. Lisochkin, G. A. Merzlikin, I. G. Morozov, Yu. I. Orekhov, Yu. A. Sergeev, P. N. Slyusarev, G. N. Ushakov, N. V. Fedorov, V. Ya. Chernyi, and V. M. Shmelev	1207	448
Physical and Operating Characteristics of the SM-2 Reactor—S. M. Feinberg, N. A. Dollezhal', E. D. Vorob'ev, V. A. Tsykanov, I. Ya. Emel'yanov, V. M. Gryazev, A. S. Kochenov, Yu. M. Bulkin, V. I. Ageenkov, and P. G. Aver'yanov	1212	452
The PGR Pulsed Graphite Reactor—I. V. Kurchatov, S. M. Feinberg, N. A. Dollezhal', P. I. Aleshchenkov, F. S. Drozdov, I. Ya. Emel'yanov, A. D. Zhirnov, M. A. Kazachenko, G. D. Knyazeva, F. V. Kondrat'ev, V. D. Lavrenikov, N. G. Morgunov, B. V. Petunin, V. P. Smirnov, V. M. Talyzin, A. G. Filippov, I. L. Chikhladze, P. M. Chulkov, and Ya. V. Shevelev	1224	463
Statistical Reactor Kinetics Equations—A. B. Govorkov	1236	474
Channel Effects in Fission of Even-Even Compound Nuclei—L. N. Usachev, V. A. Pavlinchuk, and N. S. Rabotnov	1242	479
Neutron Angular and Energy Distribution at the Boundary of Two Media—V. A. Dulin, V. G. Dvukhsherstnov, Yu. A. Kazanskii, and I. V. Shugar	1249	486
The Neutron Background at the Surface of the Earth—G. V. Gorshkov, V. A. Zyabkin, and O. S. Tsvetkov	1256	492
Addition of Hetero-Organic Compounds to Polystyrene—E. E. Baroni, S. F. Kilin, T. N. Lebsadze, I. M. Rozman, and V. M. Shoniya	1261	497

Annual Subscription: \$95

Single Issue: \$30

Single Article: \$15

All rights reserved. No article contained herein may be reproduced for any purpose whatsoever without permission of the publisher. Permission may be obtained from Consultants Bureau Enterprises, Inc., 227 West 17th Street, New York City, United States of America.

CONTENTS (continued)

	P A G E	
	ENG.	RUSS.
In Memory of Konstantin Konstantinovich Aglintsev	1265	501
LETTERS TO THE EDITOR		
Study of the Transformations of Ruthenium Dioxide in the Presence of Chromium Oxide -M. K. Baranaev, V. G. Vereskunov, and K. P. Zakharova	1267	502
Use of the Time of Flight Method for Measuring the Range/Energy Relation for 18 to 38 MeV Helium Ions in Aluminum--N. I. Venikov and N. I. Chumakov	1269	503
Charge-Exchange of Oxygen Ions of Energy 2-13.3 MeV in Thin Alundum Films -N. I. Venikov, N. I. Chumakov, and B. I. Khoroshchavin	1271	504
Neutron Radiative Capture in Copper and Molybdenum--V. A. Tolskikov, V. E. Kolesov, A. G. Dovbenko, and Yu. Ya. Stavisskii	1272	505
Radiative Capture Cross Sections for Fast Neutrons in Iron--A. V. Malyshev, Yu. Ya. Stavisskii, and A. V. Shapar'	1277	508
Use of the Monte Carlo Method for Calculating the Penetration of γ -Radiation Through Matter--L. M. Shirkin	1279	509
SCIENCE AND ENGINEERING NEWS		
Symposium on the Biological Effects of Radioisotopes	1282	512
Special-Purpose Heavy Cement with Enhanced Absorbing Power--K. S. Kutateladze and A. V. Rustambekov	1286	515
BIBLIOGRAPHY		
New Books	1288	517
Author Index, 1964	1295	
Tables of Contents	1300	

The Russian date "Podpisano k pečati" of this issue was 11/17/64 . This is equivalent to "approved for printing." Publication did not occur prior to this date, but must be assumed to have taken place reasonably soon thereafter.

Publisher

SOME WAYS OF DEVELOPMENT

FOR WATER-MODERATED WATER-COOLED POWER REACTORS*

A. Ya. Kramerov, Yu. V. Markov, S. A. Skvortsov, V. P. Denisov,
E. V. Kulikov, Yu. P. Sorokin, V. V. Stekol'nikov, A. A. Khokhlachev,
V. P. Tatarnikov, and V. A. Sidorenko

Translated from Atomnaya Énergiya, Vol. 17, No. 6,
pp. 427-438, December, 1964

FEATURES OF REACTOR CONSTRUCTION AND SCHEME FOR THE SECOND BLOCK
OF THE NOVO-VORONEZH NUCLEAR POWER STATION

Water-moderated water-cooled power reactors using water as moderator and heat carrier are represented in the USSR by two blocks of the Novo-Voronezh Nuclear Power Station (NPS), of which the first block, with 210 MW electric power, is just starting operation and the second (365 MW electric power) is being constructed.

The first block of the station was described earlier [1-3]. In constructing this, the aim was to gather experience in planning, setting up, and operating stations using as heat source heterogeneous reactors with water under pressure. Naturally in this first large NPS the parameters and planning decisions were effected with some degree of caution.

The aim in planning the second Novo-Voronezh NPS was, on the one hand, to take a step forward in the creation of atomic-power systems with economic indices approximating those of thermal power plants, and, on the other, to make full use of the experience in planning and setting up the basic equipment gained when constructing the first station, while avoiding new departures, the realization of which would demand a considerable consumption of time and resources on scientific-research and constructional work. Hence the development of the second block may be regarded as limited, by the framework indicated, to the modernization of the first station.

As in the first block, a body with dimensions limited by transport conditions will be used. This will be devoid of anticorrosion plating, which will allow the thickness of the main metal to be increased and the calculated pressure to be raised to 120 abs. atm. From considerations of unification, the active zone, as in the first block, is made up of 349 hexagonal cassettes of gage 144 mm and length 2.5 mm. The fuel elements are cylindrical, with sintered uranium dioxide in shells, ~ 0.5 mm thick, of zirconium-niobium alloy or stainless steel. To shorten the installation time it was decided to use the master-circulation glandless pumps adopted by industry and used in the first block (discharge 5250 m³/h, head 60 m water). For the same reason, recharging the fuel with removal of the roof was retained; at the same time a system for recharging without roof removal was developed so that this might be used in future.

In view of the fact that the removal and replacement of the roof, the actual fuel charging, and the restoration of the reactor system to the operating state could occupy a great deal of time, these operations should preferably be effected as rarely as possible, i. e., the length of operation between two rechargings should be fairly prolonged. For increased specific power of the reactor this means not only a corresponding increase in the depth of combustion but at the same time a rise in the initial store of reactivity, which must be compensated by absorption in the control and safety elements of the reactor.

The principle of compensating for excess reactivity based on the replacement of fuel by a fast-neutron water trap is used. The structural work showed that the number of such elements could be raised to 73. These are placed uniformly about the active zone at the nodes of a triangular lattice with a period of 294 mm.

*Report No. 304 presented by the USSR to the Third International Conference on the Peaceful Use of Atomic Energy, Geneva, 1964.

The water/uranium ratio (ratio of the volume of water to that of the fuel material) is kept the same as in the first block (1.7). This ensures a slight negative coefficient of reactivity, sufficient compensating power of the control system, and a good neutron balance.

The fuel is loaded into cassettes of roughly the same construction and with the same cross-sectional dimensions as in the first block. For a core diameter of 7.7 mm and an external diameter of the fuel elements 8.8 mm, each cassette holds 127 fuel elements in a triangular lattice with spacing 12.3 mm. In this way it proved possible to bring the thermal power of the reactor to ~ 1400 MW, i. e., 1.8 times greater than that of the first block. A further substantial increase in power could only be realized by increasing the consumption of water and revising the principles of the reactivity compensation and loading system, which would contradict the original intentions of the design.

In a campaign lasting ~ 1.5 -2 y, with three partial rechargings, a burn-up of $\sim 22,000$ -30,000 MW · day/ton uranium is achieved. The required average enrichment for the first charging is 2.5-3.5%; the feed of the reactor is maintained by 3-4% enriched fuel.

Out of the 73 control-element cassettes, 60 (CR) are intended for the compensation of slow changes in reactivity (control rods) and 13 (SR) for emergency protection (scram rods). The construction of the CR and SR is in principle analogous to that of the cassette in the first-block reactor. Provision is made, however, for hydraulically relieving them from upward stress from the flow of heat carrier, which in this more thermally-stressed reactor prevents reliable downward motion of the cassette (in the sense of reduced reactivity).

The SR cassette, just as that of the CR, consists of two parts: the absorber and the part containing fuel. Use of fuel in the SR makes it possible to improve the neutron balance in the active zone and raise the depth of burn-up.

It was decided to use a saturated-steam power cycle (pressure 30 abs. atm), although preliminary study showed the economic advantages, in principle, of using combustion heating, which, however, would complicate the arrangement of the station. Five such turbo-units are used, as in the first block; a little modernization enables the power of each to be raised to 73 MW. Thus the electrical power of the block is 365 MW with an efficiency of 26%.

In order to take off the power from the active zone without reducing the parameters of the steam coming into the turbine and the water temperature at the entrance to the reactor, it was decided to increase the maximum enthalpy of the water at the outlet from the most thermally-stressed cassette up to saturation enthalpy, and even to admit steam content (up to 3 or 4%) in individual hot streams emerging from the active zone. For an average heating of $\sim 28^\circ\text{C}$ and water temperature at the entrance into the reactor 250°C , the flow of heat carrier through the active zone is $42,000 \text{ m}^3/\text{h}$. This compelled the number of circulation loops of the system to be raised from six to eight. Abandonment of the idea of repairing separate units in working-reactor conditions considerably simplified the arrangement of the first circuit and made it possible to site the eight loops in two hermetically-sealed boxes.

In order to maintain the necessary quality of the water in the second circuit, ion-exchange filters are used in the purification system of the second block of the station, in contrast to the evaporation devices used in the first block; this enables the gas balance to be stabilized more easily. The filtration is effected while maintaining the working pressure of the water.

The pressure in the first circuit is maintained by steam volume compensators (not gas as in the first block), which also aids stabilization of the water-chemical conditions of the first circuit.

As a result of raising the specific and total power of the reactor, a considerable reduction in the fuel and capital components of the cost of electrical energy was achieved.

The reactor (Fig. 1) constitutes a vertical cylindrical vessel some 19 m high. It consists of a body 10 and upper take-off block 12 with a plane roof. Inside the body, in a special cylindrical shaft 6, is a removable bucket 7 of diameter 3000 mm and height 4000 mm, serving for the positioning of the hexagonal cassettes containing the fuel elements 5. The drive mechanisms of the movable cassettes 2 intended to compensate the reactivity and avert danger in the reactor are set in the casing of the upper take-off block. On a flange of the body is set the roof of diameter 3350 mm and thickness 520 mm. Into 85 apertures of diameter 100 mm are sealed tubes for the mechanisms of the reactivity-control systems and tubes for bringing out the cassings of the thermocouples regulating the water temperature in the cassettes. The roof-body joint is made in the form of a self-sealing lock with a

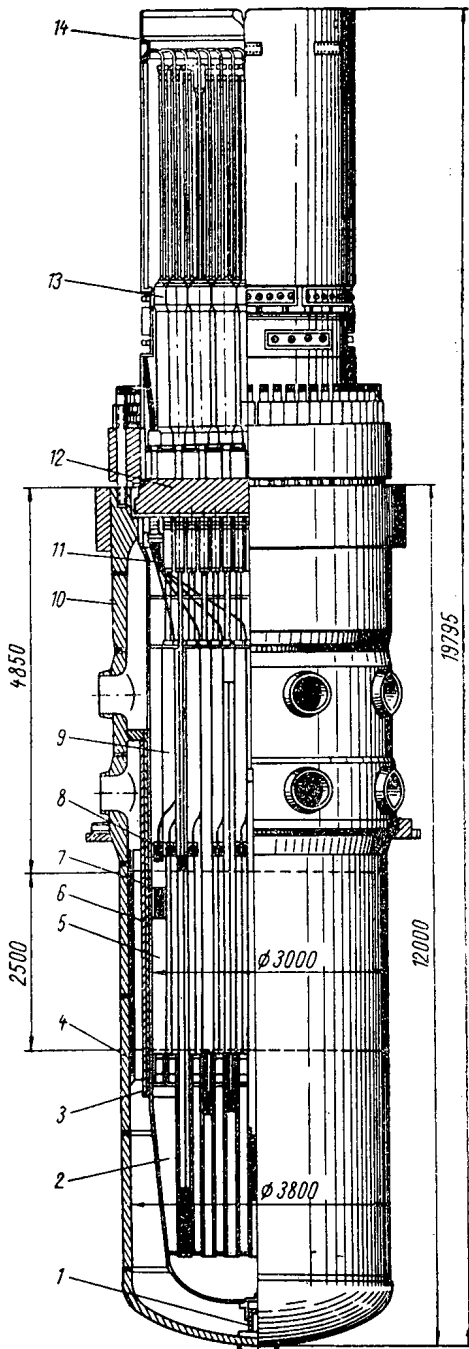


Fig. 1. General view of the reactor: 1) bushing for fixing the shaft to the body; 2) control-system cassette; 3) bottom of shaft; 4) screen; 5) working cassette; 6) shaft; 7) removable bucket; 8) spacing lattice; 9) protecting-tube block; 10) body; 11) temperature-control tubes; 12) take-off block; 13) drive for the control-system cassette; 14) servicing platform.

Figure 3 shows the dependence of the increase in the relative energy consumption on circulation Δn and the rise in the efficiency of the cycle $\Delta \eta$, after exchanging the steam generator with minimum temperature head δ

wedge-shaped nickel gasket. Sealing by the flexible element of a toroidal compensator, one end of which is welded to the roof while the other presses on the flange of the body, is provided as reserve. Sealing is here achieved by means of a rod seal of diameter 5 mm or by welding the toroidal compensator to the flange of the body. The roof is fixed to the flange of the body by a pressure ring of diameter 4000 mm and height 800 mm with 60 pins.

The outline scheme of the electrical station and the reactor-cooling system are indicated in Fig. 2. Each of the circulating loops includes a steam generator, centrifugal pump of the glandless type, two valves with electrical drive, a reverse valve, and connecting pipelines of internal diameter 500 mm.

The steam generators have a horizontal-type design. This makes it possible to establish the heat-exchange surface below the flange of the reactor body, so that in recharging the reactor the circulating loops can be kept full of water, which in turn ensures the elimination of the residual heat evolution during recharging by natural circulation, without any special circuit.

In case of a loss of supply in the self-consumption system, a safety supply system including storage batteries and a Diesel generator with automatic start is provided in the station. The electrical supply of the circulating pumps of the circuit in the first seconds after an emergency is effected from the turbine generators owing to the steam and mechanical coasting of the turbo-assemblies. As the revolutions of the generator fall below the norm, the pumps are switched on to the storage batteries and subsequently stopped, the system passing over to shut-down cooling by way of natural circulation in the reactor circuit. The grouping of the turbine and deaerating sections is analogous to that in organic-fuel electrical-stations.

2. WAYS OF IMPROVING WATER-MODERATED WATER-COOLED REACTORS (WWR)

Improvements to the WWR achieved in the design of the second block of the Novo-Voronezh NPS were strictly limited by the above-mentioned program of modernization of the first block in this station, and so by no means exhaust ways of improving WWR.

From the point of view of a possible reduction in the cost of the energy produced, let us consider some other more radical ways of changing the construction of WWR systems.

Steam-Generation Scheme

It is expedient to retain the simplest arrangement of producing steam in "boiler" evaporators, supplying saturated steam to the turbines. The production of power steam by the self-evaporation of water in the reactor circuit by throttling can only compete with this scheme at low pressures (clearly not optimum) and with fairly cheap pumps, the cost of which (per 1 kW pump power), as calculations show, must be less than half that of 1 m² heating surface.

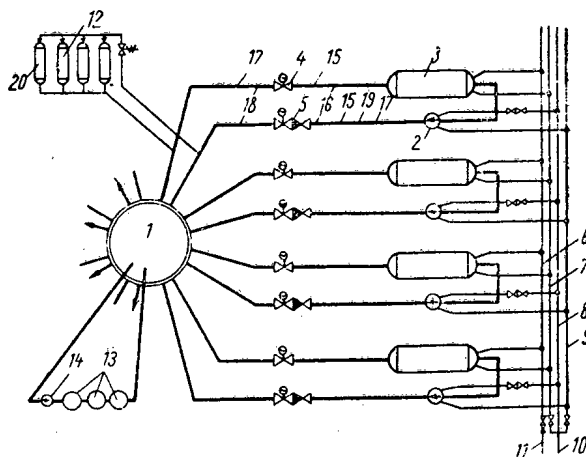


Fig. 2. Reactor-cooling scheme. 1) Reactor; 2) circulating pump; 3) steam generator; 4) valve; 5) reverse valve; 6) air-removing pipeline; 7) discharge pipeline; 8) pipeline for removing air from the pumps; 9) pump-discharging pipeline; 10) branch to collecting reservoirs; 11) branch to air-purification filters; 12) steam volume compensators; 13) filters; 14) transfer pump; 15) temperature monitor; 16) monitor for temperature difference in loop; 17) pressure monitor; 18) monitor for pressure drop in active zone; 19) flow monitor; 20) compensator-level meter.

for a throttle system, on the initial and final pressures. As we see, the increments are only equal ($\Delta n = \Delta \eta$, i. e., the net efficiency of the system is not reduced) either for steam pressures too low for large powers ($p_2 = 10-15$ abs. atm) or for unsuitably-large temperature heads ($\Delta t > 25^\circ\text{C}$).

Superheating the steam in the steam generator by Δt_{ne} leads to an increase $\Delta \eta$ in the efficiency of the cycle roughly proportional to the product of Δt_{ne} and the superheating heat $q_{ne} = C_p \Delta t_{ne} / \Delta i$. Since the possible superheating is proportional to the heating Δt of the heat carrier in the reactor, the increase in efficiency due to the introduction of superheating is approximately proportional to Δt^2 . Since for WWR small water heatings are best, the effect of introducing superheating does not, as a rule, justify the complication in the construction of the steam generator and its greater cost.

Use of a two-pressure cycle raises the efficiency as the first power of Δt , which makes the increase in efficiency more appreciable even at low Δt . For example, for $\Delta t = 40^\circ\text{C}$, the relative increase in efficiency is roughly

$$\frac{\Delta \eta}{\eta} \cong \frac{1}{4} \cdot \frac{T_x \Delta t}{\left(T_s + \frac{\Delta t}{2}\right) (T_s - T_x)} = \frac{1}{4} \cdot \frac{300 \cdot 40}{\left(500 + \frac{40}{2}\right) (500 - 300)} \cong 0.03,$$

where $T_x = 300^\circ\text{K}$ and $T_s = 500^\circ\text{K}$, the temperatures of the cold and hot sources in the one-pressure cycle.

For uniform heating of the water in the cassettes of the reactor the optimum are heating Δt rises, as a result of which the effect may increase ~ 1.5 times.

If the difficulties of drying steam at two pressures in the turbine can be successfully overcome, then evidently for a large power of each reactor-cooling loop it may be advantageous to use two similar steam generators in series in the first circuit, producing saturated steam at two temperatures differing by $20-25^\circ\text{C}$. It should be emphasized, however, that to a certain extent this complicates the arrangement of the first circuit, which should be as simple and symmetrical as possible, so as to minimize the extent and volume of its pipes and installations and to create good conditions for the natural circulation of the water in the first circuit and for compensation of the thermal expansion of the pipes.

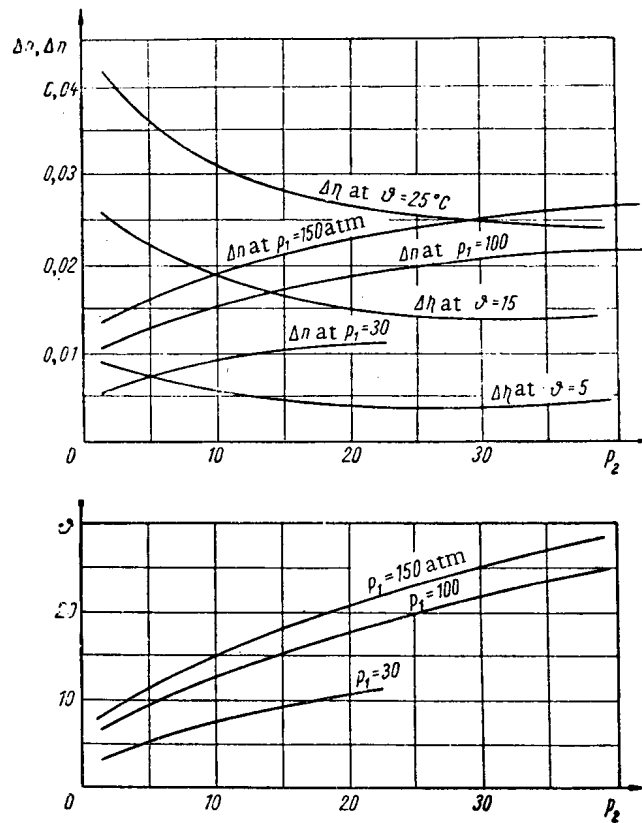


Fig. 3. Increase $\Delta\eta$ in cycle efficiency and Δn in the relative amount of energy spent on circulation after replacing the steam generator by a throttle system, expressed as a function of the temperature head in the steam generator ϑ and the pressures in the reactor p_1 and turbine p_2 . The lower graph shows the connection between the minimum temperature head ϑ and the pressures p_1 and p_2 for which $\Delta\eta = \Delta n$, i. e., the net efficiency is unaltered.

Thermal expansion of the pipes may best be allowed for by providing free movement of the equipment, with rigid, straight pipes. In this case it is convenient to have the pipes of the first circuit, the supports of the reactor, the pumps, and the steam generator, and the fittings in a single horizontal plane; the main pipes may reasonably be connected to the reactor above the active zone, which simplifies the construction and improves the reliability of the reactor body.

Motion of Water in the Reactor

For a downward motion of the water in the reactor, the space above the active zone remains free for carrying out recharging operations, and the emergency introduction of the absorbing controls into the active zone under the combined action of the flow and the force of gravity is more reliable. There arises a danger, however, of upsetting and stagnating the water circulation on an accidental switch-off of the supply to the master pumps and consequent overheating and damage to the fuel elements. This situation would apparently not have especially serious consequences. It is very hard to check this with the necessary degree of reliability. Meanwhile we must confine consideration to a lifting motion (of the water), when there are practically no doubts, but when it is also considerably more difficult to free the space above the zone and ensure the reliable downwards motion of the controls.

A two-way active zone occupies an intermediate position between oneway zones with upward and downward motion of the water. In such an active zone, with water being fed in and out underneath, it is convenient to prevent the cassettes in the central, lifting path from floating upwards by means of hydraulic pistons, and to effect cassette-by-cassette control of the water temperature only at the bottom—at the outlet from the second peripheral (hot and downward) path. Then the space above the active zone will be free for recharging without removing the roof.

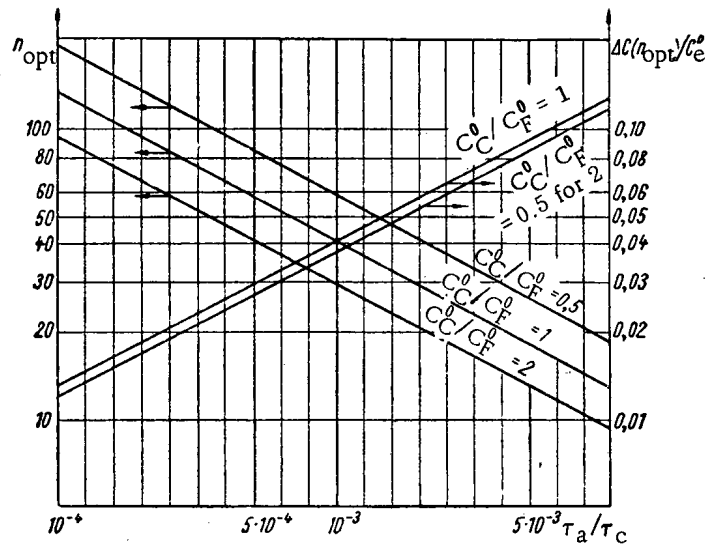


Fig. 4. Variation with auxiliary recharging time τ_a of the optimum number of rechargings n_{opt} per campaign τ_c and the corresponding relative increase in the cost of 1 kWh, ΔC , over the cost of 1 kWh C^0 for continuous recharging at full power.

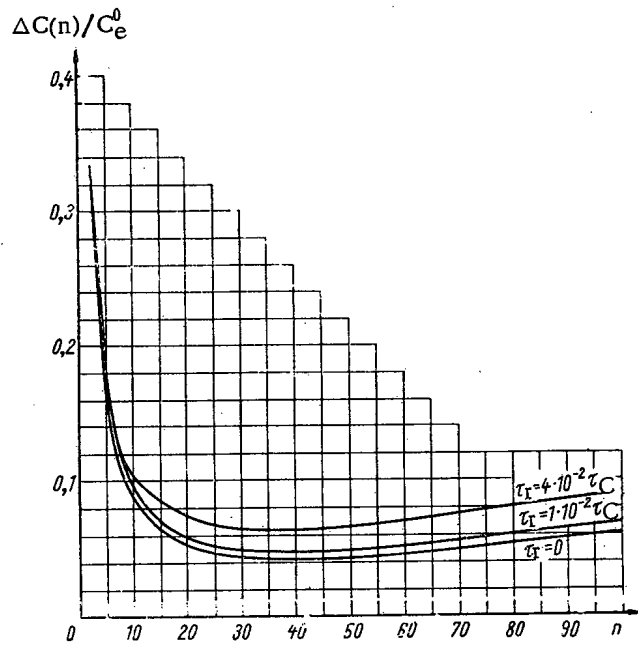


Fig. 5. Relative increase in the cost of 1 kWh over the cost 1 kWh with continuous recharging without lowering the power, plotted as a function of the number of recharging n per campaign τ_c and of the cassette-recharging time τ_r . (Auxiliary time taken as $\tau_a = 10^{-3} \tau_c$.)

Downward motion of the water can be arranged to take place in all the control channels. The two-way active zone, however, contains the possibility of neutron instability, and as before there are doubts over the reliability of effecting emergency cool-off in the downward path if forced circulation suddenly ceases. The thermotechnical advantages connected with increasing the critical loadings (by a rise in the velocity and underheating of the water at the danger point) and the possibility of increasing the heating and reducing consumption (by leveling the temperature of the water in the chamber between passes) are only substantial for a fairly high radial nonuniformity of heat

evolution, which in itself is unprofitable. Hence the two-way active zone does not normally have sufficient advantages to justify increasing the hydraulic resistance and complicating the construction.

Ways of Recharging

With high pressure of the heat carrier and a channel-free structure of the active zone, it is most realistic at the present time to recharge the fuel after removing the reactor roof. In so doing the auxiliary operations occupy a lot of time (see, for example, [4]), and are accompanied by a substantial change in the "thermomechanical" conditions of the first circuit. Hence it is economically desirable to carry out such recharging as rarely as possible (not more than a few times in each campaign), despite the fact that more frequent recharging makes it possible to deepen the burn-up of the fuel being extracted by using the reactivity of that being added [5], and simplifies the problem of compensation of excess reactivity.

Reducing the duration of recharging lowers underproduction and hence the cost of 1 kWh energy.

Using the approximate connection between the attainable depth of burn-up $\rho_C(n)$ and the number of rechargings per campaign time τ_C (see [5]) $\frac{\rho_C(n)}{\rho_C(n=\infty)} = \left(1 + \frac{\theta_r}{n}\right)^{-1}$, we obtain a relation between the optimum number of rechargings n_{opt} , the additional shutdown time τ_a of the WWR in connection with recharging, and the actual cassette-recharging time $\tau_r = m\tau_1$:

$$n_{opt} = \frac{1 - \tau_r/\tau_C}{\frac{\tau_a}{\tau_C} + \sqrt{\frac{\tau_a}{\tau_C} \cdot \frac{1}{\theta_r} \cdot \frac{C_C^0}{C_F^0}}} \approx \sqrt{\theta_r \cdot \frac{\tau_C}{\tau_a} \cdot \frac{C_F^0}{C_C^0}}, \quad (1)$$

where m is the total number of cassettes, τ_1 is the recharging time for one cassette, $\theta_r = \frac{\int_0^R r dr \int_0^R \Phi^3(r) r dr}{\int_0^R \Phi(r) r dr \int_0^R \Phi^2(r) r dr}$ is the

reduction in the depth of burn-up due to the radial nonuniformity of the neutron field $\Phi(r)$ [for $\Phi(r) = J_0(\mu r/R)$, $\theta_r = 1.69$], C_C^0 and C_F^0 are the capital and fuel components of the cost of 1 kWh energy for the ideal condition of continuous recharging at full power.

For $n = n_{opt}$, the cost of 1 kWh $C_e(n) = C_{min}$ exceeds the ideal cost $C_e^0 = C_F^0 + C_C^0$ by a fraction

$$\frac{\Delta C(n_{opt})}{C_e^0} = \frac{C_{min} - C_e^0}{C_e^0} = \frac{\frac{\tau_r}{\tau_C} + \sqrt{\frac{\tau_a}{\tau_C} \theta_r \cdot \frac{C_F^0}{C_C^0}} \left(2 + \sqrt{\frac{\tau_a}{\tau_C} \theta_r \cdot \frac{C_F^0}{C_C^0}}\right)}{\left(1 + \frac{C_F^0}{C_C^0}\right) \left(1 - \frac{\tau_r}{\tau_C}\right)} \approx \frac{2\sqrt{\theta_r \tau_a / \tau_C}}{\sqrt{C_F^0/C_C^0} + \sqrt{C_C^0/C_F^0}}. \quad (2)$$

These relationships are shown in Fig. 4, while Fig. 5 gives the relation for $\Delta C(n)/C_e^0$, the increase in the cost of 1 kWh over the "ideal," as a function of the number of rechargings n , from which we see that a reduction of n to $0.5 n_{opt}$ does not seriously raise the cost of the power. As we see, the main role is played by the auxiliary time, reducing which to $(10^{-3}-10^{-4})\tau_C$ may considerably reduce the cost of power. Together with improving the recharging after removing the roof, the realization of such short times for the auxiliary operations will stimulate the development of recharging without removing the roof and shutting down the reactor.

Recharging the fuel without removing the roof but after stopping the reaction, cooling down, and dropping the pressure can have little point, since by so doing the only improvement on open-roof recharging would be the absence of roof resealing, while the recharging itself would be harder and probably take longer. The shutting down of the reactor before recharging and its subsequent heating have to be carried out quite slowly in order to avoid thermomechanical damage.

Recharging while running requires complicated measures to restrict the flow of water through the cell of the unloaded cassette and leads to a surge in the neutron field in neighboring cassettes. This form of recharging would rather demand a reduction in reactor power. Carrying out recharging operations for a critical state of the reactor also introduces difficulties and seriously retards the recharging process. The use of solid absorbers with upper drive

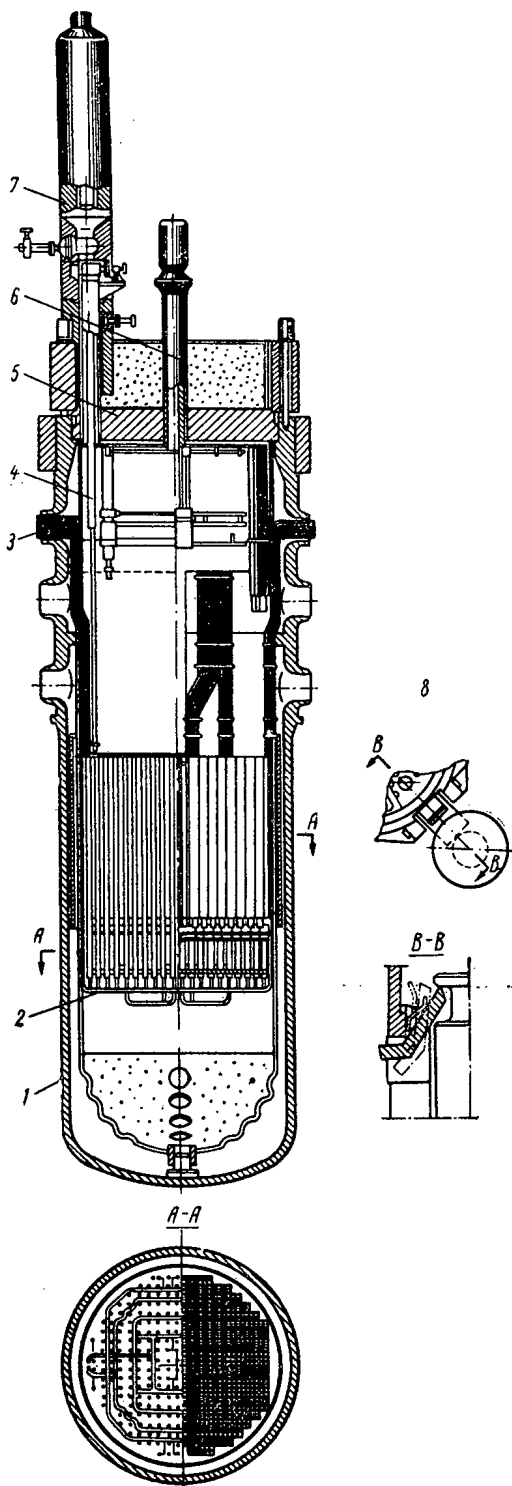


Fig. 6. Arrangement of reactor with "honeycomb" active zone and variation in the concentration of liquid absorber in the channel system: 1) body; 2) liquid-absorber collectors; 3) tubes for cassette control of the hermetic state of the fuel elements and water temperature; 4) driving-mechanism rod; 5) roof; 6) recharging machine; 7) diving system; 8) unit securing the cassette from floating up.

is entirely excluded; use of lower drive is limited by inconveniences associated with the disposition of the absorbers above the active zone. In view of this, choice of a reactivity-compensating system evidently reduces to the use of liquid compensators, i. e., changing the concentration of an absorber in solution. For this the most appropriate is probably an active zone developed into cells (kind of honeycomb) by special barriers, which, however, occupy a perceptible part of the useful volume and constitute quite a skeleton structure (Fig. 6).

Without removing the roof it is most suitable to recharge the fuel without lowering the temperature and pressure, but after switching off the reaction. This kind of recharging can be effected in two stages: 1) unloading from the active zone into intermediate storage cells (or inversely); 2) removing the cassettes from these cells through a gate in the body (or loading new cassettes into them). The more complex second stage may be effected while the reactor is running without time limitation.

The structural arrangement of this recharging is analogous to that shown in Fig. 6. Inside the body of the reactor are movable or immovable intermediate-storage cells for cassettes outside the active zone. These cells and the gate in the roof lie one over the other, thus easing the kinematics of the external charging machine. The container of this may be furnished with a "magazine" so that the gating only has to be done once per recharging.

For n rechargings per campaign, the number of intermediate-storage cells must be roughly $1/n$ -th of the number of cassettes in the active zone (for 300 cassettes and 20-100 rechargings, there should be 16 or 4 intermediate cells respectively).

If the exchange time for one cassette is $\tau_1 = 15-30$ min, then for 300 cassettes and a campaign time $\tau_c = 500$ days the increase in the cost of 1 kWh of energy owing to deviation from continuous recharging at full power is an extremely small quantity:

$$\frac{\Delta C(n_{opt})}{C_e^0} \approx \frac{1}{2} \cdot \frac{m\tau_1^3}{\tau_c} = \frac{1}{2} \cdot \frac{300(0,25 \div 0,5)}{500 \cdot 24} \approx (0,3 \div 0,6) \%$$

Estimating the length of the auxiliary operations (switching off the reaction, freeing the space above the active zone from the drives of the control systems, and restoring the working state) as $\tau_a = 5$ h, for $\theta_r = 1,69$ and $C_C^0/C_F^0 = 1$ we obtain:

$$n_{opt} \approx \sqrt{\theta_r \frac{\tau_c}{\tau_a} \cdot \frac{C_F^0}{C_C^0}} = \sqrt{1,69 \cdot \frac{500 \cdot 24}{5} \cdot 1} \approx 65,$$

and the cost of 1 kWh further increases by

$$\frac{\Delta C (n_{opt})}{C^0} \cong \frac{2 \sqrt{\theta_r \tau_a / \tau_c}}{\sqrt{\frac{C_F^0}{C_C^0} + \sqrt{\frac{C_C^0}{C_F^0}}}} = \sqrt{1,69 \cdot \frac{5}{500 \cdot 24}} = 2,6 \%$$

On placing the drives underneath the active zone, the auxiliary-operation time τ_a may be reduced, and this may diminish this figure.

Fixing the Cassette

In a spiked working reactor, the lifting force of the current flowing from bottom to top may several times exceed the weight of the cassettes, and these must therefore be braced against floating up or relieved from the pressure drop. In the presence of some kind of spacing lattice between the cassettes, these may be fixed by spring catches to the lattice walls (position 8 in Fig. 6), or by using catches or spring clamps in the tail of the cassette for fixing in the lower supporting lattice. These methods required either an increase in the space between the cassettes, or greater force in the recharging machine, or lock-control system passing through the active zone.

A more rational method of relieving the cassettes is a system of pistons fixed to the lower part of the cassette and experiencing an inverse pressure drop, due to the fact that a flow-collecting chamber, connected by a bypass tube to the space above the active zone, is formed under the pistons.

All the methods described make it possible to free the upper part of the body from apparatus preventing the recharging of the fuel.

Control and Protection Systems and Drives

Solid absorbers placed along the axis of the active zone are most widespread in WWR. In both the reactors of the Novo-Voronezh NPS, control cassettes with absorbers furnished with neutron water traps are used.

Replacement of the compensating and emergency absorbers by fuel when raised ensures a good neutron balance and increases the compensating power of the control elements, but on the other hand causes difficulties in the rapid introduction of the absorber against the direction of motion of the heat carrier. Hence it is very necessary to relieve the control cassettes from the action of the upward-moving current in the present case for high specific heat extractions. Such control elements introduce considerable nonuniformity into the distribution of the neutron field for intermediate positions, and therefore, generally speaking, it is appropriate to use them for emergency protection and the compensation of changes in reactivity due to the temperature effect, the Doppler effect, and poisoning.

It appears more justified to leave compensation for fuel burn-up to absorbers of relatively small efficiency, the movement of which does not introduce substantial nonuniformities into the neutron flux. It is possible, for example, to use lamellar and cylindrical absorbers furnished with scattering tails. For a fairly high recharging frequency (meaning recharging without removing the roof), the excess reactivity compensating the burn-up may be small, so that the over-all efficiency of the absorber need not be high.

We cannot exclude the development of combined absorbers, combining the principles of absorption in traps and in thin plates. The use of liquid absorbers, the concentration of which in the moderator or special water circuit may be varied, also deserves attention. In WWR conditions the compensation of reactivity by changing the neutron spectrum may prove hard to realize.

It is appropriate to use the following drives for solid control- and-protection systems.

1. Electromechanical or electromagnetic drives. These are placed in sheathes welded into the roof and connected with the working part by a rigid rod through a remote-release coupling. The sheathe is tight, i. e., the energy is fed to the drive electromagnetically through a close nonmagnetic screen.

During recharging, the drive rod is disconnected from the working part and taken away up, while the working part remains in the lowest position. The absorber projecting above the active zone and the rigid connecting rod may require protection from the action of the flow of water coming out of the active zone.

This scheme of electrical drive is similar to existing ones and is accessible for inspection through the upper flange of the sheathes in the roof, but in principle it is not suitable for recharging while running; it does not ensure emergency protection for recharging without roof removal, occupies a large space in the roof, and requires a reserve of travel upwards for removing the rod from the recharging space.

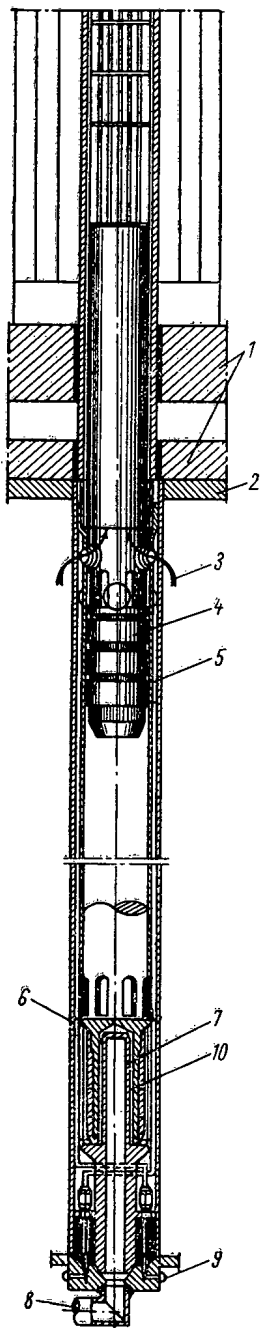


Fig. 7. Hydraulic drive system: 1) supporting plinth; 2) plinth with hydraulic-cylinder sheaths; 3) cooling-water entrance; 4) piston-tail working part (upper position); 5, 6) position indicators; 7) damper tube; 8) water supply under the piston; 9) to position indicators; 10) piston down.

2. Hydraulic drive situated beneath the active zone (Fig. 7). A piston is connected with the "tail" of the working part and moves in a hydraulic cylinder under the control of water pressure under the piston. There are units for detachably connecting the piston to the tail of the cassette and the cylinder to the controlling water, units for limiting the extreme positions and fixing intermediate positions, and also a unit for restricting the rate of lift. This kind of drive allows rapid clearing of the space for recharging without disconnecting from the working parts, and retaining the emergency protection during the recharging period.

The hydraulic drive demands extremely reliable coupling of the piston to the fuel working part, so as to eliminate the possibility of its floating up under the action of the flow. This fact forces us to consider combined drives with a mechanically movable support above, fixing the intermediate positions. This system is quite cumbersome, but facilitates a rapid downward throw of the absorber from any intermediate position. One may connect a hydraulic drive to the nonfuel elements of the control-and-protection system, which are not threatened with floating up under the action of the cooling flow of water, or go as far as a nondetachable joint of the working part with the hydraulic piston.

Compensation of Burn-up by Lowering the Power

There is some interest in the possibility of raising the burn-up and lowering the cost per kWh by gradually reducing the power of the reactor, maintaining the parameters, so as to compensate burn-up by reducing the Doppler effect (and partly diminishing poisoning). This decreases the fuel but increases the capital component, since less power will be produced in the profit period. Hence there exists an optimum lowering of power, as calculated below.

In the linear approximation, the cost of 1 kWh may be expressed in the form

$$C_e(\kappa) = C_F + C_C = C_F^0 [1 + k(1 - \kappa)]^{-1} + C_C^0 [1 - nk \ln \kappa] [1 + nk(1 - \kappa)]^{-1}, \quad (3)$$

where C_F^0 and C_C^0 are the fuel and capital components of the cost of 1 kWh for operation at nominal power and depth of burn-up ρ_c^0 ; $k = \frac{\Delta \rho_c^0}{\rho_c^0} \cong \frac{\Delta K_Q^0}{\rho_c^0 (\partial K / \partial \rho_c)}$ is the relative increase in burn-up resulting from the use of reactivity ΔK_Q^0 released on reducing the power to zero; n is the number of rechargings in campaign time τ_c for power Q_0 ; $\kappa = Q/Q_0 = \exp(-\tau_0/\tau_c k)$ gives the extent to which the power is reduced for the additional working time τ_{ex} . The components of the cost of 1 kWh may be expressed in terms of C_F (cost of 1 kg of fuel) and K (capital expenditure in setting up the NPS):

$$C_F^0 = \frac{C_F^1}{\eta \rho_c^0};$$

$$C_C^0 = \frac{K}{\tau \eta Q_0}.$$

This cost $C_e(\kappa)$ for $n = 1$ is smaller than $C_e(\kappa = 1) = C_e^0 = C_C^0 + C_F^0$ by a fraction $(\Delta C/C_e^0) = k\kappa[1 - \kappa + (1 + C_F^0/C_C^0)^{-1} \ln \kappa][1 + k(1 - \kappa)]^{-1}$, which in the case of $k(1 - \kappa) \ll 1$ is maximum for $\kappa = \kappa_{opt} = (1 + C_F^0/C_C^0)^{-1}$. For example, for $C_F^0/C_C^0 = 1$ we obtain $\kappa_{opt} = 0.5$, $\tau_{ex} = \tau_c k \ln \kappa^{-1} = 0.69 k \tau_c$ and $(\Delta C/C_e^0)_{max} = 0.15k/(1 + 0.15k)$. Hence for $k = 0.4$ the advantage in the cost of 1 kWh is $\sim 5\%$, and the duration of operation at reduced power is $\tau_{ex} = 0.28 \tau_c$.

For a large number of rechargings the advantage in the cost of 1 kWh will be smaller. In the limit $n \rightarrow \infty$, instead of (3) we obtain for the cost of 1 kWh $C_e(\kappa) = C_F^0 [1 + k(1 - \kappa)]^{-1} + (C_C^0 \ln \kappa^{-1}) / (1 - \kappa)$, which will be lower than $C_e^0 = C_F^0 + C_C^0$ only for fairly large values of k or C_F^0 / C_C^0 . For example, for $C_F^0 / C_C^0 = 1$, the value of $k = \Delta \rho_c^0 / \rho_c^0$ should be greater than 0.5.

Although the improvement in cost is not very great, we must remember that this is a gain in comparison with the cost corresponding to continuous recharging, since the unproductive use of neutrons in compensation by the absorbers is excluded. Furthermore, use of the power effect simplifies the control system thanks to the reduction in the number of burn-up-compensation controls, and makes it possible to increase the time between rechargings, i. e., to raise the chances of charging systems with roof removal.

3. OPTIMUM WWR PARAMETERS

If particular types of main components are selected for the NPS and the reactor, then optimization of the parameters characterizing these units quantitatively may also substantially lower the cost per kWh.

Since the number k' of independent parameters $x_{k'}$ is large, and their connection with the cost of energy complicated, direct optimization by simultaneous solution of a closed system of equations (minimum cost of 1 kWh corresponding to $\partial C_e / \partial x_{k'} = 0$) is only possible in exceptional cases [6]. The form of these conditions is often complex, since in varying each parameter all the rest in the chosen set are kept constant, and not just those "convenient" combinations in fixing which the form of the conditions $\partial C_e / \partial x_{k'} = 0$ becomes simple. If we select such combinations, then we may find simple relations between the optimum parameters, reducing the voluming of computing work by many orders. In particular, in a number of cases it is convenient to fix the power of the reactor and, together with this, part of the electrothermomechanical equipment of the NPS.

A considerable simplification will also be achieved if we consider that normally the relative changes in the cost per kWh C_e are much smaller than the relative changes in the independent parameters being varied. Such procedures were developed in [7] and applied to WWR of the type considered.

All the parameters were divided into three groups. The parameters of the first and second groups at the optimum are expressed analytically in terms of those of the third original group. In this are included the cost coefficients of the equipment, and also the volume fraction of water in the active zone ϵ , the pressure p_1 , the coefficients of nonuniformity of heat evolution, heating, and velocity, and other parameters the optimum value of which has not yet been obtained in analytical form.

In the first ("thermomechanical") group come the power Q , the zone length l , the heating of the water in the active zone Δt , the head \mathcal{H} in the steam generator, and other associated parameters. These quantities are optimized for a fixed cost of fuel, determined by the parameters of the second group.

The second ("fuel") group comprises the diameter d_F , the depth of burn-up ρ_C , and the length of the campaign τ_C for the fuel elements. These are connected by the definition $\rho_C = \tau_C \rho_{sp}(d_F)$ in terms of the specific power $\rho_{sp} = 4q_F / \gamma U d_F = 4q_l / \gamma U \pi d_F^2$.

The heat flow from unit length q_l or surface q_F of the fuel element must, at the "stressed point," be kept equal to the limiting permissible value q_l^0 or q_F^0 ; if $q > q^0$, then some advantage may be gained by making these flows equal to each other, increasing, for example, the corresponding diameter of the fuel element, which lowers the cost of their manufacture and the amount of covering for the same power and otherwise equal conditions.

For fixed parameters of the first group (including the power and the parameters of the heat carrier and the steam), the capital expenditure and efficiency will be constant, and the minimum cost per kWh will be obtained for those values of ρ_C , τ_C , and d_F which make the fuel component a minimum.

Analysis of the relations obtained in this way in [7] for a cycle without repeated use of fuel leads to the following:

1. In the region of fuel-element diameters* $d_F \geq d_0 = q_l^0 / \pi q_F^0$ in which the linear heat flow equals the limiting value $q_l = q_l^0$, the optimum burn-up ρ_{opt} is determined only by the relationship of $C_F M(\rho_C)$, the cost of the

*Here $d_0 = q_l^0 / \pi q_F^0$ is the diameter for which the heat flows from unit length and unit surface of the fuel element simultaneously take their limiting values, $q_l = q_l^0$ and $q_F = q_F^0$.

fuel material, to the depth of burn-up, and lies at the point $\rho_c = \rho_{opt}^0$, in which the tangent to the curve $C_{FM}(\rho_c)$ passes through the origin of coordinates (i. e., $\partial C_{FM} / \partial \rho_c = C_{FM} / \rho_c$). Here the optimum diameter is proportional to the complex $[q_l^{\partial} k_{manuf} / C_{FM}(\rho_c) \rho_c]^{1/4}$, i. e., falls with increasing depth of burn-up and cost of fuel material, and with decreasing cost of manufacturing unit length of fuel element ($0.25\pi\gamma_U k_{manuf}$, where γ_U is the specific gravity of the fuel).

This creates a tendency toward the transition of the optimum d_F into the region $d_F < d_0$.

2. In the region $d_F \leq d_0$ the heat flow q_F equals the attainable q_F^{∂} , and the optimum burn-up is somewhat smaller than the quantity ρ_{opt}^0 , tending toward it with increasing q_F^{∂} and decreasing cost of making one meter of fuel element as $\sqrt{q_F^{\partial} / \frac{\partial C_{FM}}{\partial \rho_c}} \sqrt{k_{manuf}}$. Here the optimum diameter varies as

$$\sqrt{k_{manuf} / \left(C_{FM} - \rho_c \frac{\partial C_{FM}}{\partial \rho_c} \right)}$$

3. The optimum values of ρ_c and d_F are sensitive to the relation between the cost $C_{FM}(\rho_c)$ of the fuel being loaded and the depth of burn-up of the fuel being extracted. Apparently for dioxide fuel the optimum in a number of cases lies in the range 30-50 kg/ton, and the optimum diameter is not very different from $d_0 = q_l^{\partial} / \pi q_F^{\partial} \approx 10$ mm.

The optimum campaign is more stable. It lasts around 10^3 days and increases as the complex $(k_{manuf})^{1/2} / [q_l^{\partial} (C_{FM} / \rho_c)]^{1/2}$ with increasing cost of manufacturing fuel elements and decreasing values of the attainable flows and ratio (C_{FM} / ρ_c) .

With the aid of the corresponding relations of [7], 288 sets of optimum parameters of the first group were calculated for different original parameters of the third group, which contain certain arbitrary features and were therefore varied over wide limits.

In this the following was taken into consideration:

1. The maximum heat content on emergence of the water from the cassette must not differ greatly from saturation $i_{max} \cong i' (p = p_1)$. If $i_{max} < i'$, then the enthalpy at the inlet i_{in} has to be lowered or the flow rate increased (in both cases efficiency falls), or the power reduced. These negative effects are not compensated by a certain increase in the critical loadings on increasing the underheating up to boiling in the danger region above the middle of the active zone.

For $i_{max} > i'$ there appears a steam content $x = (i_{max} - i') / r$ which worsens the neutron balance and reduces the hydraulic stability of the parallel operation of the channels; hydraulic shocks arise on condensation of the steam after mixing. For small x these effects are apparently not very great, but the quantitative aspect of the problem is not quite clear.

2. The diameter of the active zone should be made a maximum (~ 3 m), allowing for its being placed in a works-manufactured framework of maximum transportable dimensions ($D_{tr} \sim 4$ m).

Increasing the diameter above D_{tr} would be advantageous if it were not accompanied by a reduction in the thickness and strength of the body material and a corresponding sharp fall in the pressure and efficiency, which are not compensated by a rise in power (in boiling-water reactors the situation may be different).

Reducing the diameter leads to a rapid fall in power, by no means compensated by the reduction in the cost of the body and the increase in efficiency for a rise in the permissible pressure, which even for $D = 4$ m is close to optimum. As the pressure rises, the efficiency increases all the more slowly and the critical loadings fall all the more rapidly, which makes it necessary to lower the power or increase the surface of the fuel elements. For $\partial q_{crit} / \partial p_1 = -0.03 \cdot 10^6$ kcal/m²·h·abs·atm [8], the optimum pressure is ~ 120 abs·atm, which is still realizable in a transportable body. Achieving critical and hypercritical parameters, which may sharply improve many properties, is another matter. This is not considered here.

The results of applying the relations obtained reduce mainly to the following, valid at the point of minimum cost per kWh (these admit, as a rule, a fairly clear physical interpretation, although sometimes "common sense" could prompt other, false tendencies):

1. The effect of the water-uranium ratio N_U on the capital component of the cost per kWh in the optimum proves extremely weak, despite the strong variation of the fuel-element surface and the active cross section of the heat carrier with changing N_U ; this is due to the compensation of the N_U effect by the inverse effect of the relative length of the active zone l/d_F , which at the optimum rapidly increases with rising N_U [roughly as $N_U^{0.6} (1 + N_U)^{0.4}$].

2. The optimum thermal power Q_{opt} depends mainly on the radial coefficient of nonuniformity of heat evolution K_q , constituting 5-6 million kW (thermal) of $K_q = 1.5$, and $3.3-4 \times 10^6$ kW for $K_q = 3$. Approximately $Q_{opt} \sim K_q^{-0.6}$ and is practically independent of the admissible heat flows, an increase in which may more suitably be used for reducing the relative length of the active zone.

3. The average heating of the heat carrier at the optimum depends most of all on the nonuniformity of heating $K_{\Delta t} = \Delta t_{max}/\Delta t_{av}$ (roughly $\Delta t_{opt} \sim K_{\Delta t}^{-3/4}$) and is 45-65°C for $K_{\Delta t} = 1.2$ and 30-45°C for $K_{\Delta t} = 2$.

4. The optimum average velocity of the water in the active zone W_{opt} is mainly determined by the nonuniformity of velocity $K_W = W_{max}/W_{av}$, and is 3.5-4 m/sec for $K_W = 2.5$, and 6-7 m/sec for $K_W = 1.25$ (approximately $W_{opt} \sim K_W^{-0.8}$).

The maximum heating values Δt_{max} and especially velocities W_{max} depend on K_W and $K_{\Delta t}$ only weakly:

$$\Delta t_{max} = K_{\Delta t} \Delta t_{opt} \sim K_{\Delta t}^{0.25}$$

and

$$W_{max} = K_W W_{opt} \sim K_W^{0.2},$$

W_{max} changing in general very little (within 8-9 m/sec).

On varying the density of heat take-off ρ from unit volume of heat carrier, the velocity and heating of the water may advantageously be changed in the same way as $\sqrt{\rho}$.

5. The optimum fraction of energy spent on pumping over the heat carrier $n_p = N_p/Q$ depends fairly weakly on all the original varying data and forms 0.6-0.9% of the thermal power.

6. Also stable is the optimum average temperature head in the steam generator, equal to $\sim 25^\circ\text{C}$ for a non-corrosive heating surface.

7. Finally, the cost of an established 1 kWh, C_{est} , (without the cost of the first charging) is determined to a considerable extent by the relation of the cost of the second circuit and auxiliary systems of the NPS to power: $C_{NPS} = A + BQ$. The chief part is played by the coefficient B, but it is interesting to note that this has a very weak effect on the thermomechanical parameters being optimized. The value of C_{est} falls considerably on reducing the coefficients of nonuniformity K_q and $K_{\Delta t}$.

With increasing pressure, the value of C_{est} also falls, but the length of the active zone and the charge of fuel increase (owing to the fall in the permissible heat flows). Hence there is an optimum pressure p_1 of the order of 120 abs·atm, as was discussed earlier. For this pressure and a maximum heat content of the water corresponding to saturation, an average heat flow at the surface of the most-stressed fuel element $q_{max} = 1.2 \cdot 10^6$ kcal/m²·h·°C, and a radial heat-evolution nonuniformity $K_q = 1.5$, the optimum parameters of a WWR in the maximum transportable framework of diameter 4 m lie roughly within the following ranges: thermal power $Q \approx 5.5 \cdot 10^6$ kW/m²; ratio of the length of the active zone to the diameter of the fuel element ~ 500 (for a water-uranium ratio of ~ 1.6); mean heating and velocity of the water 48°C and 6.5 m/sec (for $K_{\Delta t} = 1.2$ and $K_W = 1.25$); mean head in steam generator 26°C; steam pressure $p_2 \approx 45$ abs·atm; efficiency of cycle $\sim 30\%$; proportion of power spent on circulation $n_c \approx 0.65\%$ (for pump efficiency ~ 0.7).

The parameters of the second block of the Novo-Voronezh NPS are close to the optimum values corresponding to the pressure, nonuniformity coefficients, and power of the reactor in this block ($Q \approx 1400$ MW), which, however, is considerably below optimum.

LITERATURE CITED

1. Planning of 420 MW Atomic Power Station. Report to the 11th Section Meeting of the All-World Power Conference [in Russian], Belgrade (1957).

2. S. A. Skvortsov, In the book "Transactions of the Second International Conference on the Peaceful Use of Atomic Energy," Contributions of Soviet Scientists, Vol. 2 [in Russian], Moscow, Atomizdat (1959), p. 105.
3. R. S. Ambartsumyan et al., Ibid., p. 119.
4. P. Eddy, Nucleonics, 21, 101 (1963).
5. S. M. Feinberg et al., See [2], p. 411.
6. A. Ya. Kramerov, "Atomnaya énergiya," 10, 211 (1961).
7. A. Ya. Kramerov and Ya. V. Shevelev, Engineering Calculation of Nuclear Reactors [in Russian], Moscow, Atomizdat (1964).
8. J. Aladyev et al., Boiling Crisis in Tubes, International Developments in Heat Transfer, Vol. 2, New York (1961), p. 237.

THE ORGANIC-COOLED ORGANIC-MODERATED
NUCLEAR POWER STATION "ARBUS"

K. K. Polushkin, I. Ya. Emel'yanov, P. A. Delens,
N. V. Zvonov, Yu. I. Aleksenko, I. I. Grozdov,
S. P. Kuznetsov, A. P. Sirotkin, Yu. I. Tokarev,
K. P. Lavrovskii, A. M. Brodskii, A. R. Belov,
E. V. Borisyuk, V. M. Gryazev, V. D. Tetyukov,
D. N. Popov, Yu. I. Koryakin, A. G. Filippov,
K. V. Petrochuk, V. D. Khoroshavin, N. P. Savinov,
M. N. Meshcheryakov, V. P. Pushkarev, V. A. Suroegin,
P. A. Gavrilov, L. N. Podlazov, and I. N. Pogozhkin

Translated from Atomnaya Énergiya, Vol. 17, No. 6,
pp. 439-448, December, 1964

The idea of utilizing low-rating nuclear electric power generating stations was a corollary of the need to supply electric power to remote and barely accessible areas of the USSR where the building of conventional electric power generating stations would not be justified economically principally because of the high cost of fuel delivery or the high cost of mining fossil fuels in the area itself. Engineering costs calculations show that small scale nuclear power utilities could be economically competitive in such areas even today. As is generally known, the cost of electric power produced at a nuclear power station is characterized by a relatively high capital investment component, and this holds particularly for low-power electric generating stations. The capital investment component can be lowered to manageable proportions through the use of organic coolants, by relying on cheaper structural materials, through the use of mass-produced ancillary equipment and instruments, and by weight reduction or even complete elimination of the biological shielding around the primary loop. To date, however, the widespread use of organic coolants in power reactor design practice has been held in check by several undesirable effects associated with radiolytic processes which affect organic compounds. Prominent among these effects is the buildup of high-boiling-point products of radiation-induced polymerization in the coolant, a situation which could eventually lead to the formation of insoluble compounds precipitating out in film form on the heat transfer surfaces, with a resulting vitiation of the heat transfer performance of the coolant. As experience in the operation of the OMRE experimental reactor in the USA has demonstrated, the simplest cleanup of the coolant by distillation and rectification to get rid of the high-boiling polymerizates will ensure that the concentration of these substances is kept at or below a specified level, but still will fail to prevent deposits from settling out on the surface of the fuel elements. Moreover, this approach to coolant cleanup implies the need for continuous makeup of fresh coolant supplied to the loop and the disposal of high-boiling insolubles extracted from the loop. This imposes a troublesome limiting factor on the choice of suitable organic fluids, given the heightened requirements of radiation stability.

The brunt of the efforts spent in dealing with the problem of how to best use organic coolants in nuclear power stations was therefore directed to the search for ways to recover the high-boiling radiolyzates without first extracting them from the loop, which would open the door for the use of inexpensive and accessible products exhibiting a fairly low radiation and thermal stability as reactor coolants. These efforts culminated in the design of a regeneration scheme based on the catalytic hydrocracking process. Preliminary test-loop studies indicated that this process successfully hydrates unsaturated products of radiation-induced dehydrogenation and effects a selective degradation of high-boiling-point radiolysis products, given a judicious choice of process parameters. This method of loop cleanup rendered possible the use of hydrogenation-stabilized gas oil produced on the basis of a directly distilled kerosene-gas oil cut of naphthene-aromatic base petroleum as organic coolant for the first nuclear power station. Added to

*Paper No. 307 presented by the USSR delegation to the Third International Conference on the Peaceful Uses of Atomic Energy, Geneva 1964.

the generally familiar advantages inherent in organic coolants are such advantages of gas oil as the low freezing range (-40°C to -70°C), freedom from any required use of a loop heating system, and the low cost.

Below appear some salient characteristics of gas oil:

Specific weight at 20°C ; g/cm^3	0.8558
Iodine number	Not greater than 1
Total sulfonating components, w/o	30
Low point on boiling range, $^{\circ}\text{C}$	212
High point on boiling range, $^{\circ}\text{C}$	300
Carbon content, %	86.89
Hydrogen content, %	13.11
H/C ratio	1.8
Sodium content, w/o	$2 \cdot 10^{-5}$
Sulfur content, %	$3 \cdot 10^{-3}$
Vapour pressure at 350°C , atm.	4.85
Chemical composition:	
paraffin hydrocarbons, %	30.12
aromatic hydrocarbons, %	30.03
naphthene hydrocarbons, %	39.85

The first ARBUS type nuclear power generating station was built at the Melekess Atomic Reactor Research Institute. The principal station parameters are the following:

Reactor power output, MW	5000
Turbogenerator output, kW	750
Pressure in primary-loop pressurizer, atm.	6
Coolant temperature at reactor entrance, $^{\circ}\text{C}$	230
Coolant temperature at reactor exit, $^{\circ}\text{C}$	243
Coolant flowrate in primary loop, tons/h.	600
Saturated steam temperature in steam generator, $^{\circ}\text{C}$	223

The physical startup of the organic-cooled reactor in this power station took place on June 29, 1963, and the station went on the line after heat transfer tests had been completed on August 11, 1963.

Basic Power Station Layout

The power station operates on two loops (Fig. 1). The coolant is circulated through the primary loop by two electrically driven pumps working on two parallel flow branches which are reunited by the reactor. Each pump has a throughput of 430 cubic meters per hour at a head of 43 meters liquid column. The electric motor develops 50 kW power. The coolant flows out of the reactor into steam generator units featuring a free evaporation level; the advantages of these steam generators are their simplicity, reliability, and less stringent feedwater requirements. After rejecting heat to the secondary-loop water in the steam generators, the coolant then proceeds through the pressurizers which simultaneously fulfill the function of degasifiers. Degasification takes place by virtue of the free level of the coolant and the special degasifying columns to which 10% of the total coolant flow is delivered. Mesh filters for rough purification are also installed in the pressurizer. From the pressurizer, the coolant is taken up by the circulating pumps and recycled to the reactor. The primary-loop pressure is kept constant during plant operation by the gases liberated in radiolysis of the coolant; nitrogen is used to maintain the pressure when the power station is started up cold. Excess gas is vented to the atmosphere by a pressure controller. Removal of residual heat release in the reactor in case of outage of the primary-loop circulating pumps during the initial period is taken care of by two turbine pumps working on the steam accumulated in the steam generators; this steam can keep the turbine pumps going for 90 min. The coolant flowrate is 96 tons/h in that case. Further heat removal is handled by the natural circulation of the coolant.

The primary-loop coolant is purified by means of cermet filters installed on bypass circulating pumps. The filters retain suspended particulates greater than 1.5 to 3μ across and prevent the concentration of iron in the coolant from surpassing 0.3 mg/liter. The flow through the cermet filters comprises $\sim 10\%$ of the total coolant flow.

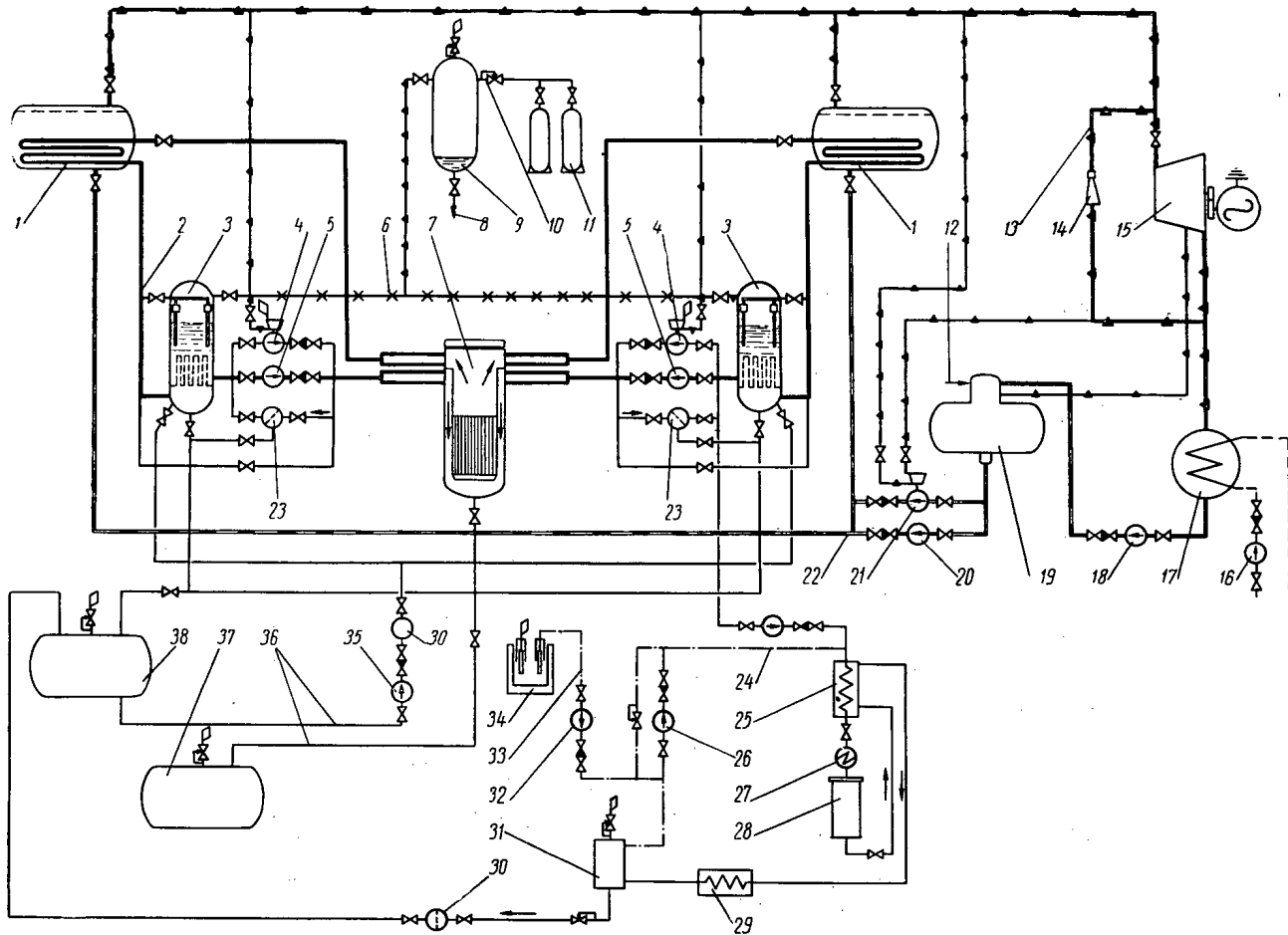


Fig. 1. Basic flowsheet of the ARBUS power generating facility: 1) steam generator; 2) basic primary-loop piping; 3) pressurizer; 4) emergency turbine pump; 5) main circulating pump; 6) gas piping; 7) reactors; 8) removal of light gas oil cuts; 9) receiver; 10) control valve; 11) nitrogen cylinder; 12) water in, from chemical water treatment plant; 13) steam lines; 14) pressure relief and cooling unit; 15) turbine with reducing valve and generator; 16) circulating pump; 17) condenser; 18) hotwell pump; 19) deaerator; 20) electric feed pump; 21) turbine feed pump; 22) secondary-loop piping; 23) cermet filter; 24) metering pump; 25) regenerative heat exchanger; 26) circulating compressor; 27) electric furnace; 28) catalyst reactor; 29) cooler; 30) mesh filter; 31) gas separator; 32) booster compressor; 33) hydrogen lines; 34) electrolyzer; 35) makeup pump; 36) auxiliary gas oil lines; 37) drainage tank; 38) overflow tank.

The primary loop and makeup for the primary loop are rounded out by a pump operating from an overflow tank of 20 m³ capacity. Coolant overflow will be cycled to the overflow tank or to the drainage tank depending on the degree of contamination. Low-boiling gas oil fractions forming during the process of decomposition of the coolant (these fractions exhibit boiling points to 120°C) become condensed in the receiver, whence they are discharged periodically into the drainage tank. Coolant is bled from the primary loop for regeneration, and the regenerated gas oil is cycled to the overflow tank. A description of the regeneration system and the operating principles of that system are given below.

The secondary loop comprises part of a conventional condensation steam turbine electric power station. In the event of a sudden drop in the turbogenerator load, a reduction cooler unit is provided for the purpose of cycling excess steam directly to the water-cooled condenser (Fig. 2).

Power Station Equipment

ARBUS is set up in discrete completely modularized units which had been run through test-stand checkouts at the site of fabrication. The power station is made up of 19 units none of which weighs more than 20 tons. The total weight of the overall plant, biological shields around the reactor included, is roughly 360 tons. The weight and

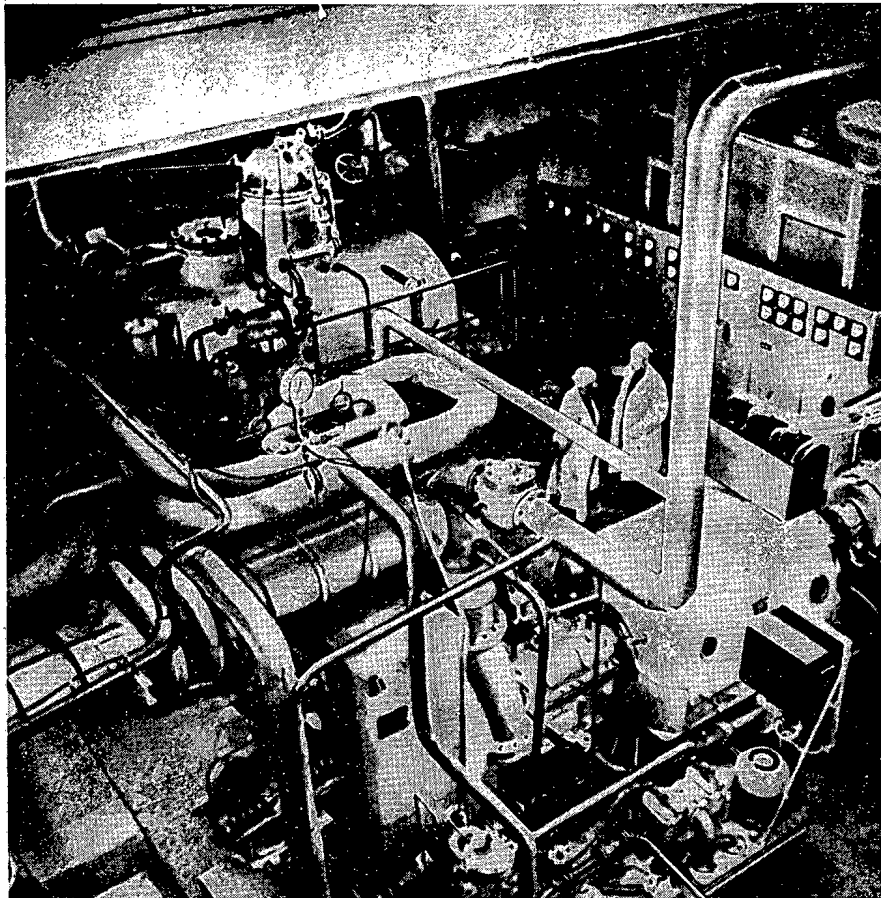


Fig. 2. Steam power equipment of the nuclear station. Turbogenerator appears up front.

sizes of the modular units facilitate transportation of the units to the construction site by water or overland routes. Assembly of the power station on the construction site was completed in a matter of two to three months.

ARBUS is housed in a building covering 12.36 by 28.5 m, and standing 6.36 m high. The electrolyzer and the overflow tanks are located outdoors. Figure 3 presents a clear picture of the layout of the equipment inside the building.

When the power station is being started up, electrical equipment is supplied with power from a diesel generator of 135 kW rating, so that the system operates in a fully autonomous manner. Natural circulation flow is used in heating up the primary loop and emergency cool-down of the primary loop, because of the different levels on which the reactor and the steam generator are located.

The power station equipment includes a fuel element container, a guiding mechanism for seating in-pile components, specialized hardware for reactor refueling operations, a storage rack for spent fuel assemblies and control and shielding sleeves with rods. The reactor is refueled with the aid of a special bridge crane boasting a load carrying capacity of 12 tons.

The reactor and plant staff numbers 17.

The equipment, valves and fittings, and piping of the primary loop are made of low-carbon steel. Mass-produced petroleum industry pumps and standard petrochemical fittings with tightened specifications on the finish of the interior surfaces are employed in the plant. The nonstandardized equipment is made of St-20 structural steel with modularized shells and bottoms for the reactor, steam generators, and pressurizers. The piping was welded in a protective argon-carbon dioxide environment.

Maximum estimates of the activity of the primary-loop coolant showed it to be $1.5 \cdot 10^{-4}$ curie/liter even taking into account a possible escape of fission products from ruptured fuel elements, as determined by deliberate

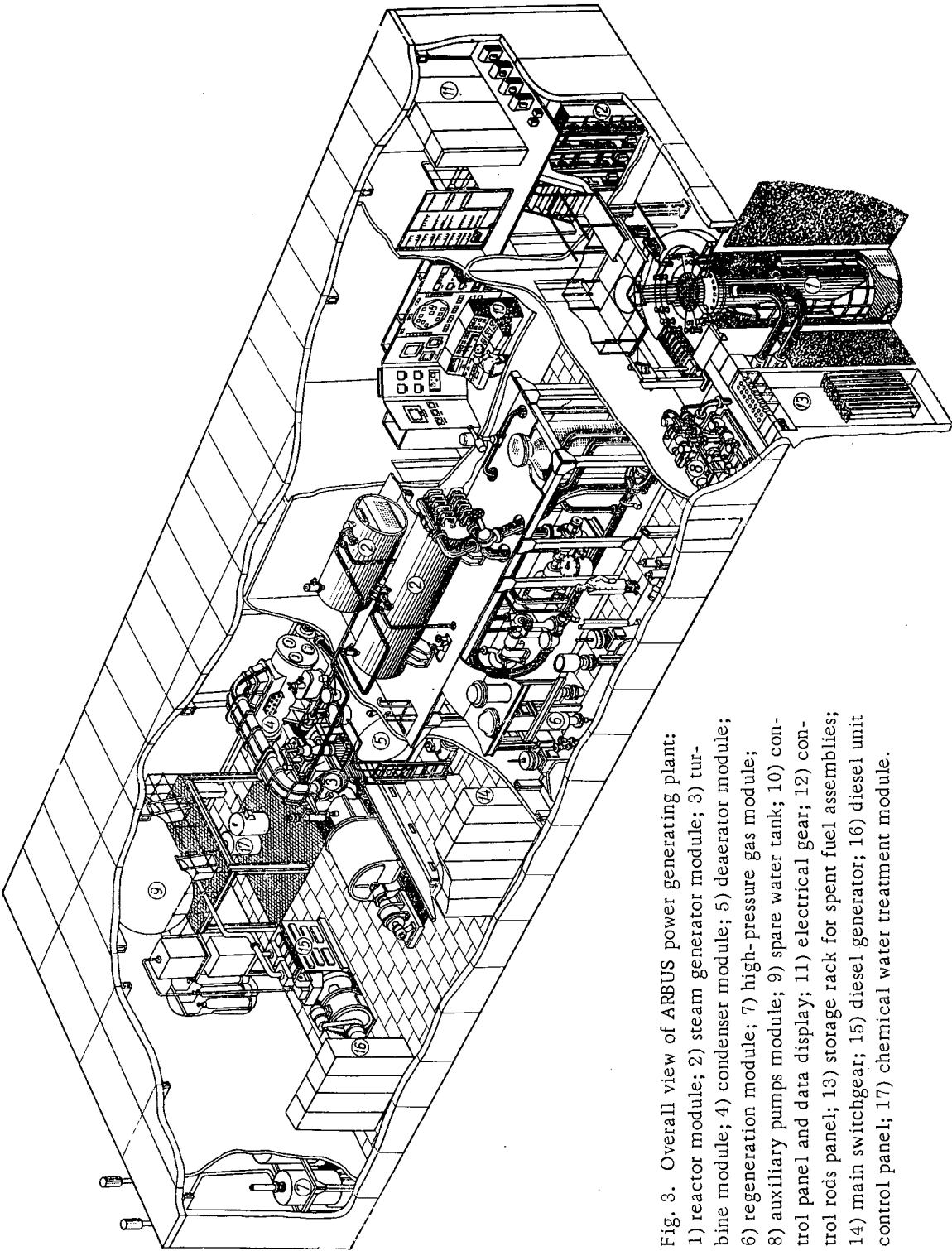


Fig. 3. Overall view of ARBUS power generating plant:
1) reactor module; 2) steam generator module; 3) turbine module; 4) condenser module; 5) deaerator module; 6) regeneration module; 7) high-pressure gas module; 8) auxiliary pumps module; 9) spare water tank; 10) control panel and data display; 11) electrical gear; 12) control rods panel; 13) storage rack for spent fuel assemblies; 14) main switchgear; 15) diesel generator; 16) diesel unit control panel; 17) chemical water treatment module.

puncturing of the cladding in loop tests. This made it possible to do without biological shields around the primary loop, and to retain only the reactor shielding made of conventional shielding materials (concrete, graphite, polyethylene, iron).

When the makeup of the central power station equipment and the operating conditions of the equipment are taken into account, the radiation level in rooms occupied by personnel were estimated at $0.5 \mu\text{rem}/\text{sec}$, and that in the piping system at 3 to $4 \mu\text{rem}/\text{sec}$. The activity of the gas effluents formed as a result of radiolytic decomposition of the coolant, was 10^{-12} curie/liter.

The total activity of the gas vented by the power station was approximately $7.2 \cdot 10^{-8}$ curie/day.

The Reactor

The reactor is a welded cylindrical vessel standing 4365 mm high, extending 1340 mm in diameter, with a wall thickness of 20 mm, a flange with support lugs and eight pipe connections 150 mm in diameter for inflow (four bottom pipes) and outflow (four top pipes) of coolant. Side and bottom shields were installed to lower the irradiation intensity of the vessel.

An internal vessel is placed inside the reactor to organize the flow of coolant, and at the same time to support the weight of the core. The uniformity of flow distribution ahead of the core is achieved by means of two perforated baffle plates.

The fuel elements are clad with low-copper D-20 aluminum alloy. Uranium-aluminum alloy used for fuel minimizes escape of fission products into the coolant loop in the event of fuel element rupture. The total U^{235} loading in the reactor is 22.5 kg, with 36% enrichment. The maximum fuel element core temperature is 336°C by rating, that of the cladding 335°C .

The physical design of the ARBUS reactor core was based on the results of earlier criticality experiments performed on experimental channels of a VVR-M reactor, a description of which may be found in the proceedings of the second Geneva conference on the peaceful uses of atomic energy. The choice of these channels is dictated by the similarity to the channels of the ARBUS facility both in geometry and in the specific U^{235} loading per running centimeter of the channel length.

During the physical startup of the ARBUS reactor, the critical level of the moderator was determined for the fully assembled core, and determinations were made of the number of control rods required to override the total excess reactivity, the neutron flux distribution, was mapped, and rods were calibrated in a hot clean system. The results of the physical startup showed that the procedure relied upon for calculations provided the accuracy required in determining the physical characteristics of the core. Adequate agreement between theoretically predicted and experimental data was attained in the determination of the critical height H_{Cr} required for a "clean" core at room temperature ($H_{\text{Cr}}^{\text{exp}} = 314 \text{ mm}$; $H_{\text{Cr}}^{\text{theor}} = 320 \text{ mm}$) and the position of the control rods in critical cold clean and hot clean systems.

Experimentally measured neutron fields, measured over the radius and height of the core, confirmed the theoretically computed values of the variation factors used in the heat transfer calculations.

The system was heated up from 20° to 200°C using an external heat source, in the determination of the temperature effect and of the temperature coefficient of reactivity. Extrapolation of the results arrived at to the operating temperature of the moderator (245°C) revealed that the experimental value of the temperature effect from 20° to 245°C exceeds the theoretically computed value of $6.1 \cdot 10^{-2}$ by approximately $k_{\text{eff}} = 1.4 \cdot 10^{-2}$. The temperature coefficient of reactivity is negative over the entire range of temperatures concerned, and is $-4.3 \cdot 10^{-4} \text{ } 1/^\circ\text{C}$ at the operating point.

Taking into account the corrections obtained in the physical startup and in the power startup, the values of the effective multiplication factor for the various states of the reactor are the following: at the beginning of the reactor period, $k_{\text{eff}} = 1.264$ for $t = 20^\circ\text{C}$; in the case of a hot clean reactor $k_{\text{eff}} = 1.189$; in the case of a hot poisoned reactor $k_{\text{eff}} = 1.148$. The duration of the reactor period with the reactor on full power is about two years.

Reactor control is achieved by means of cylindrical rods traveling through the reactor core. Two boron steel rods are designed for automatic control (the automatic control rods); 30 boron steel rods are designed to override the temperature effect and the poisoning effect (reactivity compensation rods). These rods compensate $\sim 12\%$ of the reactivity.

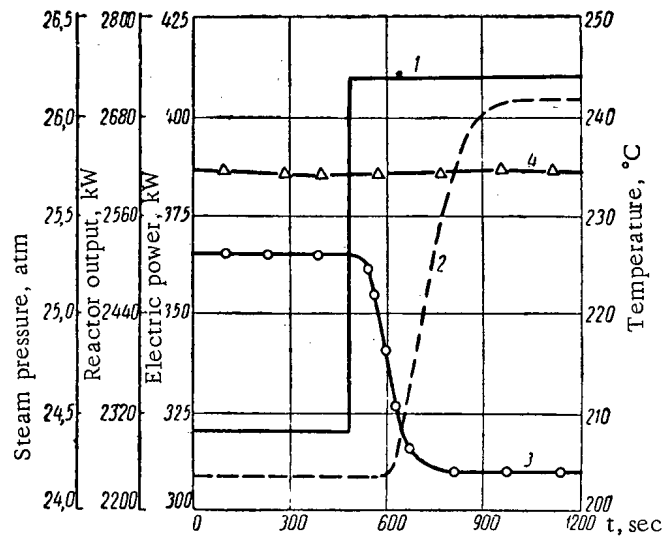


Fig. 4. Variation in power station parameters in response to increased power load: 1) electric power; 2) reactor power output; 3) steam pressure; 4) coolant temperature at reactor exit.

Under emergency conditions of the first kind (scramming conditions), (i.e., cessation of coolant flow in the primary loop or reactor runaway), all of these rods are dropped into the core. The overall design provides for either bank operation or individual operation of the rods. Two reactivity compensation rods (shim rods) working in pairs provide for emergency protection of the second kind (junior scram). The emergency signals of the second kind include signals for exceeding the preset power level, for power supply outage, and for various other process signals. 37 boron carbide rods are designed for overriding poison burnout effects. These rods compensate $\sim 18\%$ of the reactivity and are used as on-off controls.

Power monitoring, control, and protection of the reactor is carried out by monitoring neutron flux with compensated ionization chambers. These ionization chambers are placed in special pressure tight suspension supports positioned in the space between the reactor well and the reactor vessel. A total of 12 channels are available for the suspended supports. Five lead-shielded channels are designed to accommodate startup suspension supports.

The control and protection system is based chiefly on magnetic amplifiers which assure stable performance at low temperatures and easily withstand transportation over long distances.

Reactor control is performed by means of a single automatic control: a second stands on hot standby. A preset power level can be held stable to within $\pm 1\%$. An automatic startup control is available for starting the reactor up automatically, bringing the reactor up from the nominal power level of 10^{-4} to $10^{-5}\%$ up to a level of 1 to 10% with a predetermined period. Over that range, the automatic startup control also provides protection by controlling the rate of power rise.

Investigation of Dynamic Response and Control of Power Station

The dynamic response of power stations has been studied on an analog computer, and later directly on the ARBUS power station. As a result of these dynamic investigations, it has been found that one special feature of this power station is the comparatively slow unfolding of processes under both operating and scram conditions. The slowness of all the transients, accounted for by the comparatively large coolant volume in the primary loop and the large volume of boiling water in the steam generators, is an advantage from the standpoint of the temperature response of the fuel elements and the primary-loop components.

The study of temperature self-regulation of the power station showed that the power station exhibits adequate stability for normal operation at a predetermined set of operating conditions without requiring an automatic pile neutron flux control. The maximum permissible reactivity jump developed by the system in response to a permissible deviation of the process parameters is roughly $+0.1\beta$ and -0.3β .

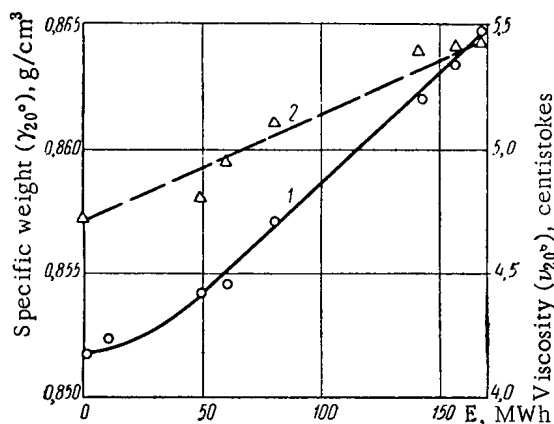


Fig. 5. Temperature variation of gas oil viscosity: 1) original gas oil in loop; 2) gas oil containing 9.03% high-boiler radiolyzates.

It was found as a result of an investigation of a scram cool-down of the primary loop when one of the circulating pumps malfunctioned that the temperature of the fuel element surface will not exceed the permissible maximum if emergency turbine pumps go into action no later than 3 sec after the emergency signal becomes operative. As direct experimentation conducted at the power station showed, this takes a time of 0.2 sec.

The off-peak operating time of the turbogenerator when working to satisfy the power requirements of the power station itself will be 18 min when the reactor emergency protection system is actuated.

The results of analog computer studies were verified by the direct power station tests. Figure 4 shows the variation in the power station parameters when the electric load was stepped up.

Maintenance and Cleanup of the Primary Loop

The basic requirements imposed on power stations whose primary loop materials are carbon steels and which require no biological shielding is the purity of the organic coolant employed. Care must be taken to keep the equipment and piping of the loop free from contamination and from corrosion products in order to meet this requirement, employing either mechanical or chemical means with subsequent protection with a volatile inhibitor (50% aqueous solution of monoethanolamine) and leakproofing during hauling and assembly operations. After assembly has been completed and the loop has been pressurized with dehumidified air, the loop may then be filled with DA fuel (close to gas oil in composition) with an iron content of roughly 1 mg/liter; this fuel is then used for hot blowdown of the loop. The temperature is kept close to operating temperature during this operation. The operation is carried out in three stages to maximize its effects. The fuel is drained out and replaced with fresh fuel for each such stage. The blowdown process is monitored by checking the iron content in the fuel.

The blowdown and purification technology so described made it possible to achieve a startup of the power station with an iron content of 0.2 to 0.3 mg/liter in the gas oil.

Coolant Regeneration

A specially designed regeneration system for treatment of the organic coolant by continuously bleeding a part of it to a hydrogenation reactor was resorted to in order to remove polymers and unsaturated compounds from the ARBUS primary loop. In this reactor (hydrogenizer), hydrogenation of unsaturated unstable compounds and degradation of polymers with the formation of compounds similar to the original compounds in their physicochemical properties was achieved under hydrogen pressure on an aluminum-cobalt-molybdenum catalyst bed, with up to 80% recovery yields. The remaining 20% consisted of lightweight off-products and coke. An additional purification of the coolant from traces of metals and sulfurs present in it also occurred in a similar regenerative process. The reader should note that the hydrocracking step is facilitated in this instance by the nature of linkages in radiation-chemical polymers. The regeneration conditions were so chosen that aromatic compounds would not undergo hydrogenation.

As studies have shown, the optimum process parameters for regeneration by hydrogenation of coolants fabricated from gas oil petroleum cuts are: hydrogen pressure 40-60 atm, reactor temperature 350°-380°C, coolant

The self-regulation operation, an automatic transition of the power station for one power level to another with the automatic controls shut off can occur given an appropriate change in the temperature level of the coolant and in the steam pressure in the secondary loop.

Investigations of perturbations in coolant flowrate have shown that flow rate oscillations with amplitudes to 10% and frequencies of 0.01 Hz and higher are tolerable. No changes in process parameters are observed at any frequency above 0.3 Hz.

When the station is operating at rated levels, an instantaneous drop of 260 kW in electric power load results in an increase of 3 atm, approximately, in the steam pressure in the secondary loop, whereas a subsequent step-up of 260 kW in the electric load will return the system parameters to their original values.

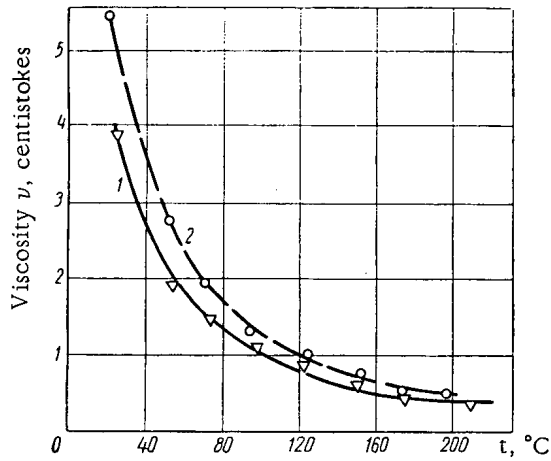


Fig. 6

Fig. 6. Variation in viscosity and in specific weight of gas oil as a function of integrated exposure dose: 1) viscosity; 2) specific weight.

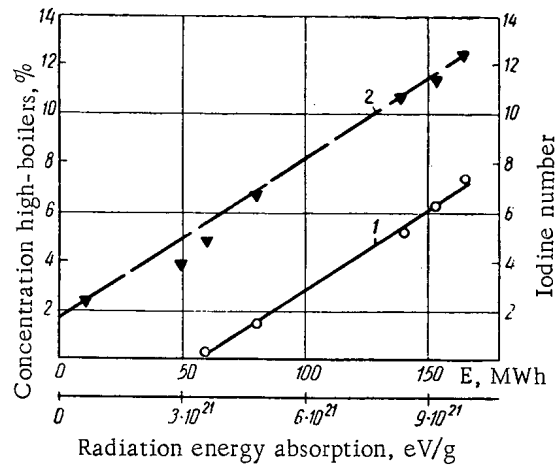


Fig. 7

Fig. 7. Accumulation of high-boilers and variation of iodine number, as functions of the integrated exposure dose: 1) concentration of high-boiling radiolyzates; 2) iodine number.

Composition of Gas Formed in Radiolysis

Components	Contents	
	w/o	v/o
Hydrogen	26.670	83.077
Methane	24.191	9.415
Ethane-ethylene	13.634	2.829
Propane	11.079	1.566
Propylene	9.060	1.343
N-butane	5.496	0.590
Acetylene	0.548	0.132
Butane	2.081	0.224
Allene	0.386	0.061
β, i + α-butylenes	6.219	0.692
β-Butylene + divinyl	0.636	0.071

volume rate 0.5 h^{-1} , and molar ratio of raw material to hydrogen from 1:5 to 1:10. The basic layout of the coolant regeneration system is seen in Fig. 1. Primary-loop coolant flows (at 200 to 250 liters/h) through a metering pump. The metering pump sends the gas oil under 45 to 60 atm pressure downstream to mix with a counterflow of hydrogen circulating in the system and obtained by electrolysis of water in the electrolyzer, whence, the hydrogen is fed to the system by a booster diaphragm compressor. The gas oil and hydrogen mixture is heated in a regenerative heat exchanger, and then becomes heated to operating temperature in an electric furnace. The mixture then arrives subsequently in the catalyst-packed reactor. The mixture of hydrogen and regenerated gas oil emerging from the catalyst-bed reactor gives up its heat in the heat exchanger and ends up cooled down to a temperature of $30\text{--}50^\circ\text{C}$ in the cooler. Downstream of the cooler, the

mixture becomes separated in a gas separator unit, whence, the gas oil, on passing through the cermet and felt filters, gains access to the primary-loop make-up tanks, while the hydrogen is recycled to the circulating compressor.

As a result of the fact that gaseous polymer degradation products (methane) are formed in the hydrogenization regeneration process, slight quantities of the circulating gas are continuously vented to the stack. The total flow-rate of hydrogen is 5 normal m^3/h , of which about 4 normal m^3/h are delivered directly to the reaction.

Radiation-Chemical Coolant Modifications

The radiation-chemical characteristics of gas oil stabilized by hydrogenation obtained at the ARBUS nuclear power plant appear on the whole to be in excellent agreement with the results of preliminary experiments and loop-test experiments. Figure 5 shows the temperature variation of the viscosity of the original primary-loop gas oil and the irradiated primary-loop gas oil in the ARBUS plant, with a content of 9.03% high-boiling radiolyzates. Figures 6 and 7 show the variation in the density, viscosity, iodine number, and content of high-boiling radiolyzates as the integrated exposure dose is increased and with the regeneration set out of operation. Figure 7 also plots the energy radiation absorption scale per gram of gas oil.

The initial molecular yield of high-boiling products was computed on the basis of the data obtained, and found to be ~ 2 mole/100 eV. This was later reduced to ~ 0.5 mole/100 eV with long-term operating experience.

The table lists the compositions of gases formed during the radiolysis. The coolant flowrate was 20 to 30 tons per year to replace losses by radiolytic decomposition at 100% power load.

SUMMARY

The installation and the experimental operation of the ARBUS nuclear electric power generating station demonstrated the feasibility of constructing organic-cooled nuclear power stations in remote regions of the USSR. The correctness of the calculations and principal design decisions, the realizability of equipment fabrication and of the carbon steel primary-loop piping without any biological shielding, and the possibility of exploiting available mass-produced petrochemical equipment and standard fittings, giving due attention to the specific requirements of a nuclear facility, were confirmed in operation. This nuclear power station exhibits adequate operational stability, with the added advantages of simplicity and reliability in operation under a variety of operating conditions.

In subsequent work, improvements can be made in the engineering costs of power stations of this type, by increasing the process parameters (employing regenerable coolant of higher thermal stability), and by introducing other power plant improvements based on the accumulated operating experience.

TÉS-3 COMPACT ATOMIC POWER STATION*

N. M. Sinev, A. K. Krasin, I. F. Bychkov,
 O. I. Blokhin, D. L. Broder, V. N. Gabrusev,
 Yu. V. Dudnikov, V. A. Zhil'tsov, M. A. Koptev,
 A. Ya. Komarov†, A. P. Kotov, M. N. Lantsov,
 G. A. Lisochkin, G. A. Merzlikin, I. G. Morozov,
 Yu. I. Orekhov, Yu. A. Sergeev, P. N. Slyusarev,
 G. N. Ushakov, N. V. Fedorov, V. Ya. Chernyi,
 and V. M. Shmelev

Translated from *Atomnaya Énergiya*, Vol. 17, No. 12,
 pp. 448-452, December, 1964

Introduction

In correspondence with the plan for the development of nuclear power in the USSR, the TÉS-3 mobile large-unit atomic power station with a water-moderated water-cooled reactor was set in operation on an experimental basis in 1961. TÉS-3 constitutes a full-scale demonstration experimental-low-power atomic power station (APS) designed for operation in those regions of the USSR where the use of small APS is economically expedient. For such APS, it is especially important that the construction and assembly work at the site of operation be kept at a minimum. In this regard, TÉS-3 constitutes an experiment in producing APS which would leave the factory in a state of maximum readiness for operation. Virtually all the equipment of TÉS-3 is assembled in four large units and mounted on four self-propelled caterpillar-track flatcars with heated coach-type bodies. This makes it possible to operate TÉS-3 without constructing special buildings, while the preparation of the site mainly consists in providing the biological shield.

It is planned to utilize TÉS-3 mainly as a stationary plant without moving it to another site. Therefore, a number of units connected with the drive of the self-propelled power cars can be dismantled after the station reaches the site of operation (diesels, transmission gear, tracks, etc.). In this case, the chassis of the cars play the role of ordinary foundation frames, while the space which becomes available can be used for auxiliary rooms.

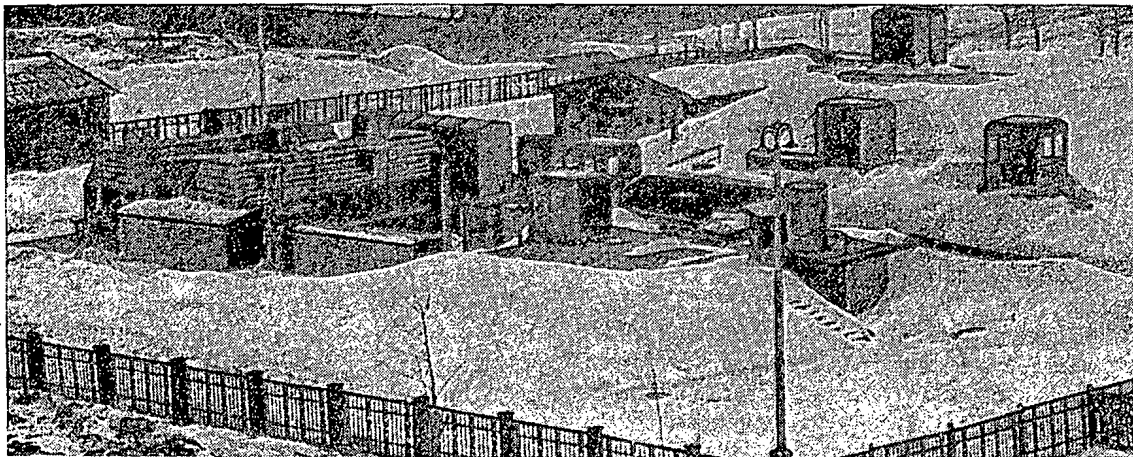


Fig. 1. General view of the TÉS-3 site.

* Report No. 310, presented by the USSR at the Third International Conference on the Peaceful Uses of Atomic Energy, Geneva, 1964.

† Deceased.

TABLE 1. Values of the Critical Height h and of $d\rho/dh$ for Cores with Different Numbers of Fuel Assemblies

Number of fuel assemblies*	Core diameter D , cm	D/h	h , cm		$d\rho/dh, \times 10^2$ cm	
			experiment	calculation	experiment	calculation
31	40.4	0.69	58.6	49.2	—	0.173
32	41.1	0.75	54.6	47.0	—	0.204
36	43.4	0.99	44.0	40.8	0.350	0.303
60	55.7	1.96	28.4	28.7	0.999	1.006
74	61.9	2.46	25.1	26.3	—	—
79	63.9	2.64	24.2	25.8	1.36	1.444

* The central cell does not contain a fuel assembly.

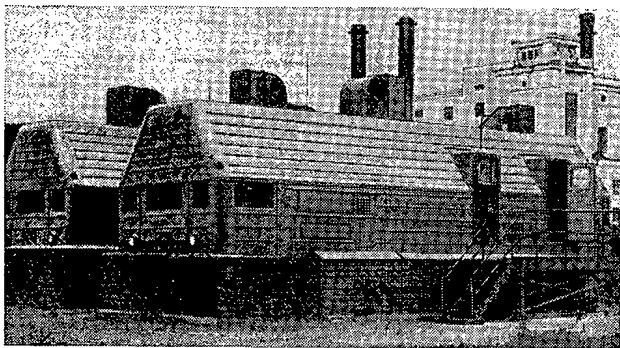
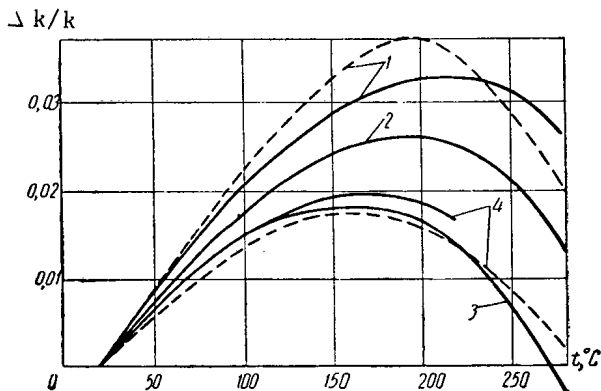


Fig. 2. View of the self-propelled power cars with the control panel and the turbogenerator. The car tracks are covered for heating purposes.

Fig. 3. Dependence of the reactor's reactivity $\Delta k/k$ on the mean water temperature t in the reactor (the solid curves represent the experimental results, while the dashed curves denote the calculation data). 1) Reactor with 74 fuel elements; 2) same (the core contains two manual-control rods); 3) same (the core contains six manual-control rods); 4) hot critical assembly with 85 fuel assemblies.

If necessary, the communications between the self-propelled units can be dismantled and the station transferred to another site. The weight and the overall dimensions of the self-propelled power cars make it possible to transport them by railway. During transport, the reactor is cooled by means of a radiator provided in the reactor car. The replacement of depleted fuel assemblies can be performed under field conditions without removing the reactor lid by using a reloading container and a 25-ton self-propelled crane.

Description of the Station

The TЭС-3 power station was installed at Obninsk at the site of the first atomic power station in the world in such a manner that the preparation of the area, the assembly, and the operation of the station corresponded most closely to these operations as they would be performed under field conditions. The TЭС-3 site (Fig. 1) comprises the self-propelled power cars, a storehouse for spare parts, and a small prefabricated building housing the turbogenerator panel, a transformer for the station's own needs, and the radiation health checkpoint.

The self-propelled power cars with the reactor and the other first-loop equipment are located in a common trench with a depth of 2.8 m, whose walls and cover are made of prefabricated reinforced-concrete sections and are covered on the outside with soil, which constitutes the basic biological shield. The self-propelled power cars with the turbogenerator and the control panel are situated at the ground level (Fig. 2).

TЭС-3 constitutes a two-loop steam turbine plant. It is provided with sectionalizing and emergency arrangements for reliable self-contained operation of the station. The station is automated; its power level varies automatically with changes in the turbogenerator load. The basic characteristics of the power station are:

Generator power, kW	1500
Reactor power, kW	8800
Pressure in the first loop, atm abs.	130
Water temperature, °C:	
at the upstream end of the reactor	270
at the downstream end of the reactor	300
Parameters of the second loop:	
steam generator pressure, atm abs	20
steam superheating temperature, °C	280
pressure in the condenser, atm abs	0.13
Cooling water discharge, t/h.	1000
Weight of the station's equipment, t.	210
Weight of transported biological shielding,	
included in the above, t.	28.5
Weight of all self-propelled cars, t.	310
Duration of run, days.	250

Reactor Physics

The physical characteristics of the TĚS-3 reactor were determined on the basis of the two-group theory by taking into account the multiplication of neutrons in moderation; they were checked by means of three critical assemblies which were put together successively. At the initial stage, the experiments were performed on a critical assembly that only approximately simulated the core of the TĚS-3 reactor. The subsequent experiments were performed by using two full-scale critical assemblies, which simulated the TĚS-3 reactor to the full extent. "Cold" experiments for checking the design of the control elements and devices for charging the reactor with uranium were performed by using one of these assemblies. It was possible to heat the last, "hot" critical assembly almost to the calculated temperature, which made it possible to investigate the temperature effect.

The initial reactivity was found by using the dependence $\rho = f(d\rho/dh)$. The critical height h was varied by changing the number of fuel assemblies (Table 1).

The thus obtained critical mass of the reactor with the calculated core, i.e., with 11 fuel assemblies removed, differed from the theoretical value by 5%. The reactivity of the cold uncontaminated reactor (0.114) also was in satisfactory agreement with the calculated value, which was equal to 0.123.

The temperature effect of reactivity determines to a large extent the safety of the reactor and convenience in operation. Therefore, a thorough investigation of this effect was carried out in experiments on all critical assemblies and during the actual start-up of the reactor. The experiments showed that the temperature effect is highly sensitive to the presence of absorbing rods in the core and to the withdrawal of individual fuel assemblies from the core (Fig. 3).

The compensating ability of the control elements was investigated for rods made of different materials, which were characterized by different designs and dimensions and were arranged within fuel assemblies and in individual cells. The data pertaining to the chosen control system are given in Table 2.

Biological Shield

The biological shield of TĚS-3 consists of two parts: the immobile part, which is provided at the operation site, and the transportable part. The transportable part of the shield is made of lead and is installed in the tank of the biological shield. The tank, which is provided with a coiled pipe for cooling, is filled with distilled water or a solution of boric acid. The thickness of the lead layer is 100-190 mm. The water (~700 mm) serves as the anti-activation shield for the tank walls, the coiled pipe, and the structure of the self-propelled car. Before transportation, the tank is emptied.

A specific feature of the biological shield of TĚS-3 is the use of lead as the heavy component, which, in its pure form, does not acquire the long-lived induced γ -activity; this component was inserted directly in the tank of the biological shield without jacketing. Another characteristic of the shield is the use of a boric acid solution, which also reduces the activation of the materials in the shield and the structure of the self-propelled reactor car. The

TABLE 2. Compensating Ability ($\Delta k/k \cdot 10^3$) of the Control Elements

Control element	Material	t = 20°C		t = 280°C	
		experiment	calculation	experiment	calculation
Manual-control rod	B ₄ C	6 ± 0.16	5.35	12 ± 0.3	8.97
Automatic-control rod . . .	Boron steel (2% boron by weight)	1.51 ± 0.04	1.78	3.4 ± 0.08	3.05
Emergency rod	B ₄ C	5.7 ± 0.15	4.84	6.9 ± 0.18	5.72
"Soft" compensating system	Stainless steel	114 ± 2	90	—	—

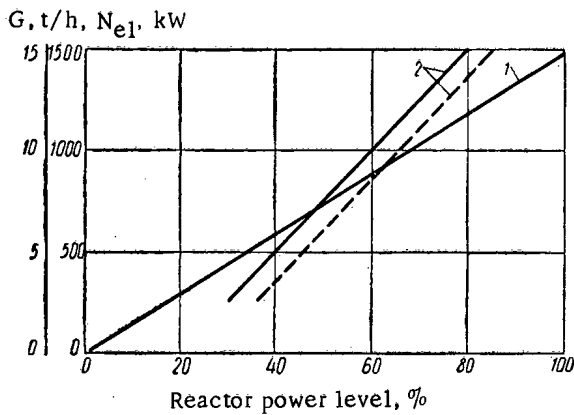


Fig. 4

Fig. 4. Dependence of the steam discharge G (1) and of the generator power N_{e1} (2) on the reactor power level. ———) Measurement; - - -) calculation.

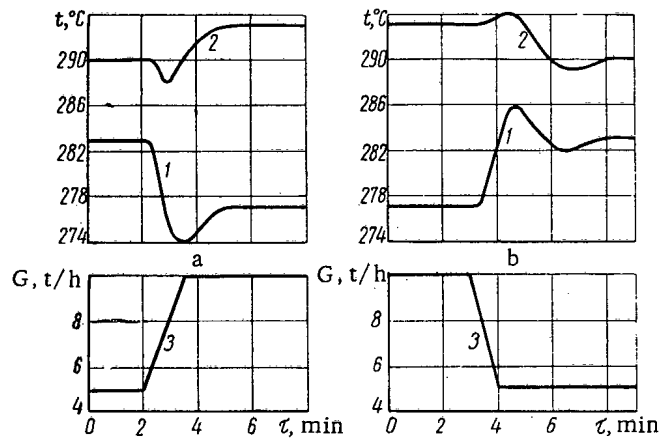


Fig. 5

Fig. 5. Reactor operation under self-control conditions (a and b—cases where the water supply discharge was increased and reduced by 5 t/h, respectively). 1) Water temperature at the upstream end of the reactor; 2) water temperature at the downstream end of the reactor; 3) water supply discharge.

TABLE 3. Radiation Level at the Lateral Surface of the Self-Propelled Reactor Car, $\mu R/sec$

Exposure time, days	Experiment	Calculation
0.1	30.2	33.2
0.5	6.92	10.4
1.0	3.02	4.36
10	0.195	0.338
20	0.087	0.279
30	0.055	0.187

effectiveness of the above measures for reducing the activation γ -radiation was confirmed during the operation of TЭС-3. The biological shield was calculated in the multigroup P_1 -approximation, where the neutron group with $E \geq 1.5$ MeV was assigned; the calculations were checked by measuring the neutron distributions in different shield variants for the critical assembly.

Table 3 provides the γ -radiation levels at the lateral surface of the self-propelled reactor car, measured at the initial period of TЭС-3 operation. Before the measurements were performed, the reactor was operating at a power level of 3000 kW for 20 days. The shield tank was filled with distilled water.

Operation of the Power Station

The purpose of the operation of TЭС-3 was a check of its operating ability under different conditions and an investigation of the problems arising in designing and operating plants of this type, which, in the final analysis, will make it possible to determine the advisability of utilizing low-power APS in the national economy of the country. Figure 4 provides data characterizing the operation of the station at various power levels. Figure 5 shows the results of one of the experiments on reactor self-control. Under conditions of self-contained operation, the power station is started up by means of a 150-kW starter generator, which is driven by the propulsion diesel of one of the self-propelled cars. The power station operates under different load conditions: at constant power and under conditions of

TABLE 4. Yield of Radiolytic Gases, norm. liter/h · m³ of Solution

Concentration of boric acid, % by weight	Reactor power level, MW			
	3.3		5.5	
	H ₂	O ₂	H ₂	O ₂
0.04	0.35	0.2	0.68	0.42
1.7	1.45	0.8	3.0	1.45
3.5	3.7	1.8	5.6	2.55

sudden changes in the turbogenerator load. Emergency shut-downs were simulated several times, in which case the TЭС-3 units and systems were first supplied from a storage battery and then from a diesel generator.

Water Conditions. Ammonia or hydrazine hydrate were added to the water in the first loop for binding dissolved oxygen and increasing the pH to its optimum value (9-10). Hydrazine hydrate proved to be much more effective. After it was introduced, the oxygen content in the first loop was equal to 0.005 mg/liter. Hydrazine hydrate was also used in the second loop, where it re-

duced the oxygen concentration in the feed water to 0.01-0.005 mg/liter. In order to control the corrosion of lead and steel in the biological shield tank, the pH value in the boric acid solution was maintained at a level of ~7 by means of ammonia. Table 4 provides data on the radiolysis of water in the biological shield tank for different concentrations of boric acid and different reactor power levels.

Conclusions

The construction and operation of the TЭС-3 plant have shown that the experiment of producing a large-unit mobile power station with a water-moderated water-cooled reactor was entirely successful. The prolonged operation of TЭС-3 confirmed the reliability, satisfactory controllability and convenient servicing of this type of power station.

At the same time, the operation of TЭС-3 has shown that further improvements are possible, in particular, a greater degree of automation, an increase in the run duration to two or three years, a switch to natural coolant circulation in reactor cooling, etc.

We should also mention the satisfactory agreement between the theoretical basic parameters of the power station and those actually obtained, which was largely due to the many experiments performed at the design stage.

PHYSICAL AND OPERATING CHARACTERISTICS OF THE SM-2 REACTOR*

S. M. Feinberg, N. A. Dollezhal', E. D. Vorob'ev,
 V. A. Tsykanov, I. Ya. Emel'yanov, V. M. Gryazev,
 A. S. Kochenov, Yu. M. Bulkin, V. I. Ageenkov,
 and P. G. Aver'yanov

Translated from *Atomnaya Énergiya*, Vol. 17, No. 6,
 pp. 452-463, December, 1964

INTRODUCTION

The SM-2 reactor was designed for extensive research in nuclear physics, solid state physics, metallurgy, radiochemistry, reactor construction physics and engineering, and in many other branches of science and engineering.

The core is a parallelepiped, $42 \times 42 \times 25$ cm in size, with a cavity measuring $14 \times 14 \times 25$ cm (neutron "trap"). The corners of the parallelepiped, measuring $7 \times 7 \times 25$ cm, are occupied by compensating rods. The core is made up of fuel element assemblies, $7 \times 7 \times 25$ cm in size, and is surrounded by a reflector made of beryllium oxide blocks with water interlayers. The fuel element assemblies contain 54 fuel element plates 0.8 mm thick which are separated by water-filled gaps 1.65 mm wide.

There are five horizontal, one sloping, and 18 vertical channels in the reactor for performing experiments. The physical features of the reactor and its basic parameters were discussed in [1]; the fundamental engineering decisions were discussed in [2]. The SM-2 reactor is the first intermediate research reactor with water moderator.

Construction of the reactor was completed in 1961. Physical startup of the reactor was achieved in October, 1961. From November, 1962, the reactor has been operating at nominal parameters. The maximum power reached by the reactor was 55 MW.

After a period of reactor operation at reduced power and particularly at planned parameters, an extensive program of scientific research work was carried out which dealt both with the study of the reactor itself and its separate units and also with the completion of a program of irradiation of various materials in the experimental channels.

In addition, operation of the reactor during the time mentioned allowed a study of the efficiency of its basic components.

The idea of building the SM-2 intermediate research reactor and the basic construction design came from S. M. Feinberg. He also directed the entire complex of operations involved in construction of the reactor. The design of reactor construction was carried out under the direction of N. A. Dollezhal' and Yu. M. Bulkin. Experimental studies in the initial stages of the project were made by E. D. Vorob'ev, V. B. Klimentov, and V. M. Gryazev. Several physical computations, consisting of a mathematical program of P_1 -approximation reactor calculations, were completed during this stage by I. K. Levin and N. Ya. Lyashchenko. During the second stage of the project, experimental studies of reactor physics were continued with the participation of V. A. Tsykanov and others. The immediate assistant to the scientific director of the project was V. A. Tsykanov who did much toward the development of the engineering plans for the reactor and who directed the construction and operation of the reactor in the later stages of the project. Construction of reactor control and protection systems was worked out under the direction of I. Ya. Emel'yanov. Starting with the second stage, the basic physical calculations were made by A. S. Kochenov. The fuel elements for the reactor core were developed in accordance with the suggestions and techniques of V. I. Ageenkov. N. G. Aver'yanov and other members of the operating staff played an important part in mastering the intricacies of operating the SM-2 reactor.

*Paper No. 320, presented by the USSR at the Third International Conference on the Peaceful Use of Atomic Energy, Geneva, 1964.

TABLE 1. Critical Masses for Various Core Configurations

Type of system	Channel conditions	Core configuration as shown in Fig. 1	Number of fuel element assemblies*	Reactivity, %		
				U ²³⁵ , kg	meas.	calc.
Beryllium oxide assemblies installed in central cavity	Channels open	a	13	8.6	0	—
Water in central cavity	Vertical channels closed with BeO plugs	b	20	13.2	0.5	1.8
	Lead plug in horizontal channel III. BeO plug in horizontal channel V					
The same	The same	c	20	13.2	0	1.1
" "	Channels open	d	21	13.9	0.7	0.8†
" "	" "	e	22	14.5	0.7	—
Beryllium inserts and water in central cavity	" "	f	18	11.9	1.0	—

*Reduction of the number of fuel element assemblies by one makes the system subcritical.
†Reactivity was computed for a system of 20 fuel element assemblies.

A large group of scientists, builders, engineers, and workers participated in the work of planning, construction, and operation of the SM-2 reactor; the authors wish to express their gratitude to all of them.

PHYSICAL CHARACTERISTICS OF THE REACTOR

The linear dimensions of the SM-2 reactor are commensurate with neutron migration length, but the core and reflector have a complex geometry. Therefore, reliance on physical calculations for reactor planning was risky, and the main consideration was given to experiments.

The first experiments have already been described [1]. Basically, the experiments were performed with a homogeneous core which contained construction materials in addition to uranium and moderator. Critical experiments performed with circular cores and water reflector were inadequate. Because of the lack of uranium in these experiments, one could not manage to introduce the required amount of construction materials into the core. Several critical experiments were performed with a uniform core and a beryllium oxide reflector which covered only a small portion of the lateral surface of the core.

On the basis of this clearly unsatisfactory information, it was expected that the critical loading for the SM-2 reactor would be 6.8-7.3 kg. Furthermore, the loss of reactivity because of the experimental channels was not taken into account. Subsequent experiments, in which the core and reflector of the SM-2 reactor were completely reproduced, showed that the critical loading was considerably greater.

Appropriate computing techniques were developed simultaneously with the experiments. It was determined that P_1 -approximation calculations [1] (with 12 energy groups) for the distribution of neutron flux throughout the core and "trap" agreed satisfactorily with experimental data. However, the magnitude of the critical loading was in satisfactory agreement with experimental values only in the case of one-dimensional core and reflector geometry. It was clear that a physical computation of some core configurations could only be made with a two-dimensional approximation.

A calculation of the neutron spectrum in the core indicated that the main absorption of neutrons (~90%) was below an energy of 10 eV. The age of the thermal neutrons is 35 cm², and the energy region from 10 to 0.1 eV contributes a total of 2 cm². Therefore, neutron leakage from the reactor is determined by the energy region above 10 eV.

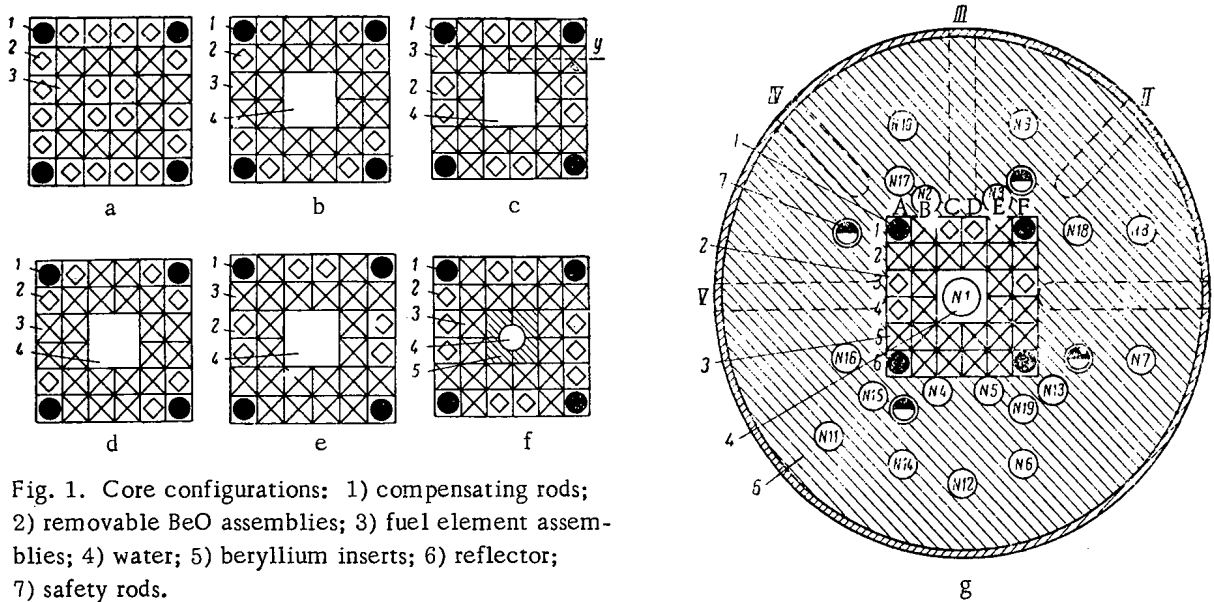


Fig. 1. Core configurations: 1) compensating rods; 2) removable BeO assemblies; 3) fuel element assemblies; 4) water; 5) beryllium inserts; 6) reflector; 7) safety rods.

In this connection, it is suitable to assume the following two-group model for neutron physics calculations: the fast neutrons are not absorbed but undergo considerable migration; only slow neutrons, whose migration is small, (with energies less than 10 eV) are absorbed.

To solve the reactor equations in the two-group, two-dimensional approximation, the mathematical program put forth in [3] was used. The SM-2 reactor calculations were carried out for both plane and cylindrical geometries. In the plane geometry case, neutron leakage in the vertical direction was taken into account by assuming that the group absorption cross sections Σ_i were

$$\Sigma_i = \Sigma_i^* + \kappa_i^2 D_i. \quad (1)$$

Here, Σ_i^* is the absorption cross section in an infinite medium for the i -th group; D_i is the diffusion coefficient for the i -th group; $\kappa_i^2 = \left(\frac{\pi}{H+2\delta}\right)^2$, where H is the height of the core; δ is the effective correction.

Neutron leakage through vertical gaseous channels was taken into account in the following manner: all macroscopic cross sections were assumed to be zero in the channel volume, and the diffusion coefficient

$$D_i = \frac{d_h}{3} + \frac{\lambda_{tr i}}{3}, \quad (2)$$

where d_h is the hydraulic diameter of the gaseous channel; $\lambda_{tr i}$ is the transport length for the i -th group in the region surrounding the channel.

The effect of the horizontal channels on reactivity was taken into account by means of experimental corrections.

For the cylindrical geometry, only the neutron flux distribution along the height of the reactor was computed. The effect of the experimental channels was not considered.

Using the two-group, two-dimensional approximation, calculations were made of the reactivity with different core configurations, of the control rod compensating capabilities, the reactivity changes with U^{235} burnup, and of the distribution of fast and slow neutron fluxes. The calculations were in satisfactory agreement with experiment.

1. Critical loading

Critical loading was investigated for various core configurations: with a central water-filled cavity, with beryllium inserts placed in the water-filled cavity, with a central cavity filled with beryllium oxide, etc.

The experiments were performed on a special test stand and directly in the reactor vessel. The critical state was achieved by gradually filling a previously assembled core with water. The results of several experiments to determine the critical mass of the reactor are given in Table 1.

TABLE 2. Compensating Rod Reactivities

Compensating rod	Reactivity, %			
	20 assemblies, Fig. 1e	measured 22 assemblies, Fig. 1e	23 assemblies, Fig. 1g	calculated 20 assemblies, Fig. 1c
I	1,11	0,81	0,81	1,15
II	1,13	1,53	1,82	1,15
III	1,11	1,35	1,25	1,15
IV	1,05	0,77	0,71	1,15

TABLE 3. Effect on Reactivity of Various Materials Located in the Peripheral Vertical Channels (see Fig. 1g)

Channel condition	Reactivity change, %	
	channels 2 and 3	channels 4 and 5
Gas replaced by water	-0,03	-0,08
Channel lining (steel pipe 69 mm in diameter, 3 mm wall)	+0,04	+0,18
BeO plug 62 mm in diameter	+0,1	+0,58
Closely packed bundle of nickel rods	-	+0,04
Loaded with 170 g of U ²³⁵	+0,23	-

TABLE 4. Effect of Reactivity of Various Materials Located in the Horizontal Channels

Channel condition	Reactivity change, %	
	closely packed bundle of nickel rods	channel directly adjoin- ing the core
BeO plug 62 mm in diameter and 300 mm long	+0,1	+0,43
Water plug 73 mm in diam- eter and 260 mm long	+0,04	+0,22
Plug of lead discs 72 mm in diameter and 8 mm thick with plastic spacers giving a total length of 262 mm	+0,1	+0,43

The critical mass for the actual construction with a water-filled cavity at the center and without experimental channels turned out to be 11 kg in contrast to the preliminary estimate of 6,8-7,3 kg mentioned above.

The experimental channels increased the critical mass to 13,5 kg. In order to reduce it, beryllium inserts were installed in the neutron trap. This lowered the critical mass to 8,6 kg without experimental channels, and to 11,2 kg with them.

A physical calculation of the two-group, two-dimensional type underestimated the value for the critical loading. However, the difference from the experimental values did not exceed 10%. Below are given values for the reactivity produced by replacing the beryllium oxide assemblies by fuel element assemblies for the core configuration shown in Fig. 1g:

Cell	A-2	A-5	B-1	B-5	B-6	C-2	C-5	C-4	F-4
Reactivity, %, . . .	0,67	1,05	0,56	1,13	1,08	1,05	1,57	1,29	1,22

As should be expected, it is clear from the results that the effect of fuel element assemblies on reactivity depends on core configuration, position of assembly insertion, and the presence of experimental channels nearby.

2. Reactivity Compensation

The compensating capabilities of the control rods were determined by means of reactor excursions. The reactivity was calculated by the "inhour" formula. On the basis of special calculations, the ratio β_{eff}/β was assumed to be 1,4 for a core containing 20 fuel element assemblies, and 1,3 for 28 fuel element assemblies.

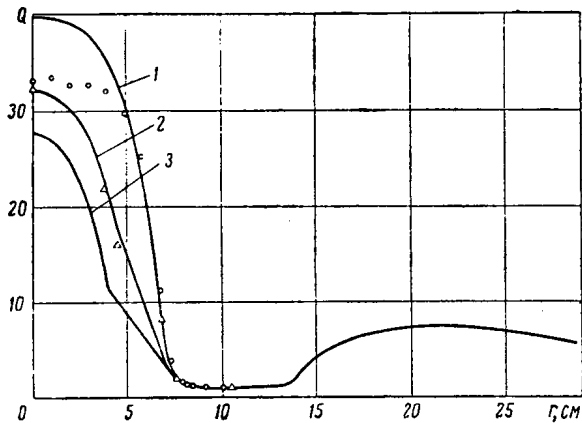


Fig. 2. Distribution of U^{235} fission density along a reactor radius (solid curves were calculated by the two-group, two-dimensional approximation; experimental values in the "trap" were increased 1.3 times): 3) water in trap; 2) 25 mm thick BeO plates in trap alongside core; 3) beryllium inserts in trap.

The reactivity of the compensating rods which were located in the corners of the core is given in Table 2 for three core configurations, from which it is evident that the reactivity of the four compensating rods was $\sim 4.5\%$ (interference between these rods was not observed). For normal operation of the reactor, this was insufficient. Therefore, to strengthen the control and protection system, four safety rods were located in the beryllium inserts installed in the neutron trap in addition to the four compensating rods. These rods consisted of a beryllium ejector and a water-filled cadmium tube (1 cm in diameter). While the reactor was running, the absorbing part of the safety rods was located above the core and consequently did not perturb the neutron flux. The compensating capability of a single rod was 1% . Because of interference, the reactivity of the four rods was 2.8% .

The four compensating rods which were positioned according to plans in the body of the reflector had little reactivity. Therefore they were removed from the reactor, and the channels thus released were used for experimental purposes.

The total reactivity of the compensating and safety rods was 6.6% with a core loading of 28 fuel element assemblies.

3. Effect of Experimental Channels on Reactivity

The effect of the experimental channels on reactivity was studied on a test stand. It was determined that loading the central channel (water-filled) with material having small absorption cross sections (aluminum, lead, beryllium oxide, beryllium) increased the reactivity. Beryllium and beryllium oxide had a strong effect in the increase in reactivity. For example, inserts of beryllium installed in the neutron trap between the central channel and the core increased reactivity by 5% . Six cylindrical slugs with 2% enrichment and a diameter of ~ 1 cm with a total U^{235} load of 18 g uniformly distributed over the cross section of the central channel increased the reactivity by $\sim 1\%$. Ten SM-2 fuel element plates installed with a 2.45 mm spacing increased the reactivity by $\sim 0.1\%$.

The effect on reactivity produced by various materials located in the peripheral horizontal and vertical channels is shown in Tables 3 and 4. Both tables refer to the core configuration shown in Fig. 1g. The outer peripheral channels have practically no effect on reactivity. The total loss of reactivity resulting from the presence of experimental channels in the external reflector amounts to $\sim 4\%$.

4. Space-Energy Neutron Distribution

Experimental studies of neutron spectra and of the spatial distribution of neutrons over the reactor volume have been carried out with miniature fission chambers containing U^{235} and with indium, uranium, and gold detectors. The diameter of the fission chambers was 1.4 mm, making it possible to make measurements in the gaps between fuel element plates. The precise displacement and location of a fission chamber was accomplished with the aid of a special measuring bridge. The U^{235} fission density in the experimental channels was measured with chambers of larger diameters (to 5 mm). Results for measurements of the quantity $Q = \int \Phi(u) \sigma_f^5(u) du$ are shown in Fig. 2.

Solution of the transport equation indicates that there is a considerable depression of the neutron flux in the fuel element. The ratio of the value in a water gap Q_w to the average value at the center of a fuel element \bar{Q}_d is ~ 1.3 . Since the ratio Q_t/\bar{Q}_d (where Q_t represents the maximum flux in the trap) enables one to relate the maximum thermal flux to the specific power of the reactor, the ratio Q_t/\bar{Q}_d , and not Q_t/Q_w , is of most interest.

Curves for the distribution of fission density, which was measured with U^{235} chambers, are given in Fig. 2. The points give experimental results in the neutron trap multiplied by 1.3.

Experiments indicated that the coefficient of variation for heat release throughout the core was ~ 3 .

¹As in Russian original text-Publisher.

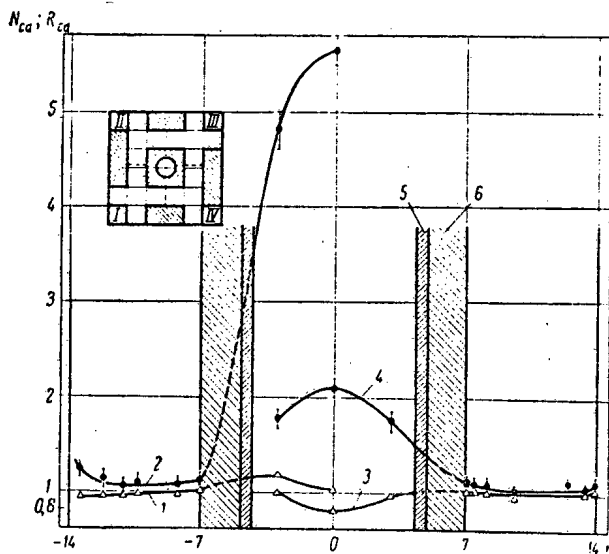


Fig. 3. Experimental distribution along a "radius" of the reactor for activation by neutrons above the cadmium cutoff (N_{Cd}) and for the cadmium ratio (R_{Cd}) in indium and gold: 1) N_{Cd}^{Au} ; 2) R_{Cd}^{Au} ; 3) N_{Cd}^{In} ; 4) R_{Cd}^{In} ; 5) wall of central channel; 6) beryllium.

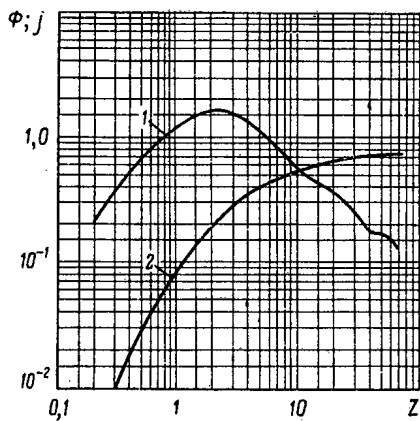


Fig. 4

Fig. 4. Energy dependence of neutron flux $\Phi(z)$ and of flux along the energy axis, $j(z)$: 1) $\Phi(z)$; 2) $j(z)$; $z = E/kT$, $T = 323^\circ K$.

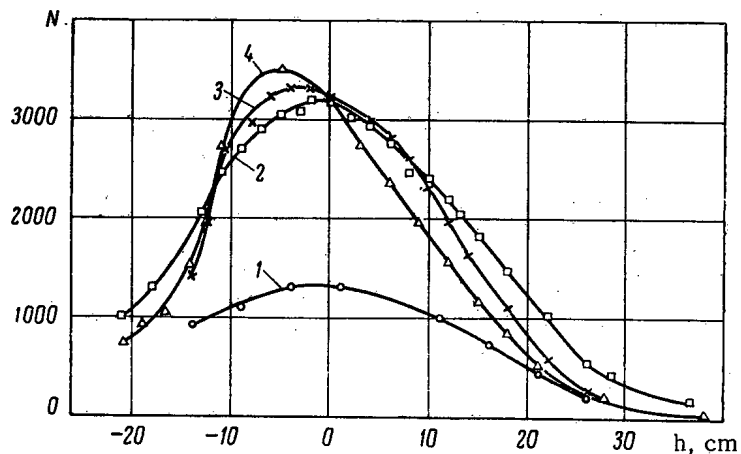


Fig. 5

Fig. 5. U^{235} fission density distribution along vertical channels: 1) channel 14; 2) channel 4; 3) channel 15 (nearby compensating rod withdrawn); 4) channel 15 (nearby compensating rod withdrawn approximately_halfway).

The radial distribution for density of activation by neutrons above the cadmium cutoff and for the cadmium ratio with indium and gold is shown in Fig. 3. Indium and gold foils 0.1 and 0.2 g/cm² thick, respectively, were used in the experiments.

The calculation of neutron fluxes was performed in various approximations. The space-energy distribution of the slowing down neutrons and the curves for fission density, which was measured with U^{235} chambers, were computed in the P_1 -approximation. The fission density curves were also calculated by the two-group, two-dimensional approximation.

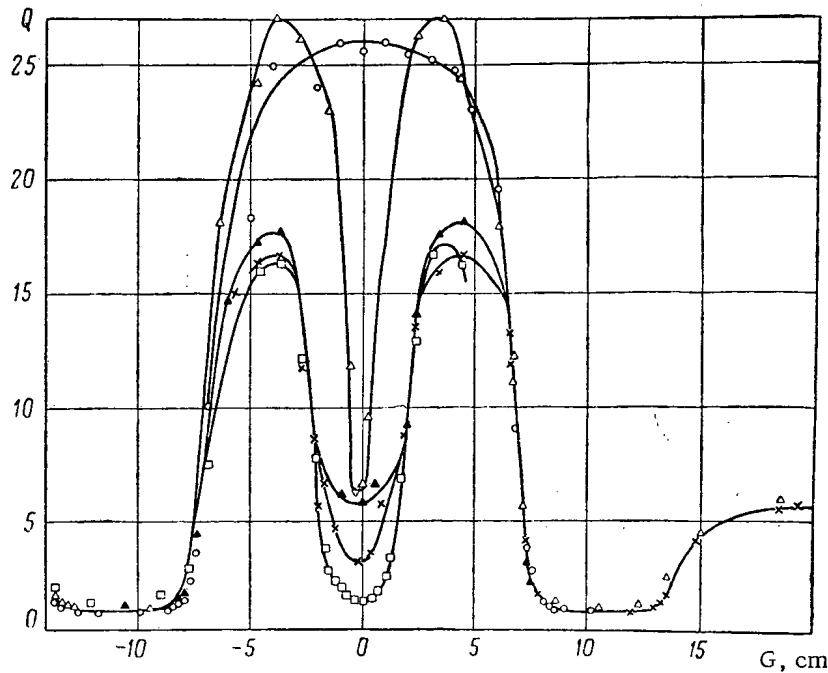


Fig. 6. U^{235} fission density distribution in the neutron trap with insertion of SM-2 fuel element plates: (O) no plates; (Δ) three plates, 2.45 mm spacing; (\blacktriangle) six plates, 7.35 mm spacing; (\times) eight plates, 4.9 mm spacing; (\square) 14 plates, 2.45 mm spacing.

The slow neutron spectrum was calculated for a homogeneous medium by means of the equation [4]

$$\Phi(z) = \frac{ze^{-z}}{1 + \frac{\gamma \sum_a}{\xi \sum_s}} \left[\int_0^z dz' \frac{\xi \sum_s z' e^{-z'} + \frac{d}{dz'} \left(\xi \sum_s z' e^{-z'} \right)}{\left(\xi \sum_s z' e^{-z'} \right)^2} \int_0^{z'} \sum_a(z'') \Phi(z'') dz'' + \text{const} \right], \quad (3)$$

where $z = E/kT$; T is the medium temperature; $\Sigma_s(z)$ is the macroscopic scattering cross section; $\Sigma_a(z)$ is the macroscopic absorption cross section; ξ is the mean logarithmic energy loss for neutron scattering by a free, stationary nucleus; γ is one half the ratio of the mean logarithmic squared energy loss to the mean logarithmic energy loss for scattering by a free, stationary nucleus.

Equation (3) was solved on an electronic computer assuming that $\xi \Sigma_s = \text{const}$ and $\gamma = 1$. The relation for the variation of absorption cross section as a function of energy was selected in accordance with the absorption cross section for U^{235} . The neutron spectrum was computed in the 0-2 eV energy range. At the same time, a computation was made of the slowing down flux along the energy axis, which is the fraction of neutrons absorbed below some given energy, i.e.,

$$j(E) = \frac{\int_0^E \sigma_c^5 \Phi dE'}{\int_0^\infty \sigma_c^5 \Phi dE'}. \quad (4)$$

The temperature of the medium was assumed to be 50°C. The energy dependence of the neutron flux $\Phi(z)$ and of the slowing down flux along the energy axis is shown in Fig. 4. The calculated cadmium ratio for U^{235} from capture was 2.44, and was 2.47 from fission. The experimental value for the cadmium ratio of U^{235} through fission varied in the range 1.5-2.1 for the center of the core.

TABLE 5. Steady-State Xe¹³⁵ Poisoning of the Reactor

Power, MW	Number of fuel element assemblies in the core	Average power, MW/liter;	Poisoning $\Delta k-k$, %.	
			measured	calculated
4,1	20	167	2,03	2,00
28,0	28	818	3,77	3,55
33,7	28	985	3,69	3,70

Measurements of the fission density distribution in the experimental channels were performed in the system shown in Fig. 1g. Vertical channels 2-7 and horizontal channels I-V were filled with air, and vertical channels 1, 8-11 and 13-15 were filled with water. The fission density distribution for U²³⁵ over height was measured in vertical channels 4, 12, 14, and 15. The results are given in Fig. 5.

Below is data on U²³⁵ fission density in the vertical channels at the level of the center of the core:

Channel number	1	4, 5, 15	2, 3, 13	12	14	6	9, 10	8	7	11
Relative fission density	1	0,11	0,067	0,057	0,045	0,034	0,030	0,027	0,017	0,013

During the measurements, all four compensating rods were inserted to the center of the core.

There is great interest in the neutron flux distribution in the central water-filled cavity when various amounts of fissionable material are placed in it. A series of measurements was made to determine this; the results are shown in Fig. 6. SM-2 fuel element plates were installed in a channel at various spacings. As can be seen from the curves, placing 14 fuel element plates at a spacing of 2.45 mm in the channel leads to a reduction in thermal neutron flux by a factor of approximately 20. The neutron spectrum in the vertical channels was measured by means of threshold detectors (Au, In, Mg, Ti, Fe, Al). The neutron spectrum for several channels is shown in Fig. 7.

5. Steady-State Xe¹³⁵ Poisoning of the Reactor

Data on the steady-state poisoning of the reactor by Xe¹³⁵ are given in Table 5. Poisoning was calculated by the formula

$$P = \frac{\frac{-\sigma_f}{\sigma_c}}{\lambda_2 + \int_0^{\infty} \sigma_{Xe} \Phi dE} \cdot \frac{(\gamma_1 + \gamma_2) \int_0^{\infty} \sigma_{Xe} \Phi dE}{\lambda_2 + \int_0^{\infty} \sigma_{Xe} \Phi dE}, \quad (5)$$

where $\gamma_1 + \gamma_2 = 0.064$ is the total yield per fission of iodine and xenon fission fragments; $\lambda_2 = 2.09 \times 10^{-5} \text{ sec}^{-1}$ is the Xe¹³⁵ decay constant.

Formula (5) embraces the following assumptions:

- 1) the nuclear density of Xe¹³⁵ is considered constant over the core and is equal to a certain value which is related to the average fission density;
- 2) the slow neutron importance is also constant over the core;
- 3) the slow neutron spectrum over the entire core is assumed the same as that within it.

In actuality, there is a spike in the neutron flux at the boundary of the core and this leads to the fact that the nuclear density of xenon at that location can be greatly different from the mean value. In addition, the importance and spectrum of slow neutrons at that position will be different from the corresponding quantities in the bulk of the core. Consideration of the boundary effects mentioned is taken into account by means of perturbation theory. Variations in reactivity because of reactor poisoning are computed by the formula

$$\frac{\Delta k}{k} = \theta P, \quad (6)$$

where θ is the fraction of neutrons absorbed in the uranium.

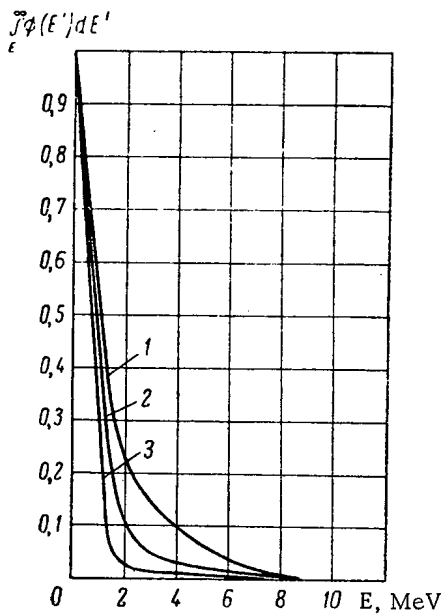


Fig. 7. Integral neutron spectrum measured with threshold detectors (E is neutron energy, MeV): 1) channel 4 spectrum; 2) channel 19 spectrum; 3) channel 6 spectrum.

increases when the water in the central channel is heated and the temperature of the water in the primary loop is maintained constant. Simultaneous heating of the water in the core and in the central cavity leads to an increase of reactivity up to $\sim 30^\circ\text{C}$, and a fall in reactivity with further heating. The results of these experiments are shown in Fig. 8.

8. Profiling Uranium Along Fuel Element Assembly

One of the most complicated problems which come up in reactors of the SM-2 type is the correct profiling of the uranium at the core boundaries.

Experiments performed with SM-2 fuel elements showed that they can operate with thermal loadings greater than 10^7 kcal/m² · h, which exceeds the maximum thermal loading in the reactor by a factor of two. Consequently, the main purpose of uranium profiling along the core is not the reduction of thermal loading but the increase of average burnup. Calculations indicate that, if the uranium loading in the fuel element assemblies is not profiled, the average uranium burnup in fuel element assemblies removed from the core will be $5k_z$ times less than attainable ($k_z = 1.3$ is the variability coefficient for energy deposition with height in the core). This means, for example, that if the attainable burnup is 35%, the average burnup will not exceed 6%.

The profiling assumed in the design (first plate containing $\frac{1}{3}$ uranium, the second $\frac{2}{3}$, the third and succeeding ones 1) made it possible to increase burnup by 1.7 times. This occurred because the first plate with a complete uranium loading was third from the inside boundary of the core where the neutron flux was less. Plates with lower uranium content, i.e., with greater possible burnup, were located in high flux regions. During operation of the reactor, a new profile (0.25; 0.4; 0.6; 0.8; 1.0) was introduced which made it possible to raise the average burnup by a factor of 2.5 in comparison with unprofiled fuel element assemblies.

All the data presented on burnup refers to a core without beryllium inserts. Placing beryllium inserts in the neutron trap somewhat reduces the neutron flux at the internal boundary, and increase the average burnup by 1.3 times.

Thus, the measures taken made it possible to bring the average burnup toward the achievable value by a factor greater than three. However, the gap between average and attainable burnup is still large and is ~ 2 .

It is clear from Table 5 that the measured reactivity poisoning at a power of 28 MW is greater than that at 33.7 MW. This contradiction points out the deficiencies in the experimental methods for measuring reactivity, and indicates the error of measurement is not less than 0.25%.

At a power of 50 MW, the Xe¹³⁵ poisoning is close to the maximum and leads to $\Delta k/k \approx 4\%$.

6. Uranium Burnup and Fuel Assembly Replacement

The loss of reactivity during reactor operation is $2.2 \cdot 10^{-4}\%$ per MW · h. A calculation of the variation in reactivity by the two-group, two-dimensional approximation assuming uniform uranium burnup within the confines of an individual fuel element assembly gives a value of $(1.7-2.3) \cdot 10^{-4}\%/MW \cdot h$. With this same approximation, replacement by fresh assemblies of four fuel element assemblies in the inside row of the core having 12.5% uniform burnup increases the reactivity by 1.3%, but the same replacement in the outside row increases the reactivity by 1%. With 25% burnup, these values are 2.8 and 2%, respectively.

7. Effect of Temperature on Reactivity

Experiments to determine the effect of temperature on reactivity have shown that reactivity monotonically falls with heating of the water in the primary loop while the temperature of the water in the central channel is held constant. On the other hand, reactivity

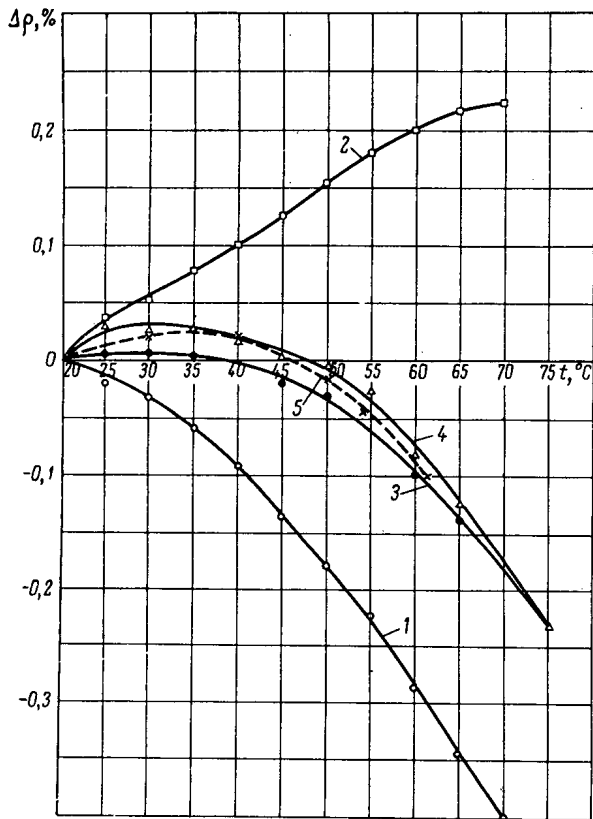


Fig. 8. Effect of temperature on reactivity ($\Delta\rho$ is the change in reactivity, t is water temperature): 1) main loop water heated; 2) channel 1 water heated; 3) simultaneous heating of main loop and channel 1 water; 4) simultaneous cooling of main loop and channel 1 water; 5) simultaneous heating of main loop and channel 1 water with small volume of free gas in main loop.

OPERATING CHARACTERISTICS

1. Reactor Fuel Elements

By design, the fuel elements of the reactor should operate at a thermal loading of $(5-6) \cdot 10^6$ kcal/m² · h. The achievement of that thermal loading and the dense packing of fuel element plates in the reactor core (fuel element thickness 0.8 mm, water gap width 1.6 mm) made it possible to obtain high specific core loading ($\bar{q} = 1600-1700$ kW per liter, $q_{\max} = 4500$ kW/liter). Although thermal engineering calculations revealed the possibility of operating fuel elements at such high thermal loadings, there were widespread misgivings as to whether they could actually be achieved. In addition, it was necessary to check the attainable U^{235} burnup.

Only experiment could furnish answers to these questions. Therefore, before bringing the reactor up to nominal power, a fuel element test was performed in channel 1 with a thermal loading of $6 \cdot 10^6$ kcal/m² · h up to a maximum U^{235} burnup of 28%. In all, six fuel element plates were tested in this experiment. With reactor operation at nominal power, a thermal loading of $6 \cdot 10^6$ kcal/m² · h was achieved simultaneously in a large number of fuel elements, and the maximum U^{235} burnup in the reactor core reached values of 35% and higher in individual fuel elements.

After a period of operation, two fuel element assemblies were removed from the core (because of suspected loss of integrity) with a 2-3% U^{235} burnup which pointed to manufacturing deficiencies.

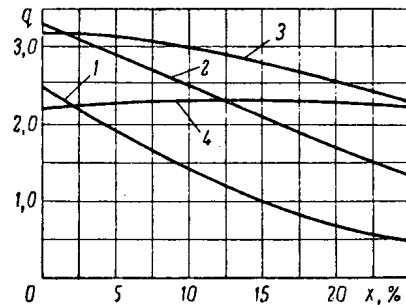


Fig. 9. Variation in thermal loading at fuel element surface as a function of average U^{235} burnup in the fuel element assembly (without beryllium inserts): q is the ratio of thermal loading in a given fuel element to the average thermal loading in the fuel element assembly; x is the average U^{235} burnup; 1, 2, 3, 4 are, respectively, the boundary, second, third, and fourth plates.

Profiling the uranium in a fuel element assembly increases the critical loading. However, the loading increases more slowly than the average burnup. For example, the design profile increased the critical loading by $\sim 5\%$, and the new profile by $\sim 10\%$. From the point of view of uranium consumption, profiling is practical.

With uranium burnup, the maximum thermal loading, gradually decreasing in magnitude, shifts toward the bulk of the core. Thus the problem of correct profiling requires time analysis of the burnup process at the edge of the core. This problem has not yet been completely solved. The redistribution of thermal loading in fuel elements at the edge of the core for the design type of profiling is shown in Fig. 9.

In order to determine the possible increase in thermal loading on the fuel element plates, tests were made on U^{235} burnup at thermal loadings of $(10-11) \cdot 10^6$ kcal/m² · h. The maximum burnup achieved in these experiments was 30%. The results of the tests showed that the thermal loading at the surface of a fuel element be increased by a factor of two over the design value, and only because of this may higher neutron fluxes be attained with the reactor.

Thus the operating experience with the reactor and the experiments that have been performed have indicated the capabilities of fuel element plates at high thermal loading in an intermediate reactor.

2. Control and Protection Systems

After the installation of additional rods during startup and adjustment operation, the control and protection system of the reactor proved to be capable of assuring the required excess reactivity consideration of the overcharging with fuel element assemblies to take care of U^{235} burnup. During reactor operation, the protective system assured safety; the number of spurious responses was small, and there were no serious failures in the electronic equipment or in the electrical circuits of the protective, power measuring, and automatic control systems. Preventive inspection and regular maintenance assured continuing operability of the systems.

The sealed drives of the compensating rods, located on the lid of the reactor, never got out of order during the entire operating period after the introduction of several improvements in the startup period. During operation, a minimum of preventive measures was taken including periodic measurements of the insulation resistance of the windings and a check on the adjustment of the control units.

Hydraulic drives were installed for the four safety rods located in the neutron trap. They operated well and, during operation, required only periodic adjustment of the indicator system.

3. Some Information About the Stability of Specific Parts of the Reactor

The stability of materials becomes an acute problem in a reactor with high neutron flux. Therefore the construction of such a reactor must provide for maximum interchangeability of parts.

In working out the plans for the SM-2, the question of the selection of reflector material was discussed many times and at great length. However, the experimental data on irradiation with high total neutron fluxes which was needed for the final decision was lacking. It was decided to use beryllium oxide as the first type of reflector material. During operation of the reactor, observations were made on samples taken from the removable assemblies and from the shafts of the compensating rods for the purpose of checking on the condition of the beryllium oxide. The samples removed had been irradiated by a fast neutron flux ($E \geq 1$ MeV); the total flux seen by the samples was $10^{20}-10^{22}$ n/cm². The data indicated that a total flux of 10^{22} n/cm² was a maximum for beryllium oxide.

At the present time, because of this, the removable beryllium oxide assemblies have been replaced by metallic beryllium assemblies. The effect of the fast neutron flux on a beryllium oxide layer in the fixed reflector is less, and the construction of the reflector provides for measures preventing the breakdown of the beryllium oxide blocks.

Another very important part of the reactor, which operates under difficult conditions, is the lining of the horizontal channels passing through the lateral reflector at the edge of the core. The lining header is irradiated by a fast neutron flux of $5 \cdot 10^{14}$ n/cm² · sec and by γ radiation from the core. In addition, it is subject to an external pressure of 50 kg/cm². Lengthy operation of channel lining leads to considerable radiation damage of the material in the walls. The latter can be held to acceptable values by replacing the channel lining from time to time. The capability for replacement is provided for in the construction.

4. Operation of Technical Equipment

During the reactor operating period, all the basic equipment in the cooling loops and in the auxiliary systems operated normally. Pumps in the primary and secondary cooling loops, heat exchangers, and a cooling tower insured removal of reactor heat at any time of the year. The technical equipment of the experimental cooling loops also operated flawlessly.

CONCLUSION

Operating experience with the SM-2 reactor verified the correctness of the basic physical and engineering ideas incorporated in the design:

1. A thermal neutron flux in the trap of about $2.5 \cdot 10^{15}$ n/cm² · sec was achieved at a power of 50 MW.
2. The flux of fast neutrons in the core with energies above 1 MeV exceeded 10^{15} n/cm² · sec.
3. A maximum thermal loading in the core of $4.5 \cdot 10^3$ kW/liter was achieved with a coefficient of variability in the core equal to ~3.
4. The fuel elements proved completely efficient at a record thermal loading of $6 \cdot 10^6$ kcal/m² · h, and, as experiment has shown, this loading can be doubled. Furthermore, the attainable burnup exceeds 35%.
5. The main engineering units of the reactor—the cooling system, the recharging system, the control and protection system, etc.—proved to be completely effective.

At the present time, plans are being developed for an increase in reactor power. The reactor vessel, the main loop, the auxiliary systems and facilities will remain unchanged. The reactor power is being increased from 50 MW to 100 MW. The core will be built with fuel elements manufactured in accordance with previously developed and tested technology. The height of the core is being increased to 40-50 cm. The beryllium oxide in the reflector will be replaced by metallic beryllium, the reflector being made up of individual, interchangeable blocks. Water-filled cavities will provide for an increase in thermal neutron flux in the immediate vicinity of the horizontal channels.

The increase in power of the SM-2 reactor permits:

- 1) an increase in thermal neutron flux in the trap to $(5-8) \cdot 10^{15}$ n/cm² · sec (depending on the number of samples which are irradiated in the core), and an increase in fast neutron flux (energies greater than 1 MeV to $2 \cdot 10^{15}$ n/cm² · sec;
- 2) sample irradiation in the "hard" spectrum of the core;
- 3) an increase in average U²³⁵ burnup.

LITERATURE CITED

1. S. M. Feinberg et al., In Reports of the Second International Conference on the Peaceful Use of Atomic Energy [in Russian], Dokl. sov. uchenykh, Atomizdat, 2, Moscow (1959), p. 334.
2. S. M. Feinberg et al., Atomnaya énergiya, 8, 493 (1960).
3. Ya. V. Shevelev and V. K. Saul'ev, Atomnaya énergiya, 14, 200 (1963).
4. N. I. Laletin, Atomnaya énergiya, 14, 458 (1963).

THE PGR PULSED GRAPHITE REACTOR*

I. V. Kurchatov,† S. M. Feinberg, N. A. Dollezhal',
 P. I. Aleshchenkov, F. S. Drozdov, I. Ya. Emel'yanov,
 A. D. Zhirnov, M. A. Kazachenko, G. D. Knyazeva,
 F. V. Kondrat'ev, V. D. Lavrenikov, N. G. Morgunov,
 B. V. Petunin, V. P. Smirnov, V. M. Talyzin,
 A. G. Filippov, I. L. Chikhladze, P. M. Chulkov,
 and Ya. V. Shevelev

Translated from *Atomnaya Énergiya*, Vol. 17, No. 6,
 pp. 463-474, December, 1964

INTRODUCTION

For investigating processes taking place in various substances irradiated by neutrons and γ rays a variety of demands may be imposed on the radiation source. For example, it is possible that intense irradiation over a short period may be required. Reactors with a small neutron lifetime are used for this, for example of the Godiva type. In other experiments it may be necessary to maintain a high neutron flux for a longer period. Pulsed reactors with high integrated neutron fluxes are necessary here. The pulsed graphite reactor (PGR) belongs to this type of reactor, whose construction was reported at the Second International Conference on the Peaceful Uses of Atomic Energy by S. M. Feinberg [1].

The integral neutron density per pulse, if no heat is given out, is calculated by the formula

$$\int n dt = \frac{i}{\Sigma v E_f} \cdot \frac{v_f}{v} \cdot \frac{1-\theta}{\theta},$$

where i is the energy which is available for absorption per 1 mole of moderator; Σ is the absorption cross section for neutrons with a velocity v by a mole of moderator, E_f is the energy release accompanying fission; θ is the absorption probability of a neutron in the fuel (uranium); v/v_f is the probability that a neutron absorbed in the fuel will cause fission. The table shows that graphite is the best material for a pulsed reactor with a large integrated flux per pulse, since it has a favorable ratio of the energy received, i , to the neutron absorption cross section.

For $(1-\theta)/\theta = 1.0$ (a very large reactor with a charge of ~ 100 kg uranium) the integrated thermal neutron flux may be of order $\int n \bar{v} dt \approx 2.2 \cdot 10^{18} \text{ cm}^{-2}$ (the average neutron velocity $\bar{v} = \int v di / \int di$ is $5.16 \cdot 10^5 \text{ cm/sec}$). In order to reduce the critical loading of the reactor it is necessary to increase the concentration of uranium in the graphite. Thus, for $(1-\theta)/\theta = 0.07$, the charge is ~ 7 kg but the integrated flux is reduced by a factor of 14. If the average temperature of the graphite is reduced to 1500°C (assuming nonuniformity of heating), the average integrated flux throughout the reactor still falls by a factor of 2.5, i.e., to a value of $0.6 \cdot 10^{17} \text{ cm}^{-2}$. These are precisely the characteristic parameters of the PGR reactor: the reactor for producing short-duration but extremely intense beams of neutrons and γ rays for irradiating samples. In constructing the reactor there arose problems in the study of its dynamics as a result of large reactivities and also in controlling the neutron flux according to a specified time law. A study of the behavior of the reactor structure with a core of graphite blocks and homogeneously-distributed nuclear fuel at high temperatures is of considerable interest and so also is an investigation of the safety of homogeneous uranium-graphite reactors as a result of the rapid injection of large reactivities.

The reactors has already operated without trouble for several years. The scientific supervisors of the project were I. V. Kurchatov and S. M. Feinberg. N. A. Dollezhal' and I. Ya. Emel'yanov supervised the engineering part

* Report No. 322a, presented by the USSR at the Third International Conference on the Peaceful Uses of Atomic Energy, Geneva, 1964.

† Deceased.

Comparison of Moderator-Diluents for Uranium According to the Magnitude of the Attainable Integrated Neutron Density per Pulse

Moderator	Permissible temperature T, °C	i, J/mole	Σ , cm ² /mole	$\int ndt$ for $\theta = 0.5$, cm ⁻³ ·sec
C	2700 (stability lost)	$6 \cdot 10^4$	$2.4 \cdot 10^{-3}$	$4.2 \cdot 10^{12}$
BeO	1300 (stability lost)	$5.9 \cdot 10^4$	$6.0 \cdot 10^{-3}$	$1.0 \cdot 10^{12}$
D ₂ O	300 (uranium separates out in residues)	$2.7 \cdot 10^4$	$6.0 \cdot 10^{-4}$	$7.6 \cdot 10^{12}$

of the project. On the basis of the planning and adjustment of the control equipment, investigations into the dynamics of pulsed reactors were initiated and were carried out by Ya. V. Shevelev, who was also responsible for developing the methods of assessing the PGR reactor.

The principal physical characteristics of the PGR reactor are presented below:

Principal Physical Characteristics of PGR

Core	Graphite, impregnated with uranium (90% U ²³⁵); dimensions 1400 × 1400 × 1400 mm; moving section 800 × 800 × 1400 mm; size of block 100 × 100 × 200 mm
Reflector	Graphite; thickness everywhere not less than 50 cm; dimensions of stack 2400 × 2400 × 4200 mm
Nuclear ratio U/C	1 : 10,000
U ²³⁵ charge, kg	7.46
Excess reactivity	$(22 \pm 2) \cdot 10^{-2}$
Effective delayed neutron fraction	0.00685
Prompt neutron lifetime, sec.	$(1.07 \pm 0.03) \cdot 10^{-3}$
Integral neutron flux with complete withdrawal of rods, cm ⁻²	$1.1 \cdot 10^{17}$
Maximum possible neutron flux in the burst regime, cm ⁻² ·sec ⁻¹	$1 \cdot 10^{18}$

Operating Regime

The PGR reactor is designed for operating in two regimes: the self-quenching burst regime and the controlled regime with a duration of several seconds or more. In order to achieve the regime of the first type, a reactivity is injected into the reactor which exceeds the delayed neutron fraction. The rate of reactivity injection must be such that after completion of motion of the trigger element several periods of excursion should elapse before the power attains the vital magnitude and leads to heating up of the core. If this condition is observed, then it can be assumed that the reactivity is being injected instantaneously and stepwise. The reactivity step $r_0 = k_e - 1/\beta_{eff}k_e$ determines the initial period of the excursion, the amplitude and shape of the burst. The burst is self-quenching as a consequence of the core heating up, since the reactor has a negative temperature coefficient of reactivity. As a result of this the reactor is found to be subcritical at a value close to r_0 . The precise final state of the reactor is described by the equation

$$\int_0^{\vartheta_{\infty}} r(\vartheta) d\vartheta = 0,$$

where $r(\vartheta)$ is the relationship between the reactivity and the accumulated heat $\vartheta = \int_0^t Q dt$, $\vartheta_\infty = \int_0^\infty Q dt$,

Q is the power. A considerable fraction of the heating occurs in the slow stage of the process when the reactivity is negative and the power is small. Forced quenching of the burst by rods reduces additional useless heating up of the reactor.

The controlled regime also begins with a self-quenched burst, but at the instant of its peak the units which compensate the drop in reactivity (the compensating rods) commence to move. The movement of the rods is programmed so that in the operative section of the pulse $0 \leq t \leq t_p$, the power is governed by a specified law $Q = Q_p(t)$ (for example, it has remained constant). In future the following nomenclature will be used for analyzing the controlled operating regime: λ_i are the decay constants of the nuclei of the sources of delayed neutrons; $l^* = 1/\beta_{\text{eff}}$ is the prompt neutron lifetime related to β_{eff} ; $\gamma(t) = \partial r / \partial \vartheta$ is the reactivity coefficient with respect to the accumulated heat; $\Delta r_p = |\int \gamma d\vartheta|$ is the magnitude of the reactivity compensated in the operative section;

$$\gamma_p = - \frac{\Delta r_p}{\int_{t=0}^{t=t_p} d\vartheta}$$

is the average value of γ in the operative section, $\alpha(t) = \Delta r_p \frac{\gamma}{\gamma_p} \cdot \frac{l^*}{t_p}$, $\bar{\lambda} = \sum_i \frac{\beta_i}{\beta} \lambda_i$, $\bar{\tau} = \sum_i \frac{\beta_i}{\beta} \lambda_i^{-1}$, $\varepsilon = \lambda \bar{l}^*$.

The actual reactor characteristics of PGR are used as an illustration.

The change of reactivity r_p in the constant power operating regime, $Q_p = \text{const}$, is described approximately by the function

$$\psi(t) = 1 - r_p(t) = \sum_i \frac{\beta_i}{\beta} (1 - e^{-\lambda_i t}).$$

This function varies from zero for $t=0$ to unity for large values of t . For $\psi < \psi_{\text{cr}} = \varepsilon^2 / (\alpha - \varepsilon)$ [$\varepsilon \approx 0.064$; $\alpha(0) = \alpha_i \approx 7 \text{ sec} / t_p$] the reactor is unstable (the formula is correct when $\alpha \geq 3\varepsilon$). But at the instant of the burst peak there is, in fact, already a certain number of delayed neutrons; $\psi_i = 2\varepsilon / (t_0 - 1)$. Since $\psi_i > \psi_{\text{cr}}$, the reactor is stable right from the beginning, i.e., perturbations lead to finite deviations of the power from Q_p . However, these deviations at small values of t_p (large values of α) bear the nature of weakly-damped oscillations which are continued so long as $\psi < 2\sqrt{\alpha}$. For $\psi > 2\sqrt{\alpha}$ an aperiodic regime is obtained. For prolonged regimes the aperiodicity begins immediately. To an accuracy of up to 10%

$$\frac{\delta Q_{\text{max}}}{Q_p} = \frac{\delta r}{\psi + \sqrt{\alpha}},$$

where δr is the stepwise change of reactivity. For identical values of $\delta r = 0.1$ at the beginning and end of the operative section of the regime with a duration of 30 sec we obtain $\delta Q_{\text{max}} / Q_p = 0.18$ and $\delta Q_{\text{max}} / Q_p = 0.12$, respectively.

The product $Q_p t_p$ in an uncooled reactor is limited by the maximum permissible temperature and therefore any excessive heating is harmful: it leads to a reduction of t_p at the time of emergence into the operative section and on completion at the time when the power falls to zero.

The loss of operating time, associated with heating as a result of arrival at the operating section is equal to

$$\frac{\delta t_i}{t_p} = \frac{\delta r_{\text{max}}}{\Delta r_p} \cdot \frac{\gamma_p}{\gamma_i},$$

where δr_{comp} is the reactivity compensated at the instant of commencement of movement of the rods ($\delta r_{\text{comp}} \approx t_0 - 1$); γ_i is the initial value of γ .

For a regime with a duration of 5 sec ($t_0 = 3.5$) $\delta t_i / t_p = 0.057$. The loss of operating time at the end of the process is considerable if forced quenching is not effected:

$$\frac{\delta t_f}{t_p} = \sqrt{\frac{\gamma_p}{\gamma_f} \cdot \frac{2}{\Delta r_p \lambda_{\text{eff}} t_p}},$$

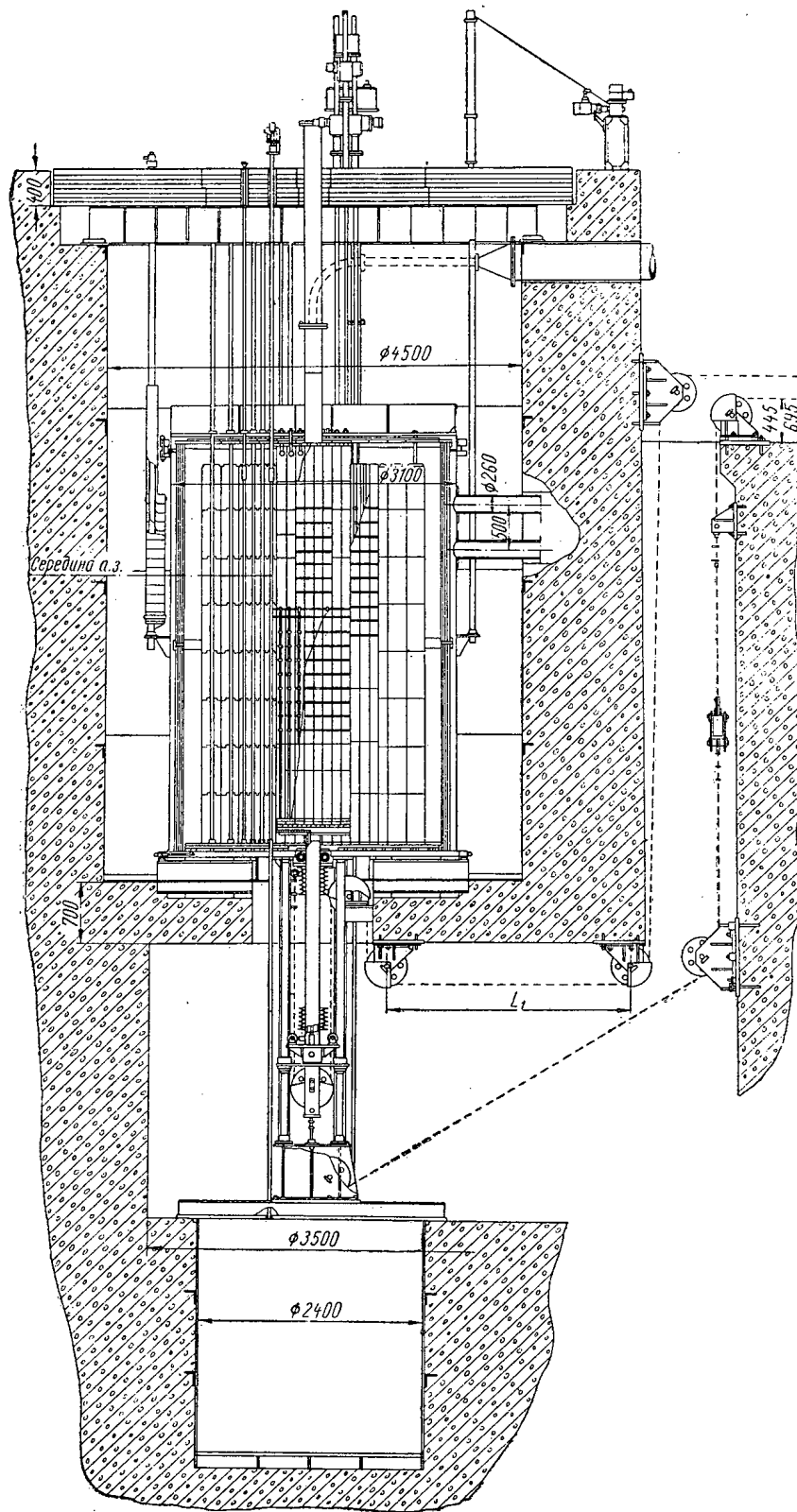


Fig. 1. Vertical section through the PGR reactor.

where λ_{eff} is the effective decay constant of the delayed neutron sources, combined into a single group. For $t_p = 5$ sec and $\lambda_{\text{eff}} \approx \lambda$, $\delta t_f = 0.35t_p$. Numerical calculation gives

$$\delta t_f = 0.3t_p.$$

Forced quenching, if it occurs after a time which is small in comparison with $0.3t_p$, can be considered as an instantaneous reduction of reactivity. It reduces very sharply the additional heating. If it be assumed that subcriticality of the hot reactor with the rods inserted is equal to Δr_p , then as a result of the instantaneous reinsertion of the shim rods

$$\frac{\delta t_f}{t_p} = \frac{\tau_{\text{eff}}}{\Delta r_p t_p}, \quad \tau_{\text{eff}} = \sum \frac{\beta_i}{\beta} \cdot \frac{1 - e^{-\lambda_i t_p}}{\lambda_i}.$$

In a regime with a duration of 5 sec we obtain $\delta t_f = 0.03t_p$. As a result of reinsertion of the rods after a time of order t_p , numerical calculation gives $\delta t_f = 0.015t_p$. In fact, quenching by the rods reduces significantly the reactivity and $\delta t_f \approx 0.1t_p$.

Reactor Construction

The PGR stack consists of a number of graphite columns. Its dimensions are $2400 \times 2400 \times 4500$ mm and it is enclosed in a cylindrical steel hull with a diameter of 3100 mm and a height of 4500 mm (Fig. 1). The columns of the core are constructed of uranium-impregnated graphite blocks with dimensions $100 \times 100 \times 150$ mm. The blocks are suspended on flexible graphite (cold) rods. The blocks, located one above the other, are not in contact with each other which allows them freely to expand and prevents their jumping as a result of rapid heating. The columns are mounted on the metal bearings of the lower reactor plates; there are gaps of 4 mm between columns. The upper and lower sections of the columns consist of blocks which are not uranium-impregnated and which form the top and bottom sections of the reflector; there is also thermal insulation between the hot core and the bearing structures. The central sections of the columns comprise the core with dimensions of $1400 \times 1400 \times 1400$ mm. The side reflector is constructed of graphite blocks, $200 \times 200 \times 600$ mm. The central columns are mounted on fixed metal stages and they form the fixed part of the core with a cross section of 800×800 mm. The stage is mounted on a vertical hollow steel column which is connected with the bottom of the casing by a rubber bellows. When the moving section of the core is lowered, it enters the cavity of the lower reflector and is then surrounded by columns containing boron absorber. The upper ends of the moving section columns are fastened to each other by graphite retainers. The corner columns of the moving section and the adjacent columns of the fixed section consist of blocks which are not uranium-impregnated. The gap between the moving and the fixed sections is 8 mm.

Above the moving section of the stack is located an additional suspended reflector formed by $100 \times 100 \times 500$ mm blocks and suspended by metal rods which are welded to the cap of the casing. In the reactor stack there is a vertical central experimental channel with a cross section of 200×200 mm. Nineteen channels with a diameter of 15 and 32 mm in the core and in the reflector serve for distributing thermocouples and also for a remotely-controlled neutron source. Thirteen cold columns of the fixed section of the core have channels with a diameter of 65 mm for inserting rods. The operative section of the rods is constructed of five flexibly-coupled graphite tubes with diameter 55 mm, filled with tablets of a graphite and gadolinium oxide mixture. The diameter of the absorbing section of a rod is 40 mm, with a gadolinium content of 0.02 g/cm^3 .

Thus, in the core of PGR there are no metallic structures and therefore the reactor heating is limited only by the thermal stability of the graphite.

Because of the high design temperature of the core, particular attention has been paid to the uniformity of distribution of the uranium in the graphite and to its identical content in the blocks. A special impregnation method has been developed for introducing the uranium into the graphite, which is distinguished by its simplicity in technical equipment. The impregnation was carried out in vacuo. The method of depositing the uranium within the blocks permitted simple drying operations at 105°C and subsequent calcining in air at a temperature of 400°C to be carried out without danger of redistribution of the uranium in the blocks. The impregnated blocks were divided into groups: a solution of specified concentration was used according to the graphite density. The average density of the core graphite was 1.71 g/cm^3 and 1.60 g/cm^3 for the reflector. The concentration of uranium, enriched to 90% in the isotope U^{235} , was 3 g/kg in the graphite. The average ratio of the number of uranium nuclei to the number of carbon nuclei per unit volume of the core is 1:10,000; the average density of the core is 1.43 g/cm^3 . Uniformity of distribution of the uranium in the graphite was controlled by the transmission of the block to a narrow beam of

cold neutrons at several points and in two perpendicular directions. The uranium content of the blocks was determined by the count of fast neutrons from the block located in the thermal column of a reactor. In assembling the core, blocks with a high uranium concentration were arranged in the less hot sections—at the periphery.

All metallic structures of the reactor are shielded from the effect of high temperatures by thermal screens. The outer side surface and the upper part of the reactor vessel are "washed" with water. Vertical tubes pass through the water in which counters and ionization chambers can be arranged. The lateral shield of concrete is lined inside with metal. A layer of water above the cover of the counter (about 1 mm thick) and a steel dismountable metal structure with a total thickness of about 400 mm (the stage of the biological shield) form the upper shield. On the staging are arranged the servos for the reactor control system. Vertical steel tubes for insertion of control rods are installed from the cover and the bottom of the casing and corresponding with channels in the graphite stack. The upper tubes pass through the stage of the biological shield and terminate in flanges for mounting the control rod motors in vacuum-tight containers. The lower tubes lead into a bunker situated below the reactor hull. The design of the reactor provides for substitution of eight of the graphite rods by light rods of thin stainless steel and cadmium. In this case, in place of the electric motors, membrane pneumatic equipment is installed which enables the rods to be removed from the core in 0.05 sec; the bunker serves as a storage site for the spent rods.

The reactor vessel and the bunker connected to it by the tubes are filled with helium; the ampoule in which the samples undergoing test are located, and which is cooled by water, is located in the central experimental channel. The PGR reactor has no special cooling system for the core. Its technological circuit includes in its gas-tight loop, three water cooling loops (the assembly hull, the stage of the moving section of the stack and the ampoule in the central experimental channel) and other auxiliary circuits. The ampoule cooling circuit consists of a heat exchanger, three vortex pumps and two centrifugal-vortex pumps operating from independent power supplies. The centrifugal-vortex pumps are included for suppressing the gas phase of radiolysis products. In the circuit at the exit from the ampoule is installed a shuttle valve, which directs the water into a settling tank during the time of operation of the reactor and into the heat exchanger after shutdown. Makeup of the circuit for water-cooling the ampoule is effected through a system of filters. In order to remove corrosion products, a loop is installed in the heat exchanger bypass for chemical purification of the water.

There is a special remotely-controlled device in the PGR reactor, designed for the withdrawal and transportation of the experimental samples into the hot laboratory.

Special Assembly Features of the Reactor Stack

Particular attention has been paid, in assembling the PGR reactor stack, to the question of operating safety, as a consequence of the large planned excess reactivity of $\sim 20\%$. The complex core configuration and the neutron absorbers inserted into it has made unreliable the use of the normal methods of controlling the subcriticality of the system (plotting the inverse count curves). The method of "shooting out" the neutron source by means of a pneumatic device has been employed. The high sensitivity of the equipment has enabled the system condition to be reliably controlled in the process of assembly of the core. This same method has been used for estimating the compensating efficiency of the rods, since measurements starting from $k_e = 0.95$ are sufficiently accurate.

Assembly of the actual stack was preceded by assembly of a simulated stack which did not contain uranium. The simulated stack was assembled in accordance with a program compiled for the assembly of the real stack and it was found to be very useful for the subsequent assembly of the reactor. The assembly techniques are worked out and the control and shielding systems were checked. Not least was the role played in the instruction of personnel, since the reactor design is not very simple: the core alone contains 2384 items. The mock-up was dismantled except for the lower reflector. The moving stage was withdrawn into the uppermost position and the moving section of the core was mounted to it. Located in it was the central rod—with a steel sleeve of 100 mm diameter, lined inside with cadmium and filled with paraffin for intensifying the compensating efficiency. The stage was then lowered to the lowermost position, the moving section of the core was positioned within the reflector and a metal dismountable structure—identical in configuration to the moving section of the core and lined inside with cadmium—was installed in its place. It was designed both for reactivity compensation and for preventing collapse of the columns of the fixed section of the core during assembly. First of all the columns fabricated from graphite which was not impregnated with uranium and with channels for inserting rods were assembled and cadmium rods in aluminum tubes with a diameter of 40 mm were inserted. Three rods, together with the central rod, were used as rods for the scram system. After assembly of the fixed section of the core and of the upper reflector, the metal structure

was removed. During the period of physical startup the central blocks of the upper reflector were suspended by a vertically moving platform. On conclusion of the physical measurements the reactor vessel was sealed off by the cover with a section of the upper reflector suspended by it. The temporary cadmium rods were subsequently substituted by the standard graphite rods. The operation of lowering the cover with the suspended reflector had been previously rehearsed on the mockup stack. The principal possible emergency situations were calculated beforehand on a computer using a two-dimensional program.

Physical Characteristics of the PGR Reactor

Considerable difficulties were encountered in the physical calculations, associated with the complex configuration of the reactor and its inhomogeneous composition. In the core there are graphite columns which are not impregnated with uranium, cold rods connecting the individual blocks, gaps between the columns, the central experimental channel cavity, channels for rods and thermocouples. In addition, as a result of lowering the moving section of the core a large-sized cavity is formed and the effect of the lower reflector with the boron absorber is manifested. Despite a number of simplifying assumptions—rounding off the transverse reactor cross section, substitution of the symmetrically arranged rods by an equivalent circular zone, the use of a diffusion equation in the central cavity—the results of the calculations are found to be in satisfactory agreement with the experimental results. The calculation was carried out on a computer mainly in two-group approximation with the introduction of a refining correction which takes into account the fast neutron leakage. Some calculations were checked in nine-group approximation. The effect of slots, channels for the rods and thermocouples [2], and nonuniformities in the fuel distribution (of the cold columns) was estimated by perturbation theory.

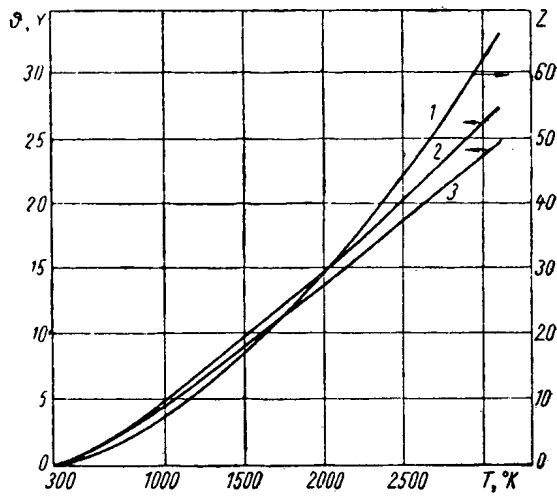
The calculated values of $(K_e - 1)/K_e$ are given below as a function of the average core temperature for the reactor without rods:

T, °K.	293.7	500	1000	1500	2000	2500
$(K_e - 1)/K_e$	0.197	0.152	0.80	0.025	-0.022	-0.066

The magnitude of the excess reactivity is one of the most important characteristics of the PGR reactor, since it determines the integrated flux per pulse. The calculated value of the excess reactivity is $(K_e - 1)/K_e \text{ calc.} = 0.19 \left. \begin{matrix} +0.016 \\ -0.018 \end{matrix} \right\}$ and agrees satisfactorily with the experimental value of $(K_e - 1)/K_e \text{ exp.} = 0.22 \pm 0.02$ obtained by the poisoning method. Forty absorbers were inserted in the core, arranged between the columns of the stack in the form of a regular lattice with a pitch of 20 cm. The absorbers were cadmium strips, sealed on both sides with aluminum plates. Their compensating efficiency was chosen such that the reactor without rods and with raised moving sections of the stack became critical. For this, holes were drilled in the plates. Then the compensating efficiency of each absorber was measured by means of two rods, previously calibrated by the excursion method. The total compensating efficiency of all the absorbers was reduced by a factor of 1.08 (0.08 is the correction to the poisoning heterogeneity, calculated to an accuracy of 10%). The value obtained is the excess reactivity. The error in the experimental value of $(K_e - 1)/K_e$ is determined mainly by an inaccurate knowledge of the delayed neutron fraction [3].

As a result of lowering the mobile section of the stack and with the rods removed completely from the core and also with the upper reflector removed, the reactor was critical at a temperature 20°C. After inserting the thermocouples and replacing the temporary cadmium rods by the standard graphite rods, the ends of which are located at the boundary of the core and the upper reflector, the reactor under these conditions was subcritical at the value $|r| \approx 2$. When the rods are inserted in the core the critical position is obtained by raising the mobile section of the stack to a level distant 530 mm from the upper position; if the mobile section of the stack is raised to the upper position then the reactor is supercritical at a value of $r = 4.5$.

The prompt neutron lifetime was calculated by the change of the effective multiplication factor K_e for an imaginary insertion of an absorber whose cross section varies according to a $1/v$ law, viz $l = \frac{1}{v} \frac{\partial k_e}{\partial (\delta \Sigma_{\text{eff}})}$. A value of $l^* = 0.190$ sec was obtained by varying $\delta \Sigma_{\text{eff}}$. The calculation was carried out for two positions of the mobile section of the stack and it was established that l depends weakly on its displacement. The prompt neutron lifetime was determined experimentally for fast reactor excursions by the period of the excursion and by the known initial reactivity generated by the movement of the calibrated rod. In two experiments ($r_0 = 1.425$ and $r_0 = 2.05$), values were obtained of $l = 0.162$ sec and $l^* = 0.153$ sec. The mean value of l^* is 0.158 sec.

Fig. 2. Functions $z(T)$, $Y(T)$ and $\Phi(T)$:

$$1) Z = \int_{T_0}^T \frac{\bar{\sigma}_f}{\sigma_f} \cdot \frac{C dT}{C_0 T_0}; \quad 2) Y = \int_{T_0}^T \frac{(\bar{\sigma}_f \bar{\nu})_0}{(\bar{\sigma}_f \bar{\nu})} \cdot \frac{C dT}{C_0 T_0};$$

$$3) \Phi = \int_{T_0}^T \frac{C dT}{C_0 T_0}.$$

neutron density on the other hand, the factor could be found for conversion from integrated fluxes to $\int n dt$:

$$\int n dt = E \int i_{ch} dt. \quad (1)$$

The relationship between the integral neutron density, integrated flux and heating is established in the following manner. If N_5 is the number of U^{235} nuclei per kg of the core, $C(T)$ is the specific heat of 1 kg of the core at a temperature T and $\bar{\sigma}_f(T)$ is the mean fission cross section of U^{235} by neutrons in the stack at temperature T , then

$$C dT = E_f N_5 \bar{\sigma}_f \bar{\nu} dt,$$

where E_f is the energy released by a single fission. Hence

$$\int n dt = F \cdot Y, \quad Y = \int_{T_1}^{T_2} \frac{(\bar{\sigma}_f \bar{\nu})_0}{(\bar{\sigma}_f \bar{\nu})} \cdot \frac{C dT}{C_0 T_0}, \quad F = \frac{C_0 T_0}{E_f N_5 (\bar{\sigma}_f \bar{\nu})_0}, \quad (2)$$

$$\int \bar{\nu} dt = G \cdot Z, \quad Z = \int_{T_1}^{T_2} \frac{\bar{\sigma}_f}{\sigma_f} \cdot \frac{C dT}{C_0 T_0}, \quad G = \frac{C_0 T_0}{E_f N_5 \bar{\sigma}_f}. \quad (3)$$

The suffix "zero" defines some reference temperature and T_1 and T_2 are the initial and final temperatures. With large heating (of order 1000°C) the chamber current is associated essentially not with the quantity n but with the quantity $\bar{\nu} \bar{\sigma}_f$, i.e., with the heat release $C(dT)/dt$. Consequently, the relationship

$$\Phi = H \int i_{ch} dt; \quad \Phi = \int \frac{C dT}{C_0 T_0}. \quad (4)$$

should be fulfilled. The coefficient H can be found from comparison of formulas (1), (2) and (3), bearing in mind that formula (1) is valid when $\bar{\sigma}_f \bar{\nu} = \sigma_f \nu_0$:

$$H = \frac{E}{F}.$$

Thus, if the initial temperature T_1 and the chamber current ($\int i_{ch} dt$) are known, then T_2 and $\int \bar{\nu} dt$ can be found (Fig. 2). Measurement of the temperature with the thermocouples makes it possible to adjust the accuracy of determining the integrated flux. Thus, during the time of the first heating up of the reactor, when the shim rods had

In order to determine the neutron flux, the peripheral thermocouple channel of the core was used, the closest to the mobile section—channel b-8—and equipped with a lock for the insertion and removal of samples without disturbing the vacuum tightness of the equipment. It was assumed that the neutrons which are incident on the chamber are fast neutrons which have been slowed down in the water around the chamber, and hence there should be a relationship between the chamber current and the release of heat in the peripheral sections of the core, whence only fast neutrons could reach the chamber. This relationship is slightly sensitive to the condition of the reactor (to the position of the rods and to the temperature) and it was determined so that in future the neutron flux could be assessed firstly on the basis of the chamber currents and secondly by the relationship between the flux at a specified position and the flux in channel b-8.

Gold foils (in cadmium and without cadmium) and a copper wire were activated in channel b-8. The ratio between the activity of the wire and the thermal neutron integral density $\int n dt$ was determined by measuring the absolute activity of the gold foils by the β - γ coincidence method. The cadmium ratio for the gold was found to be 2.7. By establishing the connection between the activation and the integrated flux on the one hand, and between the activation and the integrated neutron density on the other hand, the factor could be found for conversion from integrated fluxes to $\int n dt$:

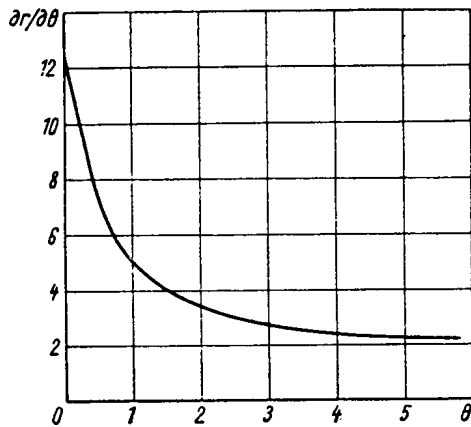


Fig. 3. Thermal reactivity coefficient.

traversed one-half of their path, the temperature in channel b-8 as determined by $\int i_{ch} dt$ was equal to 820°C . The temperature according to the thermocouple readings was almost identical with this value.

In the above-mentioned triggering the integrated flux in channel b-8 was $2 \cdot 10^{16} \text{ cm}^{-2}$ and at the center of the core it was $4 \cdot 10^{16} \text{ cm}^{-2}$. According to calculation the reactor, without rods and with the mobile section of the stack withdrawn to the upper position, becomes critical at an average temperature of 1800°K , which corresponds to a flux at the center of $1.1 \cdot 10^{17} \text{ cm}^{-2}$. If the rods are not withdrawn from the upper reflector, then this value is reduced to $0.8 \cdot 10^{17} \text{ cm}^{-2}$.

The neutron fluxes in channel b-8 at the instant of the self-quenched burst maximum are given below as a function of the magnitude of the initial reactivity jump r_0 or the initial excursion period τ_e :

r_0	τ_e	$\bar{n}\bar{v}$
5.50	0.035	$1.34 \cdot 10^{16}$
4.46	0.045	$0.84 \cdot 10^{16}$
3.65	0.059	$5.2 \cdot 10^{15}$
2.54	0.10	$1.98 \cdot 10^{15}$
1.47	0.285	$2.9 \cdot 10^{14}$

The maximum possible instantaneous value of the neutron flux in the burst regime was estimated on the basis of the calculated dependence of the reactivity on the accumulated heat $r(\vartheta)$ for the reactor without rods and with an average temperature of heating up of 1600°K :

$$(\bar{n}\bar{v})_{\max} = \frac{K_v G}{l^*} \cdot \frac{dZ}{d\vartheta} \int_0^{\vartheta_1} (r-1) d\vartheta = 1 \cdot 10^{18} \text{ cm}^{-2} \cdot \text{sec}^{-1}.$$

Here ϑ_1 is the value of ϑ for which $r=1$; K_v is the coefficient of volume inhomogeneity.

The temperature dependence of the reactivity was found for small values of ϑ during the first reactor triggerings—bursts with heating up of the core. The reactivity was calculated as a function of time from the oscillogram of the ionization chamber currents by means of a special program on the computer and, according to the integral of the chamber current it was

$$r = r_0 + k_1 \int i_{ch} dt + k_2 \left[\int i_{ch} dt \right]^2.$$

The relationship between the reactivity and the accumulated heat was expressed in the form

$$r = R_0 + \kappa_1 \vartheta + \kappa_2 \vartheta^2.$$

The coefficients $\kappa_1 = -12.6$ and $\kappa_2 = 5.7$ were determined from these relationships and the function $\Delta r = \kappa_1 \vartheta + \kappa_2 \vartheta^2$ was plotted, describing the dependence of the reactivity on the temperature in channel b-8. The temperature coefficient decreases according to the extent of heating up of the reactor; its initial value is $dr/dT = -0.042 \text{ deg}^{-1}$.

In the controlled regime the reactivity coefficient with respect to temperature depends only on the displacement of the shim rods. In order to derive it, the dependence of dr/dx_{rod} on the position of the rod x_{rod} was used. The efficiency of the shim rods in the critical reactor was determined as a function of their position (with identical extent of withdrawal of eleven rods) during cooling down of the reactor which had been heated to 1000°C (the temperature of channel b-8). The measurement procedure is as follows. Having waited until the cooling reactor becomes slightly supercritical, one of the rods is moved a few centimeters upwards, the change of reactivity is determined and all the rods are lowered to a new level. The change of reactivity found is divided by the displacement of the rod and multiplied by the number of rods. The temperature field during cooling down does not reproduce exactly the temperature field of the heated reactor, nevertheless the relationship $dr/dx_{rod} = f(x_{rod})$ obtained, was used for calculating the reactivity coefficient by the parameter ϑ for channel b-8. Oscillograms of prolonged

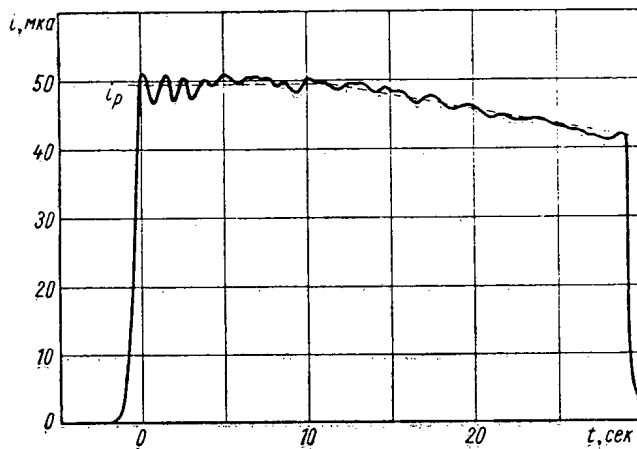


Fig. 4. Triggering oscillogram, ———) Ionization chamber current $i_{ch}(t)$; - - - -) specified law of current variation $i_p(t)$.

regimes carried out with the regulator disconnected were used. The oscillogram of the current $i_{ch}(t)$ and the known coefficient H make it possible to determine the relationships $\vartheta(t)$ and $r(t)$, i.e., $r(\vartheta)$. The relationship $x_{rod}(\vartheta)$ is found by means of the $x_{rod}(t)$ oscillograms. Further, $dr/d\vartheta$ is determined from the relationship $dr/d\vartheta = (dr/dx_{rod}) \cdot (dx_{rod}/d\vartheta) + (dr/dt)$. The graph of the relationship $dr/d\vartheta = f(\vartheta)$ is shown in Fig. 3.

PGR Reactor Control

The control mechanism of the PGR is divided functionally into trigger, compensating and control. The trigger element, which initiates the neutron burst, is the moving section of the stack. For triggering the reactor it is always raised to its top position and therefore the magnitude of the initial reactivity jump r_0 is determined by the initial temperature of the stack, by the position of the rods and by the absorption of the samples in the ampoule of the central experimental channel. The movement of the eleven compensating (shim) rods is started at the instant of the burst maximum, after operation of the threshold equipment whose detector is an ionization chamber. Synchronous movement of the rods, by a law which is defined by the profile element, is ensured by a servo-system. An automatic control rod corrects any errors.

The first triggerings of the reactor were undertaken with identical withdrawal of the shim rods and with the automatic controls detached. The ionization chamber currents $i_{ch}(t)$ were oscillographed and also the movement

of the rods $x_{rod}(t)$. At the coordinates $x_{rod}(t); J(t)$, where $J(T) = \int_0^T i_{ch} dt$, triggerings of different duration were

represented by similar curves, since in any triggering after reaching the operating region the reactivity differs but little from zero (by not more than unity). The relationship $x_{rod} = f(J)$ also represents, to a first approximation, the law of motion of the shim rods in the regime $i_{ch}(t) = \text{const}$. A more precise law was obtained after working out the results of several triggerings with a previously adjusted profile element. Because of the different extent of the graphite temperature effect on the temperature of the neutron gas in the core and in the ampoule, the ratio of the chamber current to the neutron density inside the ampoule does not remain constant. In order to adjust the profile element to the regime in which the neutron density inside the ampoule should remain constant, special measurements were carried out. In particular, a loop wire activator was positioned inside the ampoule which was provided with a device for exposing the wire by sections. The section of the wire irradiated for several seconds was discharged, after each exposure, from the core and collected in a container which was shielded from thermal neutrons. By comparing the activation of the individual sections of the wire with the current integrals during the time of irradiation, it was established that the chamber current should be reduced towards the end of the regime (Fig. 4).

The procedure worked out for the calculating allows a profile element to be produced for any operating regime of the reactor. In particular, there is the interesting possibility of producing neutron pulses of different duration, which approximate in shape to rectangular. In this case, the operating time losses at the beginning and end of the process will be minimum. A regime of this type can be divided into three stages: the initial stage, during which time the power of the reactor reaches a specified value, the operating region ($Q = Q_p$) and the final stage is

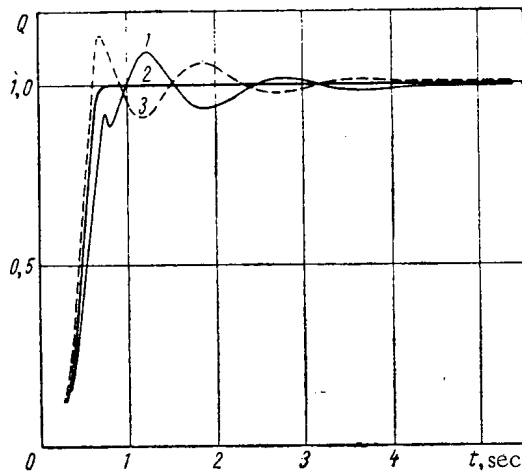


Fig. 5

Fig. 5. Effect of errors in the reactivity jump δr_0 on the behavior of the power in the regime $t_p = 10$ sec; 1) $\delta r_0 = -0.05$; 2) $\delta r_0 = 0$; 3) $\delta r_0 = 0.05$.

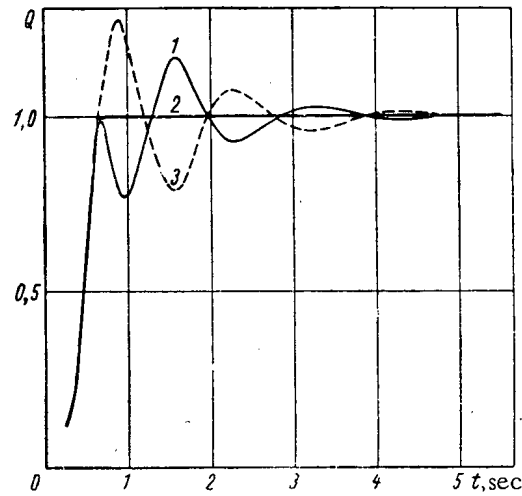


Fig. 6

Fig. 6. Effect of errors in the instant of commencement of motion of the shim rods on the behavior of the power in the regime $t_p = 10$ sec. 1) $\delta t_{rod} = -0.05$ sec; 2) $\delta t_{rod} = 0$; 3) $\delta t_{rod} = 0.05$ sec.

the forced quenching. The most important is that of reaching the operating region, since initially the reactor has the least stability. Successful arrival at the operating regime is determined mainly by the correct choice of the value of the initial reactivity jump r_0 and the instant of start of the movement of the shim rods. Errors in the reactivity or in the response threshold of the switching system, Q_{thresh} , of the shim rods give rise to considerable power fluctuations at the beginning of the operating section of the regime.

The relative error in the maximum power of the burst depends on the error in r_0 thus:

$$\frac{\delta Q_{max}}{Q_{max}} = \frac{2\delta r_0}{r_0 - 1}$$

The error at the instant of commencement of motion of the shim rods δt_{rod} leads to a reactivity perturbation:

$$\delta r_{pert.} = \frac{\delta t_{rod} \gamma_i \Delta r_p}{t_p \gamma_p}; \quad (\gamma_i / \gamma_p) \Delta r_p \approx 50.$$

The error in r_0 , equal to 0.05 in a regime with a duration of 20 sec ($r_0 = 1.78$), changes the amplitude of the burst by 13%; a shift of the instant of engaging the shim rods by 0.05 sec is equivalent to a reactivity perturbation at the commencement of the operating region of $\delta r \approx 0.13$. Figures 5 and 6 illustrate the effect of errors in the initial reactivity and in the instant of the initial motion of the rods on the behavior of the power. The curves are obtained by a numerical method by means of special program on the electronic computer.

A number of experimental relationships are used in making a correct choice of r_0 and Q_{thresh} . The value of the ionization chamber current (the unit of the servo-system of control by the rods) is determined at the beginning of the operating region, $i_{ch}(t_i)$, from specified values of t_p and Q_p . The magnitude of the initial reactivity jump is chosen from the condition $i_{ch max}(r_0) = i_{ch}(t_i)$.

In determining Q_{thresh} account should be taken that the movement of the rods commences with a delay of Δt_{rod} after actuation of the threshold circuit. Consequently, it is necessary to know not only the amplitude but also the shape of the ensuing burst. A value of Q_{thresh} is determined for which initially the motion of the rods should coincide with the burst peak.

If the position of the rods is fixed and there is no sample in the ampoule, then r_0 as a result of raising the moving section of the core is determined only by the temperature of the stack. The relationship between r_0 and the temperature (when it is uniform over the whole stack) can be represented, within the range 20-50°C, in the form of

Declassified and Approved For Release 2013/03/14 : CIA-RDP10-02196R000600120002-4
a straight line with a slope of $dr_0/dT = -0.034 \text{ deg}^{-1}$. The temperature must be measured with an accuracy of a fraction of a degree, otherwise the error in r_0 will be inadmissibly large. In the initial state, prior to triggering, the shim rods will be located in the strictly fixed lower position and the automatic and manual control rods will be in some intermediate position. By changing their position the magnitude of r_0 is also changed. Reduction of r_0 can be achieved also by a small preliminary heating of the core. The losses in integrated flux as a result of this will be small, since at low temperature the specific heat of the graphite is small and the fission cross section is large.

The compensating efficiency of samples installed in the ampoule is estimated by the position of the moving section of the stack corresponding to the critical state. The most accurate value for the compensating efficiency of the sample can be obtained by producing a burst which is quenched while the reactor is heating up (pseudoburst). The riding up period and the reactivity are determined by the chamber current oscillogram. After the personnel had acquired adequate practical experience, the error in attaining a specified value of r_0 in the majority of reactor triggerings did not exceed values of $r_0 = \pm 0.02$. The power at the start of the operating region is also found to be sensitive to the inaccuracy of adjustment of the profile element, but one and the same profile element is suitable for different, but not too strongly different, values of t_p . Figure 4 shows the form of an actual triggering with a duration of 30 sec, carried out with the profile element for the regime $t_p = 20$ sec.

The reactor has been found safe and convenient to operate as a means of producing high, although also short-duration, neutron (and γ ray) fluxes. In reactors of this type, with an enlarged core and a reduced uranium content, fluxes of up to $2 \cdot 10^{18} \text{ cm}^{-2}$ can be attained.

The injection of reactivities which are many times greater than β is safe: as a consequence of the negative reactivity temperature coefficient the reactor, as a result of this, reaches a certain limiting temperature. Control has proved feasible to an accuracy of $\pm 3\%$ by the behavior of the flux with time, by means of relatively simple equipment.

The individual columns of blocks impregnated with uranium and connected to each other by graphite rods are very flexible and they are unstable. However, the columns when connected together at the top form a system which is stable on the whole, although it is a moveable and swaying system, and which easily withstands repeated movements (up and down). No jamming has been observed, despite the contact with the surrounding stationary stack. Also, no noticeable effect whatsoever of the stack column vibrations on the reactivity has been observed.

The graphite, fireproof rods with the absorbing gadolinium oxide tablets have proved to be completely efficient.

No significant volatilization of uranium and fission products from the stack has been observed as a result of operating the reactor. There has been no appreciable contamination by fission products of the caps of the control and safety rods directly connected with the core space.

In conclusion, we take this opportunity of expressing our sincere appreciation to V. V. Goncharov for the sponsorship and assistance which he has continuously rendered in the construction of the reactor, and to B. V. Kurchatov for direct participation in developing the technology for impregnating graphite with uranium. We also express our appreciation of the scientific workers, engineers and builders, whom we have not found it possible to mention here, for having participated in the construction and commissioning of the PGR reactor.

LITERATURE CITED

1. S. M. Feinberg, Data from the Second International Conference of the United Nations Organization [in Russian], 10, Discussion of reports P/419 and P/1848.
2. Ya. V. Shevelev, *Atomnaya Énergiya*, 14, 4 (1963).
3. G. R. Keepin et al., *Nucl. Energy*, 6, No. 1/2 (1957).

STATISTICAL REACTOR KINETICS EQUATIONS

(UDC 621.039.512)

A. B. Govorkov

Translated from *Atomnaya Énergiya*, Vol. 17, No. 6,
pp. 474-479, December, 1964
Original article submitted December 13, 1963

In addition to the kinetic equation for the flux of prompt neutrons, which determines their mean behavior in the reactor, we have the kinetic equations for the "production densities" of the neutron fluxes which describe the statistical behavior of the prompt neutrons in the reactor. Taking into consideration the space and energy distribution of the neutrons, a method is given for making an effective averaging of the statistical behavior characteristics of the reactor. A discussion is given of the theory of the Rossi α experiment.

In the elementary theory of statistical methods of determining reactor parameters, the behavior of neutrons in a reactor is described by means of the one-group and the one-zone approximations [1]. However, there is some interest in a more general treatment which includes the space-energy distribution of the neutrons. In the present paper, a treatment of this type is made for the prompt neutrons, while the delayed neutrons in fission are taken account of formally in the external source. A similar problem has been treated in the papers of [7] by a somewhat different method.

A neutron located in the reactor has the coordinate \mathbf{r} , the energy E , and the direction of its velocity $\mathbf{n} = \mathbf{v}/v$. In abbreviated form, the state of the neutrons $(\mathbf{r}, E, \mathbf{n})$ is designated by the letter x , and the element $dVdEd\Omega$ is designated by the symbol dx . The symbols x and $x + h$ designate the finite volume of the reactor, and the finite energy intervals and the directions of the velocities.

The probability of having in the reactor, at a chosen instant of time, a given number of neutrons, distributed, in addition, in a definite way over the points x , is designated by $W_N(x_1, x_2, \dots, x_N; t) dx_1, dx_2, \dots, dx_N$. We average the production densities of the neutron fluxes over these probabilities at several different points:

$$\begin{aligned}
 & F_s(x', x'', \dots, x^{(s)}; t) \\
 &= \sum_{N=1}^{\infty} \frac{1}{N!} \int dx_1 \dots \int dx_N \left[\sum_{i=1}^N v_i \delta(x_i - x') \right] \left[\sum_{\substack{j=1 \\ (j \neq 1)}}^N v_j \delta(x_j - x'') \right] \dots \left[\sum_{\substack{k=1 \\ (k \neq i, j, \dots)}}^N v_k \delta(x_k - x^{(s)}) \right] \\
 & \quad \times w_N(x_1, x_2, \dots, x_N; t).
 \end{aligned} \tag{1}$$

The above densities have been given the name of production densities in the theory of random point processes [2]. The factorial moments of the number of neutrons in the finite interval $x, x + h$ are expressed in the following way:

$$\overline{N(N-1) \dots (N-s+1)} = \int_x^{x+h} dx_1 \dots \int_x^{x+h} dx_s \frac{F_s(x_1, \dots, x_s; t)}{v_1 \dots v_s} \tag{2}$$

The production densities satisfy the equations: [see Eq. (3) on following page]

$$\begin{aligned}
\frac{1}{v_1 \dots v_s} \frac{\partial F_s(x_1, \dots, x_s; t)}{\partial t} &= \sum_{i=1}^s \frac{v_i}{v_1 \dots v_s} \left\{ -\mathbf{n}_i \nabla_i F_s(x_1, \dots, x_i, \dots, x_s; t) \right. \\
&\quad - \frac{F_s(x_1, \dots, x_i, \dots, x_s; t)}{l_{asf}(x_i)} + \int dx'_i \frac{F_s(x_1, \dots, x'_i, \dots, x_s; t)}{l_{sc}(x'_i)} p^{(sc)}(x'_i | x_i) \\
&\quad + \int dx \frac{F_s(x, x_1, \dots, x_{i-1}, x_{i+1}, \dots, x_s; t)}{l_f(x)} \left[\sum_{\nu=1}^{\infty} \frac{\nu}{\nu!} \int dx'' \dots \int dx^{(\nu)} \right. \\
&\quad \quad \left. \times p_{\nu}^f(x | x_i, x'', \dots, x^{(\nu)}) \right] + Q(x_i; t) \\
&\quad \left. \times F_{s-1}(x_1, \dots, x_{i-1}, x_{i+1}, \dots, x_s; t) \right\} + \sum_{\mu=2}^s \sum_{1 \leq i_1 < i_2 < \dots < i_{\mu} = \mu, \dots, s} \frac{v_{i_1} \dots v_{i_{\mu}}}{v_1 \dots v_s} \\
&\quad \times \frac{F_{s-\mu+1}(x, x_1, \dots, x_{i_1-1}, x_{i_1+1}, \dots, x_{i_{\mu}-1}, x_{i_{\mu}+1}, \dots, x_s; t)}{l_f(x)} \\
&\quad \times \left[\sum_{\nu=\mu}^{\infty} \frac{\nu(\nu-1) \dots (\nu-\mu+1)}{\nu!} \int dx^{(\mu+1)} \dots \int dx^{(\nu)} p_{\nu}^{(f)}(x | x_{i_1}, \dots, x_{i_{\mu}}, x^{(\mu+1)}, \dots, x^{(\nu)}) \right], \quad (3) \\
&\quad s = 1, 2, \dots
\end{aligned}$$

Here, $1/l_a(x)$, $1/l_{sc}(x)$, $1/l_f(x)$ are the macroscopic cross-sections for capture, scattering, and fission respectively, occurring when a neutron collides with a nucleus. The total macroscopic cross-section for all processes is $1/l_{asf}(x)$. The density of the relative probability that the neutron as a result of scattering at the point \mathbf{r} will change its energy E and the direction of its velocity \mathbf{n} to E' and \mathbf{n}' is written in the form:

$$p^{(sc)}(x | x') \equiv p^{(sc)}(\mathbf{r}, E, \mathbf{n} | E', \mathbf{n}') \delta(\mathbf{r} - \mathbf{r}').$$

This function is normalized in the following way:

$$\int p^{(sc)}(x | x') dx' = 1. \quad (4)$$

The densities of the relative probabilities that as a result of fission of a nucleus produced at the point \mathbf{r} by a neutron with energy E and the direction of its velocity \mathbf{n} , ν secondary prompt neutrons will be formed with energies $E', E'', \dots, E^{(\nu)}$, and the directions of the velocities $\mathbf{n}', \mathbf{n}'', \dots, \mathbf{n}^{(\nu)}$, may be written in the form:

$$p_{\nu}^{(f)}(x | x', \dots, x^{(\nu)}) \equiv p_{\nu}^f(\mathbf{r}, E, \mathbf{n} | E', \mathbf{n}', \dots, E^{(\nu)}, \mathbf{n}^{(\nu)}) \delta(\mathbf{r} - \mathbf{r}') \dots \delta(\mathbf{r} - \mathbf{r}^{(\nu)}).$$

These functions are normalized in the following way:

$$\sum_{\nu} \frac{1}{\nu!} \int dx' \dots \int dx^{(\nu)} p_{\nu}^{(f)}(x | x', \dots, x^{(\nu)}) = 1. \quad (5)$$

The density of the probability of emission in unit time by an external source of one neutron at the point \mathbf{r} with the energy E and the direction of its velocity \mathbf{n} is $Q(x, t) \equiv Q(\mathbf{r}, E, \mathbf{n}; t)$.

The function $F_1(x, t)$ is the usual mean density of the flux of prompt neutrons, while Eq. (3) for $s = 1$ is the usual kinetic equation. For $s = 2$, we obtain the kinetic equation for the "binary density of the fluxes," discussed previously by the author as applied to the problem of the spread in pulse amplitudes in a pulsed reactor [3].

The Eqs. (3) may be solved successively, since the equation for each successive function includes expressions depending on it itself and on the preceding functions. This "breakup" of the functions into following and preceding is based on the assumption that the inherent liberation of energy in the reactor, which accompanies the nuclear fission processes, has no effect on the magnitude of the critical parameters of the reactor. Otherwise, Eqs. (3) are

incorrect. For example, for pulsed fast neutron reactors of "Godiva" type, our treatment only holds in the stage of the pulse where the liberation of energy in the chain fission reacting does not yet have any effect on the value of the critical parameters of the reactor. But the very start of the neutron chains in the individual pulses may fluctuate greatly, although after the chains are sufficiently developed, the fluctuations stop [4].

The boundary conditions for the production densities are formulated in a way similar to the boundary conditions for the usual neutron flux density. For a reactor bounded by a convex surface, and surrounded by a void, they are of the form:

$$\begin{aligned} F_s(\mathbf{r}_i, \mathbf{E}_i, \mathbf{n}_i, \dots, \mathbf{r}_i \text{ bn } \mathbf{E}_i, \mathbf{n}_i \text{ int} \\ \dots, \mathbf{r}_s, \mathbf{E}_s, \mathbf{n}_s; t) = 0, \\ i = 1, \dots, s, \end{aligned} \quad (6)$$

where $\mathbf{r}_i \text{ bn}$ designates a point on the boundary, and $\mathbf{n}_i \text{ int}$ is the direction of the velocity of the neutron inside the system. The number of boundary conditions for each function is s .

For the majority of cases of practical interest, the solution of Eqs. (3) for the production densities may be assumed in the form:

$$F_s(x_1, \dots, x_s; t) = F_s(x_1, \dots, x_s) \varphi_s(t). \quad (7)$$

Then, Eqs. (3), using transformations analogous to the transformations of L. N. Usachev for the usual kinetic equation [5], may be written in the following way:

$$\begin{aligned} T(s) \frac{d\varphi_s(t)}{dt} = s \frac{k_{\text{eff}} - 1}{k_{\text{eff}}} \varphi_s(t) \\ + sq(s, t) \varphi_{s-1}(t) + \sum_{\mu=2}^s \binom{s}{\mu} \gamma_{\mu}(s) \varphi_{s-\mu+1}(t). \end{aligned} \quad (8)$$

Here, k_{eff} is the multiplication factor for prompt neutrons, $\binom{s}{\mu}$ is the binomial coefficient, and $T(s)$ is the effective lifetime of the neutrons in the reactor:

$$T(s) = \frac{1}{\mathcal{J}(s)} \int dx_1 \dots \int dx_s \frac{F^+(x_1) \dots F^+(x_s)}{v_1 \dots v_s} F_s(x_1, \dots, x_s). \quad (9)$$

The worth of the prompt fission neutrons is:

$$\begin{aligned} \mathcal{J}(s) = \int dx_2 \dots \int dx_s \frac{F^+(x_2) \dots F^+(x_s)}{v_2 \dots v_s} \left\{ \int dx \int dx' \frac{F_s(x, x_2, \dots, x_s)}{l_f(x)} \right. \\ \left. \times \left[\sum_{\nu=1}^{\infty} \frac{\nu}{\nu!} \int dx'' \dots \int dx^{(\nu)} p_{\nu}^{(f)}(x | x', x'', \dots, x^{(\nu)}) \right] F^+(x') \right\}. \end{aligned} \quad (10)$$

The quantity $q(s, t)$ has the sense of the power of the external neutron source, including the worth of the neutrons:

$$q(s, t) = \frac{1}{\mathcal{J}(s)} \int dx_1 F^+(x_1) Q(x_1, t) \int dx_2 \dots \int dx_s \frac{F^+(x_2) \dots F^+(x_s)}{v_2 \dots v_s} F_{s-1}(x_2, \dots, x_s). \quad (11)$$

The coefficients $\gamma_{\mu}(s)$ which relate the different functions $\varphi_s(t)$, are expressed in the following way:

$$\begin{aligned} \gamma_{\mu}(s) = \frac{1}{\mathcal{J}(s)} \int dx_{\mu+1} \dots \int dx_s \frac{F^+(x_{\mu+1}) \dots F^+(x_s)}{v_{\mu+1} \dots v_s} \left\{ \int dx \int dx_1 \dots \int dx_{\mu} \frac{F_{s-\mu+1}(x, x_{\mu+1}, \dots, x_s)}{l_f(x)} \right. \\ \left. \times \left[\sum_{\nu=\mu}^{\infty} \frac{\nu(\nu-1) \dots (\nu-\mu+1)}{\nu!} \int dx^{(\mu+1)} \dots \int dx^{(\nu)} p_{\nu}^{(f)}(x | x_1, \dots, x_{\mu}, x^{(\mu+1)}, \dots, x^{(\nu)}) \right] \right. \\ \left. \times F^+(x_1) \dots F^+(x_{\mu}) \right\}. \end{aligned} \quad (12)$$

In all these expressions, the function $F^+(x)$ is a characteristic solution of the equation conjugated with the usual kinetic equation with no external source for a reduction in neutron multiplication by the factor k_{eff} [5].

It is very inconvenient that the quantities $T(s)$, $q(s, t)$, and $\gamma_\mu(s)$ depend on the subscripts s of the function $\varphi_s(t)$, and can thus not be regarded as universal characteristics of the reactor kinetics. In many cases, however, it is possible to make use of the additional assumption that the production densities decompose into the product of the densities of the usual neutron flux:

$$F_s(x_1, x_2, \dots, x_s) = F(x_1) F(x_2) \dots F(x_s). \quad (13)$$

Then, we obtain the mean lifetime of a neutron in the reactor:

$$T = \frac{1}{\mathcal{J}} \int dx \frac{F^+(x) F(x)}{v}; \quad (14)$$

The worth of the prompt fission neutrons is:

$$\mathcal{J} = \int dx \int dx' \frac{F(x)}{l_f(x)} \left[\sum_{\nu=1}^{\infty} \frac{\nu}{\nu!} \int dx'' \dots \int dx^{(\nu)} p_\nu^{(f)}(x|x'; x'', \dots, x^{(\nu)}) \right] F^+(x'); \quad (15)$$

The power of the external source is:

$$q(t) = \frac{1}{\mathcal{J}} \int dx F^+(x) Q(x, t); \quad (16)$$

and the coupling coefficients are:

$$\begin{aligned} \gamma_\mu &= \frac{1}{\mathcal{J}^\mu T^{\mu-1}} \int dx \int dx_1 \dots \int dx_\mu \frac{F(x)}{l_f(x)} \left[\sum_{\nu=\mu}^{\infty} \frac{\nu(\nu-1)\dots(\nu-\mu+1)}{\nu!} \right. \\ &\times \left. \int dx^{(\mu+1)} \dots \int dx^{(\nu)} p_\nu^{(f)}(x|x_1, \dots, x_\mu, x^{(\mu+1)}, \dots, x^{(\nu)}) \right] F^+(x_1) \dots F^+(x_\mu). \end{aligned} \quad (17)$$

The set of Eqs. (8) determines the statistical behavior of the neutrons in the reactor.

We now determine the number of coincidences in counting neutrons with a detector in the time intervals dt and dt_0 , separated by the interval $t-t_0$ (Rossi α experiment [6]*). The probability of the event under discussion is defined in the following way:

$$\begin{aligned} R(t, t_0) dt dt_0 &= \sum_{N=1}^{\infty} \sum_{N_0=1}^{\infty} \frac{1}{N! N_0!} \int dx_1 \dots \int dx_{N_0} \int dx'_1 \dots \int dx'_N \\ &\times \left\{ \int dx \varepsilon(x) \int dx' \varepsilon(x') \left[\sum_{i=1}^N \delta(x' - x_i) \right] \left[\sum_{j=1}^{N_0} \delta(x - x_j) \right] \right. \\ &\times w_{N, N_0-1}(x'_1, \dots, x'_N; t | x_1, \dots, x_{j-1}, x_{j+1}, \dots, x_{N_0}; t_0) \left. \right\} \\ &\times w_{N_0}(x_1, \dots, x_{N_0}; t_0) \} dt dt_0. \end{aligned} \quad (18)$$

Here, $\varepsilon(x)$ is the neutron counting efficiency at the point x (macroscopic absorption cross-section of the neutron counter, multiplied by its velocity); the function,

*It should be noted that independently of Rossi, a similar idea for an α experiment was proposed in the Soviet Union by Ya. B. Zel'dovich and N. A. Dmitriev.

$$w_{N, N_0-1}(x'_1, \dots, x'_N; t | x_1, \dots, x_{j-1}, x_{j+1}, \dots, x_{N_0}; t_0)$$

is the probability of finding N neutrons in the reactor at the points x'_1, \dots, x'_N at the instant of time t , if, at the instant t_0 after counting one neutron at the point x_j , $N_0 - 1$ neutrons remain at the points $x_1, \dots, x_{j-1}, x_{j+1}, \dots, x_{N_0}$.

Multiplying this function by $\sum_{i=1}^N \delta(x' - x_i)$, summing over the number of neutrons N and integrating over the arguments x'_1, \dots, x'_N on the right-hand side of Eq. (18), give the density of the mean number of neutrons at the point x' at the instant of time t for the condition that at the instant of time t_0 , this density is $\sum_{i=1}^{N_0} \delta(x_i - x')$

$-\delta(x_j - x')$. The solution for this density may be found in the form of an expansion in the eigenfunctions of the kinetic equation $\Phi_n(x)$, corresponding to the eigenvalues α_n . After substituting this expansion in the right-hand side of Eq. (18), using the relation (1) in summing over the number of neutrons N_0 , and integrating over their positions x_1, \dots, x_{N_0} , we obtain the following expression for the coincidence frequency:

$$R(t, t_0) dt dt_0 = \int dx \frac{\varepsilon(x) F(x)}{\nu} dt_0 \int dx' \frac{\varepsilon(x') F(x')}{\nu'} dt + \sum_n e^{\alpha_n(t-t_0)} \int dx' \frac{\varepsilon(x') \Phi_n(x')}{\nu'} dt \frac{\int dx \int dx'' \varepsilon(x) \left[\frac{F(x, x'')}{\nu \nu''} + \frac{F(x) Q(x'')}{\alpha_n \nu} \right] \Phi_n^+(x)}{\int dx \frac{\Phi_n^+(x) \Phi_n(x)}{\nu}} dt_0. \quad (19)$$

The functions $F(x)$ and $F(x, x'')$ are the steady state solutions of the usual and binary kinetic Eqs. (3) for the reactor. The first term on the right-hand side of Eq. (19) gives the usual random coincidences in counting neutrons in the time intervals dt and dt_0 , and the second term gives the coincidences due to the genetic relation between the neutrons in the chain reaction. If the period of time $t - t_0$ is considerably greater than the time interval required to set up the characteristic distribution in the reactor ($t - t_0 \gg 1/\alpha_n$, $n = 2, \dots$), in the second term on the right-hand side of Eq. (19) we can keep only the first term of the series in n , corresponding to the eigenvalue:

$$\alpha_1 = \frac{1}{T} \cdot \frac{k_{\text{eff}} - 1}{k_{\text{eff}}}. \quad (20)$$

In order to simplify the preexponential multiplier in the resulting expression, we make an additional assumption. We shall assume that quite good equality is maintained between the steady state solution of the kinetic equation and its first eigenfunction, and that the binary density may be written as the product of two such solutions:

$$F(x, x'') = \varphi_2 F(x') F(x''), \quad (21)$$

where φ_2 is determined by the steady state Eq. (8) for $s = 2$. After all the transformation, we obtain:

$$R(t, t_0) dt dt_0 = \varepsilon^2 \bar{N}^2 dt dt_0 + \varepsilon^2 \bar{N} \frac{\Gamma_2/2}{(1/k_{\text{eff}}) - 1} \exp \times \left[\frac{t-t_0}{T} \left(1 - \frac{1}{k_{\text{eff}}} \right) \right] dt dt_0, \quad (22)$$

where the mean number of neutrons in the reactor, from Eq. (2), is:

$$\bar{N} = \int dx \frac{F(x)}{\nu}. \quad (23)$$

The averaged neutron counting efficiency is expressed in the following way:

$$\varepsilon = \frac{\int dx \frac{\varepsilon(x) F(x)}{\nu}}{\int dx \frac{F(x)}{\nu}}. \quad (24)$$

The coefficient is:

$$\Gamma_2 = \frac{1}{T} \cdot \frac{\int dx \int dx' \int dx'' \frac{F(x)}{l_f(x)}}{\left\{ \int dx \int dx' \frac{F(x)}{l_f(x)} \right\}} \quad (25)$$

$$\times \frac{\left[\sum_{v=2}^{\infty} \frac{v(v-1)}{v!} \int dx''' \dots \int dx^{(v)} p_v^{(f)}(x | x', x'', \dots, x^{(v)}) \right] F^+(x') F^+(x'')}{\left[\sum_{v=1}^{\infty} \frac{v}{v!} \int dx'' \dots \int dx^{(v)} p_v^{(f)}(x | x', x'', \dots, x^{(v)}) \right] F^+(x')^2 \left\{ 1 / \int dx \frac{F(x)}{v} \right\}}$$

In conclusion, I express my gratitude to Yu. A. Romanov and N. A. Dmitriev, for discussion of the results of the work.

LITERATURE CITED

1. F. Hofman, Scientific and Engineering Bases of Nuclear Power, Vol. 2 [Russian translation], Moscow, IL (1950), p. 103.
2. M. S. Bartlett, Introduction to the Theory of Random Processes [Russian translation], Moscow, IL (1958).
3. A. B. Govorkov, "Atomnaya Énergiya," 13, 152 (1962).
4. G. Hansen, Nucl. Sci. and Engng., 8, 709 (1960).
5. L. N. Usachev, Reactor Construction and the Theory of Reactors, Paper presented by the Soviet delegation at the International Conference on the Peaceful Uses of Atomic Energy (Geneva, 1955) [in Russian], Moscow, Academy of Sciences Press, USSR (1955), p. 251.
6. J. Orndoff, Nucl. Sci. and Engng., 2, 450 (1957).
7. L. Pal, Suppl. Nuovo Cimento, 7, 25 (1958); L. Pal and H. Nemet, Pile Neutron Research in Physics, Vienna, IAEA (1962), p. 491.

CHANNEL EFFECTS IN FISSION OF EVEN-EVEN COMPOUND NUCLEI

(UDC 539.173)

L. N. Usachev, V. A. Pavlinchuk, and N. S. Rabotnov

Translated from *Atomnaya Énergiya*, Vol. 17, No. 6,
pp. 479-485, December, 1964
Original article submitted December 12, 1963

An analysis is made of the experimental data on the fission of even-even compound nuclei in the reactions (d, pf) , (γ, f) , and (n, f) at the threshold. Calculations are made of the fission which is based on the Bohr-Wheeler formula. All the experimental data given are in agreement with the structure of the fission channels proposed by A. Bohr. It is found in this case that the fission channels with negative parity lie 0.6-0.8 MeV higher than the first channels having positive parity. For the fission channels arranged in this way, the Bohr-Wheeler formula gives a quantitative description of the mean fission widths for the resonances of the (n, f) reaction in the nuclei U^{233} , U^{235} , and Pu^{241} . To account for the large difference in the case of Pu^{239} , it is necessary to assume that the ground state of this nucleus has negative parity.

The experimental data are being analyzed for the purpose of finding what effect the spin and parity of the fissioning nucleus have on the fission barrier. If the barrier may be assumed to be approximately parabolic, the form of the barrier is completely determined by two quantities, the height E_f and the parameter E_{curv} , which gives the curvature of the barrier at the saddle point [1]. The principal theoretical ideas as to the relation between the fission process and the quantum characteristics of the fissioning nucleus were developed in the papers by N. Bohr, A. Bohr, Hill, and Wheeler [1-3], which presented a number of points of view used in the present paper. These may be generalized in the following way:

1. At the saddle point, a considerable part of the excitation energy goes into potential energy of deformation, the nucleus "cools off," and the number of ways of exciting degrees of freedom not associated with fission is greatly limited. There are accordingly not a large number of ways,—"fission channels"—by which the nucleus can pass through the saddle point.

2. For even-even nuclei at the saddle point, there will be pairing effects, and the spectrum of the fission channels will be similar to the spectrum of the low lying excited levels. Accordingly, on A. Bohr's hypothesis, the fission channels are arranged in the following way in order of increase in the fission thresholds corresponding to them (Fig. 1): 1) the rotation band of positive parity, based on the level 0^+ (there is no 1^+ level in it), 2) the rotation band of negative parity, starting with the level 1^- , the distance of which from the level 0^+ we designate by Δ_1 (there is no 0^- level in this band), and 3) at a distance of $\Delta_2 \approx 1$ MeV above the lower of the fission channels (the channel 0^+) there begin to be channels corresponding to single-frequency excitations, which, generally speaking, may have any characteristics, including 0^- and 1^+ .

3. For the mean fission width of the states with spin J and parity Π , we have the Bohr-Wheeler formula:

$$\bar{\Gamma}_f^{J, \Pi} = \frac{\bar{D}^{J, \Pi}}{2\pi} \sum_{i=1}^v P(E_f^{(i)}, E_{curv}^{(i)}, E), \quad (1)$$

where $\bar{D}^{J, \Pi}$ is the mean distance between the levels of the compound nucleus, i is the number of the fission channels, and P is the penetrability of the barrier for the i -th channel, which is given by the expression [1]:

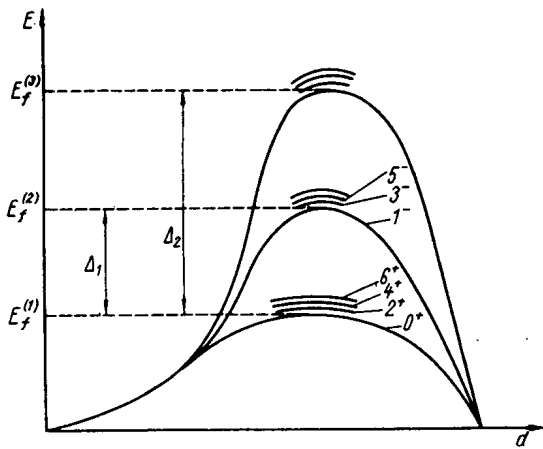


Fig. 1. Schematic representation of the structure of the fission channels corresponding to A. Bohr's hypothesis.

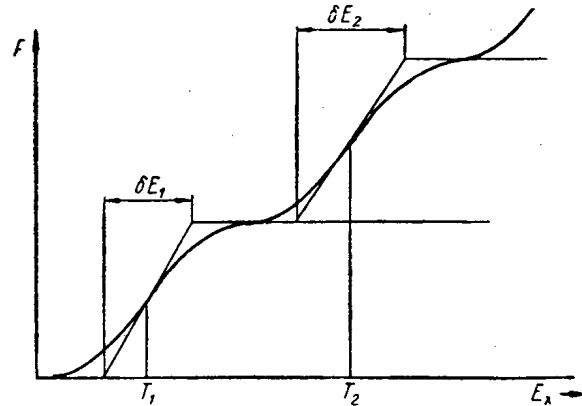


Fig. 2. Schematic representation of the fission curves in the (d, pf) reaction, as found in [4].

Values of the Parameters $E_f^{(1)}$, $E_f^{(2)}$, $E_{curv}^{(1)}$, and $E_{curv}^{(2)}$, Determined from the Data Found in Different Reactions, MeV

Compound nucleus	$E_f^{(1)}$	$E_{curv}^{(1)}$	$E_f^{(2)}$	$E_{curv}^{(2)}$	B_n
Th ²³²	5,7 (γ, f)	0,41 (γ, f)	6,4 (γ, f)	0,68 (γ, f)	6,4
U ²³⁴	5,5 (d, pf)	0,45 (d, pf)	6,2 (d, pf)	0,45 (d, pf)	6,8
U ²³⁶	6,0 (d, pf)	0,58 (d, pf)	6,4 (γ, f)	—	6,4
U ²³⁸	6,0 (γ, f)	0,68 (γ, f)	6,6 (n, f)	—	6,0
Pu ²⁴⁰	5,0 (d, pf)	0,31 (d, pf)	6,6 (γ, f)	0,38 (d, pf)	6,4
Pu ²⁴²	~ 6,0 (n, f)	—	5,8 (d, pf)	—	6,4

$$P(E_f^{(i)}, E_{curv}^{(i)}, E) = \frac{1}{1 + \exp \frac{2\pi(E_f^{(i)} - E)}{E_{curv}^{(i)}}} \quad (2)$$

Equation (1) is used to find the characteristics of the fission channels.

The (d, pf) Reaction

In [4], using the (d, pf) reaction, curves were obtained for the fissionability of the compound nuclei U²³⁴, U²³⁶, and Pu²⁴⁰ below the neutron binding energy in the corresponding nucleus. The curves have the characteristic form shown in Fig. 2. Below the neutron emission threshold, the only process competing with fission is emission of γ-quanta, so that the fissionability measured in [4] is expressed by the formula:

$$F = \frac{\sigma_{d, pf}}{\sigma_{d, p}} = \sum_{J, \Pi} \left\langle \frac{\Gamma_f^{J, \Pi}}{\Gamma_f^{J, \Pi} + \Gamma_\gamma^{J, \Pi}} \right\rangle \sigma_{d, p}^{J, \Pi} \frac{1}{\sum_{J, \Pi} \sigma_{d, p}^{J, \Pi}} \quad (3)$$

where $\sigma_{d, p}^{J, \Pi}$ is the mean cross-section for the formation of a compound nucleus with spin J and parity Π in the d, p reaction, and the partial mean fissionability is obtained by averaging over the distribution of fission widths and is equal to:

$$\left\langle \frac{\Gamma_f^{J, \Pi}}{\Gamma_f^{J, \Pi} + \Gamma_\gamma^{J, \Pi}} \right\rangle = \frac{1}{1 + \alpha} S(\alpha) \quad (4)$$

Here, $\alpha = \frac{\bar{\Gamma}_f^{J, \Pi}}{\bar{\Gamma}_\gamma^{J, \Pi}}$, and $S(\alpha)$ is the "fluctuation function" (see below). It follows from Eqs. (1)-(3) that the fissionability curve will have the characteristic step form observed in the experiment, for one of the following two cases:

A. If $\bar{\Gamma}_f \ll \bar{\Gamma}_\gamma$, even for $P = 1$ (i. e., on the plateau), the quantity $\bar{\Gamma}_f$ may be neglected in comparison with $\bar{\Gamma}_\gamma$ in the denominator. Since $\bar{\Gamma}_\gamma$ is only very slightly dependent on the energy, the fissionability will be simply proportional to the fission width, and hence to the penetrability. On the plateau, the fissionability takes the value:

$$F^{\text{plateau } J, \Pi} = \sigma_{d, p}^{J, \Pi} \frac{\bar{\Gamma}_f^{\text{plateau } J, \Pi}}{\bar{\Gamma}_\gamma} \sigma_{d, p}^{-1} \quad (5)$$

if $\bar{\Gamma}_f^{J, \Pi} = \bar{\Gamma}_f^{\text{plateau } J, \Pi}$.

B. If, at some energy, the mean fission width is comparable with the radiation width, and continues to increase more rapidly, then, for $\bar{\Gamma}_f \gg \bar{\Gamma}_\gamma$, the fissionability at the plateau is given by the ratio:

$$F^{\text{plateau } J, \Pi} = \frac{\sigma_{d, p}^{J, \Pi}}{\sigma_{d, p}} \quad (6)$$

If, for the same energy, there are barriers for several combinations of the moment and the parity, Eqs. (5) and (6) must be summed over all such combinations.

Assumption A is used in [4], from which it follows that the threshold value of the energy coincides with T (see Fig. 2), — the point on the energy axis where $F = (1/2)F^{\text{plateau}}$. The parameter $E_{\text{curv}} = (\pi/2)\delta E = \pi/2S$ [here S is the slope of the curve $F'(E) = F(E)/F^{\text{plateau}}$ at the point where $F' = 1/2$].

For this interpretation to be correct, it is necessary for the value of $\bar{\Gamma}_f$, with a penetrability equal to unity, to be several times less than $\bar{\Gamma}_\gamma$ for the energy corresponding to going out onto the first plateau. The width $\bar{\Gamma}_\gamma$ for $E = B_n$ is 30-40 MeV for all fissioning elements. Even if it is assumed that this value does not decrease for an increase of 1 MeV in the excitation energy, for Pu^{240} , with $E = 4.9$ MeV, we should have $\bar{\Gamma}_f \approx 5$ MeV. When using the expression for the level density based on the Fermi gas model:

$$\rho(E, J) = \rho(E) \frac{2J+1}{2\sqrt{2\pi}\sigma^3} \exp \times \left[-\frac{\left(J + \frac{1}{2}\right)^{1/2}}{2\sigma^2} \right], \quad (7)$$

where

$$\rho(E) = \frac{\sqrt{\pi}}{12(a)^{1/4}(E')^{5/4}} \exp[2(aE')^{1/2}] \quad (7')$$

[here $E' = E - \Delta$ (the parameters σ , a , and Δ were found by A. V. Malyshev from a comparison with the experimental data for $E = B_n$)], calculation from Eq. (1) gives a hundred times greater values. Accordingly, we shall try to analyze the experimental data, starting with the assumption B, and using Eqs. (1)-(7).

According to assumption B, the fissionability reaches half its value at the plateau for $T < E_f$. We shall find how the experimental values of the quantities T and δE are related to E_f and E_{curv} in this case. Making the natural assumption that in subbarrier fission a role is being played by only one lower channel (for fixed values of J and Π), and that the distribution of fission widths is described accordingly by χ^2 , the distribution with one degree of freedom [5], we find that in our case F' is equal to the mean partial fissionability:

$$F' = \frac{1}{1+\alpha} S(\alpha), \quad (8)$$

and

$$S_1(\alpha) = (1+\alpha) \left(\frac{\alpha}{2\pi}\right)^{1/2} \int_0^\infty \frac{x^{1/2}}{1+x} e^{-dx/2} dx \quad (9)$$

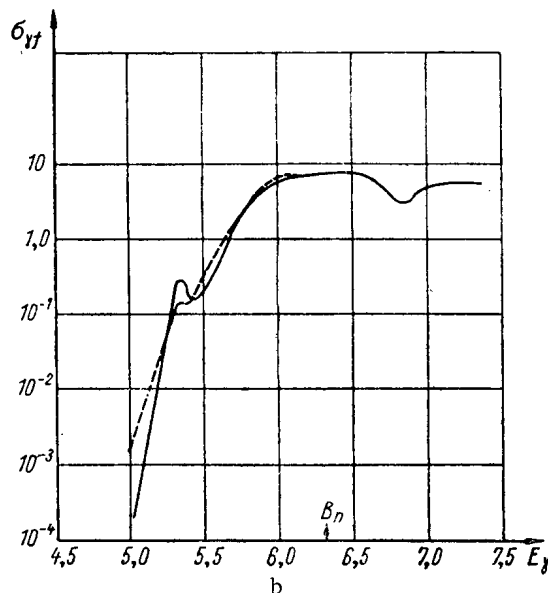
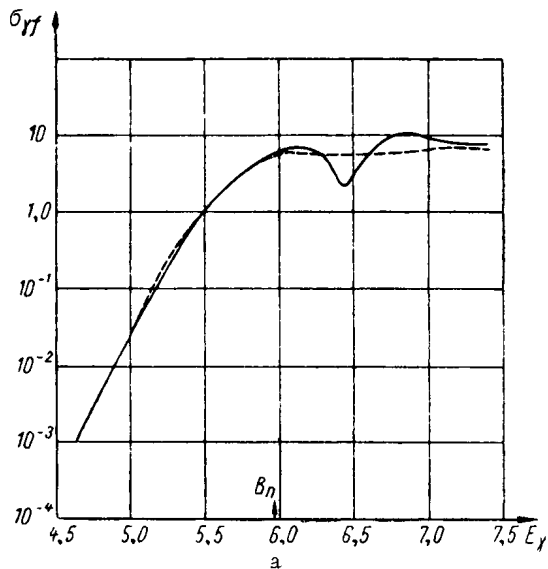


Fig. 3. Energy dependence of the photofission cross-sections of U^{238} (a) and Th^{232} (b).

found in the preliminary calculations which were made in [7] neglecting the fluctuations in the fission widths.

Since, in the (d, pf) reaction, for a deuteron energy of 14 MeV, the neutrons captured by the target nucleus can have a considerable orbital moment, the compound nucleus is formed in states with all possible combinations of spin and parity. According to our assumptions, the plateau on the fissionability curve first shows up for $\bar{\Gamma}_f \gg \bar{\Gamma}_\gamma$. Accordingly, the subsequent rise in fissionability cannot be accounted for by further increase in the fission width, i. e., by opening up of new fission channels for compound nuclei, the fission probability of which was already very large. The second rise accordingly means that at an excitation energy corresponding to the beginning of the first plateau, for a considerable, and possibly even greater part of the compound nuclei, fission is still strongly prohibited [there are at least two groups of combinations of the spin and parity of the compound nucleus for which the thresholds are equal respectively to $E_f^{(1)}$ and $E_f^{(2)}$ (see table)], i. e., they differ by approximately 0.6-0.8 MeV. This is also shown by the fact the value of the fissionability F at the first plateau is considerably less than unity. However, it is impossible to make a direct identification of the value of the fissionability at the first plateau with the

is the "fluctuation function" for the one-channel distribution, as found in [6]. Differentiating (8) with respect to the energy, using (1), (2), and (9), and assuming that the level density and the radiation width change slowly with increase in energy in comparison with the rapid increase in the fission width, we obtain:

$$\frac{\partial F'}{\partial E} = -\frac{\pi}{E_{\text{curv}}} [S(\alpha) - 1]. \quad (10)$$

For $F' = 1/2$, the solution of the transcendental Eq. (8) in α gives the values $\alpha^* = 0.37$ and $S(\alpha^*) = 0.675$. Substituting the experimental values $\left. \frac{\partial F'}{\partial E} \right|_{F' = \frac{1}{2}} = \frac{1}{\delta E}$ in the left-hand side of (10) and $\alpha = \alpha^*$ in the right-hand side gives the following relation between δE and E_{curv} :

$$E_{\text{curv}} = \pi \delta E \cdot 0,325 \approx \delta E. \quad (11)$$

This shows that according to our analysis, the values of E_{curv} are a factor of 1.5 less than those found by the authors of [4] when using assumption A. It should be noted that when making calculations from formula (11) it is possible to use the values of δE given in [4], since the fissionability curves in assumptions A and B, but with different values of E_{curv} , are very nearly the same, and the finite energy resolution changes them in the same way.

To calculate E_f , we use the condition:

$$\alpha^* = \alpha(T) = \frac{\bar{\Gamma}_\gamma}{\bar{\Gamma}_f(T)}. \quad (12)$$

Applying Eqs. (1) and (7) we obtain:

$$E_f = T + \frac{E_{\text{curv}}}{2\pi} \ln \left[\frac{\alpha_0}{2\pi Q(T)} - 1 \right]. \quad (13)$$

The results of the calculations made by Eqs. (11) and (13) are given in the table. The values found for the "threshold shift" $E_f - T$ are approximately a factor of 1.5 less than those

fraction of the compound nuclei that fission through the lower barrier, since the height of the plateau may depend on the spin of the target nucleus, as well as because of the possibility of an effect being exerted on this quantity by anisotropy in the angular distributions of the protons and fragments. This last fact is also pointed out by the authors of [4].

If it is assumed that Δ_1 (see above) is several hundred kiloelectronvolts, the second rise in the fissionability curve corresponds to fission of compound nuclei with negative parity. The consequences of this assumption may be compared with the experimental data on photofission, and fission by resonance neutrons.

Photofission

The energy dependence of the photofission thresholds and the angular distributions of the fragments have been investigated by many authors both with monochromatic γ -rays [8-10], and with a bremsstrahlung spectrum [11, 12]. Those that have been best studied are the nuclei Th^{232} and U^{238} . In heavy nuclei, γ -quanta with an energy of 5-7 MeV experience only electric dipole and quadrupole absorption, which leads, for even-even target nuclei, to the formation of compound nuclei in the states 1^- and 2^+ . The photofission cross section is equal to

$$\sigma_{\gamma, f} = \sigma_{\gamma}^{(2+)} \left\langle \frac{\Gamma_f^{2+}}{\Gamma_f^{2+} + \Gamma_c} \right\rangle + \sigma_{\gamma}^{(1-)} \left\langle \frac{\Gamma_f^{1-}}{\Gamma_f^{1-} + \Gamma_c} \right\rangle, \quad (14)$$

where $\sigma_{\gamma}^{(2+)}$ and $\sigma_{\gamma}^{(1-)}$ are the cross-sections for quadrupole and dipole photoabsorption respectively, and Γ_c is the total width of the decay processes, competing with fission. Below the (γ, n) reaction threshold, we have $\Gamma_{\gamma} = \Gamma_c$. From general considerations, the dipole absorption cross section will be considerably greater than the quadrupole cross section. If this is true, then, for a large difference between the thresholds in favor of quadrupole photofission, the curve giving the energy dependence of the photofission cross section, with the ordinates plotted to a logarithmic scale, should be qualitatively a straight line with the slope $2\pi/E_{\text{curv}}^{(1)}$ for $E < E_f^{(1)}$, and a straight line with the slope $2\pi/E_{\text{curv}}^{(2)}$ for $E_f^{(1)} < E_{\gamma} < E_f^{(2)}$. The change in slope occurs at the point where the quadrupole photofission cross section reaches saturation, i. e., for $\bar{\Gamma}_f^{(2+)} = \bar{\Gamma}_{\gamma}$. Since, qualitatively, the curvature at the peak and hence the corresponding value of E_{curv} will be greater for a higher barrier, the above change in slope will be in the direction of a decrease. Experimental curves for Th^{232} and U^{238} , taken from [12], are shown in Fig. 3. It may be seen that the form of the curves is qualitatively in complete agreement with our assumptions, especially for Th^{232} , in which the two linear segments are clearly visible. The values of $E_{\text{curv}}^{(1)}$ for both nuclei may be found directly from the slope, and are equal to 0.41 for Th^{232} , and 0.68 for U^{238} . If it is assumed that $\bar{\Gamma}_{\gamma} \approx \bar{\Gamma}_{\gamma}$ at the break point, Eq. (13) may be used to find the values of the quadrupole photofission thresholds. They are equal to 5.7 and 6.0 MeV respectively. For Th^{232} , it may also be found that $E_{\text{curv}}^{(2)} = 0.68$ MeV. To find the position of the second threshold, it is necessary to know the total cross section for dipole absorption of γ -quanta in this energy range. A lower limit for this quantity may be found if it is assumed that the photofission cross sections reach saturation at $E_{\gamma} = B_n$. Then:

$$\sigma_{\gamma}^{(1-)} + \sigma_{\gamma}^{(2+)} = \sigma_{\gamma f}(B_n). \quad (15)$$

It is known from the experiments of [8] on the angular distribution of the photofission fragments that at $E_{\gamma} = 6.14$ MeV for U^{238} , fission through the 2^+ channel makes up about 20% of the total photofission cross section. Judging from the curves in Fig. 3, the contribution from quadrupole fission in Th^{232} is even less. Then, using Eq. (15), and assuming that the photoabsorption cross section changes only slightly as E_{γ} changes by several hundred kiloelectronvolts, it is possible to construct a curve for the fissionability through the 1^- channel in the range $E_{\gamma} = 5.5$ -6 MeV, and determine $E_f^{(2)}$ by means of Eq. (13). The results are given in the table.

It should be noted that the contribution made by the quadrupole component to the angular distribution of the photofission fragments was first observed in [11], while making measurements with a bremsstrahlung spectrum with the limiting energy $E_{\gamma} = 9.3$ MeV, and was found to be equal to 10%. If our values for the partial photofission cross sections are averaged over a bremsstrahlung spectrum of this type, we get precisely the ratio $\sigma_{\gamma f}^{2+}/\sigma_{\gamma f}^{1-} \approx 10\%$. For U^{234} and U^{236} nuclei, the photofission cross section has been measured in [10] with monochromatic γ -radiation at only the two points: $E_{\gamma} = 6.14$ MeV and $E_{\gamma} = 7.0$ MeV. For U^{234} , $\sigma_{\gamma f}(6.14) = 5_{-2}^{+10}$ mbarn and $\sigma_{\gamma f}(7.0) = 52 \pm 16$ mbarn. The second point already lies higher than the binding energy of the neutron, and no definite conclusion can be drawn as to the position of the threshold of the channel 1^- .

Our assumptions as to the mutual location of the 1^- and 2^+ thresholds lead to certain conclusions for which there are not sufficient experimental data to check. Thus, for example, for $E_\gamma < E_f^{(1)}$, as we get further down into the subbarrier region, the angular distribution of the fission fragments shows an ever increasing role being played by the quadrupole component, observation of which requires measuring the fragment yields at an angle of 45° to the beam of γ -quanta as well as at the angles 0 and 90° . This has been pointed out in [18].

Fission by Resonance Neutrons

Experimental data are known which may be used to make a direct check of the Bohr-Wheeler formula. These are the results of experiments on the resonance structure of the neutron cross sections. Such data exist for the four fissionable nuclei U^{233} , U^{235} , Pu^{239} , and Pu^{241} .

Several of the first resonances in each of the above isotopes are divided by multilevel analysis into two groups with different spins, and, for each group, the mean values are found of the distances between levels \bar{D}^J , and of the fission widths. If the Bohr-Wheeler formula (1) is correct, the "effective number of channels:"

$$\nu_{\text{eff}}^{J,\pi} = \sum_{i=1}^{\nu} P_i(E_i; E) = \frac{2\pi \bar{\Gamma}_f^{J,\pi}}{\bar{D}^J, \pi} \quad (16)$$

may be expressed in terms of the quantities observed experimentally. We shall now verify whether or not the values of ν_{eff} obtained in this way for different nuclei agree with our assumptions as to the structure of the fission channels.

1. $U^{233} + n$. Ground state $5^+/2$. Accordingly, the resonances correspond to the levels 2^+ and 3^+ of U^{234} . If the nucleus is axially symmetric at the saddle point, the rotation band of positive parity, which, according to our assumptions corresponds to the lower fission channel, contains only the level 2^+ , while the level 3^+ is a single particle level. The lower fission threshold of U^{234} (see table) lies more than 1 MeV below the neutron binding energy. At $E = B_n$, the one particle channels will already be making a contribution, and, hence, $\nu_{\text{eff}}^{2^+} > \nu_{\text{eff}}^{3^+} \approx 1$. The experimental values calculated from our papers [13, 14] are $\nu_{\text{eff}}^{2^+} \approx 2$ and $\nu_{\text{eff}}^{3^+} \approx 0.7$.

2. $U^{235} + n$. The ground state of U^{235} is $7^-/2$, and the compound nucleus fissions from the states 3^- and 4^- . In U^{236} , only the position of the first threshold is known, which lies approximately 0.4 MeV below the neutron binding energy (see table). The rotation band of negative parity, which contains the level 3^- , will lie 0.6–0.8 MeV above the lower threshold, i. e., in the vicinity of $E = B_n$. Also near B_n , several hundred kiloelectronvolts higher, will be the first channels corresponding to single-particle excitations. Accordingly, the relation $\nu_{\text{eff}}^{4^-} < \nu_{\text{eff}}^{3^-} \leq 1$ will be approximately satisfied. According to the results of [15], the values of ν_{eff} are equal to 0.6 and 0.15 for the two systems of resonances. The values of the spins in these groups have not been determined experimentally. It may be seen that our assumptions will give better agreement with the experimental data if it is assumed that the levels with the larger fission width have spin 3.

3. $Pu^{241} + n$. Ground state of Pu^{241} , $5^+/2$. The fission widths have only been measured for nine resonances [16], and the position of the fission thresholds is unknown. The values of ν_{eff} are equal approximately to 1.5 and 0.2. If all our assumptions are correct, this means that the broad resonances correspond to $J = 2$, while the narrow resonances correspond to $J = 3$, and the threshold of the lower channel is located approximately 0.5 MeV below the neutron binding energy. A study of the (d, pf) reaction in the Pu^{241} nucleus is of particular interest in this respect.

4. $Pu^{239} + n$. Ground state $1^+/2$. The mean distance between resonances is $\bar{D} = 2.9$ eV, which corresponds to $\bar{D}^{0^+} = 11.6$ eV, $\bar{D}^{1^+} = 3.9$ eV. According to the most recent measurements [15], $\bar{\Gamma}_f^{0^+} \approx 40$ MeV, $\bar{\Gamma}_f^{1^+} \approx 160$ MeV, and, hence, $\nu_{\text{eff}}^{0^+} = 0.26$, $\nu_{\text{eff}}^{1^+} = 0.02$. Thus, the assumptions as to the structure of the fission channels, which, in other cases, are in complete agreement with experimental data, here lead to an error of two orders of magnitude. This inconsistency may be removed if it is assumed that the ground state of the Pu^{239} nucleus has negative parity. There is no 0^- level in rotation bands of negative parity, and the channel corresponding to it is necessarily a single-particle one. If it lies approximately 2.0 MeV above the lower threshold, this will give the small penetrability observed. The fluctuations in the fission widths of the Pu^{239} resonances are well described by the one-channel Porter-Thomas distribution [5]. This also shows that the threshold for fission of Pu^{239} by S-neutrons is located high.

In [17], a systematic scheme was proposed for the parities of the ground states of α -active nuclei. The positive parity of Pu^{239} is one of the very few places where the scheme differs from the experimental data.

CONCLUSIONS

It has been assumed in this paper that the Bohr-Wheeler formula (1) gives an order of magnitude description of the mean fission width. In analyzing the data on the (d, pf) reaction, it follows unambiguously from this assumption that, first, there are at least two sets of combinations of spin and parity of a fissionable nucleus for which the fission thresholds differ by 0.6–0.8 MeV, and, second, these thresholds are located higher than had previously been assumed. The data on the (γ, f) reaction were analyzed under the additional assumption that the photoabsorption cross section is only slightly dependent on the energy in intervals of the order of 1 MeV, as compared with the exponential increase in the fission width in the range $E_\gamma = 5-7$ MeV. Our treatment also leads to appreciably higher values of the photofission thresholds than those accepted up to the present time, with the fission barrier in quadrupole photoabsorption located 0.6–1.0 MeV below the dipole photofission barrier. In comparing the results of analyzing the (d, pf) and (γ, f) reactions, it is natural to assume that the first rise in fissionability in the (d, pf) reaction corresponds to channels with positive parity, while the second corresponds to channels with negative parity. All these conclusions are in agreement with A. Bohr's hypothesis as to the structure of the fission channels of even-even nuclei, if the distance between the rotation bands of positive and negative parity is $\Delta_1 \approx 0.6-1.0$ MeV.

In accordance with the results of treating the (d, pf) and (γ, f) reactions, and within the framework of A. Bohr's hypothesis, a distribution of the fission channels may be given for which the Bohr-Wheeler formula gives a quantitative description of the experimental data on the mean fission widths of the resonances of the (n, f) reaction, except for the data on the Pu^{239} nucleus. To get rid of the large difference noted in this last case, it must be assumed that the ground state of the Pu^{239} nucleus has negative parity.

LITERATURE CITED

1. D. Hill and J. Wheeler, *Phys. Rev.*, **89**, 1102 (1953).
2. N. Bohr and J. Wheeler, *Phys. Rev.*, **56**, 426 (1939).
3. A. Bohr, In the book: "Materials from the International Conference on the Peaceful Uses of Atomic Energy (Geneva, 1955)," Vol. 2 [Russian translation], Moscow, Fizmatgiz (1958), p. 176.
4. J. Northrop, R. Stokes, and K. Bayer, *Phys. Rev.*, **115**, 1227 (1959).
5. C. Porter and R. Thomas, *Phys. Rev.*, **104**, 483 (1956).
6. A. Lane and J. Lynn, *Proc. Phys. Soc.*, **70**, 557 (1957).
7. L. N. Usachev, V. A. Pavlinchuk, and N. S. Rabotnov, *ZhÉTF*, **44**, 1950 (1963).
8. B. Forkman and S. Tohansson, *Nucl. Phys.*, **20**, 136 (1960).
9. H. De Carvalho, A. Manfredini, and M. Muchnik, *Nuovo Cimento*, **25**, 136 (1960).
10. J. Huizenqa et al., *Nucl. Phys.*, **34**, 439 (1962).
11. A. I. Baz' et al., In the book: "Transactions of the Second International Conference on the Peaceful Uses of Atomic Energy," Papers presented by Soviet scientists, Vol. 1 [in Russian], Moscow, Atomizdat (1959), p. 362.
12. L. Catz, A. Baerg, and F. Brown, P/200, Proc. of II-d UN Conference on PUAE (Geneva, 1958), Vol. 15 (1958), p. 183.
13. C. Reich and M. Moore, *Phys. Rev.*, **118**, 718 (1960).
14. E. Vogt, *Phys. Rev.*, **118**, 724 (1960).
15. I. V. Kirpichnikov et al., "Atomnaya Énergiya," **16**, 110 (1964).
16. A. Simpson and M. Moore, *Phys. Rev.*, **123**, 559 (1961).
17. V. N. Andreev, *ZhÉTF*, **42**, 913 (1962).
18. J. Griffin, *Phys. Rev.*, **116**, 107 (1959).

NEUTRON ANGULAR AND ENERGY DISTRIBUTION
AT THE BOUNDARY OF TWO MEDIA

(UDC 539.125.52)

V. A. Dulin, V. G. Dvukhshestnov, Yu. A. Kazanskii,
and I. V. Shugar

Translated from *Atomnaya Énergiya*, Vol. 17, No. 6,
pp. 486-492, December, 1964

Original article submitted August 8, 1963; in revised form, July 2, 1964

Measurements were made of the angular and energy distributions for fast neutrons (0.4-3.4 MeV) emerging from water, graphite, aluminum, iron, nickel, and lead at a water-medium interface after penetration of thicknesses equalling 1.5-4.6 mean free paths. The reaction $D(D, n)He^3$ was the neutron source. Measurements were made with a single-crystal fast neutron scintillation spectrometer having γ -ray discrimination. The results of the measurements are compared with calculations.

The most complete characterization of a neutron flux in a medium is the angular and energy distribution. An exact solution of the transport equation for the purpose of defining this characterization is fraught with great difficulty. Approximate methods require experimental verification, and all the more so if the system of constants is not complete. Combined experiments are of interest since they furnish recommendations which are important for practical shielding construction; in addition, they can serve as criteria for the correctness of a selected approximate method, and, finally, they enable one to refine the system of constants.

The intensities of existing monoenergetic sources and the efficiencies of fast neutron spectrometers were unsatisfactory, until recently, for detailed studies of the neutron flux in materials. High-efficiency neutron detectors [1, 2] have made it possible to carry out measurements of angular and energy distributions for the case of a point isotropic, 3.2 MeV source at distances of 1.5-4.6 mean free paths and in the angular range $20-70^\circ$. This work is a continuation of work started in [3].

Experimental Arrangement

A cascade neutron generator was the neutron source. Deuterons with an energy of 400 keV were incident on a Zr-D target 200 keV thick, and thus there were neutrons with energies of 3.08-3.4 MeV along the deuteron beam. A diagram of the experimental apparatus is shown in Fig. 1. Selection of a neutron beam at a definite angle was accomplished by using a conical collimator with an angular resolution of $\sim 8^\circ$. In order that neutrons which emerged from the experimental material in the vicinity of point A in the 0° direction not be scattered in water, there was an air space at the boundary. The neutron background was recorded with a collimator filled with water. About 1% boric acid was added to the water, and the spectrometer was enclosed on the end and sides with a 1.5 cm thick layer of lead. In this way, the ratio

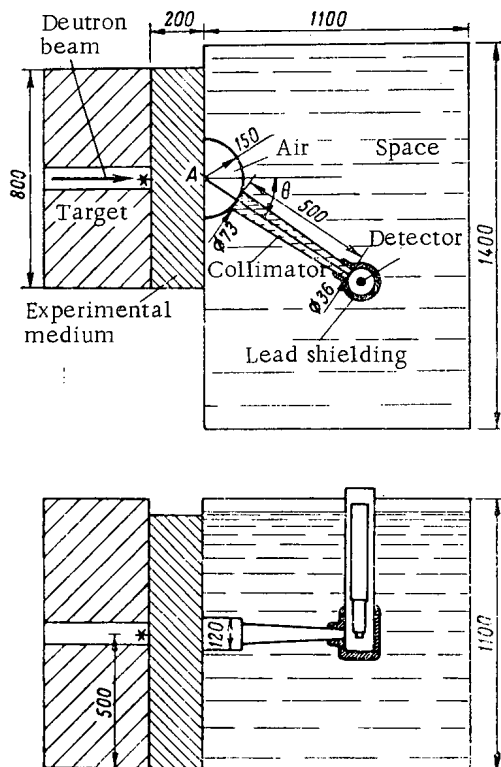


Fig. 1. Diagram of experimental apparatus.

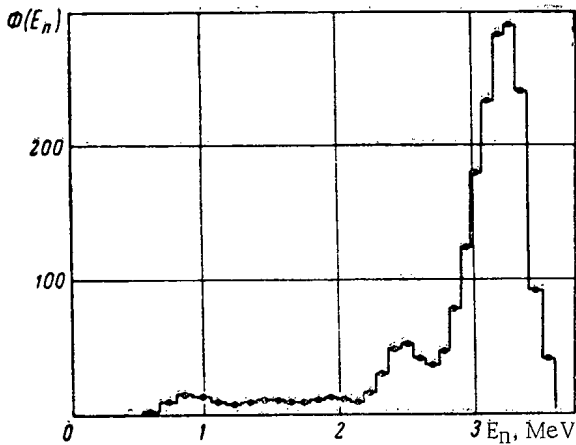


Fig. 2. Neutron energy distribution at 0° with no experimental medium.

pulse height distribution was measured with a one hundred channel analyzer. The energy scale of the spectrometer was set, and periodically checked, by measurements of the pulse height distribution at the 0° angle. Instrumental stability (chiefly that of the photomultiplier) was 2-3% during the course of all the measurements. The pulse height distribution was measured three to five times at each angle.

Conversion of the pulse height distributions to energy spectra was carried out by means of the formula

$$\Phi(E_n) = - \frac{E_n}{1 - \exp[-\Sigma(E_n)d]} \cdot \frac{dV}{dE} \times \frac{d}{dV} \left[N(V) \frac{dV}{dE} \right], \quad (1)$$

where $\Sigma(E_n)$ is the macroscopic neutron scattering cross section of hydrogen in the crystal; d is the crystal thickness; dV/dE is the derivative of pulse height with respect to energy.

Thus the analysis of results was reduced to a multiplication of the measured pulse height distribution $N(V)$ by dV/dE (each channel), differentiation with respect to the pulse height scale by the "sliding zone" method, followed by multiplication by dV/dE and correction for detection efficiency. It has been shown that differentiation by the sliding zone method makes it possible to use reasonably small steps (~ 70 keV), and this does not lead to "oscillation" of the results.

As is well known, differentiation of the instrumental spectrum is not a rigorous method of analysis since the shape of the line from the crystal differs from a "plateau" (dE/E_n). However, as V. G. Zolotukhin has shown, this is unimportant for continuous spectra even when working with crystals of large diameters. Results which were obtained by the method described for the neutron spectrum at 0° with no experimental medium are shown in Fig. 2. It is apparent that there is a weak maximum in the spectrum at ~ 2.5 MeV which is principally the result of not considering the actual shape of the line from the crystal.

Discussion of Results

Fast Neutron Angular and Energy Distributions. Fig. 3 gives the experimentally obtained neutron energy distributions at angles of 20, 40, and 70° , and Fig. 4 gives the angular distributions for neutrons in the energy groups 0.4-1.2, 1.2-2.0, 2.0-2.8, and 2.8-3.4 MeV after penetrating layers of water ($3.3 \lambda_T$), graphite ($3.3 \lambda_T$), aluminum ($1.5 \lambda_T$), iron (3.0 and $4.6 \lambda_T$), nickel (2 and $4 \lambda_T$), and lead ($3 \lambda_T$). All thicknesses are given in mean free paths for 3.4 MeV neutrons. It is clear from the figure that the shape of the energy spectrum varies irregularly in all media. But in every case except that of water, the elastic scattering peak appears rather clearly (in iron, a peak caused by inelastic scattering appears), and softening of the spectrum with increasing angle is observed. To a first approximation, the dependence of the energy groups on angle is the same for all media. The length of path also has little effect on the angular dependence of the energy groups.

In Fig. 5, the angular distributions for the 2.8-3.4 MeV group are shown along with results from a single-scattering approximate calculation which was done with isotropic, and actual anisotropic, scattering cross sections.

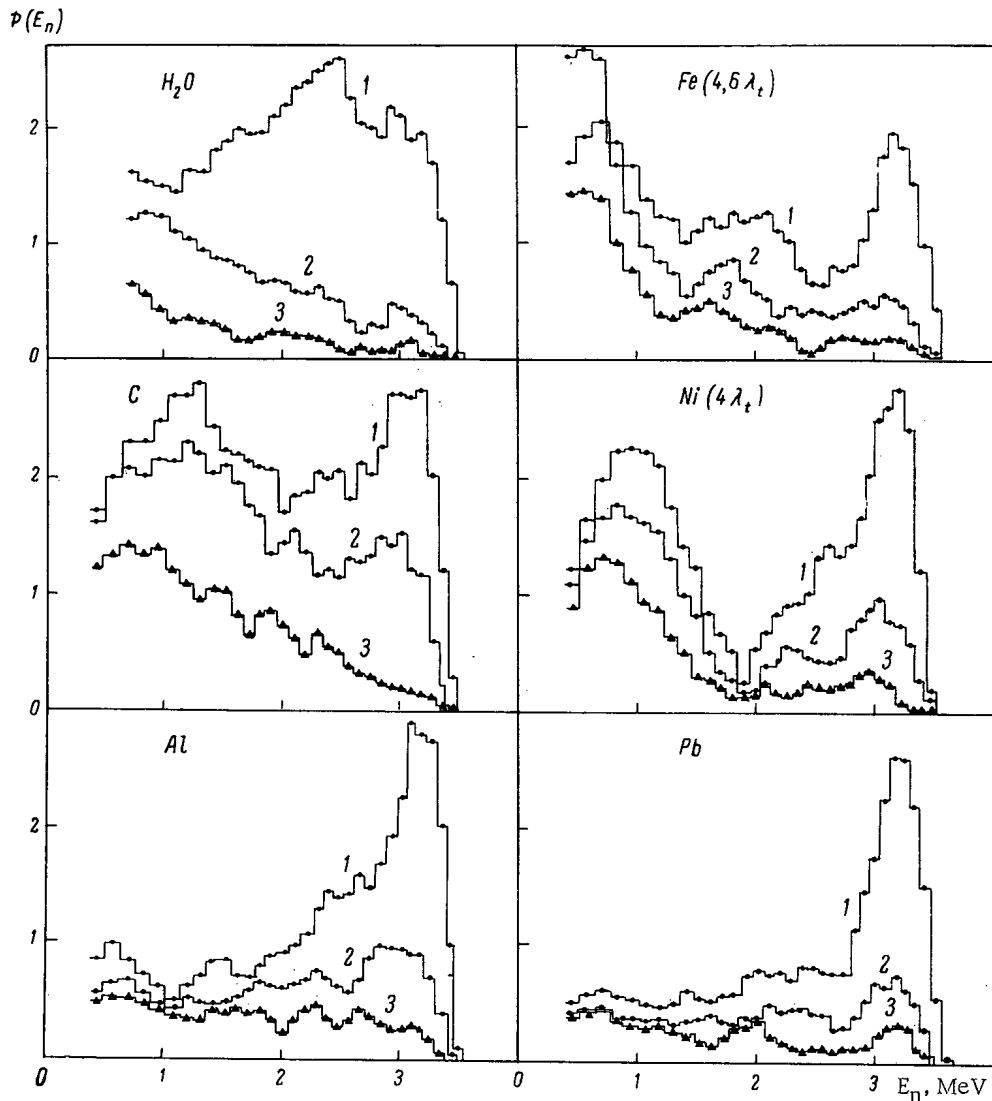


Fig. 3. Neutron energy distributions in water, graphite, aluminum, iron, nickel, and lead at angles of: 1) 20°; 2) 40°; 3) 70°.

The experimental and calculated angular distributions were multiplied by $\sin \theta$. The disagreement between experiment and theory for the 2.8-3.4 MeV group indicates the importance of the role of multiple scattering.

For practical purposes, the angular distribution of neutron dose can be extremely useful. The angular distribution of dose for neutrons with energies of 0.4-3.4 MeV multiplied by $\sin \theta$, i. e., $\sin \theta \int_{0.4}^{3.4} \Phi(E, \theta) D(E) dE$ is shown in Fig. 6.

The dependence of dose on energy $D(E)$ was taken from [6]. Data for the angles 0-20° can be obtained from single-scattering approximate calculations for the 2.8-3.4 MeV group and by means of extrapolation for the remaining energy groups. As can be seen from Fig. 6, the magnitude of the dose in the range 20-70° for all media except water depends slightly on angle, and can be described by the formula

$$D(\theta) \sim \frac{1}{\sin \theta} \exp\left(-\frac{\theta}{\theta_0}\right), \quad (2)$$

where $2\pi/3 \leq \theta_0 \leq 2\pi$. For water, the dose dependence on angle is close to that for γ -rays [7] ($\theta_0 \approx \pi/4$).

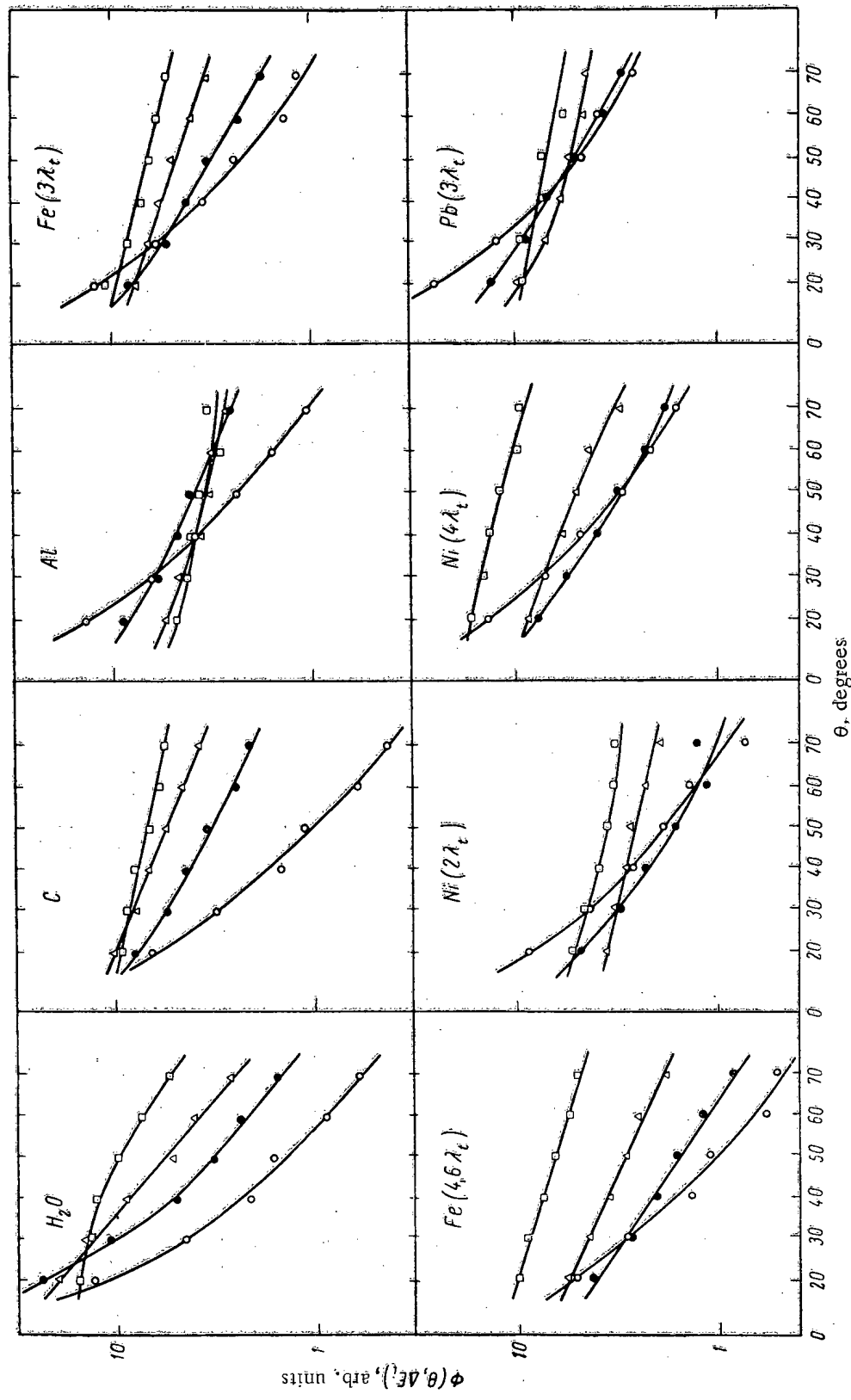


Fig. 4. Neutron angular distributions in water, graphite, aluminum, iron, nickel, and lead per unit solid angle for the energy groups: \circ) 2.8-3.4 MeV; \bullet) 2.0-2.8 MeV; Δ) 1.2-2.0 MeV; \square) 0.4-1.2 MeV.

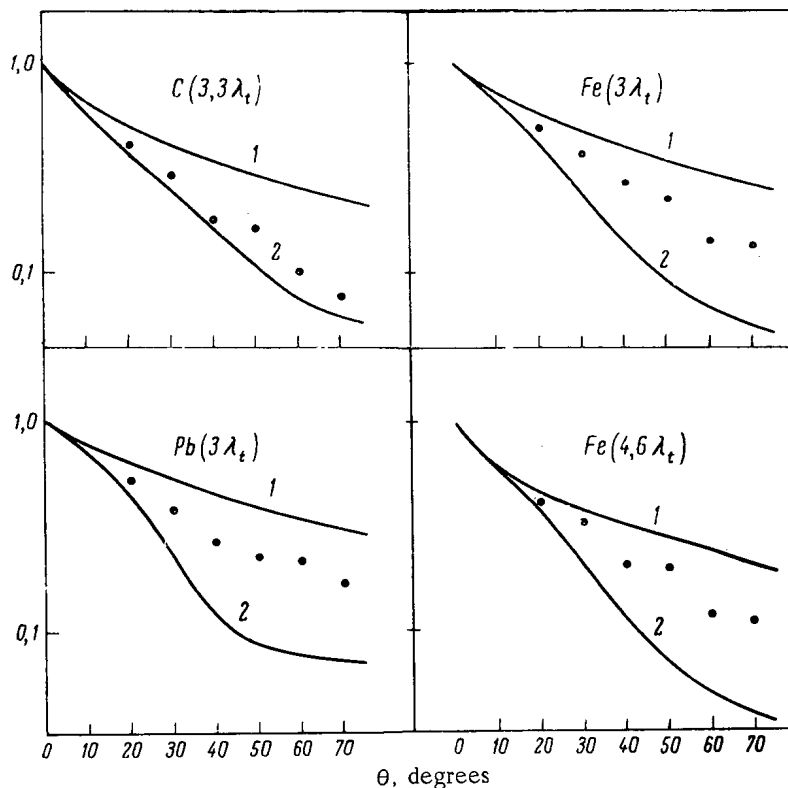


Fig. 5. Angular distribution of the 2.8-3.4 MeV group for graphite, lead, and iron in the solid angle $d\Omega$: 1) single-scatter approximate calculation assuming isotropic differential scattering cross section; 2) single-scattering approximate calculation using actual differential scattering cross sections for neutrons with energies close to 3.4 MeV.

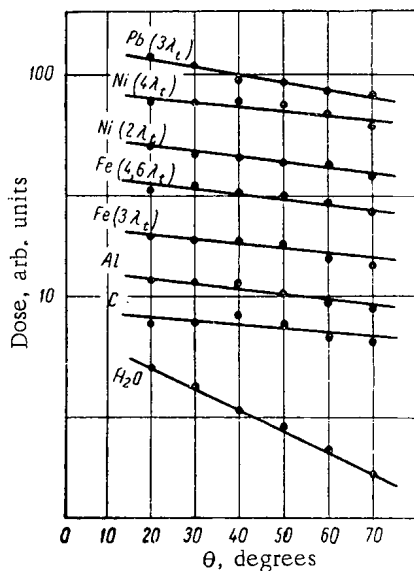


Fig. 6. Angular distribution of dose in the solid angle $d\Omega$ for 0.4-3.4 MeV neutrons.

Fast Neutron Energy Distributions

The fast neutron energy distributions at the boundary of two media $\Phi(E_0, E, R)$ are not only of interest in themselves, but also may be used for checking the angular energy distributions obtained. In Fig. 7, there are shown neutron energy distributions both measured at the water-medium boundary (in the space A) and obtained by integration of angular energy distributions. Extension of the results to the region of angles greater than 70° was obtained by exponential extrapolation. Extrapolation into the range of angles $0-20^\circ$ for the 2.8-3.4 MeV group was made in accordance with the results from a single-scatter approximate calculation. The energy distribution of neutrons in the space A is the sum of scattered and unscattered radiation. The integral over angle only takes into account scattered radiation. Measurement of the energy distribution at 0° makes it possible to determine the contribution of unscattered radiation. The satisfactory agreement between measured spectra and the spectra obtained by integration indicates that the choice of exponential extrapolation was a good one and apparently one that reflects the main features of the angular energy distributions. Results are also given in Fig. 7 for moments method calculations of the energy distributions in water, graphite, and iron with an isotropic point source of neutrons [8] and for Monte Carlo calculations [9] in iron with an effectively plane, monodirectional source of 3.0 MeV neutrons. The same figure gives the

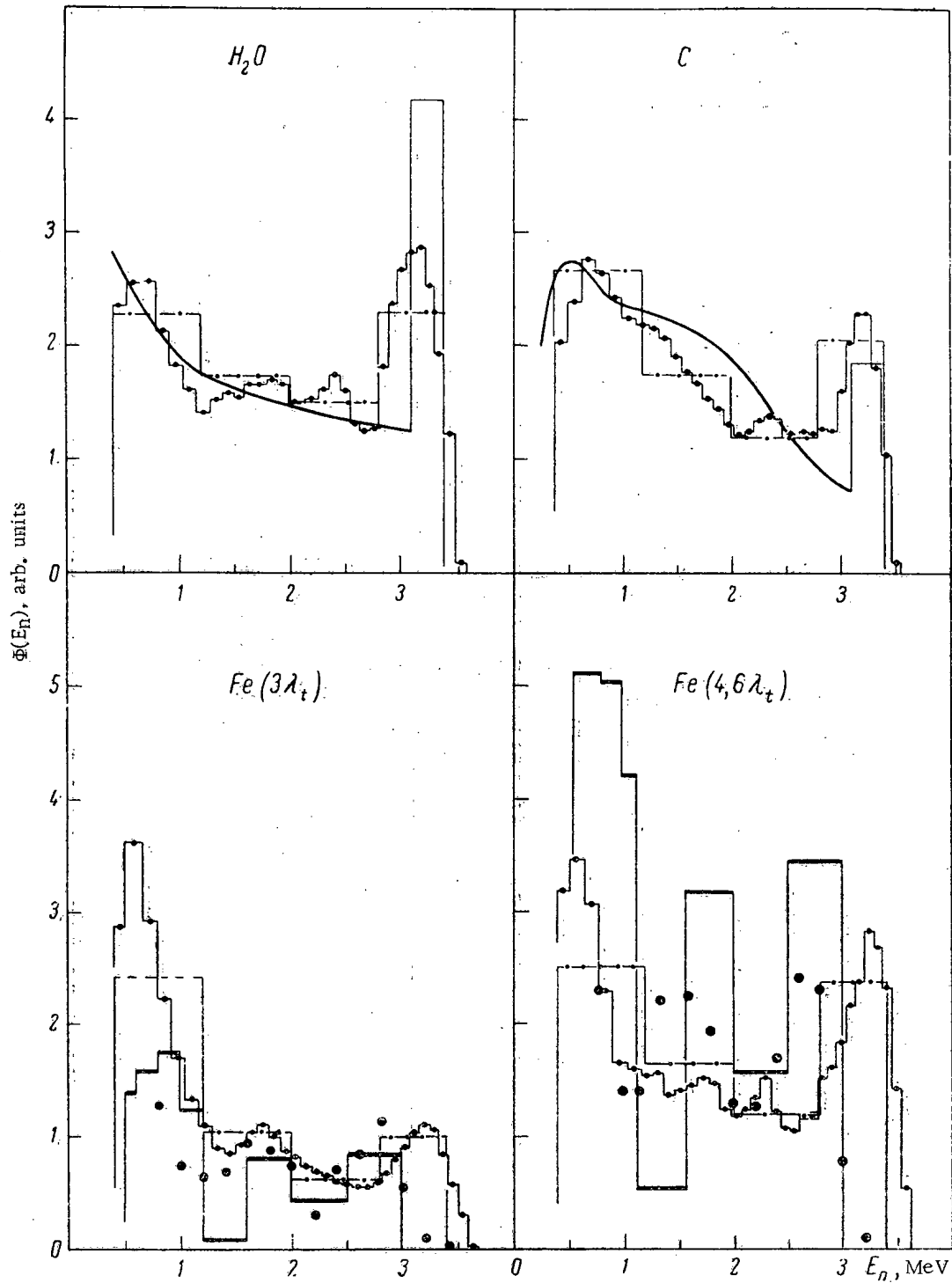


Fig. 7. Neutron energy distributions: $-\bullet-$ measured at the water-medium boundary (in space A); $-\cdot-\cdot-$ angular energy distributions obtained by integration with allowance for unscattered neutrons; $—$ results of calculations in water and graphite [8]; $—$ (histogram) calculation [9]; \bullet results of measurements in shield geometry [10].

results of fast neutron measurements with a single-crystal scintillation spectrometer under shielding geometry conditions and for an effectively plane, monodirectional source of ~ 3 MeV neutrons [10]. A detailed comparison of the energy distributions is difficult because of the differences of initial energies and of geometries. However, the differences between the energy distributions is not very great even with such differing geometries.

The authors consider it their pleasure to express thanks to S. G. Tsypin for valuable remarks and discussions and to L. A. Trykov for helpful advice. In addition, the authors thank A. P. Klimov for maintaining successful operation of the neutron generator and A. T. Bakov for help with the measurements.

LITERATURE CITED

1. F. Brooks, Nucl. Instrum. and Methods, No. 4, 151 (1959).
2. R. Owen, Atomnaya tekhnika za rubezhom, No. 1, 16 (1960).
3. V. A. Dulin, Yu. A. Kazanskii, and I. V. Shugar, Atomnaya énergiya, 14, 488 (1963).
4. V. A. Dulin, et al., Pribory i tekhnika éksperimenta, No. 2, 35 (1961).
5. K. Laniosh, Practical Methods of Applied Analysis [in Russian], Moscow, Fizmatgiz (1961), p. 327.
6. Kh. D. Androsenko and G. N. Smirenkii, Pribory i tekhnika éksperimenta, No. 5, 64 (1962).
7. Yu. A. Kazanskii, Atomnaya énergiya, 8, 432 (1960).
8. H. Goldstein, Fundamentals of Reactor Shielding [Russian translation], Moscow, Gosatomizdat (1961).
9. M. Leimdörfer, FOA 4A 4196-411 (May, 1961); AB Atomenergi, Internat. Repots RFA-88 (1962).
10. G. Doring, R. Jansson, and N. Starfelt, Symposium on the Detection, Dosimetry, and Standardization of Neutrons (Harwell, 10-14, December, 1962), Vienna, IAEA, SM-36/102.

THE NEUTRON BACKGROUND AT THE SURFACE OF THE EARTH

(UDC 537.591:550.35)

G. V. Gorshkov, V. A. Zyabkin, and O. S. Tsvetkov

Translated from *Atomnaya Énergiya*, Vol. 17, No. 6,

pp. 492-496, December, 1964

Original article submitted December 24, 1963

Measurements were made of the slow neutron flux above soil and water surfaces. The slow neutron flux above soil was 3.1 times greater than that above a water surface. Possible reasons are discussed for the increase in slow neutron flux above soil as compared with water. The thermal neutron flux was computed at the surface of a material in which fast neutrons are formed by cosmic rays.

It was concluded that the difference in the slow neutron fluxes above soil and water is caused to a considerable degree by the cosmic ray generation of neutrons in the upper layers of the earth's crust.

The curve for the altitude dependence of the neutron flux produced by cosmic radiation is distorted close to the surface of the earth by a number of factors, chief among which are the following:

1. Cosmic ray production of neutrons in the upper layers of the earth's crust.

2. Distortion of the neutron spectrum by the surface of the earth. In 1940, this factor was pointed out by Bethe, Korff, and Placzek [1] who considered the case of an infinitely extended water surface. A part of the fast neutrons produced in the atmosphere close to a water surface are incident on the water, and are moderated in it to thermal energies. Some of these thermal neutrons, diffusing back into the air, increase the thermal neutron density close to the water surface in comparison with that in the free atmosphere where the relative thermal neutron density is considerably lower because of capture by nitrogen in the $N^{14}(n, p)C^{14}$ reaction (formation of radioactive carbon).

Since the efficiency of any neutron detector depends on the neutron spectrum being recorded, a distortion of this spectrum can influence the results of a measurement.

3. Production of neutrons in the earth's crust as a result of natural radioactivity.

In this paper, we attempt to estimate the slow neutron flux at sea level above water and soil surfaces.

Experiment

Neutron radiation was recorded with a scintillation counter which consisted of a slow neutron detector and photomultiplier 200 mm in diameter.

The detector, prepared by us of enriched boric acid (enriched in B^{10} to 91%) and zinc sulfide by the method of joint fusion [2] with consideration of the changes mentioned in [3], was in the form of a 200 mm disc. The construction of the scintillation counter is briefly described in [4, 5]. Detection efficiency was determined with a thermal neutron flux which had been measured by activation of indium foils and of manganese (in the form of $KMnO_4$) with subsequent radiochemical concentration of the radioactive manganese by the Szilard-Chalmers method.

The absolute number of In^{116} and Mn^{56} decays was determined through the γ -radiation of these isotopes by means of a scintillation γ -counter calibrated by the β - γ coincidence method [6].

The slow neutron flux at sea level was measured at the following points:

1. in the environs of Leningrad at Zelenogorsk, approximately 3 km from the Gulf of Finland;
2. on a pier in Zelenogorsk (soil-water boundary);

Results of Neutron Background Measurements at the Earth's Surface

Point of observation	Type of measurement	Number of pulses recorded	Counting time, h	Counting rate, cts/h	Signal difference with and without cadmium	
					cts/h	neuts/cm ² ·day
1	Without cadmium	5287	8.92	593 ± 8	392 ± 10	285 ± 7
	With cadmium	1435	7.13	201 ± 5		
2	Without cadmium	1204	3.09	391 ± 11	186 ± 13	136 ± 9
	With cadmium	718	3.92	205 ± 7		
3	Without cadmium	2276	7.16	318 ± 7	126 ± 9	93 ± 6
	With cadmium	1246	6.5	192 ± 5		

3. above the surface of the water in the Gulf of Finland approximately 1 km from shore. Measurements were made from June 29 to July 2, 1960.

The absolute height above sea level did not exceed 30 m. Atmospheric pressure during the measurements underwent only insignificant changes (1013-1018 mbar).

For measurement of the neutron flux above the water surface, the apparatus was installed in a light, wooden boat. The depth of the gulf at the point of measurement was about 5 m. For all measurement points, the neutron detector was placed 1 m from the surface.

All neutron radiation measurements were carried out by the difference method using cadmium shields which completely surrounded the counter. From the difference in counter readings with and without the cadmium shields (1 mm thick), the net effect produced by slow neutrons was determined. The result obtained with the counter covered by cadmium was taken as background. By a special experiment, performed in a deep underground location it was demonstrated that the detector background produced by natural contamination with α -active element was (6.1 ± 0.1) cts/cm²·day. Results of the measurements are given in the table.

The value obtained for the slow neutron flux at sea level in the vicinity of the ground $[(285 \pm 7)$ neuts/cm²·day] is in excellent agreement with previous results [7-9] (240, 230, and 290 neuts/cm²·day, respectively). The value of the slow neutron flux above a water surface $[(93 \pm 6)$ neuts/cm²·day] is in agreement with other results [10] $[(78 \pm 2)$ neuts/cm²·day].

The main feature of the results is the fact that the slow neutron flux above the surface of the ground (see table, point 1) is 3.1 times greater than the neutron flux above a water surface (point 3). The magnitude of the flux at the water-ground boundary has an intermediate value.

It is impossible to explain the increase in the value of the slow neutron flux close to the surface of the ground by a contribution from neutrons of purely terrestrial origin, i. e., because of (α , n) reactions, spontaneous fission of heavy nuclei, etc. As has been shown [4], the slow neutron flux measured in underground workings (in granite and marble, for example) at a depth of about 200 m water equivalent is (13 ± 2) and (6 ± 1) neuts/cm²·day, respectively, which is 5 and 2% of the magnitude of the slow neutron flux at the surface of the ground.

Measurements at other points on the earth's surface have shown that the slow neutron flux which is obtained at the same geographic latitude (60° N) at sea level and normalized to a pressure of 760 mm Hg exhibits some variation (approximately 200-300 neuts/cm²·day) depending on the chemical composition of underlying rock, the moisture content and the topography of a location, and the presence of surrounding objects.

In addition, the neutron flux at point 1 was also measured in winter with a snow cover present. With snow cover present, it was shown that the slow neutron flux, normalized to a pressure of 760 mm Hg, was 1.65 times less than the neutron flux measured at the very same spot during the dry summer season.

The reduction in slow neutron flux with the transition from a soil to a water surface was observed in [11] and also in [12, 13]. According to the data in [13], the slow neutron flux in firm areas of the high mountain regions is

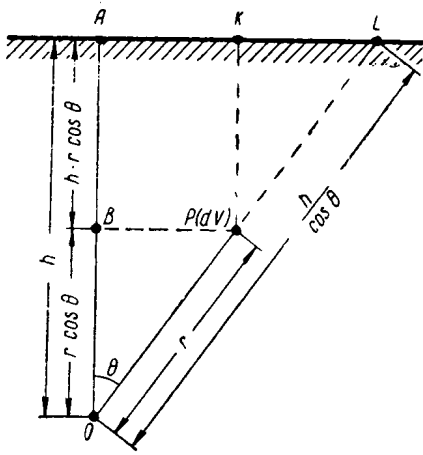


Diagram for calculating the rate of thermal neutron production.

reduced by a factor of 1.4 in comparison with the flux at granite outcroppings in the same area. The neutron flux at granite intrusions in the high mountain regions is several times greater than the neutron flux at a glacier located in the same area [12].

It is impossible to explain the reduction of the slow neutron flux above water as compared with that above rock by a distortion of the energy spectrum of the neutron component of the cosmic radiation since, in that case, the slow neutron density above water surface should be greater than the neutron density above rock. As indicated above, the slow neutron intensity of purely terrestrial origin in rock is also insufficient to explain this effect.

The next factor that one must take into account is neutron production through the action of cosmic radiation in underlying rock and in water. We shall consider whether the strength of this additional source of neutron formation at sea level is sufficient to exert a noticeable effect on the magnitude of the neutron component of cosmic radiation.

Theoretical Considerations

We compute the thermal neutron flux per unit area at the surface of an infinitely extended material in which cosmic rays are producing fast neutrons. To simplify the calculations, we assume: 1) the cosmic radiation is normally incident on the surface of the material; 2) there is a vacuum above the surface of the material; 3) there is no fast neutron capture in the material.

We introduce the following notation: I is the thermal neutron flux per unit area at the surface of the material, $\text{cm}^{-2}\text{-sec}^{-1}$; q_0 is the rate of fast neutron production by cosmic rays in the given material at its surface, $\text{g}^{-1}\text{-sec}^{-1}$; ρ is the density of the material, g/cm^3 ; x_c is the absorption length of the neutron-producing cosmic ray component in the given material, cm; L is the fast neutron slowing down length in the given material, cm; l is the thermal neutron diffusion length in the given material, cm; D is the thermal neutron diffusion coefficient in the given material, cm.

We compute the rate of thermal neutron formation per unit volume of the material at the point 0 at a depth h (see figure) because of slowing down of fast neutrons produced by cosmic rays at the point P in a volume element dV of the material.

The rate of fast neutron production q in a volume element $dV = r^2 dr \sin \theta d\theta d\phi$ located at a distance $PK = h - r \cos \theta$, from the surface of the material will be a factor $\exp[-(h - r \cos \theta)/x_c]$ less than at the surface. This is explained by the absorption of the neutron-generating component in the layer of material, i. e.,

$$q = q_0 \rho dV e^{-\frac{h - r \cos \theta}{x_c}}$$

The fast neutron flux through unit area at point 0 produced by fast neutrons arising from the volume element dV at a distance $PO = r$ from the point 0 will be

$$\frac{q}{4\pi r^2} e^{-\frac{r}{L}}$$

The number of fast neutrons emitted at point P in the volume element dV and converted to slow neutrons per unit volume at point 0 will be

$$\frac{q}{4\pi r^2} e^{-\frac{r}{L}} \frac{1}{L} \quad (1)$$

This expression gives the rate of formation of slow neutrons per unit volume at the point 0 because of the slowing down of fast neutrons emitted from the volume element dV at P:

$$Q(h, r, \theta, \varphi) = \frac{q}{4\pi r^2} e^{-\frac{r}{L}} \frac{1}{L} = \frac{q_0 Q}{4\pi r^2} e^{-\frac{h-r \cos \theta}{x_c}} e^{-\frac{r}{L}} \frac{1}{L} r^2 dr \sin \theta d\theta d\varphi.$$

The rate of formation of slow neutrons per unit volume at point 0 because of fast neutrons which are produced throughout the entire thickness of material will be

$$\begin{aligned} Q(h) &= \frac{q_0 Q}{4\pi L} \int_0^{2\pi} d\varphi \left\{ e^{-\frac{h}{x_c}} \left[\int_0^{\pi/2} \sin \theta d\theta \int_0^{h/\cos \theta} e^{-\frac{r}{x_c} \left(\frac{\cos \theta}{x_c} - \frac{1}{L} \right)} dr + \int_{\pi/2}^{\pi} \sin \theta d\theta \int_0^{\infty} e^{-\frac{r}{x_c} \left(\frac{\cos \theta}{x_c} - \frac{1}{L} \right)} dr \right] \right\} \\ &= \frac{q_0 Q x_c}{2} \left[\int_0^{\pi/2} \frac{\sin \theta}{L \cos \theta - x_c} e^{-\frac{h}{L \cos \theta}} d\theta - e^{-\frac{h}{x_c}} \int_0^{\pi} \frac{\sin \theta d\theta}{L \cos \theta - x_c} \right]. \end{aligned}$$

In an unbounded medium, the thermal neutron flux at a distance h from an infinitely thin layer of thickness dh in unit volume of which Q thermal neutrons are formed per unit time is according to diffusion theory,

$$dI_{\text{inf}}(h) = \frac{Ql}{2D} e^{-\frac{h}{l}} dh.$$

For approximate calculations, one can consider that the thermal neutron flux at the material-vacuum boundary is reduced by a factor of two in comparison with the flux in an unbounded medium at the same distance from an infinitely thin layer since the thermal neutron flux from the vacuum into the material is zero.

Then we have for the thermal neutron flux at the surface of the material from an infinitely thin layer of thickness dh located at a depth h

$$dI(h) = \frac{Ql}{4D} e^{-\frac{h}{l}} dh. \quad (2)$$

In order to determine the total thermal neutron flux at the surface of the material, it is necessary to integrate expression (2) over the entire thickness of the material, considering further that the rate of slow neutron formation per unit volume also depends on depth:

$$\begin{aligned} I &= \int_0^{\infty} \frac{Q(h)l}{4D} e^{-\frac{h}{l}} dh \\ &= \frac{q_0 Q x_c l}{8D} \left\{ \int_0^{\pi/2} \frac{\sin \theta d\theta}{L \cos \theta - x_c} \int_0^{\infty} e^{-h \left(\frac{1}{L \cos \theta} + \frac{1}{l} \right)} dh \right. \\ &\quad \left. - \int_0^{\pi} \frac{\sin \theta d\theta}{L \cos \theta - x_c} \int_0^{\infty} e^{-h \left(\frac{1}{x_c} + \frac{1}{l} \right)} dh \right\}. \end{aligned}$$

The final result for the thermal neutron flux at the surface of the material takes the form

$$I = \frac{q_0 Q x_c l^2}{8DL(x_c + l)} \left\{ l \ln \left(1 + \frac{L}{l} \right) + x_c \ln \left(1 + \frac{L}{x_c} \right) \right\}. \quad (3)$$

In order to estimate the thermal neutron flux above water and granite resulting from the generation of fast neutrons in these materials by cosmic rays, one needs to know the slowing down length for the fast neutrons which are produced in water and granite by cosmic radiation. The exact energy spectrum of these neutrons is unknown. In [14], the mean neutron energy for neutrons produced in lead and carbon by cosmic rays was estimated to be approximately 3 MeV. We used the slowing down length for fast neutrons with an energy of 3 MeV.

Water Surface: $q_0 = 2.89 \cdot 10^{-5} \text{ g}^{-1}\text{-sec}^{-1}$ [10]; $\rho = 1 \text{ g/cm}^3$; $x_c = 169 \text{ g/cm}^3$ [10] or $x_c = 169 \text{ cm}$; $l = 2.3 \text{ cm}$ [15]; $L = 6.4 \text{ cm}$ [16]; $l_{tr} = 0.49 \text{ cm}$ [17] (l_{tr} is the transport mean free path); $D \approx l_{tr}/3 = 0.49/3 = 0.16 \text{ cm}$.

Substituting these values into formula (3), we find $I = 1.72 \cdot 10^{-5} \text{ neutrons/cm}^2 \cdot \text{sec} \approx 15 \text{ neutrons/cm}^2 \cdot \text{day}$.

Granite: $\rho = 2.78 \text{ g/cm}^3$ [15]; $l = 10.3 \text{ cm}$ [15]; $D = 1.03 \text{ cm}$ [15]; $L = 45 \text{ cm}$ (our calculation).

The mean atomic weight of granite is 27.6 [15], i. e., close to the atomic weight of aluminum - 27. For the estimate, we assumed that the magnitudes of q_0 and x_c were equal to the corresponding values for aluminum: $q_0 = 5.2 \cdot 10^{-5} \text{ g}^{-1}\text{-sec}^{-1}$ [18]; $x_c = 220 \text{ g/cm}^2$ [19] or $x_c = 220/2.78 = 79 \text{ cm}$.

From formula (3), we find $I = 1.94 \cdot 10^{-3} \text{ neutrons/cm}^2 \cdot \text{sec} \approx 170 \text{ neutrons/cm}^2 \cdot \text{day}$.

It should be noted that the rate of neutron formation by cosmic rays in granite is only 1.8 times as much as in water, but the thermal neutron fluxes resulting from their formation differ by an order of magnitude. This is explained by the differing slowing down and diffusion characteristics of granite and water.

CONCLUSIONS

The calculations that were made have shown that the production of neutrons by cosmic rays in the upper layers of the earth's crust can exert a strong influence on the slow neutron flux at sea level.

In order for us to compare calculation with experiment, it would have been necessary to compute the slow neutron flux at surface of the ground which arises from neutrons produced in the atmosphere. For such an estimate, it is necessary to know the intensity and spectrum of atmospheric neutrons and the possible distortions of them at the surface of the earth. We did not have such data available, and therefore such an estimate was not made in this paper.

However, it is clear that the contribution of the neutrons which are produced in granite by cosmic rays to the total neutron flux above its surface is considerably greater than in the case of water. Therefore, one can suppose that the difference in slow neutron fluxes above water and soil surfaces are caused to a considerable degree by the cosmic ray production of neutrons in the upper layers of the earth's crust.

LITERATURE CITED

1. H. Bethe, S. Korff, and G. Placzek, *Phys. Rev.*, 57, 573 (1940).
2. T. V. Timofeeva and S. P. Khormushko, *Izv. AN SSSR, Ser. fiz.*, 22, 14 (1958).
3. B. S. Grebenskii et al., *idem*, 25, 500 (1961).
4. G. V. Gorshkov, V. A. Zyabkin, and O. S. Tsvetkov, *Atomnaya Énergiya*, 13, 65 (1962).
5. G. V. Gorshkov and O. S. Tsvetkov, *In Chemistry of the Earth's Crust, Vol. 2, Moscow, Izd-vo, AN SSSR (1963), p. 409.*
6. G. V. Gorshkov, A. N. Silant'ev, and O. S. Tsvetkov, *Radiokhimiya*, 4, 244 (1962).
7. A. P. Zhdanov and A. S. Serdakov, *Dokl. AN SSSR*, 31, 861 (1941).
8. N. Kaplan and H. Yagada, *Rev. Scient. Instrum.*, 23, 155 (1952).
9. K. Mather, *Austral. J. Phys.*, 9, 147 (1956).
10. E. Bagge and S. Skorka, *Z. Phys.*, 152, 34 (1958).
11. G. V. Gorshkov, S. P. Khormushko, and O. S. Tsvetkov, *Dokl. AN SSSR*, 131, 933 (1960).
12. V. V. Cherdyn'tsev and V. I. Meshkov, *Bulletin of the Committee for the Determination of the Absolute Age of Geological Formations, No. 1, Moscow, Izd-vo, AN SSSR (1955), p. 61.*
13. L. I. Shmonin et al., *Uch. zap. Kazakhsk. un-ta*, 30, No. 5, 25 (1957).
14. V. Cocconi-Tongiorgi, *Phys. Rev.*, 76, 517 (1949).
15. E. M. Filippov, *Applied Nuclear Geophysics [in Russian], Moscow, Izd-vo, AN SSSR (1962).*
16. N. A. Vlasov, *Neutrons [in Russian], Moscow, Gostekhteorizdat (1955).*
17. *Nuclear Physics Handbook [English translation], L. A. Artsimovich, edited, Moscow, Fizmatgiz (1963).*
18. A. Tobey and C. Montgomery, *Phys. Rev.*, 81, 517 (1951).
19. G. Benardini, G. Cortini, and A. Manfreclini, *Phys. Rev.*, 76, 1792 (1949).

ADDITION OF HETERO-ORGANIC COMPOUNDS TO POLYSTYRENE

(UDC 621.387.464:678.746)

E. E. Baroni, S. F. Kilin, T. N. Lebsadze, I. M. Rozman,
and V. M. Shoniya

Translated from *Atomnaya Énergiya*, Vol. 17, No. 6,
pp. 497-499, December, 1964

Original article submitted November 30, 1963

To obtain polystyrene containing Pb, Bi, Hg, Sn, and Se, the solubilities of their phenyl compounds in the monomer are determined. The optimum conditions for thermal polymerization of styrene containing these compounds are described in detail. Data are given on the preparation of polymerization products containing phenyl compounds of Pb (12%), Bi (19%), Hg (33%), As (12%), Sn (11%), and Se (10%, by weight). The polymerization products are transparent and stable in air. The material is intended for the production of scintillation detectors and γ -ray and neutron shielding. Data are given on the luminescent yield of plastic scintillators containing Pb, Hg, and Sn.

Scintillation methods of detecting neutrons, x-rays and γ -rays make use of inorganic crystal phosphors, organic monocrystals and liquid solutions [1-5], and also of plastic scintillators (PS) [6-9]. The atomic composition of PS prepared by polymerizing solutions of organic phosphors in certain monomers (styrene and vinyltoluene) is limited to the light elements C, H, and O. These substances have very small coefficients of photoelectric absorption, which causes considerable difficulty in the use of PS for γ -ray spectroscopy—though large PS are very efficient for detecting low-intensity radiation.

Methods have been described for increasing the photoelectric absorption of plastics by incorporating heavy elements in the form of organic compounds [10-12]. For example, 9.4 wt. % lead and 10% bismuth can be added to polystyrene-based PS with 1,1', 4,4'-tetraphenyl-butadiene-(1,3) as luminous additive [10]. However, these polymerization products are unstable in air owing to the insufficient stability of the compounds used (bismuth and lead hexahydrobenzoates, lead naphthenate, triphenylmethyl lead). An attempt to use Pb, Hg, or Bi isobutyrate or trimethylacetates, together with polycyclohexylmethacrylate in polyvinyltoluene, was unsuccessful [11].

We have performed experiments on incorporation into polystyrene-based PS of Pb, Bi, Hg, As, Sn, and Se in the form of more stable and easily prepared compounds. The present paper gives test results on procedures for thermal polymerization of styrene containing the phenyl compounds of these elements. [13] describe another method which we have developed for incorporating hetero-organic compounds in PS.

The incorporation of various chemical elements in PS is not only of interest for use in the measurement of ionizing radiation, but is also important for the preparation of comparatively cheap γ -ray and neutron shielding materials [14-16].

Preparation of PS with Organometallic Additives

We used the following hetero-organic compounds: tetraphenyl lead [17], diphenyl mercury, tetraphenyl tin, triphenyl arsenic, triphenyl bismuth [18] and diphenyl selenium [19]. The best method of purifying these compounds (except diphenyl selenium) is sublimation in a vacuum of $\sim 10^{-4}$ mm Hg. In order to incorporate the maximum amounts of these compounds into the polystyrene, and to study the conditions for thermal polymerization, the temperature dependences of their solubilities in pure monostyrene were roughly determined. The results are given in Table 1.

To avoid polymerization of the specimens during the solubility determinations (especially at the higher temperatures), the experiments were performed rapidly (within 5 min) in a previously temperature-stabilized glycerine bath.

TABLE 1. Solubilities of Phenyl Compounds in Styrene at Various Temperature

Substance	M. p., °C	Temp., °C	Solubility in styrene wt. %	Content of elementary metal, wt. %
Pb(C ₆ H ₅) ₄	224— 225	20	0,5	0,2
		140	46	18,4
Bi(C ₆ H ₅) ₃	76	20	40	19,0
		60	60	28,5
Hg(C ₆ H ₅) ₂	120	20	20	11,3
		60	60	33,9
As(C ₆ H ₅) ₃	57	20	30	7,35
		50	50	12,2
Sn(C ₆ H ₅) ₄	222— 223	20	0,5	0,14
		140	70	19,5
Se(C ₆ H ₅) ₂	Liquid	20	50	21,55

TABLE 2. Conditions for Polymerizing Styrene with Organometallic Additives

Substance	Content of organometallic compound, wt. %	Content of elementary metal in polystyrene, wt. %	Polymerization temperature, °C	Polymerization time, h	Properties
Pb(C ₆ H ₅) ₄	30	12	140	16	Transparent, hard
			160		
Bi(C ₆ H ₅) ₃	40	19	120	144	Ditto, with yellow tint
Hg(C ₆ H ₅) ₂	60	33.9	120	60	Transparent, hard
As(C ₆ H ₅) ₃	50	12	120	144	Ditto
Sn(C ₆ H ₅) ₄	40	11.1	150	24	" "
Se(C ₆ H ₅) ₂	30	10.2	140	170	Transparent, hard, rubbery

Preliminary experiments showed that, in the presence of these hetero-organic compounds, polymerization cannot be effected by the procedure developed in [8] for preparing polystyrene-based PS. Each compound requires definite temperature conditions for polymerization. For this reason the polymerization conditions were investigated for each compound separately.

Polymerization Conditions for Styrene Containing Tetraphenyl Lead. Experiments on the incorporation of tetraphenyl lead in styrene showed that, if thermal polymerization is carried out at 200°C, addition of 10, 15, or 20 wt. % tetraphenyl lead causes blackening of the product. With 10 wt. % tetraphenyl lead blackening occurred 6 h, and with 20 wt. % 4 h after polymerization began. In every case blackening began in the lower part of the test flask, and during polymerization gradually penetrated the upper part of the specimen. It should be noted that in all cases the specimen became yellow before turning black. This may be due to the fact that the Pb(C₆H₅)₄ molecule (m. p., 224-225°C) is markedly dissociated at these temperatures owing to the radical processes involved in styrene polymerization. In fact, on decreasing the polymerization temperature to 190, 180, or 170°C, the blackening was lessened.

The conditions for thermal polymerization of styrene containing Pb(C₆H₅)₄ are as follows: a sealed ampoule containing pure styrene and the required amount of tetraphenyl lead is placed in a glycerine bath at 145°C. The contents of the ampoule are kept under nitrogen. The bath is gradually heated over a period of 6 h to 160°C, then

TABLE 3. Light Outputs of PS with Organometallic Additives

Additive		Rel. output on excitation	
Composition	Wt. %	γ -rays	UV light (2967 Å)
Pb(C ₆ H ₅) ₄	—	100	100
	5	75	90
	10	54	85
Hg(C ₆ H ₅) ₂	5	50	80
	10	30	64
Sn(C ₆ H ₅) ₄	5	95	100
	10	79	100

kept at this temperature for a further 10 h. With this procedure, 30% tetraphenyl lead was added to the polystyrene (12 wt. % elementary lead). To avoid turbidity, the products were cooled by a stream of water immediately on completion of polymerization. Specimens prepared in this way were transparent and possessed adequate mechanical strength. They do not alter on being left in the light, and are stable in air.

Polymerization Conditions for Styrene Containing Tetraphenyl Tin. Products containing large quantities of tetraphenyl tin do not become blackened during thermal polymerization at 200°C. Sudden temperature changes during polymerization involve no risk, as the possible precipitation of a crystalline tin compound on temperature reduction can be eliminated by quickly raising the bath temperature—no visible changes, such as becoming black or yellow, then being observed.

The conditions for polymerization of styrene containing Sn(C₆H₅)₄ are as follows: a sealed ampoule, containing styrene plus the required amount of tin compound in an atmosphere of nitrogen, is placed in a bath previously heated to 135°C. The temperature is smoothly raised to 145-150°C over a period of 4 h. At this temperature polymerization goes to completion in 24 h. The specimens must be cooled like those containing tetraphenyl lead. The amount of tin added is 11.1 wt. %. The product is transparent, colorless, and stable in light and air.

Polymerization Conditions for Styrene Containing Diphenyl Mercury, Triphenyl Bismuth, Triphenyl Arsenic and Diphenyl Selenium. Preliminary experiments on the incorporation of triphenyl bismuth in polystyrene showed that, with polymerization at 200°C, blackening occurs as for tetraphenyl lead. In the same polymerization conditions specimens with diphenyl mercury and diphenyl selenium turned yellow, and the former became brittle. The specimens with triphenyl arsenic were colorless but brittle. The brittleness sharply increased with increasing concentrations of the phenyl compounds of Hg, Bi, As, and Se (20, 30, 40, and 50 wt. %). To eliminate this undesirable property, especially at maximum concentrations [60% Hg(C₆H₅)₂, 40% Bi(C₆H₅)₃, 50% As(C₆H₅)₃], polymerization should be performed at 120°C. With 30 wt. % diphenyl selenium the optimum polymerization temperature is 140°C. The polymerization conditions for various additives are compared in Table 2. The products containing these elements are adequately hard and transparent. Despite preliminary purification of the initial materials, the specimens with triphenyl bismuth all had a pale yellow tint. The polymers with diphenyl selenium, though transparent, were rubbery and had a reddish tint owing to the presence of colloidal selenium in the diphenyl selenium. The styrene containing additives was polymerized in the thermostat under nitrogen in sealed glass ampoules.

Effect of Organometallic Additives on the Luminescence of PS

To prepare scintillators, organometallic compounds were added to the styrene together with luminescent substances—3 wt. % terphenyl and, as spectral displacer, 0.08% 1,3,5-triphenyl- Δ^2 -pyrazoline. Polymerization of the specimens with additives was performed in the conditions given in Table 2, and for the pure specimens in the usual conditions [8]. Cylindrical specimens, of diameter 29 mm and length 26 mm, were cut from the polymerization products. A photomultiplier and mirror galvanometer were used to compare the light intensities from the

TABLE 4. Luminescence of PS with p-Terphenyl and Diphenyl Mercury

Concentration of Hg(C ₆ H ₅) ₂ , wt. %	I _β	I _f	I _R	τ, nsec
0	100	100	100	2.2
1	90	99	250	2.2
2	73	92	290	2.1
3	54	85	310	2.0
4	48	82	340	1.9
5	41	78	330	1.9
6	33	75	280	1.9

Note. Here I_β = luminescent intensity on excitation by β-rays from Ce¹⁴⁴ - Pr¹⁴⁴; I_f = ditto on excitation by UV light (λ = 3130 Å); I_R = ditto on excitation by x-rays from 60 kV tube; τ = mean duration of fluorescence on excitation by x-rays. PS diameter 16 mm, length 10 mm.

specimens on excitation with γ-rays from Co¹³⁷. Teflon reflectors were used to collect the light. The results (Table 3) agree with the data for diphenyl mercury [12] and for pressed scintillators [13].

From Table 3 it is evident that the presence of organometallic compounds quenches the luminescence of PS. It was of interest to discover at what stage of the scintillation process this quenching occurs. A phase fluorometer was used to measure the duration of luminescence of the scintillators on direct excitation of the spectrum displacer with UV light (λ ≈ 3600 Å). This was found to be independent of the presence of the organometallic compounds, i. e., the fluorescence of the displacer is not quenched. Measurements of the fluorescent yield of p-terphenyl on direct excitation in PS by the line λ ≈ 2967 Å revealed the occurrence of quenching in the presence of tetraphenyl lead, and especially of diphenyl mercury (see Table 3). However, the degree of quenching was much less than with excitation by γ-rays. Quenching by diphenyl mercury was also studied in a scintillator with a single luminescent additive (1.5% p-terphenyl).

From Table 4 it is evident that radioluminescence is quenched less strongly than fluorescence of terphenyl. So the quenching of radioluminescence occurs mainly during transfer of excitation energy from the polystyrene to the p-terphenyl.

PS containing organometallic compounds might be useful for measuring soft x-rays. For example, the absorption of bremsstrahlung x-radiation (u = 60 kV) by PS increases by a factor of eight on adding 5% diphenyl mercury. Despite the reduced yield, the fluorescent intensity is increased more than three times (see Table 4).

LITERATURE CITED

1. H. Kallman, M. Furst, and F. Brown, *Nucleonics*, 14, No. 4, 48 (1956).
2. A. Ronzio, *Internat. J. Appl. Radiation Isotopes*, 4, 196 (1959).
3. R. Axtmann and Le Conter Cathey, *Internat. J. Appl. Radiation Isotopes*, 4, 261 (1959).
4. H. Gilman, E. Weipert, and F. Hayes, *J. Organ. Chem.*, 23, 361, 628, 760, 910 (1958).
5. J. Birkes, *Scintillation Counters* [Russian translation], Moscow, Izd-vo, Inostr. lit. (1955).
6. L. Pichat and Y. Köchlin, *J. Chim. Phys.*, 48, 225 (1951).
7. W. Buck and R. Swank, *Nucleonics*, 11, No. 11, 48 (1953).
8. E. A. Andreeshchev et al., *Pribory i tekhnika éksperimenta*, No. 1, 32 (1956); *Izv. AN SSSR, Ser. Fiz.*, 22, 67 (1958); *Zh. Fiz. Khimii*, 34, 665 (1960).
9. E. E. Baroni and V. M. Shoniya, *Atomnaya Énergiya*, 6, 330 (1959).
10. L. Pichat, P. Pesteil, and J. Clement, *J. Chim. Phys.*, 50, 26 (1953).
11. M. Hyman and J. Ryan, *IRE Trans. Nucl. Sci.*, MS-5, 87 (1958).
12. L. Basile, *J. Chem. Phys.*, 27, 801 (1957).
13. E. A. Andreeshchev et al., *Pribory i tekhnika éksperimenta*, No. 4, 151 (1961).
14. A. Restaino, *Nucleonics*, 15, No. 9, 188 (1957).
15. N. Hosgen and R. Sowden, *Nucleonics*, 19, 158 (1961).
16. E. E. Baroni, T. N. Lebsadze, and V. M. Shoniya, *Author's Certificate* 115, 458 (March 11, 1958).
17. H. Gilman and J. Robinson, *J. Amer. Chem. Soc.*, 51, 3112 (1929).
18. P. Preiffer and P. Truskier, *Ber. Dtsch. Chem. Ges.*, 37, 1127 (1904); P. Preiffer and H. Pietsch, *Ber. Dtsch. Chem. Ges.*, 37, 4622 (1904).
19. *Organic Syntheses* [Russian translation], Symposium 2, Moscow, Izd-vo. Inostr. lit. (1949), p. 237.

IN MEMORY OF KONSTANTIN KONSTANTINOVICH AGLINTSEV

from his fellow workers

Translated from Atomnaya Énergiya, Vol. 17, No. 6,
p. 501, December, 1964

Professor Konstantin Konstantinovich Aglintsev, Doctor of Technical Sciences, the head of a department and laboratory at the V. G. Khlopin Radium Institute where he was one of the leading scientists, has died after a long illness.

His scientific activity was entirely devoted to problems of dosimetry, radiometry and the measurement of ionizing radiation. His work was closely linked with the protection of the people's health. As an outstanding specialist in nuclear physics, he enjoyed considerable authority among Soviet and foreign biophysicists and doctors.

Aglintsev was born in Leningrad in 1905, and after graduating from the Physics and Mathematics Faculty of Leningrad State University he began work in 1926 in the X-Ray and Radiological Institute; from 1928 onwards his career was for many years linked with VNIIM, the D. I. Mendeleev All-Union Research Institute of Metrology. His early work was on x-rays, in particular on their standardization. He continued to study these problems to the end of his life. In 1940 he became head of the VNIIM radiometric laboratory and carried out important investigations on metrology and radioactivity, aimed in particular at setting up a USSR state standard of radiation and the development of new absolute methods for measuring radioactivity. During this period he worked on the national coordination of measurement and the rational organization of a State measurement and instrumentation service for ionizing radiation.

In 1950 he published the first edition of "Dosimetry of Ionizing Radiations": this is his chief publication and at once became the principal text in the field. It was later revised by the author. Translations of this important work were soon issued in Poland, Czechoslovakia and East Germany. Aglintsev wrote eight books and his total publications numbered eighty-two; much of his work is also to be found in the archives of scientific institutions.

His investigations of radioactivity naturally led him to the Radium Institute, where in 1950 he carried out work the new field of spectroscopy by β and γ -ray dosimetry. He devised a means for the quantitative detection of γ -rays by means of ionization chambers, counter tubes and photographic plates. He established the shapes of the effective electron spectra in the fields of various β -emitters. He discovered a simple, important empirical law on the constancy of the dose per β -particle for a given β spectrum.



Throughout his life Aglintsev continually worked in scientific education. He lectured at Leningrad State University (where many of us were taught by him) and also in the Mechanical Institute, where he was head of a department. In his work at the Radium Institute he paid much attention to the education of his fellow-workers—not only his immediate associates, but also those in other laboratories. His students include many who are now working on lines originally laid down in his work.

He has repeatedly represented Soviet science in the international forum; even in the last few years he attended eight conferences and symposia abroad. In 1959 at the Ninth International Radiological Congress he was elected as a member of the International Commission on Radiological Units and Measurement.

Besides this strenuous scientific, technical and teaching ability Aglintsev was always active in social work. His responsiveness and

attention to social interests won him the sympathy and recognition of his associates: he was elected to the Leningrad Town Council of Workers' Deputies.

His activities won him a number of Government awards. He was twice decorated with the Order of Lenin, twice with the Order of Honor, and received the Leningrad Defense Medal, and the medal "For Valorous Work in the Great Patriotic War."

Aglintsev's premature death has robbed us of a man of great soul, who loved life and people. He had friends in very varied spheres and was also at home in the world of sport.

All will remember his great sympathy and his attentiveness to the interests and needs of his associates, especially the young. They came to him for advice, support, instruction and ideas, not only as to a long-standing scientific associate, but also as to a good friend, always ready to give aid in word and deed,

We will always remember Konstantin Konstantinovich Aglintsev as a scientist, a man and a friend.

STUDY OF THE TRANSFORMATIONS OF RUTHENIUM DIOXIDE
IN THE PRESENCE OF CHROMIUM OXIDE

(UDC 546.96)

M. K. Baranaev, V. G. Vereskunov, and K. P. Zakharova

Translated from *Atomnaya Énergiya*, Vol. 17, No. 6,
pp. 502-503, December, 1964
Original article submitted May 16, 1964

A study of the conditions for the formation of RuO_4 is necessary in view of the considerable amount which passes into the vapor phase during the heat treatment of atomic industry waste. Usually either nitric acid solutions or hydroxide pulps are subjected to heat treatment; these contain a mixture of fission products, including Ru^{106} . Apart from technological impurities, such solutions and pulps contain corrosion products, especially chromium and iron.

We investigated transformations taking place on heating ruthenium hydroxide and a mixture of this with chromium hydroxide. The ruthenium hydroxide used was obtained by alkali precipitation of ruthenium chloride. The hydroxide precipitates were washed to remove all traces of alkali and chlorine ions, and then dried at a temperature of 25 to 27°C.

Determination of the volatilization of the RuO_4 was made with ruthenium hydroxide obtained by alkali precipitation of a tagged solution of RuCl_3 . The radioisotope of ruthenium was introduced in the form of the chloride of Ru^{106} . The chromium hydroxide was obtained by alkali precipitation of a solution of chromium nitrate. The behavior of the material under examination was studied by the complex thermal analysis method [1]. The transformation of the ruthenium into the vapor phase during heating, associated, as shown in [2, 3], with the formation of volatile RuO_4 , was estimated from the change in the activity of the sample, measured on an end-window counter MST-17. In order to reduce the effect of self-diffusion, we used samples with a material layer thickness not exceeding 100 mg/cm^2 . The thermal analysis was made with large quantities of a stable ruthenium isotope.

As a result of thermal analysis of the hydrate of ruthenium oxide, it was established that the loss of water from the material took place in stages in three temperature ranges (endothermic effects at 100, 260, and 330°C) and ceased at 360°C. In this process, as shown earlier [2], RuO_2 was formed. The loss of weight* from the ruthenium hydroxide in the temperature range indicated was 15%. Theoretically, passage from ruthenium hydroxide, bearing the formula $\text{Ru}_2\text{O}_5 \cdot 2\text{H}_2\text{O}$ [2], to RuO_2 should involve a 16% loss in weight. The weight loss of the sample at temperatures above 700°C is associated with the oxidation of RuO_2 to volatile RuO_4 beginning at these temperatures [2, 3].

The exothermic effect observed around 410°C corresponds to the transformation of RuO_2 from the amorphous into the crystalline state, as confirmed by x-ray analysis. The crystalline phase is absent from unroasted ruthenium hydroxide. X-ray diffraction patterns of samples roasted at 475°C show sharp lines indicating the presence of a crystalline phase.

In the case of chromium hydroxide, the exothermic effect associated with the transformation of chromium oxide from the amorphous into the crystalline state takes place at 450°C. In the thermal diagram of the binary mixture $\text{Ru}_2\text{O}_5 \cdot 2\text{H}_2\text{O} - \text{Cr}(\text{OH})_3$, however, no exothermic effects appear, and this strongly suggests interaction between the substances in question.

In order to confirm this, we studied the volatilization of ruthenium on heating a mixture of tagged ruthenium hydroxide and chromium hydroxide in air and in nitrogen. The sample spent 30 min in each temperature range.

Volatilization of ruthenium on heating the mixture began around 400°C. It was shown in [2, 3] and confirmed by our own experiments that marked oxidation of RuO_2 by atmospheric oxygen to volatile RuO_4 only took place at

*Determined by weighing the samples.

temperatures above 700°C. Since no ruthenium evaporated on heating the mixture to 900°C in nitrogen, we may assume that in the present case chromium oxide does not constitute an oxidizing agent, but simply catalyzes the process, leading to the oxidation of RuO₂ at lower temperatures. The catalytic power of chromium oxide, associated with its transformation into a form containing active oxygen on heating in air, is examined in detail in [4].

The insignificant volatilization of ruthenium on heating the mixture in a nitrogen atmosphere is determined by the reaction of disproportionization of RuO₂ [2]. As a result of this reaction, which takes place above 800°C, RuO₄ and metallic ruthenium are formed.

Our experiments thus show that, on heating the hydrate of ruthenium oxide to a temperature around 410°C, there is an exothermic effect corresponding to the transformation of RuO₂ from the amorphous into the crystalline state. They also show the catalytic effect of chromium oxide on the oxidation of RuO₂ by atmospheric oxygen to RuO₄ at 300-700°C.

LITERATURE CITED

1. L. G. Berg and G. G. Tsurinov, The Kurnakov Pyrometer [in Russian], Moscow, izd. AN SSSR (1942).
2. P. Pascal, Nouveau traite de chimie minerale, 19, Paris (1958).
3. L. Gmelin, Gmelins Handbuch der Anorganischen Chemie, H, 63, Berlin (1926).
4. T. V. Rode. Oxygen Compounds of Chromium and Chromium Catalysts [in Russian], Moscow, izd. AN SSSR (1962).

USE OF THE TIME OF FLIGHT METHOD FOR MEASURING
THE RANGE/ENERGY RELATION FOR 18 TO 38 MeV
HELIUM IONS IN ALUMINUM

(UDC 539.128.53)

N. I. Venikov and N. I. Chumakov

Translated from *Atomnaya Énergiya*, Vol. 17, No. 6,
pp. 503-504, December, 1964
Original article submitted November 20, 1963

The time of flight method [1] is suitable for measuring the energies of ions absolutely to a high degree of accuracy. We used this method in determining the range/energy relationship for He₃ ions in aluminum over an energy range of 18 to 38 MeV. The measurements were made in the emergent beam of the 1.5-m cyclotron in the I. V. Kurchatov Institute of Atomic Energy [2], using a multichannel time analyzer described in [3]. Around 10% of the ion beam deflected by the sectoral magnet fell on a graphite target, and the remaining ions were intercepted by a graphite grid set at a distance of 5515 mm in front of the target. The γ -quanta from the target and grid were recorded simultaneously by the time analyzer. In order to calibrate the time scale, recordings were made of γ -peaks from two high frequency periods. So that the intensity of γ -peaks from the target and grid should be approximately the same, the γ -quantum detector, a stilbene crystal with an FÉU-36 type photomultiplier, was placed at a distance of roughly 2.8 m beyond the target. In order to eliminate this distance from the calculation, the detector was set at zero angle to the beam axis. Use of short ion bursts (less than 2 nsec) ensured an accuracy of around 0.15 nsec in the accuracy of time of flight measurements by the analyzer.

As we know, the kinetic energy of the ion is

$$E = E_0 \left(\frac{1}{\sqrt{1-\beta^2}} - 1 \right). \quad (1)$$

Here E_0 is the ion rest energy, $\beta = \frac{v}{c}$, where v is the velocity of the ion, and c is the velocity of light.

If we confine ourselves to two terms in the expansion of expression (1), we obtain

$$E = E_0 \frac{\beta^2}{2} \left(1 + \frac{3}{4} \beta^2 \right), \quad (2)$$

in which

$$\beta = \frac{L}{c \left(\frac{\tau}{T} \cdot \frac{10^{-6}}{f} + \frac{L}{c} \right)}, \quad (3)$$

where L is the distance from grid to target in cm, τ is the time of flight of an ion from the grid to the target, T is the time interval between two γ -peaks from the target (or grid), corresponding to the high frequency period, and f is the frequency of the cyclotron hf generator in Mc/sec. The error in measuring the energy of the ions is given by the expression

$$\frac{\Delta E}{E} = 2 \left[\frac{\Delta L}{L} + \frac{\Delta \tau}{\tau} + \frac{\Delta T}{T} + \frac{\Delta f}{f} \right]. \quad (4)$$

Range/Energy Relationship for He₃ Ions in Aluminum

Energy, MeV.	18,15	22,29	24,34	27,01	30,34	32,82	35,95	37,60
Measured range, mg/cm ²	53,1	74,2	86,9	104,4	128,9	147,3	162,7	190,6
Range as given in [4], mg/cm ²	54,3	76,5	89,4	107	—	—	—	—

In our case, L was measured with an accuracy of 2 mm, $\Delta\tau$ and ΔT were around 0.15 nsec for $T = 85$ to 120 nsec, and $\tau = 120$ to 165 nsec, while $\Delta f = 5$ kc/sec for $f = 8.3$ to 12 Mc/sec.

In all the maximum error in determining the ion energies was no greater than $\pm 0.4\%$.

In order to determine the range of the ions in aluminum, a pile of foils was placed at intervals in the path of the beam, the total foil thickness being so chosen as to reduce the intensity at the target by a factor of two. To eliminate error arising from secondary emission, the target was made in the form of a Faraday cylinder and placed in a magnetic field (~ 200 Oe) directed along the normal to the cylinder axis. In order to control the stability of the beam falling on the foils, a current monitor in the form of a grid was placed in front of these. Piles of foils were turned on a lathe (the diameter of each foil being 60 mm) to an accuracy of 0.06 mm, and then weighed to an accuracy of 1 mg. The error in determining the range may be found from the formula

$$\frac{\Delta R}{R} = \frac{\Delta p}{p} + 2 \frac{\Delta D}{D} + \frac{\varphi^2}{2} + \xi, \quad (5)$$

where $\frac{\Delta p}{p}$ is the weighing error, equal to $2 \cdot 10^{-4}$, $\frac{\Delta D}{D}$ in determining the diameter of the pile of foils, equal to 10^{-3} , φ is the maximum deviation of the direction of the beam incident on the foil from the normal, equal to 0.05 (3°), and ξ is the error due to foil inhomogeneity and some current instability, less than $2 \cdot 10^{-3}$. The over-all error in determining the range is no more than $\pm 0.3\%$.

The table shows the range/energy relationship measured for He₃ ions in aluminum; for comparison, some range values taken from the computed curve of [4] are presented. No other data on the range/energy relation for He₃ in aluminum in the energy range considered are known to the authors. As seen from the table, the values given in [4] for the range of He₃ are a little (2.5 to 4%) higher for comparable energies. The precision of measuring the range/energy relation by the method described is also confirmed by the good agreement (better than 1%) between the range/energy relation measured by the authors using the same method for 6 to 17 MeV protons in aluminum (12 points in all) and that given in [4].

The authors are grateful to N. A. Vlasov for valuable comments, to S. P. Kalinin, V. P. Rudakov, and R. V. Rybakov for interest in the work, and also to V. D. Krupochkin, V. V. Paramonov, and B. I. Khoroshavin for assistance rendered.

LITERATURE CITED

1. B. V. Rybakov and V. A. Sidorov, Spectroscopy of Fast Neutrons [in Russian]. Supplement No. 1 to the magazine "Atomnaya Énergiya," Moscow, Atomizdat (1958).
2. A. A. Kurashov and V. A. Sidorov, "Pribory i tekhnika éksperimenta," No. 6, 69 (1961).
3. D. Bromley and E. Almigvist, Reports on Progress in Physics, AECL, No. 950, Chalk River, Ontario (1959).
4. Experimental Nuclear Physics, Editor E. Segre, 1, [Russian translation], Moscow, IL, (1955), p. 190.

CHARGE-EXCHANGE OF OXYGEN IONS OF ENERGY 2-13.3 MeV
IN THIN ALUNDUM FILMS

(UDC 539.188)

N. I. Venikov, N. I. Chumakov and B. I. Khoroshchavin

Translated from *Atomnaya Énergiya*, Vol. 17, No. 6,

pp. 504-505, December, 1964

Original article submitted November 20, 1963

In connection with linear accelerators for oxygen-ions acceleration and electrostatic generators with charge-exchange, interest attaches to the relation between the concentrations of variously charged ions and the energy of the "stripped" beam. A relation of this type was obtained in experiments, performed with the cyclotron of the I. V. Kurchatov Institute of Atomic Energy, in which O_{16}^{2+} ions were accelerated with the third, fifth and seventh hf subharmonics. The ion beam from the cyclotron impinged on an alundum film of thickness $\sim 20 \mu\text{g}/\text{cm}^2$ and area $20 \times 40 \text{ mm}^2$, prepared by a method similar to that in [1]. After passing through the film the ion beam was analyzed according to charge by a sector magnet. To eliminate errors due to secondary emission from the target, the ion detector (a conventional Faraday cylinder) was mounted in a magnetic field of intensity $\sim 100 \text{ Oe}$. The energies of the ions penetrating the alundum film were determined

from the field of the sector magnet, which was previously calibrated to within $\pm 1\%$ throughout its range, using a beam of protons whose energy was determined from their time of flight.

Fig. 1 plots the relative concentrations of variously charged O_{16} ions versus the energy of the beam penetrating the alundum film.

In calculating the angular scattering of a beam on passing through a thin target, it is necessary to know the equilibrium charge on the ions. Fig. 2 plots the energy dependence of the equilibrium charge on the O_{16} ions, calculated as

$$\bar{Z} = \frac{\sum_i n_i Z_i}{\sum_i n_i},$$

where \bar{Z} is the equilibrium charge, n_i the concentration of ions with charge Z_i (in our case $\sum_i n_i = 1$).

The authors would like to thank A. A. Shubin for help in preparing the alundum film.

LITERATURE CITED

1. G. B. Andreev et al., *Pribory i tekhnika éksperimenta*, No. 6, 149 (1961).

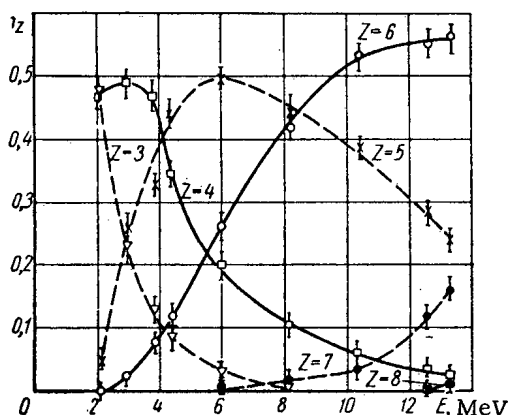


Fig. 1. Relative concentration n_Z of variously charged O_{16} ion, plotted versus energy of beam penetrating film.

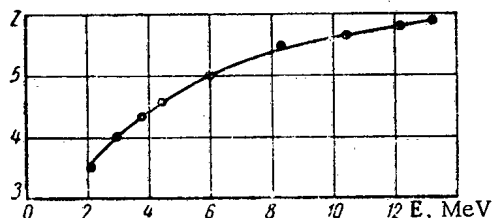


Fig. 2. Equilibrium charge of O_{16} ions versus energy.

NEUTRON RADIATIVE CAPTURE IN COPPER AND MOLYBDENUM

(UDC 539.172.4)

V. A. Tolskikov, V. E. Kolesov, A. G. Dovbenko,
and Yu. Ya. Stavisskii

Translated from *Atomnaya Énergiya*, Vol. 17, No. 6,
pp. 505-508, December, 1964
Original article submitted October 10, 1963

The energy dependence of the radiative capture cross section in the isotopes Cu^{65} and Mo^{100} was measured experimentally for neutrons with energies of 5-200 keV. The measurements were made using the relative activation method in a ring geometry. The reaction $\text{Li}(p, n)$, produced in a Van de Graaf accelerator, was used as the neutron source. The technique of measurement has been described in [1, 2].

Normalization of the Cu^{65} cross sections was done by using a weighted mean value of 44.9 ± 1.7 mb for the radiative capture cross section of neutrons from an Sb-Be source [1, 3, 4]; the neutron energy was 24 keV. The

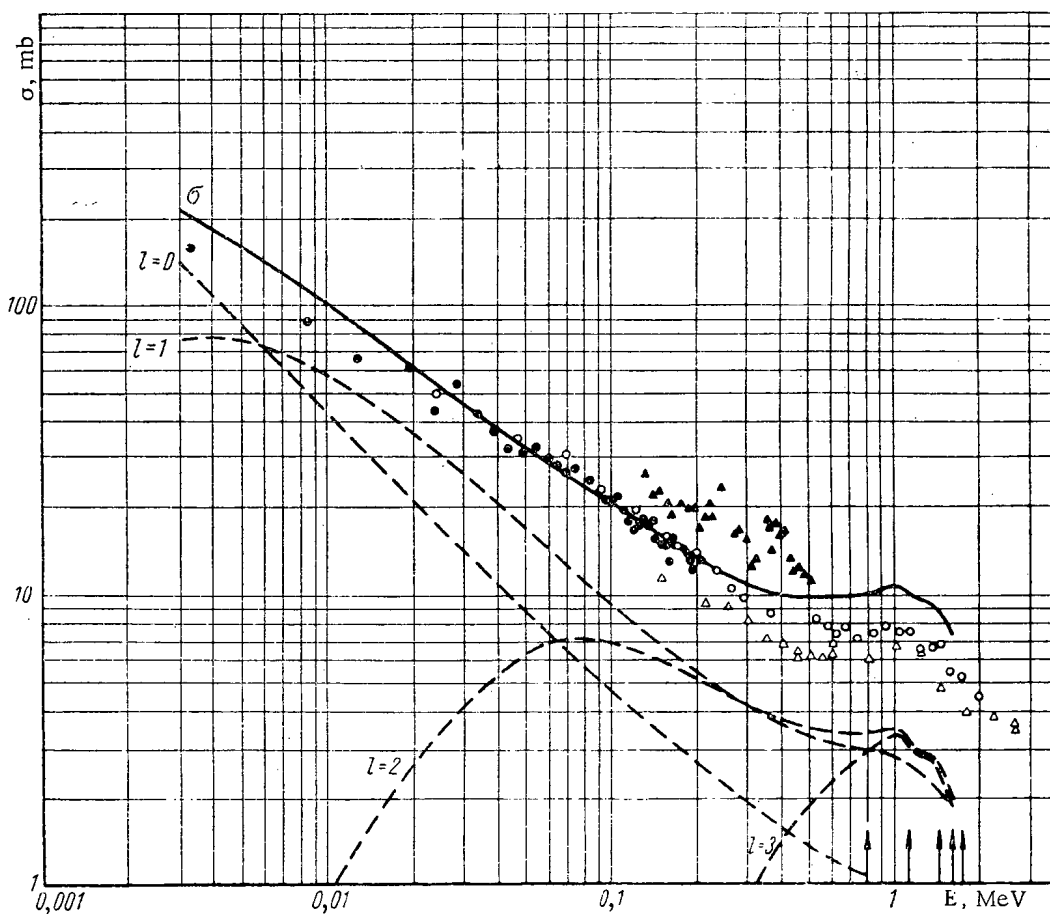


Fig. 1. Measured cross sections for radiative neutron capture in Cu^{65} in comparison with theory and with results of others. Data from: ● this experiment; ○ [1]; ▲ [5]; △ [11].

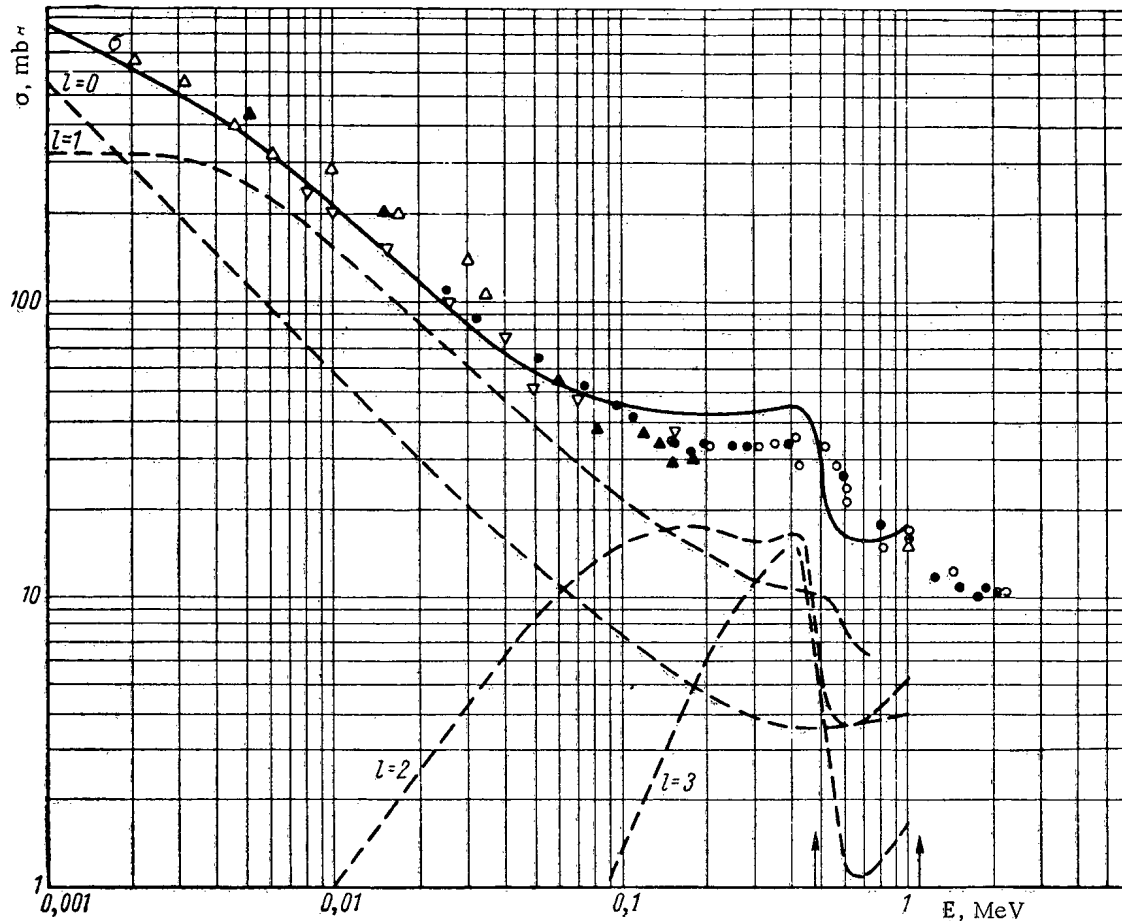


Fig. 2. Measured cross sections for radiative neutron capture in Mo^{100} in comparison with theory and with results of others. Data from: \blacktriangle) this experiment; \bullet) [1]; ∇) [6]; Δ) [7]; \circ) [11].

TABLE 1. Compound Nucleus Parameters Used in the Calculations.

Nucleus	B, MeV	α , MeV ⁻¹	\bar{D} , eV	$\bar{\Gamma}_\gamma$, eV	ξ
Cu^{63}	7,916	7,86	2400	0,4	956
Cu^{65}	7,06	8,1	4000	0,4	1590
Mo^{100}	4,61	17,1	650	0,09	1150

TABLE 2. Parameters for Target Nuclei Levels

Cu^{63}		Cu^{65}		Mo^{100}	
Energy MeV	Spin and parity	Energy MeV	Spin and parity	Energy MeV	Spin and parity
0	3/2 ⁻	0	3/2 ⁻	0	0+
0,67	1/2 ⁻	0,8	1/2 ⁻	0,474	2+
0,97	5/2 ⁻	1,12	5/2 ⁻	1,105	4+
1,34	7/2 ⁻	1,43	7/2 ⁻	—	—
—	—	1,62	3/2 ⁻	—	—
—	—	1,73	5/2 ⁻	—	—

results for the Cu^{65} cross section are shown in Fig. 1 in comparison with the results of other work. The nonmonotonicity of the cross section energy dependence curve is apparently associated with the effect of a group of resonances. In the 120-200 keV region, the cross section fluctuations are correlated with resonances in the capture cross section which were obtained in [5], but the absolute cross section values differ by a factor of one and one half to two. Within the limits of error, our results are in good agreement with the data in [1, 2].

The results of the Mo^{100} measurement are given in Fig. 2. Normalization of the relative cross section curve was done with data from [1] at $E_n = 138$ keV ($\sigma_{n\gamma} = 33.9 \pm 1.7$ mb). In the overlapping range of energies, the results are in good agreement with those in [1] and also with those from [6, 7] which were obtained by somewhat different methods.

Experimental errors are not indicated in Figs. 1 and 2 since they would fall but slightly outside the edges of the symbols on the plot.

The cross section $\sigma_{n\gamma}$ has been calculated in a number of papers [8]. Fundamental to the theory is the

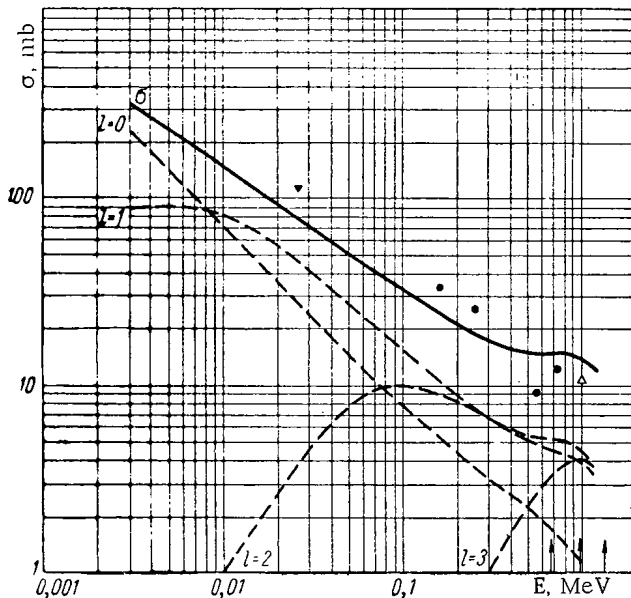


Fig. 3. Computed energy dependence of the neutron radiative capture cross section in Cu^{63} . Data from: \circ [3]; Δ [12]; \ominus [13].

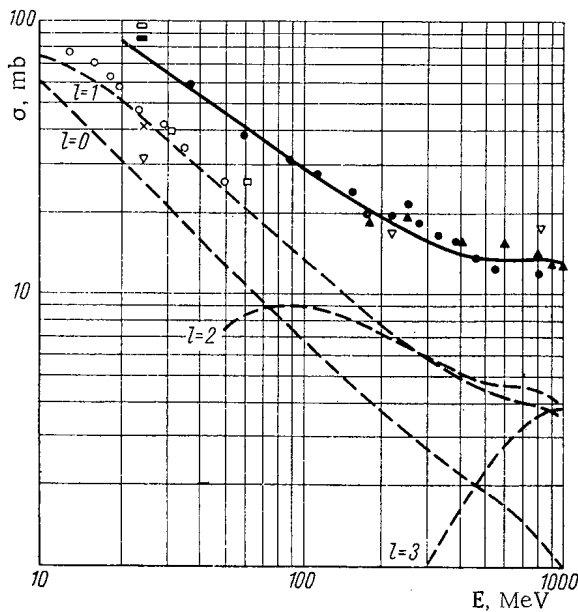


Fig. 4. Comparison of computed neutron radiative capture cross sections in natural copper with experimental results. Data from: \circ [3]; \circ [4]; \circ [7]; \ominus [14]; \times [15]; \blacktriangle [16]; ∇ [17]; \square [18].

agreement between calculated and experimental capture cross sections over the entire energy range shown in Fig. 1 for reasonable values of ξ and α .

To talk of a quantitative comparison of theory with experiment for Cu^{63} would hardly make sense because of the extreme scarcity of experimental data. However, the existing experimental points (see Fig. 3) lie on both sides of the calculated curve, and deviate from it by a factor of no more than one and a half.

assumption that the radiative capture process goes through the stage of compound nucleus formation.

The energy dependence of the mean radiation width was selected in the following form:

$$\bar{\Gamma}_{\gamma}^{(J)}(B+E) \approx \bar{D}^{(J)}(B+E) \int_E^{B+E} \frac{E_{\gamma}^3 dE_{\gamma}}{\bar{D}^{(J)}(B+E-E_{\gamma})}$$

The calculations were carried out for the simplest type of average spacing between levels in the compound nucleus

$$\bar{D}^{(J)}(x) = \text{const} (2J+1)^{-1} \exp(-2\sqrt{\alpha x})$$

The ratio $D/2\pi\bar{\Gamma}_{\gamma}$ at an energy equal to the neutron binding energy, B , in the compound nucleus enters into the calculation in the form of the parameter ξ .

In this paper, the neutron radiative capture cross sections in Cu^{63} , Cu^{65} , and Mo^{100} were calculated. The cross section calculations were performed on an electronic computer by means of a special program. Nuclear transparency T_l was computed according to the optical model for a Woods-Saxon potential with the parameters

$$V_0 = 45 \text{ MeV}; a = 0.5 \cdot 10^{-13} \text{ cm}, \zeta = 0.1, \\ R = 1.35 A^{1/3} \cdot 10^{-13} \text{ cm}.$$

The compound nucleus parameters [9] used in the calculation are given in Table 1, and the level schemes for the target nuclei are in Table 2 [9, 10].

Computed results are presented in Figs. 1-4. The arrows indicate the location of excited nuclear states. The solid lines are the total capture cross sections; the dashed lines are the contributions to the cross section by neutrons with different orbital momenta.

The theory does well in giving the general course of the capture cross section for Cu^{65} over a broad energy region (see Fig. 1). In addition, good agreement with the experimental results of this paper and those of [1, 2] with respect to absolute values is observed up to 250 keV. At higher energies, the calculated cross section is somewhat higher than the experimental. Since D and $\bar{\Gamma}_{\gamma}$, and consequently the parameter ξ also, are determined with no great precision, calculations were performed for various ξ and α . However, we did not succeed in obtaining agree-

Allowing for percent content, the capture cross section for natural copper was computed from the computed isotopic cross sections for Cu^{63} and Cu^{65} . It is compared with experiment in Fig. 4. Good agreement is noted with data from [4, 14, 16, 17]. However, the computed curve is considerably higher than the results in [7, 15, 18], where the neutron radiative capture cross section was investigated at $E_n < 60$ keV.

The fundamental difficulty in the theoretical analysis of $\sigma_{n\gamma}$ for Mo^{100} is the absence of a reliable level scheme for the target nucleus. The scheme given in Table 2 is tentative, and was obtained from an analysis of neighboring even-even isotopes.

A comparison of the experimental and calculated values of $\sigma_{n\gamma}$ for Mo^{100} is shown in Fig. 2. Calculation is in good agreement with experiment in the energy range 1-100 keV. In the energy range 0.1-1 MeV, the theoretical curve only gives the shape of the energy dependence of $\sigma_{n\gamma}$ differing from experiment in absolute value. As in the case of copper, a trial-and-error selection of the parameters ξ and α was not successful in producing agreement of theory with experiment over the entire energy range under consideration. Calculations in the region above 1 MeV cannot be made because of the absence of data concerning the Mo^{100} levels.

The theory for Mo^{100} does well in giving the sharp bend in the cross section curve at 500 keV. It results from the competition of inelastic neutron scattering with excitation of the 2^+ level at 474 keV. Furthermore, the neutron capture cross section for $l = 3$ falls most sharply of all.

In all the cases we considered, the capture of neutrons with $l \geq 1$ begins to play a significant role even at comparatively low energies. Certain general regularities are observed in the behavior of the cross section for all the nuclei studied. With the exception of very low energies, the partial cross section for p-waves is everywhere higher than the cross section for s-neutrons. A more rapid fall in cross section is observed for the case $l = 0$ than for the case $l = 1$.

In the neighborhood of 10 keV, the d-wave contribution becomes noticeable, and by 60-70 keV, the radiative capture for these waves becomes comparable with s-neutron capture. At a somewhat higher energy, the d-neutron radiative capture cross section reaches the magnitude of the p-neutron capture cross section. From that point on, these two cross sections remain approximately equal.

The partial capture cross section for neutrons with $l = 3$ begins to have an effect in copper at 300 keV, and reaches values corresponding to those for $l = 1$ and $l = 2$ at 1 MeV. At that energy, s-neutron capture is already several times less. In Mo^{100} , the f-waves come into play at 100 keV, and by 300 keV, their partial cross section is comparable with the cross sections for $l = 1$ and $l = 2$.

The calculations that were performed show that even a comparatively crude theory such as was used here is able to describe satisfactorily the energy dependence of the neutron radiative capture cross sections. Further, the theoretical parameters from [9] proved to be optimal.

The nature of the approximations in the calculations that were made should be indicated. In particular, no consideration was given to spin-orbit interaction, the distribution of reduced neutron widths, the dependence of level density on spin, etc. At the present time, a program is being written which will take into account the situations mentioned above.

LITERATURE CITED

1. V. A. Tolstikov, dissertation (1960).
2. Yu. Ya. Staviskii and V. A. Tolstikov, *Atomnaya Énergiya*, 10, 508 (1961).
3. R. Macklin, N. Lazar, and W. Lyon, *Phys. Rev.*, 107, 504 (1957).
4. J. Vervier, *Nucl. Phys.*, 9, 569 (1958/59).
5. R. Henkel and H. Barshall, *Phys. Rev.*, 80, 145 (1950); D. Hughes and R. Schwartz, *Neutron Cross Sections*, Supl. 1, Upton, N. Y., BNL. (1957).
6. E. Bilpuch, L. Weston, and H. Newson, *Ann. Phys.*, 10, 455 (1960).
7. S. P. Kapchigashev and Yu. P. Popov, *Atomnaya Énergiya*, 15, 120 (1963).
8. B. Margolis, *Phys. Rev.*, 88, 327 (1952); A. Lane and J. Lynn, *Proc. Phys. Soc. A*, 70, 557 (1957); P. E. Nemirovskii, *ZhÉTF*, 39, 1737 (1960); V. A. Tolstikov, V. E. Kolesov, and V. S. Stavinskii, *Atomnaya Énergiya*, 11, 56 (1961).
9. I. V. Gordeev, D. A. Kardashev, and A. V. Malyshev, *A Handbook of Nuclear Physics Constants*, Moscow, Gosatomizdat (1963).

10. B. S. Dzhelepov and L. K. Peker, Decay Schemes of Radioactive Nuclei, Moscow-Leningrad, Izd-vo AN SSSR (1958).
11. A. Johnsrud, M. Silbert, and H. Barschall, Phys. Rev., 116, 927 (1959).
12. D. Hughes, R. Garth, and J. Levin, Phys. Rev., 91, 1423 (1953).
13. D. Hughes and R. Schwartz, Neutron Cross Sections, Supl. 1, Upton, N. Y., BNL. (1957).
14. Yu. Ya. Staviskii and A. V. Shapar', Atomnaya Energiya, 15, 323 (1963).
15. H. Schmitt and C. Cook, Nucl. Phys., 20, 207 (1960).
16. B. Diven, J. Terrell, and A. Hemmendinger, Phys. Rev., 120, 556 (1960).
17. T. S. Belanova, ZhETF, 34, 574 (1958).
18. J. Gibbons et al., Phys. Rev., 122, 182 (1961).

RADIATIVE CAPTURE CROSS SECTIONS
FOR FAST NEUTRONS IN IRON

(UDC 539.170.2:539.172.4)

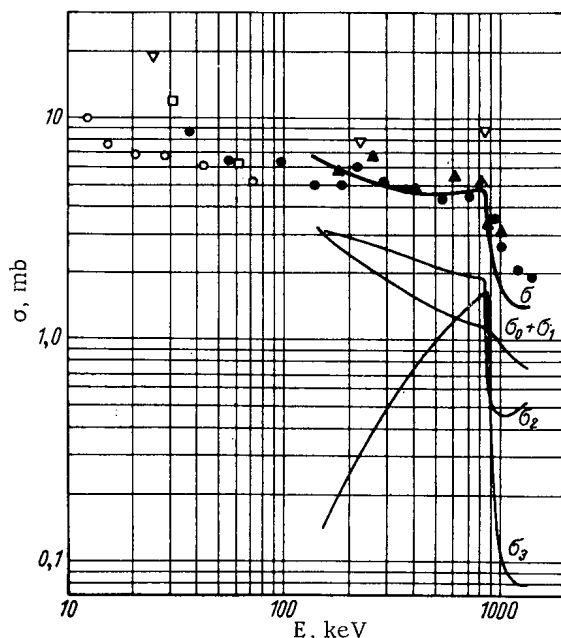
A. V. Malyshev, Yu. Ya. Stavisskii, and A. V. Shapar'

Translated from Atomnaya Énergiya, Vol. 17, No. 6,

pp. 508-509, December, 1964

Original article submitted December 28, 1963.

It is well known that inelastic scattering of neutrons can have a powerful effect on the energy dependence of the radiative capture cross sections for fast neutrons. A typical example is the behavior of the cross section for neutron capture by the isotope Fe^{56} . Previously, we measured the energy dependence of the neutron capture cross section in the energy range 0.03-0.9 MeV for a natural mixture of iron isotopes [1]. In these measurements, as in [2], a drop in the capture cross section was observed for neutron energies greater than the energy of the 845 keV level ($J = 2^+$) in the main iron isotope Fe^{56} , the drop being connected with competition from inelastic scattering. To clarify the behavior of the cross section at high neutron energies, measurements were made of σ_γ for a natural mixture of iron isotopes with 1, 1.2, and 1.4 MeV neutrons. The technique of measurement was similar to that described previously [1]. The energy resolution was 40 keV, and the accuracy of the results 20%. The results, together with previously obtained data, are shown in the figure. It is clear that the capture cross section falls at neutron energies above 900 keV. Further, the magnitude of the cross section is reduced to ~ 2 mb at neutron energies of 1.2 and 1.4 MeV. The solid lines give the calculated values for the radiative capture cross section in Fe^{56} which were obtained by using the formulas of statistical theory [6]. The symbol σ_i denotes the radiative capture cross section curve for neutrons with orbital momentum i .



Energy dependence of the radiative capture cross section for iron. Data from: ●) this experiment; ▲) [2]; □) [3]; ○) [4]; ▽) [5].

Transparency of the nucleus in the optical model was computed [7] for the potential

$$U = U_0 \frac{1 + i\xi}{1 + \exp\left[-\frac{R-r}{a}\right]} \quad \text{for } R = 1,25 A^{1/3} \cdot 10^{-13} \text{ cm.}$$

$U_0 = 45$ MeV; $\xi = 0.1$; $a = 0.5 \cdot 10^{-13}$ cm. The average spacing between levels with $l = 0$ ($D = 2.2 \cdot 10^4$ eV) was taken from [8]. In doing the calculations, the average radiation width was varied since precise data as to its magnitude was lacking. Agreement between calculation and experimental data was obtained for $\Gamma_\gamma = 0.45$ eV. This value is related to an excitation energy of the compound nucleus equalling 7.64 MeV, which corresponds to thermal neutron capture.

Some deviation of the calculations from experimental data at neutron energies above 845 MeV can be explained by contributions from other iron isotopes since the measurements were made with a natural mixture of isotopes. The strong excitation of the level at $E = 845$ keV ($J = 2^+$) leads to a sharp drop of the capture cross section in the principal iron isotope Fe^{56} . The radiative capture cross sections for the other isotopes, whose content is 8.4%, apparently behaves more smoothly in the neutron energy range

0.845-1.4 MeV. Doing reliable calculations for these isotopes is difficult because the required parameters are not known. The radiative capture cross sections for Fe^{54} and Fe^{57} were estimated for an incident neutron energy of 1345 keV. The average spacing between levels in these isotopes was computed on the basis of data published in [9]. The value of Γ_γ was assumed to be the same as that for Fe^{56} . The resulting cross sections were 7.8 mb for Fe^{54} and 4.9 mb for Fe^{57} ; the radiative capture cross section for the natural isotopic mixture was 1.9 mb which is in good agreement with measurements.

LITERATURE CITED

1. Yu. Ya. Stavisskii and A. V. Shapar', *Atomnaya énergiya*, 10, 264 (1961).
2. B. Diven, I. Terrel, and A. Hemmendinger, *Phys. Rev.*, 120, 556 (1960).
3. I. Gibbons et al., *Phys. Rev.*, 122, 182 (1961).
4. A. I. Isakov, Yu. P. Popov, and F. L. Shapiro, *ZhÉTF*, 38, 989 (1960).
5. T. S. Belanova, *idem.*, 34, 574 (1958).
6. B. Margolis, *Phys. Rev.*, 88, 327 (1952).
7. V. E. Kolesov, S. M. Ermakov, and G. I. Marchuk, in *Neutron Physics* [in Russian], Moscow, Gosatomizdat (1961), p. 310.
8. H. Newsom et al., *Ann. Phys.*, 14, 387 (1961).
9. A. V. Malyshev, *ZhÉTF*, 45, 316 (1963).

USE OF THE MONTE CARLO METHOD FOR CALCULATING
THE PENETRATION OF γ -RADIATION THROUGH MATTER

(UDC 539.122)

L. M. Shirkin

Translated from *Atomnaya Énergiya*, Vol. 17, No. 6,

pp. 509-511, December, 1964

Original article submitted December 11, 1963; in revised form, April 24, 1964

In this paper, methods are described for reducing the volume of computation in calculating individual γ -quanta histories by the Monte Carlo method. The methods that have been developed make it possible to calculate rather easily approximately 20-60 histories per hour by hand computations. Because of this, it has been possible to treat many problems dealing with γ -quantum penetration, whose solution was impossible by other methods, without using electronic computers.

From the widely accepted schemes [1, 2] for calculating the penetration of radiation through a slab of matter by the Monte Carlo method, we pick out three of the most time-consuming operations: 1) the determination of the γ -quantum path length; 2) the determination of the Compton scattering angle ω ; 3) the determination of the angle between the normal to the plane of the slab and the direction of motion of the γ -quantum after $(n+1)$ scatterings, $-\theta_{n+1}$. We present methods for finding these quantities.

To determine the path length for a γ -quantum, x , it is necessary to substitute a number y taken from a table of random number in the formula

$$x = \frac{1}{\mu} \ln \frac{1}{1-y}, \quad (1)$$

where μ is the linear attenuation coefficient, and to carry out the respective operations.

If $d\sigma/d\omega$ is the differential scattering cross section and y is a random number, the Compton scattering angle is determined from

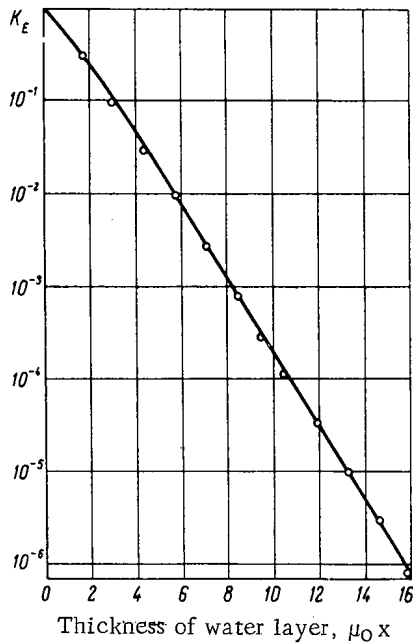
$$y = \frac{\int_0^{\omega} \frac{d\sigma}{d\omega} \sin \omega \, d\omega}{\int_0^{\pi} \frac{d\sigma}{d\omega} \sin \omega \, d\omega}.$$

Finally, the angle θ_{n+1} is found from the formula

$$\cos \theta_{n+1} = \cos \theta_n \cos \omega_{n+1} + \sin \theta_n \sin \omega_{n+1} \cos \chi_{n+1}, \quad (2)$$

where χ_{n+1} is the azimuthal scattering angle.

We consider methods for reducing the computations involved in these operations. In order to calculate a γ -quantum history by the Monte Carlo method with random numbers taken from a table, it is necessary to make a number of transformations. The volume of computation is determined by their complexity. The transformation is particularly simple for discrete random quantities, i.e., quantities whose possible values can be tabulated beforehand. In this situation, one can associate with each value of the discrete quantity a definite combination of digits in a table of random numbers [3]. Thus, for a discrete random quantity, a number taken from a table of random numbers immediately determines the value of this quantity.



Energy attenuation coefficient of water, K_E , for 4 MeV γ -rays from a plane, monodirectional source: (—) theoretical data [5]; (O) Monte Carlo calculation.

The method for determining the value of a continuous random quantity is more complicated. If the continuous random quantity x has a probability density $f(x)$, and if y is a random number, x can be found from the equation

$$y = \int_0^x f(x) dx.$$

Much time is consumed in the solution of this type of equation.

To shorten the computations, we approximately replace the random quantity with distribution density $f(x)$ by a discrete random quantity (for example, the possible values for the Compton scattering angle are broken down into a number of intervals, and the scattering probability for each of these intervals is determined).

We chose 21 intervals; the magnitude of each of the first seven intervals, which covered from 0 to $7/36\pi$, was $1/36\pi$, and the magnitude of each of the remaining 14 intervals was $1/18\pi$. In order not to have to compute θ_{n+1} by the unwieldy formula (2) every time, tables were constructed in which θ_{n+1} was defined for given θ_n , ω_{n+1} , and χ_{n+1} . In these tables, the range of possible values for the angle ω_{n+1} was broken down into 21 intervals as indicated above, the angle χ_{n+1} was assumed equal to $1/10\pi$, and the angle θ_n was assigned values $1/18\pi$, $1/12\pi$, $1/9\pi$, $5/36\pi$, $1/6\pi$, $7/36\pi$, $1/4\pi$, and then for each additional $1/18\pi$.

To pick out the γ -quantum path length, the following method was used instead of a calculation by means of formula (1).

The probability for interaction of a γ -quantum with energy E_0 while penetrating Δx cm of the slab is determined. Let it equal 0.23. Since any digit in a table of random numbers occurs with a probability 0.1, and a combination of any two digits with a probability 0.01, an interaction with a probability 0.23 can be associated with entries in a table of random numbers, for example, 1, 2, 31, 32, 33.

Several numbers from an arbitrarily selected location are copied from a table of random numbers [4]: 60835, 42323, etc. A γ -quantum trajectory Δx cm long is laid off in the slab. According to assumptions, an interaction occurs during penetration of Δx cm of the slab if the digits 1, 2 or the combinations 21, 32, 33 occur. In the table of random numbers (at the selected location), the first digit will be six. Therefore, an interaction does not occur, and the γ -quantum continues to move in its original direction. A second segment Δx is laid off, and the digit six is crossed off as having been used. Repeating the previous argument, it is concluded that the second segment of the γ -quantum trajectory is also traversed without collision. The same will hold true for the third, fourth, and fifth segments.

Finally, the γ -quantum traverses the sixth segment Δx . After six trials, the next digit is a two. Consequently, an interaction occurs in this segment according to assumption, and the first γ -quantum path length equals $6\Delta x$ cm.

Thus the determination of γ -quantum path length is reduced to the determination of the location of previously given digits, or combinations of them, in a table of random numbers. To do this, it is necessary to perform only one operation actually instead of five operations required by formula (1).

The computational procedure for γ -quantum path length close to a boundary of the slab is now considered. Let the γ -quantum traverse a distance R without collision. There remains a segment of the trajectory ΔR to a boundary of the slab with $\Delta R < \Delta x$. It is determined whether an interaction occurs in the next segment Δx . For a negative result, it is obvious that the γ -quantum also traverses the segment ΔR without collision, and leaves the slab. Assume that a collision occurs in the segment Δx . Then it is necessary to determine the probability of a γ -quantum interaction in the segment ΔR .

It can be shown that this probability is

$$W = \frac{1 - e^{-\mu \Delta R}}{1 - e^{-\mu \Delta x}}$$

or, approximately, $W \approx \Delta R / \Delta x$. Therefore, close to a boundary, we proceed in the following manner. If $\Delta R < \Delta x$, and if no interaction occurs in the segment Δx , the γ -quantum escapes from the slab. If an interaction does occur, and if y is a random number, when $y > \Delta R / \Delta x$, the γ -quantum leaves the slab; for $y \leq \Delta R / \Delta x$, an interaction is considered to have occurred at the slab boundary.

Thus the laborious operation for determining the angles ω and θ is reduced to the location of the required data in the appropriate tables, and the determination of γ -quantum path length by formula (1) is replaced by the determination of the location of a previously given combination of digits in a table of random numbers.

To make practical computations by the proposed method requires the existence of random number tables in which all the digits are uniformly distributed in the interval 0-1. Unfortunately, existing tables fail to satisfy this requirement. For example, in the tables of [4], the probability for the appearance of one is 0.1087, that for two is 0.1023, that for eight is 0.0945, etc. Therefore, we used revised tables in which "excess" digits were removed in accordance with the laws of chance, and those lacking were substituted.

The proposed method was used to determine the energy attenuation coefficient for scattering of radiation in water. To speed up the calculations, the splitting technique [1] was used; the slab was subdivided into 12 layers. The number of γ -quanta emerging from a layer was tripled for the calculation of the succeeding layer. The number of γ -quanta histories in the first water layer was 450. The segment Δx was 10 cm.

In the calculation, 10 energy groups were considered. Tables for the determination of the scattering angle ω were constructed for energies of 4.0, 3.0, 2.0, and 1.0 MeV.

The relative probable error for a single layer was computed from the formula [2].

$$(\delta_{\text{prob}})_i = 0.67 \sqrt{\frac{B_i (1 - B_i)}{N_0^i}},$$

where $B_i = \frac{N_i}{N_0^i}$; N_0^i is the number of γ -quanta incident on the i -th layer; N_i is the number of γ -quantum penetrating the i -th layer. In the calculations that were made, $(\delta_{\text{prob}})_i$ was 4-5%.

The figure gives the results of the Monte Carlo calculation as compared with theoretical data. One can conclude that the approximations used in the method developed for the purpose of speeding up the calculations do not have a significant effect on the accuracy of the final results.

LITERATURE CITED

1. H. Goldstein, Fundamentals of Reactor Shielding [Russian translation], Moscow, Gosatomizdat (1961).
2. O. I. Leipunskii, B. V. Novozhilov, and V. I. Sakharov, Propagation of γ -Quanta in Matter [in Russian], Moscow, Fizmatgiz (1960).
3. Modern Mathematics for the Engineer, E. F. Beckenbach, ed. [Russian translation], Izd-vo inostr. lit. (1958).
4. F. M. Morse and D. E. Kimball, Methods of Operational Research [Russian translation], Moscow, Izd-vo Sovetskoe radio (1956).
5. M. Berger and J. Dogget, J. Res. Nat. Bur. Standards, 56, 89 (1956).

SCIENCE AND ENGINEERING NEWS

SYMPOSIUM ON THE BIOLOGICAL EFFECTS OF RADIOISOTOPES

Translated from *Atomnaya Énergiya*, Vol. 17, No. 6,
pp. 512-514, December, 1964

The biological effects of radioactive isotopes incorporated in living beings constitute one of the most intricate problems in contemporary radiobiology. The reason for this is that, in addition to the radiation factor, the distribution of the substance throughout the organism, the form of the emitter chemical compound, the rate at which it is removed from the organism, the path of uptake into the organism, and miscellaneous other factors are also important. At the same time, the study of these processes is particularly necessary in order to ensure safety in the use of radioactive isotopes, since their tolerance concentrations in the human body cannot be computed reliably without prior knowledge of the appropriate radiobiological constants. A large supply of new data of value in this field was communicated to the scientific public in June 1964 at a symposium on the biological effects of radioactive substances held in Moscow. Of the 83 papers submitted to this symposium, 60 papers devoted to the most important emitters (Sr^{90} , Pu^{239} , Po^{210} , I^{131} , H^3 , etc.) were heard and discussed at the gathering.

A large number of the papers dealt with the most dangerous long-lived β -emitter, viz. Sr^{90} , which is found in radioactive fallout. L. N. Burykina, in her study of the kinetics of the buildup of this isotope in dogs subjected to chronic exposure through food intake, found that the rate of deposition of the isotope in the skeleton slowed down measurably as the duration of observation lengthened, while the distribution (both in individual bones and in various portions of the same bone) smoothed out. It was also found that inoculation of $0.2 \cdot 10^{-4} \mu\text{Ci/kg}$ body weight per day over a period from 3 to 3.5 years brought the rate of Sr^{90} buildup in the skeleton, as determined by the ratio of the whole body burden of Sr^{90} to the activity introduced daily, to 75 for young animals, decreasing to a figure as low as 8 with increased age. After the inoculation experiment was terminated, the rate of removal was found to be 2300 ± 300 days.

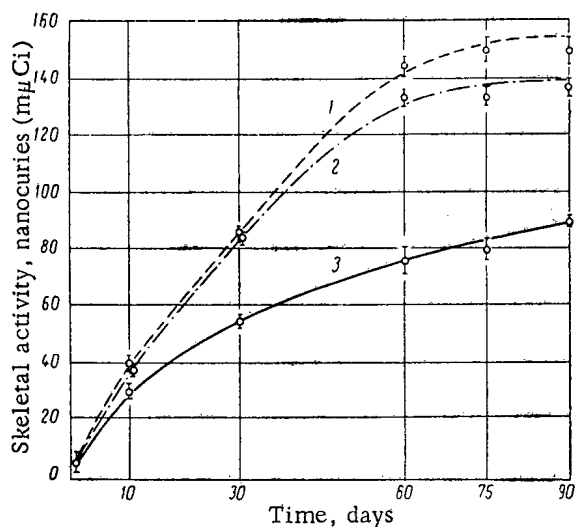


Fig. 1. Effect of ultraviolet exposure and feeding of vitamin D_2 on the kinetics of Sr^{90} accumulation in rat skeletons: 1) Sr^{90} fed with ultraviolet exposure; 2) same, but with additional feeding of vitamin D_2 ; 3) Sr^{90} introduced.

L. A. Buldakov and R. A. Erokhin reported that the amount of Sr^{90} deposited in mice skeleton after a single introduction of various quantities of the substance (from 0.1 to $74 \mu\text{Ci}$) and the rate of removal from the skeleton are independent of dose. 76% of the Sr^{90} deposited is removed in a biological half-life (T_{eff}) of 3 days, and 24% is removed in 537 days. At the same time, the fraction of strontium turnover at a rapid rate decreases in chronic uptake, while the slow turnover fraction increases with a simultaneous increase in T_{eff} . Great care should be taken, therefore, in converting radiobiological data obtained with experimental animals in an acute exposure experiment to critical tolerance data applicable to humans.

A. A. Mirzoyan, in a protracted experiment performed on 500 rats fed $9 \cdot 10^{-2} \mu\text{Ci}$ Sr^{90} orally in the form of SrNO_3 daily, made a reliable determination of the increased buildup of this isotope in the skeletons of rats subjected to additional ultraviolet exposure ($420 \text{ microerg/cm}^2$) or to UV treatment combined with feeding of D_2 vitamin (200 units). The Sr^{90} skeletal burden observed on the 60-th day of observations with in animals treated with combined β -ray and ultraviolet exposures was almost twice that in animals subjected to β exposure alone (Fig. 1).

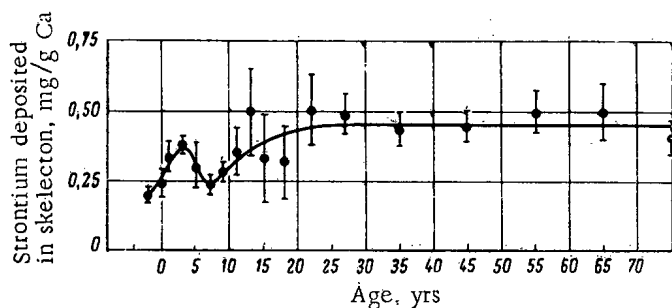


Fig. 2. Dynamics of accumulation of stable strontium in the human skeleton.

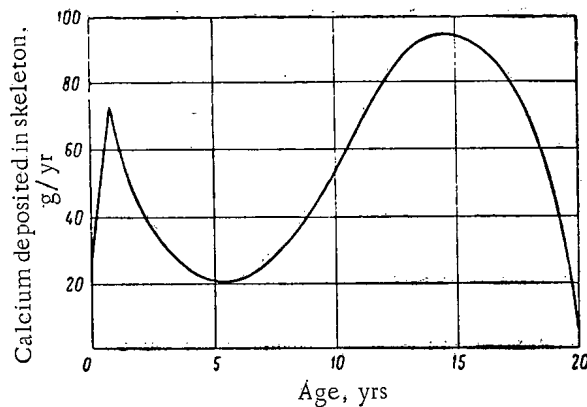


Fig. 3. Dynamics of calcium deposition in the human skeleton.

TABLE 1. Frequency of Incidence of Osteogenic Sarcomas (in animals living more than 200 days) at Various Levels of Effect Produced by Pure Radioisotopes and Mixtures

Amount of optimal sarcomogenic doses		Isotopes								
		Sr ⁹⁰	Ce ¹⁴⁴	Pu ²³⁹	Sr ⁹⁰ + Ce ¹⁴⁴	Sr ⁹⁰ + Pu ²³⁹	Ce ¹⁴⁴ + Pu ²³⁹	Sr/Ce	Pu/Sr	Pu/Ce
2	a	33	100	23	—	100	76	—	—	3,9
	b	419	210	402	—	178	285	—	—	
	c	76,5	104	4,26	—	25+1,2	60+1,7	—	—	
1	a	48,6	54,5	24,3	47	59,5	67,2	—	7,5	7,4
	b	274	275	460	256	261	349	—	—	
	c	32	59	2,26	15,2+28,6	15,3+0,8	32+0,97	—	—	
0,5	a	34,8	46,2	15,7	80	36,7	14,1	—	—	—
	b	335	335	552	268	393	522	1	8,5	
	c	17	32	1,27	7,8+14,6	9,1+0,5	17,8+0,6	—	—	
0,25	a	15	27,3	4,3	—	—	—	—	—	—
	b	609	391	670	—	—	—	—	—	
	c	10,8	16,7	0,70	—	—	—	—	—	

a) Fraction of animals with sarcomas, %
 b) Lifetime of rats dying from osteosarcomas, days
 c) Absorbed dose in skeleton, filorads.

I. K. Dibodes et al., presented some unique data on the content of stable strontium in the diet and skeleton of humans. This information, as we know, is valuable in making accurate measurements of the buildup ratio of radioactive strontium, and in computing on that basis the critical tolerance content of that isotope in the human diet. On the basis of a spectroscopic determination of the content of stable strontium in 180 bone tissue samples, the authors uncovered the dynamics of the variation of quantities of this element in the human skeleton (Fig. 2). It was found that the average content of stable strontium in bones of infants is 240 μg per gram of Ca, but 450 μg in adults above 20 years of age. Placental discrimination may be characterized thus by a coefficient of ~ 0.5 . It was also found that calcium deposition in the skeleton is nonconstant (Fig. 3), and attains a maximum in the 14th to the 16th year. The strontium buildup ratio was estimated by these authors at ~ 200 in the skeleton of adults, the discrimination factor of strontium with respect to calcium as these elements pass from the food to bone tissue is of the order of 0,2.

One of the most important problems of a practical nature in radiobiology is the study of the combined effects of radiation factors, but the number of papers dealing with this area of investigation was exceedingly scanty. Special attention was therefore due to a paper by Yu. I. Moskalev et al., containing the basic findings of research

TABLE 2. Number of Tumors Induced by Pm¹⁴⁷ in Experimental Rats (in percentage of number of animals surviving longer than 200 days)

Type of malignancy	Control	Amount of Pm ¹⁴⁷ , $\mu\text{Ci/g}$				
		10-3	10-2	0,1	0,5	1,1
Osteosarcoma	0	0	0	8,6	9,0	10,4
Leucosis	4,8	0	5,2	4,3	4,5	47,3
Tumors of the liver and gastrointestinal tract	4,7	6,0	5,2	4,3	27,3	21,1
Total tumors induced on rat	$\frac{1}{21}$	$\frac{1}{15}$	0,10	0,17	0,40	0,80

to date on the combined effects of incorporated Sr⁹⁰, Ce¹⁴⁴, and Pu²³⁹ on the organism of rats in acute, subacute, and chronic radiation injury periods. These authors were successful in revealing a synergism at work in various cases investigated, in addition to biological and effective half-lives for several isotopes: when a pair of isotopes having the same or different type of distribution is introduced jointly, most of the resulting injuries not only sum additively (Ce¹⁴⁴ + Pu²³⁹), but even appear earlier, or, in a large percentage of cases (Sr⁹⁰ + Ce¹⁴⁴ and Sr⁹⁰ + Pu²³⁹) at equal or lesser absorbed doses in the skeleton (Table 1).

T. Mukhamedov, performing an analysis of the combined effect of I¹³¹ and noise on a group of experimental dogs, introduced I¹³¹ in amounts to 4 $\mu\text{Ci/kg}$ body weight in one group, and subjected a similar group of inoculated animals to the additional effect of noise of 100-105 db intensity (20-25 db above the tolerance level) with a noise spectrum from 280 to 1300 Hz. A comparison of the critical organs (thyroid gland) on the 247-th day revealed absorbed doses in dogs subjected to the combined effect of various harmful factors to average at 75,000 rads, as compared to 47,000 rads in animals exposed solely to I¹³¹, and this was ascribed to variations in the dynamics of iodine accumulation. It was also found that alterations of the thyroid gland were of a more malignant nature in response to these combined effects.

V. N. Strel'tsova reported on the blastomogenic effectiveness of the hepatotropic isotope Pm¹⁴⁷ as a function of the amount of that isotope gaining access to the organism. In cases of a single intraperitoneal injection of Pm¹⁴⁷ in amounts of 1,1-0.011 μCi per kg body weight of a rat, in experiments carried out on 120 animals, the findings were that tumors made their appearance in 63 animals, i. e., 26% of the rats surviving a period longer than 100 days. The frequency of tumor incidence decreased in correspondence with a decreased amount of Pm¹⁴⁷ injected (Table 2). The spectrum of the tumors varied as a function of the amount of isotope incorporated. Osteosarcomas, liver tumors, and tumors of the gastrointestinal tract appear when Pm¹⁴⁷ is injected in amounts ranging from 1,1 0.14 $\mu\text{Ci/g}$. When lesser amounts are injected, tumors in internal secretion glands prevail. The absorbed doses at which tumor development is observed ranged from 400-700 all the way to 4000 rads in this case.

A. E. Ivanov and K. I. Gorel'chik discovered, in an ingenious and elegant radiometric investigation of the consequences of injection of Ce¹⁴⁴ fluoride into the lungs of experimental rabbits, a fact of fundamental importance in the redistribution of the radioactive material in the lungs. In-vivo scanning of the thoracic cage, as well as radiometric analyses of the pulmonary tissue, and autoradiographic and historadiographic investigations, aided in establishing two phases in the process of decontamination of the lungs, which biological half-lives of 7 and 126 days respectively. It was shown in very clearcut fashion that special features of the organ are responsible for the radioactive material becoming unevenly distributed in the organ, and for the comparatively rapid concentration of the material in the root zone where its blastomogenic effect is manifested.

Important data bearing directly on estimates of the tolerable Sr⁹⁰ burden in humans were presented by N. A. Zapol'skaya et al. Removal of Sr⁹⁰ from a single bone was found to vary in time (Fig. 4): the first biological half-life involved is 1,5-3 days, the second 90-100 days. A sharp contrast was also seen in the rates at which this isotope

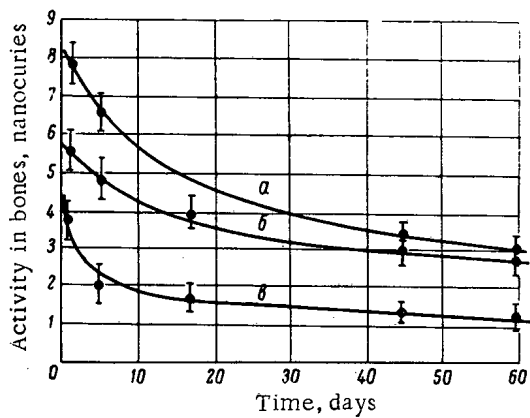


Fig. 4. Variation in Sr^{90} concentration in bones of spinal column (a), skull (b), and extremities (c) after termination of the injection of this isotope into the organisms of experimental animals.

effectiveness of 14 distinct ion exchange resins of Soviet manufacture for subsequent use in "artificial kidney" systems. A second paper dealt with the practical implementation of this apparatus in medical practice, and studied the effectiveness of hemodialysis in injuries brought about by Sr^{90} incorporated by a small group of experimental dogs. The findings were that, depending on the length of time the artificial kidney is in use and on the time elapsed from the time the animal is injected subcutaneously with Sr^{90} to the initiation of the hemodialysis, from 28 to 47% of this substance was successfully extracted from the organism.

The state publishing house "Meditsina" is scheduling the proceedings of this symposium for publication in 1965.

was removed from different portions of the skeleton (the power exponent of the removal function is -0.33 for bones in the extremities, -0.23 for the vertebral column, and -0.15 for the skull). This permits us to infer that the rate of strontium removal from the skeleton will be, on the whole, the sum of the rates of several processes, and may be described by a power-law model.

V. K. Lemberg et al., in a study of the effect of additional pathological factors on remote sequelae of radiation injury brought about in mice by Pu^{239} nitrate in amounts of $2 \cdot 10^{-3}$ and $6.3 \cdot 10^{-4} \mu\text{Ci/g}$, discovered that repeated aseptic inflammations inhibit the development of skeletal malignancies, while repeated hemorrhages and mechanical traumas (bone fractures) evince a certain tendency to contribute to the development of skeletal tumors when the organism is exposed to Pu^{239} α -radiation.

K. P. Krylov and M. G. Petrovnin presented some extremely promising papers in the field of protection against internal exposure. The first of these papers described the ef-

SPECIAL-PURPOSE HEAVY CEMENT WITH ENHANCED ABSORBING POWER

K. S. Kutateladze and A. V. Rustambekov

Translated from Atomnaya Énergiya, Vol. 17, No. 6,
pp. 515-516, December, 1964

Special heavy concrete containing a heavy aggregate is currently being employed for biological shielding in various nuclear installations; the binder used is customarily Portland cement. This cement is a comparatively weak absorber of radiation, so that the basic radiation load falls on the heavy aggregate. That accounts for the need to minimize the content of binder in the concrete.

Moreover, Portland cement has a relatively low bulk weight (1,5 ton per cubic meter), so that when a heavy aggregate is employed the concrete mass settles out into layers in the vibration tamping process and the cost of preparing and laying the special heavy concrete is greatly increased.

Experimental work on replacing Portland cement by some special heavy cement mix exhibiting enhanced absorbing properties and having a high bulk weight was therefore undertaken at the laboratory for binding materials of the Tbilisi (Tiflis) State Research Institute for Structural Materials. A fabrication technology was developed for a heavy binder based on scrap lead slag and Portland cement clinker.

The study of the physico-mechanical properties of the resulting slag binder consisting of 60-75% lead slag and 25-40% Portland cement clinker with 5% gypsum showed, under the GOST standards 310-41 and 310-60, that the material exhibits the following properties: amount of water required to produce grout of normal thickness is 24,0-24,2%, normal thickness of grout 6.8-7%, a cone spread of 110/110 mm (at a water/cement ratio of 0.40), setting is initiated in anywhere from 2 h 40 min to 3 h 35 min, and setting is completed in anywhere from 7 h 55 min to 14 h 05 min, the ultimate strength of standard cubes sized 7 x 7 x 7 cm under compressive stress and of 1:3 composition is 180-310 kg (force) per cm² in 28 days, or 640-740 kg (force) per cm² in a year of exposure to water. One

Determination of Water-Retaining Capacity of Slag Cement at Various Temperatures

Temperature, °C	Type of cement	Stored under moist conditions		Stored wet	
		average loss moisture, %	R _c compression, kg (force) per cm ²	average loss moisture, %	R _c compression kg (force) per cm ²
50	1	2,96	660	9,33	750
	2	4,11	330	9,99	365
	3	3,87	470	7,00	650
100	1	9,64	740	10,78	775
	2	9,37	235	14,09	225
	3	9,22	395	12,56	525
150	1	11,20	740	13,17	920
	2	10,25	245	14,09	225
	3	9,48	360	13,82	445
200	1	11,66	650	14,90	900
	2	11,53	270	15,61	290
	3	10,10	440	14,91	550
250	1	13,15	775	15,12	1025
	2	9,70	300	15,74	270
	3	10,16	440	15,40	525
300	1	14,13	700	16,35	800
	2	8,69	215	15,24	260
	3	15,24	380	15,24	420

*1) Portland cement; 2) lead slag - 75%; Portland cement clinker - 25%; gypsum - 5%; 3) lead slag - 60%; Portland cement clinker - 40%; gypsum - 5%.

typical feature of the slag binder is the extremely high flexural strength, attaining a figure on the order of 71-108 kg (force) per cm² in a year of exposure to water. The specific weight of the slag cement is 3.80-3.95 ton per cubic meter, and the bulk weight of the cement block is 2.9-3.2 tons per cubic meter.

A calculation of the absorbing properties on the basis of empirically derived formulas reveals that the specific slag binder exhibits a higher absorbing power than ordinary structural concrete [1].

The water-retaining capacity of slag cements at different temperatures was investigated in the course of the study. A. E. Desov's approach [2] was used in determining the water-retaining capacity, with one difference in that the weighed sample of the material was replaced by cubes of grout sized 2 x 2 x 2 cm. In this way, researchers were able to check any variations in the physico-mechanical properties of the material in response to temperature changes, as well as to determine moisture losses. Specimens solidified in water and under air-moisture conditions were tested. The results of the tests appear here in tabulated form.

The reader will see from the accompanying table that slag cements lose about as much water as does Portland cement over the temperature range from 50-300°C.

We may infer, then, that:

1) replacing Portland cement in biological shielding by this special-mix heavy cement means a simplification in the technology of concrete fabrication and laying of heavy concrete, can facilitate the transition to industrial production methods and pre-assembly of shields, and, in combination with the heavy aggregates generally used in practice will make it possible to cut down on the volume of the shielding;

2) the use of binder material having enhanced absorbing power will render possible an increased total cement content in the finished concrete, and this entails in turn a higher total water content in the concrete structure, a particularly important point for the attenuation of neutron flux;

3) the low cost of slag cement supports the hope that this material will win widespread favor in the construction of nuclear facilities.

LITERATURE CITED

1. A. N. Komarovskii, *Stroitel'nye materialy dlya zashchity ot izlucheni yadernykh reaktorov i uskoritelei* [Structural Shielding Materials for Nuclear Reactors and Accelerators], Moscow, Atom Press (1958).
2. A. E. Desov, *Tyazhelye i gidratnye betony (dlya zashchity ot radioaktivnykh vozdeistvii)* [Heavy and Hydrate Concretes for Biological Shielding], Moscow, State Construction Industry Press, Gosstroizdat (1956).

NEW BOOKS

Translated from *Atomnaya Énergiya*, Vol. 17, No. 6,
pp. 517-520, December, 1964

Books by Atomizdat

M. P. Grechushkina. *Tablitsy sostava produktov mgnovennogo deleniya U^{235} , U^{238} , and Pu^{239}* [Tables of composition of prompt-fission products of U^{235} , U^{238} , and Pu^{239}]. 1964, 67 pages, 19 kopeks.

These tables present the composition of fragments for five modes of fission, $U_{n, 14 MeV}^{238}$, $U_{n, thermal}^{235}$, $U_{n, fission}^{235}$, $U_{n, fission}^{238}$, and $Pu_{n, fission}^{239}$ for time intervals lasting from 1 h to 100 years after fission.

The tables give reference information and will be of interest to engineers and physicists working with fission fragments, as well as to specialists engaged in the study of radioactive fallout.

Izmerenie pogloshchennoi dozy v neitronnykh polyakh i v smeshannykh polyakh "gamma-izluchenie i neitrony." [Absorbed-dose measurement in neutron fields and in mixed gamma-neutron fields]. Translations of English-lang. papers. 102 pages, 42 kopeks.

Extensive material on neutron dose measurements is collected and generalized in this compendium by the U. S. National Bureau of Standards. The compilers, all prominent scientists who have made essential contributions to the development of neutron dosimetry, showed their ability to present in lucid and concise form the fundamental questions constituting the subject of current neutron dosimetry.

A. I. Zhernovoi and G. D. Latyshev. *Yadernyi magnitnyi rezonans v protochnoi zhidkosti* [Nuclear magnetic resonance in flowing fluid]. 1964, 253 pages, 76 kopeks.

In line with the automation of chemical and other process industries, special attention is being given to nuclear magnetic resonance in a flowing fluid, which allows for noncontacting and remote process on-stream monitoring of the quantity and quality of material in flow. This acquires particular importance in work with active and corrosive fluids.

The book described the general theory of NM resonance developed by the authors and discussions for making practical use of a through-flow sensor to measure liquid flowrate, for measuring and stabilizing of magnetic fields, and miscellaneous applications.

A list of pertinent literature appears at the end of the book.

Gidrodinamika i massoperedacha v psevdoozhizhennom sloe [Fluidized bed hydrodynamics and mass transfer]. Collection of papers presented at symposium on fluidization. Translations from Engl., 1964, 178 pages, 69 kopeks.

This symposium reflects a program of fundamental research on fluidized bed work carried out in the chemical engineering section of the Harwell atomic energy research center [Britain].

The book presents documents on the use of fluidized beds in such technological processes as the production of uranium hexafluoride, calcination of liquid radioactive wastes, processes in heat exchangers at nuclear power facilities.

The reader will find a description of research findings on the homogeneity of pressure and pressure variations in a fluidized bed with respect to height and diameter of the bed; various designs of fluidization apparatus and their effect on the behavior of fluidized beds are discussed.

N. P. Rudenko and A. I. Sevast'yanov. *Radioaktivnye izotopy Be^7 and Be^{10}* [The radioberyllium isotopes Be^7 and Be^{10}]. 1964, 24 pages, 5 kopeks.

This brochure presents information on beryllium radiochemistry, on nuclear processes involved in the formation of radioactive beryllium isotopes, on methods for extracting the irradiated material, and measuring techniques.

The applications of radioberyllium isotopes in industry and several phases of research are considered. A list of pertinent literature is appended.

B. Lustman. Radiatsionnye yavleniya v dvoukisi urana [Radiative phenomena in uranium dioxide]. Translated from Engl., 1964, 288 pages, 1 ruble, 46 kopeks.

This book is a translation of chapter 9 of the English-language monograph "Uranium dioxide; properties and nuclear applications" [edited by J. Belle. U.S. Government Printing Office, Washington D. C., 1961]. Extensive information is cited on radiation effects on uranium dioxide and on various other uraniferous oxide materials. A review of the theory of radiation damage in ionic-bond solids appears, along with experimental data on structural changes and changes in the properties of refractory oxides in response to radiation treatment.

The kinetics of the evolution of fission products from irradiated uranium dioxide, the behavior of uranium dioxide in corrosive media under irradiation, and the ability of the oxide to retain fission fragments are discussed.

There is a detailed treatment of the heat transfer behavior of fuel elements containing uranium dioxide. The use of uranium dioxide in three types of fuel elements is described: fuel elements with compacted uranium dioxide, in thin rod type elements and dispersion type elements; and the range of applications of each of these fuel element types, are also discussed.

The appendix provides a complete description of existing techniques for microscopic investigation of uranium dioxide existing in various states; in the form of powder, single crystals, pressed and sintered dioxide, in a zircaloy sheath, etc. The technique of fabricating preparations for electron and optical microscopy is described in close detail.

G. N. Popov, B. I. Nifontov, D. P. Lobanov, and A. V. Kulikov. Osobennoisti razrabotki mestorozhdenii radioaktivnykh rud [Aspects of mining radioactive ores]. 1964, 219 pages, 80 kopeks.

The history of the development of a raw materials base for the country, of the mining of radioactive ores, is discussed briefly, and a description is presented of engineering and costs factors in the uranium industry in the capitalist countries. Some attention is given to mining geological and engineering costs features of industrially profitable mine and alluvial deposits of radioactive ores.

Examples in foreign mining practice illustrate the basic conditions found in applications and the special features of open-pit and underground operations, and ways in which mining processes are engineered. Basic radiation safety principles observed in mining operations are discussed.

A list of literature is appended.

A. A. Khonikevich. Dezaktivatsiya sbrosnykh vod radiokhimicheskikh laboratorii i eksperimental'nykh atomnykh reaktorov [Deactivation of effluent water from radiochemical laboratories and experimental reactors]. 1964, 110 pages, 29 kopeks.

This brochure outlines problems in the treatment of radioactive effluents, describes the related process equipment, and discusses the principles observed in assembling water treatment facilities. Close attention is given to public health and radiation safety measures.

The deactivation of liquid wastes of low activity level from radiochemical laboratories and experimental reactors is illustrated by source material from many Soviet and non-Soviet articles. This brochure is the first known attempt to generalize this material.

A list of useful literature is appended.

P. L. Gruzin, V. N. Afanas'ev, S. V. Zemskii, and V. G. Smirnov. Primenenie radioaktivnykh izotopov dlya kontrolya domennogo protsessa [Radioisotope applications in blast furnace process control]. 1964, 170 pages, 44 kopeks.

This book generalizes Soviet and foreign experience in using radioactive isotopes to monitor and study the flow of charge materials and gases in blast furnaces, to monitor charge level, quality of burden, quality of the refractory furnace lining, and the operation of auxiliary units. An evaluation of isotope process monitoring techniques in comparison with rival techniques is an added feature.

131 Titles are included in the list of pertinent literature.

A. I. Abramov. Izmerenie "neizmerimogo." [Measuring the "unmeasurable"].

This renders an account of how Man hit upon the existence of atoms, how scientists learned to measure these unmeasurably tiny particles of matter: how to determine their size, weight, electrical charge, energy; what instruments are used in modern laboratories to investigate atoms and elementary particles, and what problems are ahead for physicists in the realm of measuring objects in the microcosmos.

Appendices furnish: the latest values of various constants mentioned in the book, a table of the elementary particles known to date, and a list of reference literature on atoms and atomic nuclei.

Releases by Other Publishers

W. Riezler and K. Kopitzki. Kernphysikalisches Praktikum [in German: Practical handbook of nuclear physics]. Stuttgart, 1963, 152 pages, 134 figures.

The book is based on long years of experience in practical nuclear physics work at the Institute of Radiation and Nuclear Physics of Bonn University, and has been recommended as a manual for use in West German higher educational institutions.

The book is in two parts and contains a concise but yet at the same time quite adequate description of 50-odd experiments.

The first part of the book deals with nuclear physics experimental technique.

The first chapter familiarizes the reader with the basic properties of radioactive sources and with the methods used to fabricate the sources, as well as with rules governing handling of radioactive materials.

In the next chapter, devoted to instruments designed to detect and measure radioactive radiations, experiments geared to acquaint practical laboratory trainees not only with the performance characteristics of ionization chambers, gas-discharge and scintillation counters, semiconductor radiation detectors and nuclear photographic emulsions, and some of the properties of radioactive sources, are described.

The third chapter takes up the fundamentals of the theory of quadrupole networks and the operational method in electronic network theory, as well as amplification and counting of electrical pulses.

The brief fourth chapter presents the basic laws characterizing the statistical nature of nuclear physics processes, cites formulas useful in ascertaining errors in measurements and methods for recording effects which are slight compared to possible deviations of the measured variable.

The concluding chapter in the first part of the book is devoted to special-purpose measuring apparatus used in experiments designed to ascertain the effect of target and counter geometry on counting efficiency and back-scattering of radiation from the target substrate on measurement results, or used in experiments designed to determine the absolute intensity of radioactive preparations (with the aid of a 4π -counter and coincidence techniques).

The second part of the book contains a description of experiments relating to various domains in nuclear physics.

The first chapter offers a description of three experiments on determination of the half-lives of short-lived and long-lived radionuclides, or of radionuclides having an average lifetime.

The experiments described in the following chapter are devoted to determination of the maximum beta-ray energy and the simplest decay schemes of radionuclides, the study of internal conversion and gamma-ray spectra.

The study of the properties of alpha-particles furnishes the content of experiments presented in the third chapter. The energy, scattering, and free path length of particles are measured, and the radioactive thorium series is studied by photographic emulsions.

After a brief fourth chapter dealing with the theory of mass spectrometers, experiments designed to familiarize students with the basic properties of neutrons, with techniques and procedures in the measurement of such neutron characteristics as diffusion length, transport length and albedo of thermal neutrons, neutron distributions, neutron source intensity, are described.

The concluding chapter of the book is devoted to radiochemical techniques in the separation of radioactive elements. A description of three experiments involving distinct separation techniques appears (these include solvent extraction, ion exchange work, and the Szilard-Chalmers reaction).

V. S. Bulakov and A. A. Narusbaev. Proektirovanie atomnykh podvodnykh lodok [Design of nuclear submarines]. Based on translations from foreign literature. Leningrad, Shipbuilding press [Sudostroenie], 1964, 288 pages, 1 ruble, 06 kopeks.

The authors here analyze engineering problems in current submarine design on the basis of material published in marine engineering and naval literature outside of USSR, throw light on various aspects of the design of nuclear submarines, associated power and electronic equipment, systems and devices, on-board weapons, and shipboard living problems.

Chapter I, "Nuclear submarines: strike force of the modern navy," contains a large number of tables, illustrations, layouts, and serves to acquaint the reader quite adequately with the latest achievements in the field of submarine building.

Chapter II centers its attention on the organization of design and on basic submarine design data. Layouts of the general disposition of equipment in submarine compartments and of submarine cargo vessels of various types, data on the subdivision of rigid hulls into compartments, high-weight cargo loadings, stability and unsinkability, economic competitiveness, and maneuverability, are given here.

Particular features of hull design are described in chapter III. After an analysis of available information on submersion depths and hull design data (with indications as to the chemical composition and mechanical properties of American steels and titanium and aluminum alloys), hull strength and structure, the authors consider the problem of increasing the depth to which submarines can effectively submerge. These data are illustrated by means of graphs and tables.

Chapter IV provides a description of systems (submersion and surfacing, trim and drydocking, compressed air, hydraulics) and rudder, propulsion, emergency, anchoring, and loading units.

Such problems in rendering a vessel habitable as self-contained independence, the radiation environment, maintenance of the normal gas composition and microclimate in compartments of the vessel, are taken up in chapter V. This chapter also provides some data on noise levels in compartments, on organization of shipboard labor, respiration, nutrition, and medical care.

The brief chapter VI presents an analysis of automation (particularly with the use of shipboard computers). A detailed description of the armaments and various components for protection against enemy action is found in chapter VII. In the last chapter, the reader will find some information on the nuclear power units used on submarines.

The list of literature contains 27 titles of books and foreign journals relevant to the subject, generally without reference to the concrete publications made use of in the text.

INDEX

SOVIET ATOMIC ENERGY

Volumes 16 and 17, 1964

SOVIET ATOMIC ENERGY

Vols. 16 and 17, 1964

A translation of Atomnaya Énergiya

A

Abdreev, V. D. - 775
 Abramov, A. I. - 192
 Abramov, A. S. - 1071
 Adamchuk, Yu. V. - 58
 Adamov, I. Yu. - 109
 Ad'yasevich, B. P. - 703
 Afanas'ev, V. P. - 537
 Afrikantov, I. I. - 1090, 1094
 Ageenkov, V. I. - 1212
 Aglintsev, K. K. - 940
 Agranovich, V. - 862
 Akalaev, G. G. - 555
 Akimov, I. S. - 619
 Akopov, Yu. R. - 1133
 Aleksenko, Yu. I. - 1197
 Aleshchenkov, P. I. - 606, 1078,
 1224
 Alfimov, N. N. - 317, 1044
 Alikhanov, R. A. - 769
 Alkhazashvili, G. M. - 53
 Alkhazov, I. D. - 170
 Amonenko, V. M. - 525
 Andreev, O. L. - 304
 Antonenko, V. G. - 703
 Arkhangel'skii, Yu. V. - 982
 Arkharova, I. I. - 53
 Aron, P. M. - 447, 450
 Artamkin, V. N. - 906
 Artsimovich, L. A. - 886, 1000
 Avaev, V. N. - 431
 Aver'yanov, P. G. - 1212
 Avzyanov, V. S. - 41
 Azarenko, A. V. - 396
 Azhazha, V. M. - 525

B

Babkin, G. I. - 366
 Bagdasarov, Yu. E. - 503
 Bakai, A. S. - 669
 Barabanov, I. R. - 258
 Baranaev, M. K. - 1267
 Baranov, I. A. - 63
 Barashenkov, V. S. - 636

Barbier, M. - 793
 Barchugov, V. V. - 443
 Baroni, E. E. - 1261
 Barsukov, O. A. - 41
 Bartoshek, V. - 383, 1126
 Bashkirtsev, M. - 467
 Basin, Ya. N. - 323
 Batalin, V. A. - 245
 Batenin, I. V. - 453
 Batov, V. V. - 800
 Baturov, B. B. - 973
 Batyrbekov, G. A. - 1025
 Bayadzhiev, A. V. - 636
 Beda, A. G. - 167
 Begzhanov, R. B. - 647
 Belinskaya, N. T. - 1105
 Belov, A. R. - 1197
 Belov, L. M. - 170
 Belov, S. V. - 639
 Belovintsev, K. A. - 427
 Berezhnoi, V. M. - 1031
 Berlin, I. K. - 1150
 Bezuglyi, V. D. - 762
 Biberger, A. V. - 87
 Bibikova, E. V. - 404
 Biryukov, V. - 565
 Blokhin, O. A. - 1207
 Blyumkina, Yu. A. - 295, 641
 Bochagov, B. A. - 943
 Boganov, F. F. - 1159
 Bogdanov, A. P. - 429
 Bol'shov, V. I. - 715
 Bondarenko, I. I. - 821, 1025
 Borishanskii, V. M. - 562, 649
 Borisyuk, E. V. - 1197
 Breger, A. Kh. - 314
 Brill', O. D. - 161
 Broder, D. L. - 26, 113, 1207
 Brodin, B. V. - 531
 Brodskii, A. M. - 1197
 Bugorkov, S. S. - 450
 Bulkin, Yu. M. - 1212
 Burgov, N. - 460
 Bushuev, A. V. - 653
 Butt, Yu. M. - 832

Bychkov, A. P. - 639
 Bychkov, I. F. - 1207

C

Cherkasov, A. S. - 445
 Chernyi, V. Ya. - 1207
 Chesnokov, N. - 467
 Chikhladze, I. L. - 1224
 Chistov, B. G. - 1175
 Chulkov, P. M. - 1224
 Chumakov, N. I. - 1269, 1271
 Chursin, G. N. - 445
 Chuvilo, I. V. - 186

D

Danelyan, L. S. - 58
 Danilov, V. I. - 7
 Daruga, V. K. - 754, 757, 854
 Delens, P. A. - 1197
 Denisov, F. P. - 427
 Denisov, V. P. - 1183
 Denisov, Yu. N. - 1054
 Dmitriev, M. T. - 341
 Dollezhal', N. A. - 1078, 1212,
 1224
 Donets, E. D. - 233, 564
 Dorofeev, G. A. - 1162
 Dorokhov, V. V. - 192
 Dorosh, M. M. - 937
 Doroshenko, G. G. - 176, 258
 Dovbenko, A. G. - 113, 1038, 1272
 Drapchinskii, L. V. - 164
 Drozdov, F. S. - 1224
 Druin, V. A. - 1046
 Dubovskii, B. G. - 15, 20
 Dubrovskii, I. Ya. - 735
 Dudnikov, Yu. V. - 1207
 Dulin, V. A. - 1249
 Dushin, L. A. - 109
 Dvukhshestnov, V. G. - 1249
 D'yachenko, K. K. - 1017
 D'yachkova, R. A. - 151
 Dymkov, Yu. M. - 531

E

Efremov, A. A. - 1071
 Egorov, Yu. A. - 34, 431
 Egorov, Yu. V. - 50
 Eleonskii, V. M. - 848
 Él'tekov, V. A. - 355
 Emel'yanov, I. Ya. - 1078, 1197,
 1212, 1224
 Enchevich, I. B. - 7
 Ermakov, V. A. - 233
 Érshler, B. V. - 522
 Esikov, V. I. - 515

F

Fedin, V. G. - 1071
 Fedorenko, R. P. - 906
 Fedorov, V. V. - 323
 Fedorov, N. V. - 1207
 Feinberg, S. M. - 1212, 1224
 Filippov, A. P. - 925
 Filippov, A. G. - 1197, 1224
 Filyushkin, I. V. - 176, 258
 Finkel', V. A. - 525
 Firsov, E. I. - 429
 Firsova, É. V. - 562
 Flerov, G. N. - 1046
 Fomenko, D. E. - 703
 Fominykh, V. I. - 301
 Fradkin, G. M. - 323
 Frank-Kamenetskii, A. D. - 131
 Frid, E. S. - 443
 Frolov, V. V. - 1049

G

Gabrusev, V. N. - 1207
 Gagarin, Yu. F. - 361
 Galustashvili, V. V. - 70
 Ganazha, V. D. - 560
 Garapov, É. F. - 1162
 Garusov, E. A. - 1121
 Gashev, M. A. - 1017
 Gavrillov, K. A. - 1046
 Gavrillov, P. A. - 1197
 Gel'fman, A. Ya. - 768
 Gladyshev, D. A. - 647
 Glagolev, V. I. - 258
 Gol'din, M. L. - 77, 205
 Golubev, V. I. - 821
 Goncharov, V. V. - 989
 Gordienko, Ya. I. - 396
 Gordievskii, A. V. - 832
 Gorlov, L. V. - 1071
 Gorn, L. S. - 61, 549
 Gorshkov, G. V. - 1256
 Govorkov, A. B. - 1236

Granovskii, G. L. - 768
 Granovskii, Ya. I. - 624
 Grigorovich, B. M. - 893
 Grishanin, E. I. - 276, 282, 619
 Gromov, V. - 771
 Grozdov, I. I. - 1197
 Gruzin, P. L. - 1008
 Gryazev, V. M. - 1197, 1212
 Gryaznov, Yu. N. - 1162
 Gubanov, Yu. D. - 1071
 Gur'ev, M. V. - 290
 Gustov, G. K. - 1017
 Gverdtsiteli, I. G. - 1071, 1133

I

Ignat'ev, K. G. - 121, 251
 Ignatov, A. A. - 1035
 Ioffe, M. S. - 1112
 Iokhel'son, S. V. - 180
 Isaev, P. S. - 79
 Ivanov, V. A. - 1105
 Ivanov, V. E. - 396, 525, 1071
 Ivanov, V. I. - 615
 Ivanovskii, N. N. - 1155
 Ivashchenko, N. I. - 649
 Izraél', Yu. A. - 844

K

Kaipov, R. L. - 323
 Kalinina, M. D. - 290
 Kamaev, A. V. - 15, 20
 Kamaeva, L. A. - 641
 Kaminskii, V. A. - 1133
 Kandaritskii, V. S. - 982
 Kanevskii, E. A. - 925
 Kapchigashev, S. P. - 306
 Kaplan, S. A. - 172
 Karamyan, A. S. - 298
 Kasatkin, I. P. - 940
 Katkovskaya, K. Ya. - 735
 Kazachenko, M. A. - 1224
 Kazachkovskii, O. D. - 503, 1090
 Kazanskii, Yu. A. - 1249
 Kazarinov, N. M. - 63
 Keirim-Markus, I. B. - 537
 Khachaturyan, M. N. - 546
 Khaidarov, T. - 647
 Khazanov, B. I. - 61, 549
 Kheifets, L. Ya. - 768
 Khlopkin, N. S. - 1094
 Khodakov, V. A. - 1071
 Khokhlachev, A. A. - 1183
 Khoroshavin, V. D. - 1197
 Khoroshchavin, B. I. - 1271
 Khramchenkov, V. A. - 744

Khromov, V. V. - 918
 Khrushchev, B. I. - 751
 Kilin, S. F. - 1261
 Kirichenko, V. N. - 945
 Kirichenko, V. V. - 1031
 Kirpichnikov, I. V. - 121, 251
 Knyazeva, G. D. - 606, 1078, 1224
 Kochenov, A. S. - 1212
 Kochetkov, L. A. - 601, 1105
 Kochin, A. E. - 304
 Kolchin, O. P. - 1150
 Koleganov, Yu. F. - 1025
 Kolesov, V. E. - 113, 1038, 1272
 Kolesov, V. F. - 377
 Kolomenskii, A. A. - 748
 Kolychev, B. S. - 867
 Komar, E. G. - 1017
 Komarov, A. Ya. - 1207
 Kompaniets, G. V. - 1071
 Kondratenko, A. N. - 493
 Kondrat'ev, F. V. - 1224
 Kondrat'ev, L. N. - 167
 Konochkin, V. G. - 601, 1105
 Kononenko, V. I. - 109
 Kononov, V. I. - 1078
 Kononovich, A. A. - 425
 Konoplev, K. A. - 72, 560
 Konstantinov, A. A. - 301
 Koptelov, E. A. - 326, 1071
 Koptev, M. A. - 1207
 Kopytin, N. S. - 312
 Korpusov, V. I. - 945
 Koryakin, Yu. I. - 800, 1197
 Korzh, I. A. - 246, 312
 Kosovskii, V. G. - 1071
 Kostochkin, O. I. - 447
 Kostritsa, A. A. - 624
 Kostyu, Ya. É. - 937
 Kotel'nikov, R. B. - 333
 Kotov, A. P. - 1207
 Kovalenko, S. S. - 164
 Kovalev, E. E. - 537
 Kovyrzin, V. K. - 1071
 Kozhevnikov, D. A. - 722
 Kozlov, F. A. - 1155
 Kozlov, V. Ya. - 601, 1105
 Kozlova, I. E. - 832
 Kramerov, A. Ya. - 1183
 Krasin, A. K. - 1207
 Krasnoyarov, N. V. - 1090
 Kress, R. P. - 298
 Krisyuk, I. T. - 168
 Krivokhatskii, A. S. - 170
 Krot, N. N. - 615
 Kruglov, S. P. - 309

Kryukov, K. A. - 1078
 Kucharenko, N. K. - 323
 Kucherov, R. Ya. - 1071
 Kukavadze, G. M. - 522
 Kukharkin, N. E. - 1071
 Kukhtevich, V. I. - 557
 Kulikov, E. V. - 1183
 Kulyukina, L. A. - 636
 Kunchenko, V. V. - 396
 Kurchatov, I. V. - 1224
 Kutateladze, K. S. - 1286
 Kutovoi, V. I. - 950
 Kutsenko, L. A. - 832
 Kuzeev, B. I. - 298
 Kuzin, M. E. - 87
 Kuz'michev, Yu. S. - 740
 Kuz'min, A. M. - 918
 Kuznetsov, F. M. - 15, 20
 Kuznetsov, S. P. - 1197
 Kuznetsov, V. A. - 201
 Kuznetsov, V. I. - 1046

L

Laletin, N. I. - 498, 911
 Lalykin, S. P. - 1071
 Lantsov, M. N. - 1207
 Lashuk, A. I. - 113
 Lavrenikov, V. D. - 1224
 Lavrovskii, K. P. - 1197
 Lazutkin, I. I. - 754, 757
 Lebedev, R. - 565
 Lebsadze, T. N. - 1261
 Leipunskaya, D. I. - 323
 Leipunskii, A. I. - 1090
 Lelek, V. - 1126
 Leshchinskii, N. I. - 477, 573
 Lisochkin, G. A. - 1207
 Litvinenko, A. S. - 669
 Lobanov, Yu. V. - 1046
 Lomakin, S. S. - 269
 Lopatin, I. V. - 309
 Lü Min, - 10
 Lunina, L. I. - 606, 1078
 Lupakov, I. S. - 740

M

Makhlis, F. A. - 856
 Makhon'ko, K. P. - 659
 Malakhov, S. G. - 659, 952
 Malkin, L. Z. - 170
 Mal'tsev, V. M. - 636
 Malyshev, A. V. - 1277
 Malyshev, I. F. - 1017
 Mamedov, A. M. - 578
 Marchenko, B. N. - 7

Marchuk, G. I. - 1038
 Markov, Yu. V. - 1183
 Martynenko, Yu. V. - 932
 Martynova, O. I. - 735
 Mashkovich, V. P. - 760
 Matusevich, E. S. - 557
 Matveev, O. A. - 432, 436, 439, 440, 671
 Matveev, V. I. - 570
 Matyzov, N. I. - 1044
 Memelova, L. Ya. - 522
 Menabde, N. E. - 1042
 Merkin, V. I. - 1071
 Merzlikin, G. A. - 1207
 Meshcheryakov, M. N. - 1197
 Migachev, A. I. - 631
 Mikhaleva, T. N. - 851
 Millionshchikov, M. D. - 1071
 Mirnov, S. V. - 886, 929
 Miroshnikov, G. V. - 443
 Mishev, I. T. - 416
 Mitel'man, M. G. - 425
 Mityaev, Yu. - 328, 475, 606, 1078
 Mogil'ner, A. I. - 336
 Moiseev, G. G. - 431
 Monozon, N. A. - 1017
 Mordvinov, N. M. - 1094
 Morgunov, N. G. - 1078, 1224
 Morokhov, I. D. - 879, 982
 Morozov, I. G. - 1207
 Moskalev, O. B. - 372
 Moskalev, S. S. - 58
 Mostovaya, T. A. - 1
 Mostovoi, V. I. - 1
 Mukhovatov, V. S. - 893

N

Nagornaya, L. L. - 762
 Nasyrov, F. - 552
 Nechaev, Yu. A. - 1071
 Nesmeyanova, G. M. - 146, 827
 Nesterov, V. G. - 641
 Nevskii, B. V. - 53, 921
 Nikeshichev, V. N. - 676
 Nikitin, V. - 455
 Nikolaev, A. N. - 754, 757, 760, 854
 Nikolaev, M. N. - 821, 1025
 Nikolaeva, A. - 213
 Nosov, V. I. - 810, 815
 Novikov, A. N. - 330
 Novikov, D. L. - 7
 Novikov, P. D. - 1094

Novozhilov, G. N. - 317
 Nozik, V. Z. - 15

O

Oganesyan, Yu. Ts. - 1046
 Ogorodnikov, B. I. - 945
 Okolovich, V. N. - 644, 715
 Oraevskii, V. N. - 541
 Orekhov, Yu. I. - 1207
 Orlov, M. Yu. - 821
 Orlov, Yu. V. - 34
 Osinenko, B. P. - 671
 Ostroumov, V. I. - 361
 Otroshchenko, I. V. - 906
 Otstavnov, P. S. - 178

P

Palamarchuk, Yu. D. - 15, 20
 Panchvidze, M. V. - 355
 Pankratov, V. M. - 161
 Pankrat'ev, Yu. V. - 34
 Pantuev, V. S. - 546
 Parfenov, L. B. - 569
 Partsakhashvili, G. L. - 1133
 Pasechnik, M. V. - 246, 312
 Pavlichenko, O. S. - 109
 Pavlinchuk, V. A. - 709, 1242
 Perelygin, V. P. - 1046
 Pertsovskii, E. S. - 87
 Petrochuk, K. V. - 1197
 Petros'yants, A. M. - 596, 1065
 Petrov, V. A. - 1078
 Petrov, Yu. P. - 852
 Petrov, Yu. V. - 1121
 Petrzhak, K. A. - 164, 170, 447, 450
 Petunin, B. V. - 1224
 Petushkov, A. A. - 314
 Pevzner, M. I. - 58
 Pikel'ner, L. B. - 1165
 Pikulik, R. G. - 72
 Pinkhasik, D. M. - 757
 Pinkhasik, D. S. - 854
 Pinkhasik, M. S. - 503, 1090
 Pirkovskii, S. A. - 201, 921
 Plotko, V. M. - 1046
 Podlazov, L. N. - 1197
 Podymakhin, V. N. - 859
 Pogozhkin, I. N. - 1197
 Poido, M. S. - 1090
 Polferov, E. A. - 7
 Polikanov, S. M. - 83
 Pologikh, B. G. - 1094
 Polumin, Yu. P. - 703

Polushkin, K. K. - 1197
 Polyak, Yu. Ya. - 848
 Polyakov, A. A. - 1035
 Polyakov, V. K. - 515
 Ponomarev-Stepnoi, N. N. - 269,
 810, 815, 1071
 Popkovich, A. V. - 1017
 Popov, D. K. - 180
 Popov, D. N. - 1197
 Popov, G. A. - 15, 20
 Popov, Yu. P. - 306
 Portnoi, K. I. - 815
 Potetyunko, G. N. - 421
 Pozdnyakov, B. S. - 1071
 Pravdivyi, N. M. - 312
 Prokhorova, L. I. - 715
 Pugacheva, E. V. - 282
 Pushkarev, V. P. - 1197
 Pushkarev, V. V. - 50
 Pyshin, V. K. - 503

R

Rabotnov, N. S. - 709, 1242
 Radicheva, M. A. - 416
 Radyvanok, A. - 1052
 Raizer, M. D. - 901
 Ratnikov, B. K. - 1017
 Reva, N. I. - 787
 Rozanov, E. I. - 7
 Rozenblyum, N. D. - 425
 Rozhdestvenskii, B. V. - 1017
 Rozman, I. M. - 1261
 Rudakov, V. P. - 161, 436, 667,
 Rudenko, V. N. - 174
 Rumyantsev, N. N. - 1017
 Rustambekov, A. V. - 1286
 Rybakov, B. V. - 161
 Ryvkin, S. M. - 432, 440

S

Sadokhin, I. P. - 113
 Safonov, A. N. - 7
 Sakharov, V. K. - 754, 757
 Sakodynskii, K. I. - 766
 Sakovich, V. A. - 537
 Saksaganskii, G. L. - 1017
 Samarin, E. N. - 1071
 Samoilov, L. N. - 687
 Samoilov, P. S. - 555
 Savel, Pierre - 662
 Savel'yev, E. G. - 815
 Savenkov, A. L. - 7
 Savinov, N. P. - 1197
 Savitskii, P. S. - 229
 Savosin, S. I. - 323

Sclyar, N. T. - 312
 Semenchuk, G. G. - 943
 Senchenkov, A. P. - 631
 Sergeev, Yu. A. - 1207
 Serikov, I. N. - 436
 Serov, V. Ya. - 1071
 Sever'yanov, V. S. - 601, 1105
 Shabalin, E. P. - 10
 Shapar', A. V. - 1277
 Sharov, B. V. - 453
 Sharov, V. T. - 560
 Shchebolev, V. T. - 298
 Shchegolets, V. A. - 233
 Shestakov, B. I. - 323
 Shevelev, Ya. V. - 1224
 Shikhov, S. B. - 918
 Shimanskaya, N. S. - 694
 Shimelevich, Yu. S. - 323
 Shirkin, L. M. - 1279
 Shkoda-Ul'yanov, V. A. - 937
 Shmelev, A. N. - 918
 Shmelev, V. M. - 973, 1207
 Shoniya, V. M. - 1261
 Shopauskas, K. K. - 655
 Shpakov, V. I. - 447
 Shugar, I. V. - 1249
 Shuvalov, V. M. - 606
 Sidorenko, V. A. - 1183
 Silin, Yu. S. - 298
 Simonenko, D. L. - 837
 Sinaev, A. N. - 464
 Sinev, N. M. - 973, 1088, 1207
 Sinitsyn, B. I. - 754, 757, 760, 854
 Sinitsyn, V. I. - 84, 206, 338
 Sirotkin, A. P. - 1197
 Sivintsev, Yu. V. - 1170, 1173
 Sizov, I. V. - 199
 Skurat, V. E. - 1142
 Skvortsov, S. A. - 1183
 Sledzyuk, A. K. - 1094
 Slozhenikin, N. I. - 443
 Slyusarev, P. N. - 1105, 1207
 Smirenkin, G. N. - 615, 641, 644,
 715
 Smirenniy, L. N. - 537
 Smirnov, I. P. - 921
 Smirnov, V. G. - 800
 Smirnov, V. P. - 1224
 Smirnova, I. N. - 735
 Smolin, V. N. - 515, 1078
 Smukalov, A. I. - 396
 Sobol', N. V. - 314
 Sobolev, R. I. - 932, 1112
 Solyakin, G. E. - 943
 Sorokin, Yu. P. - 1183

Sorokina, A. V. - 450
 Spevakov, F. M. - 1017
 Spitsyn, Vikt. I. - 151, 472, 827
 Spoloso, N. - 865
 Starodubtsev, S. V. - 647, 751
 Stavisskii, Yu. Ya. - 1272, 1277
 Stekol'nikov, V. V. - 1183
 Stirsky, Pavel - 804
 Stolov, A. M. - 1017
 Strelkov, G. P. - 445
 Strelkov, V. S. - 886
 Strel'tsov, N. S. - 1017
 Stetsenko, V. I. - 950
 Stukov, G. M. - 298, 304
 Styre, B. I. - 655
 Styrikovich, M. A. - 735
 Sudnitsyn, O. A. - 601, 1105
 Sukhomlin, E. A. - 787
 Sukhoruchkin, S. I. - 121, 251
 Suprunenko, V. A. - 787
 Suroegin, V. A. - 1197
 Sychev, B. S. - 26
 Sychkov, M. A. - 537

T

Tal'roze, V. L. - 1142
 Talyzin, V. M. - 1224
 Tarkhin, D. V. - 440
 Tatarnikov, V. P. - 1183
 Terent'ev, B. M. - 355
 Tetyukov, V. D. - 1197
 Tikhinskii, G. F. - 525
 Timashev, V. V. - 832
 Tkachenko, E. V. - 50
 Tokarev, Yu. I. - 1197
 Tol'skikov, V. A. - 1272
 Toropygina, É. G. - 859
 Tot'skii, I. A. - 246, 312
 Trenin, V. D. - 560
 Tret'yakov, E. F. - 167
 Tret'yakova, S. P. - 1046
 Troshev, T. M. - 416
 Trykov, L. A. - 557
 Tsarev, N. M. - 1094
 Tskhvirashvili, D. G. - 70
 Tsvetkov, O. S. - 1256
 Tsykanov, V. A. - 1212
 Tsypin, S. G. - 754, 757, 760, 854
 Tsytovich, V. N. - 901
 Tugarinov, A. I. - 404
 Tugolukov, A. M. - 26
 Tunitskii, N. N. - 290
 Tyapkin, A. - 455
 Tyrina, L. V. - 396
 Tyutyugin, I. I. - 164

U

Usachev, L. N. - 192, 709, 1242
 Ushakov, G. N. - 601, 1105, 1207
 Usov, V. A. - 1071
 Uznadze, O. P. - 821, 1025

V

Vartanov, N. A. - 555
 Vasenkova, G. V. - 906
 Vasil'ev, S. S. - 943
 Vavilov, V. V. - 15
 Vebra, É. Yu. - 655
 Venikov, N. I. - 1269, 1271
 Ventsel', P. - 509
 Vereskunov, V. G. - 1267
 Veselkin, A. P. - 34
 Vikulov, A. I. - 146, 827
 Vladimirova, M. V. - 947
 Vladykov, G. M. - 15, 20
 Vlasov, N. - 574, 581, 687
 Volkov, S. A. - 766

Volovik, V. D. - 445
 Vorob'ev, E. D. - 1212
 Vorob'ev, G. A. - 158
 Vorob'ev, V. A. - 74
 Vyalov, G. N. - 543

Y

Yablokov, B. N. - 578
 Yagovoi, P. N. - 317, 1044
 Yakovlev, G. V. - 1
 Yakovlev, V. V. - 1071
 Yakutovich, M. V. - 1071
 Yaritsyna, I. A. - 298, 301, 304
 Yastrebov, S. S. - 58
 Yavno, A. Kh. - 1017
 Yazvitskii, Yu. S. - 10
 Yurova, L. N. - 653, 1035
 Yutlandov, I. A. - 192

Z

Zablotskaya, T. V. - 649
 Zaitsev, L. N. - 26

Zaitsev, V. V. - 172
 Zakharova, K. P. - 1267
 Zaletskii, E. G. - 694
 Zamolodchikov, B. I. - 7
 Zavel'skii, F. S. - 319
 Zavoiskii, V. K. - 68
 Zelenskii, V. F. - 396
 Zhezherun, I. F. - 136, 264
 Zhileiko, G. I. - 155
 Zhil'tsov, V. A. - 1207
 Zhirnov, A. D. - 606, 1078, 1224
 Zhukov, V. F. - 1071
 Ziv, D. M. - 323
 Zolotarev, V. S. - 673
 Zolotavin, V. L. - 50
 Zvereva, G. A. - 1078
 Zvonarev, A. V. - 821
 Zvonov, N. V. - 1197
 Zyabkin, V. A. - 1256
 Zykov, S. I. - 404

ATOMNAYA ÉNERGIYA
EDITORIAL BOARD

A. I. Alikhanov	A. I. Leipunskii
A. A. Bochvar	M. G. Meshcheryakov
N. A. Dollezhal'	M. D. Millionshchikov
K. E. Erglis	(<i>Editor-in-Chief</i>)
V. S. Fursov	I. I. Novikov
I. N. Golovin	V. B. Shevchenko
V. F. Kalinin	A. P. Vinogradov
N. A. Kolokol'tsov	N. A. Vlasov
(<i>Assistant Editor</i>)	(<i>Assistant Editor</i>)
A. K. Krasin	M. V. Yakutovich
I. F. Kvartskhava	A. P. Zefirov
A. V. Lebedinskii	

SOVIET ATOMIC ENERGY

A translation of **ATOMNAYA ÉNERGIYA**
A publication of the Academy of Sciences of the USSR

© 1964 CONSULTANTS BUREAU ENTERPRISES, INC.
227 West 17th Street, New York 11, N. Y.

Vol. 16, No. 1

January, 1964

CONTENTS

	P A G E	
	ENG.	RUSS.
The Probability of the Ternary Fission of U^{235} by Monochromatic Neutrons in the 0.06-10 eV Energy Range—T. A. Mostovaya, V. I. Mostovoi, and G. V. Yakovlev.	1	3
Increasing the Proton Beam Intensity in the Six-Meter Dubna Synchrocyclotron—V. I. Danilov, I. B. Enchevich, B. I. Zamolodchikov, B. N. Marchenko, D. L. Novikov, E. A. Polferov, E. I. Rozanov, A. L. Savenkov, and A. N. Safonov	7	9
Experimental Investigation of Fluctuations in a Pulsed Reactor—Lü Min, E. P. Shabalin, and Yu. S. Yazvitskii	10	12
Interaction of Subcritical Reactors—B. G. Dubovskii, A. V. Kamaev, G. M. Vladykov, F. M. Kuznetsov, V. Z. Nozik, Yu. D. Palamarchuk, G. A. Popov, and V. V. Vavilov	15	16
Critical Parameters of Aqueous Solutions of $UO_2(NO_3)_2$ Salt—B. G. Dubovskii, A. V. Kamaev, F. M. Kuznetsov, G. M. Vladykov, G. A. Popov, and Yu. D. Palamarchuk	20	21
Effect of Water Content in Concrete on Thickness and Cost of Reactor Shielding—D. L. Broder, L. N. Zaitsev, B. S. Sychev, and A. M. Tugolukov	26	26
Spectra of Fast Reactor Neutrons After Passing Through Graphite, Lead, and Iron—A. P. Veselkin, Yu. A. Egorov, Yu. V. Orlov, and Yu. V. Pankrat'ev	34	32
Metal-Water Shielding From Point Neutron Sources—O. A. Barsukov and V. S. Avzyanov	41	40
The Clarification and Purification of Radioactive Waste Water by the Flotation Method—V. V. Pushkarev, Yu. V. Egorov, E. V. Tkachenko, and V. L. Zolotavin	50	48
An Investigation of Uranium Sorption on Minerals of the Surrounding Rock—G. M. Alkhashevili, B. V. Nevskii, and I. I. Arkharova	53	51
LETTERS TO THE EDITOR		
Radiative Capture Cross Sections of Dysprosium Isotopes in the 0.023-1 eV Energy Interval—L. S. Danelyan, Yu. V. Adamchuk, S. S. Moskalev, M. I. Pevzner, and S. S. Yastrebov	58	56
On Instrumental Errors in Determining the Intensity of Overlapping Spectral Lines—L. S. Gorn and B. I. Khazanov	61	58
Surface-Barrier Silicon Counters in Neutron and Fission-Fragment Fluxes—I. A. Baranov and N. M. Kazarinov	63	60
Size Distribution of Vapor Bubbles in Boiling Liquids—V. K. Zavoiskii	68	64
The Behavior of Borates and Boric Acid in Boiling Reactors—D. G. Tskhvishvili and V. V. Galustashvili	70	65
Measurement of Temperature Fields in the Shielding of the VVR-M Reactor—K. A. Konoplev and R. G. Pikulik	72	68

(continued)

Annual Subscription: \$95

Single Issue: \$30

Single Article: \$15

All rights reserved. No article contained herein may be reproduced for any purpose whatsoever without permission of the publisher. Permission may be obtained from Consultants Bureau Enterprises, Inc., 227 West 17th Street, New York City, United States of America.

CONTENTS (continued)

	P A G E	
	ENG.	RUSS.
Gamma-Field Structure of Plane Isotropic Cs ¹³⁷ Sources—V. A. Vorob'ev	74	69
How to Select Gamma Emitters to Monitor Density of Pulp of Atomic Number ≤ 30 M. L. Gol'din	77	71
NEWS OF SCIENCE AND TECHNOLOGY		
[The Role of Elementary Particle Research in the Development of Modern Physics		
Source: V. F. Weisskopf Physics Today, 16, No. 6, 26 (1963)		73]
International Conference on the Structure of the Nucleon—P. S. Isaev	79	79
Symposium on Transplutonium Elements—S. M. Polikanov	83	82
Industrial Applications of High-Level Radiation Facilities—V. Sinitsyn.	84	83
Gamma Radiation Facility for Cereals and Grains—A. V. Bibergal', E. S. Pertsovskii, and M. E. Kuzin	87	84
Discussion on the Costs Aspects of the Utilization of Radioactive Isotopes—I. R.	89	86
Patents	92	88
Brief Communications.	94	89
BIBLIOGRAPHY		
New Literature	95	90

ATOMNAYA ÉNERGIYA
EDITORIAL BOARD

A. I. Alikhanov
A. A. Bochvar
N. A. Dollezhal'
K. E. Erglis
V. S. Fursov
I. N. Golovin
V. F. Kalinin
N. A. Kolokol'tsov
(Assistant Editor)
A. K. Krasin
I. F. Kvartskhava
A. V. Lebedinskii

A. I. Leipunskii
M. G. Meshcheryakov
M. D. Millionshchikov
(Editor-in-Chief)
I. I. Novikov
V. B. Shevchenko
A. P. Vinogradov
N. A. Vlasov
(Assistant Editor)
M. V. Yakutovich
A. P. Zefirov

SOVIET ATOMIC ENERGY

A translation of **ATOMNAYA ÉNERGIYA**
A publication of the Academy of Sciences of the USSR

© 1964 CONSULTANTS BUREAU ENTERPRISES, INC.
227 West 17th Street, New York 11, N. Y.

Vol. 16, No. 2,

February, 1964

CONTENTS

P A G E
ENG. | RUSS.

Microwave Emission from an Electrodeless Induction Discharge. <u>I. Yu. Adamov, L. A. Dushin, V. I. Kononenko, and O. S. Pavlichenko</u>	109	99
Level Excitation Cross Sections of Mg, Cr ⁵² , Ni ⁵⁸ , Ni ⁶⁰ and Nb ⁹³ by Inelastic Neutron Scattering. <u>D. L. Broder, V. E. Kolesov, A. I. Lashuk, I. P. Sadokhin, and A. G. Dovbenko</u>	113	103
Measurement of η and Partial Cross Sections of Nuclides U ²³⁵ and Pu ²³⁹ for Resonance Neutrons. <u>K. G. Ignat'ev, I. V. Kirpichnikov, and S. I. Sukhoruchkin</u>	121	110
Use of the Monte Carlo Method for Multi-Group Reactor Calculations. <u>A. D. Frank-Kamenetskii</u>	131	119
Study of the Effect of Empty Channels in the Medium of a Moderator on the Diffusion Length of Thermal Neutrons. <u>I. F. Zhezherun</u>	136	123
Influence of Certain Halogen Compounds of the Oxidation of U(IV) in a Sulfuric Medium. <u>G. M. Nesmeyanova and A. I. Vikulov</u>	146	130
Concentration of Pa ²³¹ from Uranium Process Wastes. <u>Vikt. I. Spitsyn and R. A. D'yachkova</u>	151	134
LETTERS TO THE EDITOR		
Equation of the Energy Balance in a Linear Electron Accelerator. <u>G. I. Zhilëiko</u>	155	138
The Performance of the Arkad'ev-Marks High-Duty-Cycle Pulse Circuit. <u>G. A. Vorob'ev</u>	158	139
The Cross Sections of the T(d, n)He ⁴ and D(d, n)He ³ Reactions in the 3-19 MeV Deuteron Energy Range. <u>O. D. Brill', V. M. Pankratov, V. P. Rudakov, and B. V. Rybakov</u>	161	141
The Ratio of the Probabilities of Ternary Fission of U ²³⁵ and U ²³⁸ by Neutrons with Different Energies. <u>L. V. Drapchinskii, S. S. Kovalenko, K. A. Petrzhak, and I. I. Tyutyugin</u>	164	144
The Cross Section of the Activation of Cd ¹⁰⁸ by Thermal Neutrons. <u>A. G. Beda, L. N. Kondrat'ev, and E. F. Tret'yakov</u>	167	145
Estimating the Contribution of Iodine and Bromine Isotopes to the Process of Delayed-Neutron Emission. <u>I. T. Krisyuk</u>	168	146
Spontaneous Fission of Cm ²⁴⁴ with Emission of a Long-Range Alpha Particle. <u>L. Z. Malkin, I. D. Alkhazov, A. S. Krivokhatskii, K. A. Petrzhak, and L. M. Belov</u>	170	148
Contribution to the Theory of the Transient Multiple Compton Scattering of Gamma-Quanta. <u>V. V. Zaitsev and S. A. Kaplan</u>	172	149
The Distribution of Doses in Crystals of Alkali Halides on Irradiation by an Electron Beam. <u>V. N. Rudenko</u>	174	151

(continued)

Annual Subscription: \$95

Single Issue: \$30

Single Article: \$15

All rights reserved. No article contained herein may be reproduced for any purpose whatsoever without permission of the publisher. Permission may be obtained from Consultants Bureau Enterprises, Inc., 227 West 17th Street, New York City, United States of America.

1302

CONTENTS (continued)

	PAGE	RUSS. PAGE
The Spectra of Fast Neutrons from a Po-Be Source which have Passed Through Water Shielding. <u>G. G. Doroshenko and I. V. Filyushkin</u>	176	152
Fluxes of Fast and Slowed-Down Neutrons in Rooms. <u>P. S. Otstavnov</u>	178	154
Sb ¹²⁵ Content in the Soil Covering and in Flora. <u>S. V. Iokhel'son and D. K. Popov</u>	180	155
NEWS OF SCIENCE AND TECHNOLOGY		
Weak Interactions of Elementary Particles. <u>I. V. Chuvilo</u>	186	160
Second International Conference on Nuclide Masses. <u>L. N. Usachev, A. I. Abramov, V. V. Dorokhov, and I. A. Yutlandov</u>	192	164
Conference on Low-Energy Nuclear Physics. <u>I. V. Sizov</u>	199	169
Symposium on Exponential and Critical Experiments. <u>V. A. Kuznetsov</u>	201	171
Fourth International Conference on Techniques in Nondestructive Testing.	203	172
The Use of Isotopes in the Ukraine. <u>M. L. Gol'din</u>	205	173
Applications of Gamma Flaw Detection Techniques in Several COMECON Nations. <u>V. I. Sinitsyn</u>	206	174
Dosimeters and Radiometers on Display at the Nucleonic Instruments Exposition for COMECON. <u>Yu. T.</u>	209	176
The Atom in the Service of Agriculture. <u>A. Nikolaeva</u>	213	180
Patents	214	181
BIBLIOGRAPHY		
New Literature	216	182

ATOMNAYA ÉNERGIYA
EDITORIAL BOARD

A. I. Alikhanov	A. I. Leipunskii
A. A. Bochvar	M. G. Meshcheryakov
N. A. Dollezhal'	M. D. Millionshchikov
K. E. Erglis	(<i>Editor-in-Chief</i>)
V. S. Fursov	I. I. Novikov
I. N. Golovin	V. B. Shevchenko
V. F. Kalinin	A. P. Vinogradov
N. A. Kolokol'tsov	N. A. Vlasov
(<i>Assistant Editor</i>)	(<i>Assistant Editor</i>)
A. K. Krasin	
I. F. Kvartskhava	M. V. Yakutovich
A. V. Lebedinskii	A. P. Zefirov

SOVIET ATOMIC ENERGY

A translation of **ATOMNAYA ÉNERGIYA**
A publication of the Academy of Sciences of the USSR

© 1965 CONSULTANTS BUREAU ENTERPRISES, INC.
227 West 17th Street, New York 11, N. Y.

Vol. 16, No. 3

March, 1964

CONTENTS

	P A G E	
	ENG.	RUSS.
Nuclear Energy and the Chemical Processing Industry - P. S. Savitskii	229	191
Synthesis of the Element 102 of Mass Number 256 - E. D. Donets, V. A. Shchegolets, and V. A. Ermakov	233	195
Scattering of 0.5 and 0.8 MeV Neutrons by Medium and Heavy Nuclei - M. V. Pasechnik, V. A. Batalin, I. A. Korzh, and I. A. Totkii	246	207
Interference Effects in Fission Cross Sections - I. V. Kirpichnikov, K. G. Ignat'ev, and S. I. Sukhoruchkin	251	211
Analysis of the Reliability of Methods of Investigating the Continuous Spectra of Fast Neutrons and Gamma Quanta - G. G. Doroshenko, V. I. Glagolev, I. R. Barabanov, and I. V. Filyushkin	258	218
The Study of Neutron Diffusion in Beryllium by a Pulse Method - I. F. Zhezherun	264	224
A Study of Critical Assemblies with a Beryllium Moderator - N. N. Ponomarev-Stepnoi and S. S. Lomakin	269	228
Calculating the Efficiency of Multi-Layer Control Rods - E. I. Grishanin	276	234
Calculating the Efficiency of Multi-Layer Control Rods Containing a Moderator - E. I. Grishanin and E. V. Pugacheva	282	238
An Investigation of the Effect of Co ⁶⁰ γ -Radiation on Strongly Basic Anionites AV-17 and AM - M. D. Kalinina, M. V. Gur'ev, and N. N. Tunitskii	290	245
LETTERS TO THE EDITOR		
Electronic Equipment for Control and Protection of the Fast Physics Reactor BR-1 - Yu. A. Blyumkina	295	250
Methods of Absolute Neutron Measurements	297	251
Absolute Determination of the Number of Neutrons Emitted by a Source, Using the Method of Accompanying Particles - A. S. Karamyan, B. I. Kuzeev, R. P. Kress, Yu. S. Silin, G. M. Stukov, V. T. Shchebolev, and I. A. Yaritsyna	298	252
Absolute Measurement of the Yields of Neutron Sources by the Manganese Activation Method - A. A. Konstantinov, V. I. Fominykh, and I. A. Yaritsyna	301	253
Absolute Measurement of the Yield of a Neutron Source by the Gold-Foil Activation Method - O. L. Andreev, A. E. Kochin, G. M. Stukov, and I. A. Yaritsyna	304	255
Capture Cross Sections for Neutrons of Energy Up to 50 Kev for Cr, Cr ⁵⁰ , Cr ⁵² , Cr ⁵³ Nuclei - S. P. Kapchigashev and Yu. P. Popov	306	256

(continued)

Annual Subscription: \$95

Single Issue: \$30

Single Article: \$15

All rights reserved. No article contained herein may be reproduced for any purpose whatsoever without permission of the publisher. Permission may be obtained from Consultants Bureau Enterprises, Inc., 227 West 17th Street, New York City, United States of America.

1304

CONTENTS (continued)

	P A G E	
	ENG.	RUSS.
Measurements of Energy in a Bremsstrahlung Beam in the $E_{\gamma} = 15-80$ MeV Range by Three Methods - S. P. Kruglov and I. V. Lopatin	309	258
Scattering of Neutrons with Energies 0.5 and 0.8 Mev by Light and Medium Nuclei . . . -I. A. Korzh, N. S. Kopytin, M. V. Pasechnik, N. M. Pravdivyi, N. T. Sclyar, and I. A. Totskii.	312	260
Basis for Regulations on Air Circulation in the Working Areas of High-Level Gamma Irradiation Facilities - N. V. Sobol', A. A. Petushkov, and A. Kh. Breger	314	262
Results of an Investigation of the Total Beta Activity in Water and Air in Several Areas of the Pacific Ocean - N. N. Alfimov, P. N. Yagovoi, and G. N. Novozhilov . . .	317	264
Mass Absorption Coefficients of Gamma Radiation in Soils, and Errors in Measurements Made by the Gamma Method - F. S. Zavel'skii	319	266
The Use of Ac-Be Neutron Sources in Industrial Geophysics - R. L. Kaipov, D. M. Ziv, D. I. Leipunskaya, S. I. Savosin, V. V. Fedorov, G. M. Fradkin, Yu. S. Shimelevich, Ya. N. Basin, N. K. Kucharenko, and B. I. Shestakov	323	269
NEWS OF SCIENCE AND TECHNOLOGY		
Conference on Reactor Physics and Engineering - E. A. Koptelov	326	271
Montreal Power Reactor Conference - Yu. Mityaev	328	272
Conference on Power Reactor Operating Experience (IAEA) - A. N. Novikov	330	274
Conference on the Technology of New Nuclear Materials and on the Technology of Nonmetallic Fuels - R. B. Kotel'nikov	333	275
II International Congress on Automatic Control - A. I. Mogil'ner	336	278
How Radioactive Isotopes are Being Used in the Metallurgical Industries of Various Comecon Nations - V. I. Sinitsyn	338	279
Doses of Ionizing Radiation Affecting the Composition of the Atmosphere at Radiation Laboratories - M. T. Dmitriev	341	282
BIBLIOGRAPHY		
New Literature	344	284

ATOMNAYA ÉNERGIYA
EDITORIAL BOARD

A. I. Alikhanov
A. A. Bochvar
N. A. Dollezhal'
K. E. Erglis
V. S. Fursov
I. N. Golovin
V. F. Kalinin
N. A. Kolokol'tsov
(Assistant Editor)
A. K. Krasin
I. F. Kvartskhava
A. V. Lebedinskii

A. I. Leipunskii
M. G. Meshcheryakov
M. D. Millionshchikov
(Editor-in-Chief)
I. I. Novikov
V. B. Shevchenko
A. P. Vinogradov
N. A. Vlasov
(Assistant Editor)
M. V. Yakutovich
A. P. Zefrov

SOVIET ATOMIC ENERGY

A translation of **ATOMNAYA ÉNERGIYA**
A publication of the Academy of Sciences of the USSR

© 1965 CONSULTANTS BUREAU ENTERPRISES, INC.
227 West 17th Street, New York 11, N. Y.

Vol. 16, No. 4

April, 1964

CONTENTS

	P A G E	
	ENG.	RUSS.
Gamma Radiation Spectrum and Fractional Values of Absorbed Energy in an Arbitrary Homogeneous Mixture—V. A. Él'tekov, B. M. Terent'ev, and M. V. Panchvidze	355	291
Effect of Recoil on the Angular Correlation Between the Fragments and Charged Particles Emitted in Uranium Fission—Yu. F. Gagarin and V. I. Ostroumov	361	296
Calculation of Fission Fragment Excitation Energy—G. I. Babkin	366	300
Some Nonlinear Problems of Nuclear Reactor Theory—O. B. Moskalev	372	304
Some Problems of Pulsed Reactor Dynamics—V. F. Kolesov	377	309
Concerning the Transitional States of a Reactor as a Result of Recharging Fuel Elements—V. Bartoshek	383	315
Texture of Quenched Uranium as a Function of the Character of Heating and Other Heat Treatment Parameters—V. E. Ivanov, V. F. Zelenskii, A. I. Smukalov, A. V. Azarenko, L. V. Tyrina, Ya. I. Gordienko, and V. V. Kunchenko	396	325
Metamorphism of Uranium Deposits and Individual Uranium Minerals—A. I. Tugarinov, E. V. Bibikova, and S. I. Zykov	404	332
Investigation of Radioactive Contamination Round the IRT-100 Nuclear Reactor—I. T. Mishev, M. A. Radicheva, and T. M. Troshev	416	344
LETTERS TO THE EDITOR		
Nomograms for Calculating the Kinematic Elements of Nuclear Reactions with Two-Particle Yields—G. N. Potetyunko	421	349
Designing Direct-Charging Nuclear Current Sources—A. A. Kononovich, M. G. Mitel'man, and N. D. Rozenblyum	425	351
The Possibility of the Generation and Acceleration of Positrons in a Microtron—K. A. Belovintsev and F. P. Denisov	427	353
Gamma-Radiation from the IRT-2000 Reactor of the Belorussian Academy of Sciences—A. P. Bogdanov and E. I. Firsov	429	354
Attenuation of Neutrons with an Energy of More than 1.5 Mev in Iron—V. N. Avaev, Yu. A. Egorov, and G. G. Moiseev	431	355
Silicon Spectrometric Detectors with a Wide Sensitivity Region—O. A. Matveev and S. M. Ryvkin	432	356
Spectrometry of Heavy Charged Particles in the Medium-Energy Range by n-i-p Silicon Detectors—O. A. Matveev, V. P. Rudakov, and I. N. Serikov	436	360
Spectrometric Germanium Gamma Detector—O. A. Matveev	439	362

(continued)

Annual Subscription: \$95

Single Issue: \$30

Single Article: \$15

1306

All rights reserved. No article contained herein may be reproduced for any purpose whatsoever without permission of the publisher. Permission may be obtained from Consultants Bureau Enterprises, Inc., 227 West 17th Street, New York City, United States of America.

CONTENTS (continued)

	P A G E	
	ENG.	RUSS.
Fast Response Silicon Detectors for Pulsed X-Rays—O. A. Matveev, S. M. Ryvkin, and D. V. Tarkhin	440	363
"Long" Counter-Based Neutron Dosimeter—E. S. Frid, G. V. Miroshnikov, N. I. Slozhenikin, and V. V. Barchugov	443	365
Determination of the Moisture Content of Sand from the Attenuation of a Fast Neutron Flux —V. D. Volovik, G. P. Strelkov, A. S. Cherkasov, and G. N. Chursin	445	366
Probability of Delayed Neutron Emission from Halogens—P. M. Aron, O. I. Kostochkin, K. A. Petrzhak, and V. I. Shpakov	447	368
Radiochemical Determination of the $Al^{27}(n,\alpha)Na^{24}$ Reaction Cross Section for a Neutron Energy of 14.6 Mev—P. M. Aron, S. S. Bugorkov, K. A. Petrzhak, and A. V. Sorokina . .	450	370
Hardening Orientation of Uranium Rods—I. V. Batenin and B. V. Sharov	453	372
NEWS OF SCIENCE AND TECHNOLOGY		
International Conference on Elementary Particles—V. Nikitin and A. Tyapkin	455	374
III International Conference on the Mössbauer Effect—N. Burgov	460	377
Symposium on Nuclear Electronics Sponsored by Member Nations of the Joint Institute for Nuclear Research—A. N. Sinaev	464	379
Symposium on Radiological Shielding and Safety Techniques in the Mining and Processing of Nuclear Materials—M. Bashkirtsev and N. Chesnokov	467	381
Symposium on the Biological Effects of Neutrons	469	382
The Indian Nuclear Research Center at Trombay—Vikt. I. Spitsyn	472	384
Nuclear Power in Brazil—Yu. Mityaev	475	385
Minimum Permissible Distances for Storing Packages Containing Radioactive Materials —N. I. Leshchinskii	477	386
Spectrometric and Electronic Equipment at the Comecon Exhibit	479	387
Exhibit of Polish Nuclear Physics Instrumentation	482	390
Patents	485	390
BIBLIOGRAPHY		
New Literature	486	393

ATOMNAYA ÉNERGIYA
EDITORIAL BOARD

A. I. Alikhanov	A. I. Leipunskii
A. A. Bochvar	M. G. Meshcheryakov
N. A. Dollezhal'	M. D. Millionshchikov
K. E. Erglis	(<i>Editor-in-Chief</i>)
V. S. Fursov	I. I. Novikov
I. N. Golovin	V. B. Shevchenko
V. F. Kalinin	A. P. Vinogradov
N. A. Kolokol'tsov	N. A. Vlasov
(<i>Assistant Editor</i>)	(<i>Assistant Editor</i>)
A. K. Krasin	M. V. Yakutovich
I. F. Kvartskhava	A. P. Zefrov
A. V. Lebedinskii	

SOVIET ATOMIC ENERGY

A translation of **ATOMNAYA ÉNERGIYA**
A publication of the Academy of Sciences of the USSR

© 1965 CONSULTANTS BUREAU ENTERPRISES, INC.
227 West 17th Street, New York 11, N. Y.

Vol. 16, No. 5

May, 1964

CONTENTS

	P A G E	
	ENG.	RUSS.
On the Nonlinear Theory of Electron Cyclotron Resonance—A. N. Kondratenko	493	399
Slow Neutron Spectra in Water Containing Absorbers—N. I. Laletin	498	402
The Study of Non-Stationary Regimes of Natural Circulation in Multi-Loop Nuclear Reactor Circuits—Yu. E. Bagdasarov, O. D. Kazachkovskii, M. S. Pinkhasik, and V. K. Pyshin	503	407
The Calculation of Thermal Neutron Reactors with Plutonium Recycling—P. Ventsel'	509	413
Experimental Study of a Heat Transfer Crisis—V. N. Smolin, V. K. Polyakov, and V. I. Esikov	515	417
Mass Spectrometric Determination of Very Small Quantities of Boron in Certain Materials —L. Ya. Memelova, G. M. Kukavadze and B. V. Érshler	522	423
Deformation and Failure of Rolled Beryllium of Differing Degrees of Purity—V. M. Amonenko, V. M. Azhazha, V. E. Ivanov, G. F. Tikhinskii and V. A. Finkel'	525	426
Solid Bitumens in Uranium-Bearing Veins—B. V. Brodin and Yu. M. Dymkov	531	432
Experimental Method of Studying the Shielding Properties of Materials Using the Proton Beam of the Dubna Synchrocyclotron—V. P. Afanas'ev, I. B. Keirim-Markus, E. E. Kovalev, V. A. Sakovich, L. N. Smirenniy and M. A. Sychkov	537	437
Instability of Langmuir Electron Plasma Oscillations in the Presence of a Magnetic Field —V. N. Oraevskii	541	441
Calculating the Phase Relations in a Cyclotron—G. N. Vyalov	543	442
Pulse Amplitude Analysis by Photographing on a Moving Film—V. S. Pantuev and M. N. Khachatryan	546	444
The Optimum Thickness of α -Specimens for Use in Spectrometric Measurements on Low Activity Samples—L. S. Gorn and B. I. Khazanov	549	447
Specific Ionization Along the Fission Fragment Tracks from U^{235} and Cm^{244} —F. Nasyrov	552	449
Low Energy α -Transitions in Pu^{238} and Pu^{240} —G. G. Akalaev, N. A. Vartanov and P. S. Samoilov	555	452
Spatial Distribution of the Scattered Radiation Dose from a Source of Unidirectional α -Quanta in an Infinite Medium Near the Source—V. I. Kukhtevich, E. S. Matusevich and L. A. Trykov	557	453
Ion Exchange Equipment for Producing Reactor Feed Water—V. D. Ganzha, K. A. Konoplev, V. D. Trenin and V. T. Sharov	560	456
Heat Exchange in Separated Bundles of Rods with Metallic Sodium Flowing Longitudinally —V. M. Borishanskii and É. V. Firsova	562	457

(continued)

Annual Subscription: \$95

Single Issue: \$30

Single Article: \$15

1308

All rights reserved. No article contained herein may be reproduced for any purpose whatsoever without permission of the publisher. Permission may be obtained from Consultants Bureau Enterprises, Inc., 227 West 17th Street, New York City, United States of America.

CONTENTS (continued)

	P A G E	
	ENG.	RUSS.
NEWS OF SCIENCE AND TECHNOLOGY		
Session of the Nuclear Physics Division of the USSR Academy of Sciences—E. D. Donets	564	459
Fifteenth Session of the Learned Council of the Joint Institute for Nuclear Research		
—V. Biryukov and R. Lebedev	565	459
Polarized Beams and Polarized Targets—L. B. Parfenov	569	462
Symposium on Nuclear Electronics—V. Matveev	570	463
Second Conference on Revising the "Rules and Regulations for the Safe Transportation of Radioactive Materials"—N. I. Leshchinskii	573	464
Antimatter and the Universe—N. Vlasov	574	465
Redesign of the Bevatron—B. N. Yablokov	578	468
Radioactive Isotope and Nuclear Radiation Applications in the Azerbaidzhan SSR		
—A. M. Mamedov	578	468
Patents	580	469
BIBLIOGRAPHY		
Review—N. Vlasov	581	470
Articles from the Periodical Literature	582	470

ATOMNAYA ÉNERGIYA
EDITORIAL BOARD

A. I. Alikhanov	A. I. Leipunskii
A. A. Bochvar	M. G. Meshcheryakov
N. A. Dollezhal'	M. D. Millionshchikov
K. E. Erglis	(<i>Editor-in-Chief</i>)
V. S. Fursov	I. I. Novikov
I. N. Golovin	V. B. Shevchenko
V. F. Kalinin	A. P. Vinogradov
N. A. Kolokol'tsov	N. A. Vlasov
(<i>Assistant Editor</i>)	(<i>Assistant Editor</i>)
A. K. Krasin	M. V. Yakutovich
I. F. Kvartskhava	A. P. Zefrov
A. V. Lebedinskii	

SOVIET ATOMIC ENERGY

A translation of **ATOMNAYA ÉNERGIYA**
A publication of the Academy of Sciences of the USSR

© 1965 CONSULTANTS BUREAU ENTERPRISES, INC.
227 West 17th Street, New York 11, N.Y.

Vol. 16, No. 6

June, 1964

CONTENTS

	P A G E	
	ENG.	RUSS.
In Memoriam: Igor'Il'Ich Bondarenko	593	
A Decade of Nuclear Power Engineering—A. M. Petros'yants	596	479
Operating Experience with the World's First Atomic Power Station—G. N. Ushakov, L. A. Kochetkov, V. G. Konochkin, V. S. Sever'yanov, V. Ya. Kozlov, and O. A. Sudnitsyn	601	484
The I. V. Kurchatov Atomic Power Station at Beloyarsk—P. I. Aleshchenkov, Yu. I. Mityaev, G. D. Knyazeva, L. I. Lunina, A. D. Zhirnov, V. M. Shuvalov	606	489
Distribution of the Ratio of Radiation Capture and Fission Cross Sections for Pu ²³⁹ with Respect to Height in the BR-5 Reactor—V. I. Ivanov, N. N. Krot, and G. N. Smirenkin	615	497
Analytical Method of Calculating the Nonuniform Burn-up of Fuel in Nuclear Reactors —I. S. Akimov and E. I. Grishanin	619	500
Nonstationary Problems in the Kinetic Theory of Neutron Transport—Ya. I. Granovskii and A. A. Kostritsa	624	504
Radiation-Chemical Effect of Fast Electrons on Uranium Fluorides—A. I. Migachev and A. P. Senchenkov	631	510
LETTERS TO THE EDITOR		
Cascade Interactions of Nuclei with High-Energy Particles—V. S. Barashenkov, A. V. Bayadzhiev, L. A. Kulyukina, and V. M. Mal'tsev	636	515
Determining the Mean β -Radiation Energy of Low-Activity Samples—S. V. Belov and A. P. Bychkov	639	518
Angular Distribution of Fragments from Fission of U ²³⁵ and Pu ²³⁹ by 0.08–1.25 MeV Neutrons —V. G. Nesterov, Yu. A. Blyumkina, L. A. Kamaeva, and G. N. Smirenkin	641	519
Mean Kinetic Energy of Fragments from Fission Above the (n, nf) Threshold —V. N. Okolovich and G. H. Smirenkin	644	521
Interaction Cross Section of Neutrons with Sm ¹⁴⁹ and In ¹¹⁵ Nuclei—R. B. Begzhanov, D. A. Gladyshev, S. V. Starodubtsev, and T. Khaidarov	647	523
Heat Transfer by Flow of Metallic Sodium in a Tube—V. M. Borishanskii, T. V. Zablotskaya, and N. I. Ivashchenko	649	524
Measurement of Pu ²³⁹ Build-Up from U ²³⁹ Gammas—L. N. Yurova and A. V. Bushuev	653	527
Some of the Physical Characteristics of Hot α -Active Aerosol Particles—B. I. Styre, É. Yu. Vebra, and K. K. Shopauskas	655	528
Hot Aerosol Particles in the Surface Air Around Moscow—S. G. Malakhov and K. P. Makhon'ko	659	530

Annual Subscription: \$95

Single Issue: \$30

Single Article: \$15

1310

All rights reserved. No article contained herein may be reproduced for any purpose whatsoever without permission of the publisher. Permission may be obtained from Consultants Bureau Enterprises, Inc., 227 West 17th Street, New York City, United States of America.

CONTENTS (continued)

	P A G E	
	ENG.	RUSS.
FROM THE ARCHIVES OF SCIENCE		
The Discovery of Artificial Radioactivity—Pierre Savel	662	534
NEWS OF SCIENCE AND TECHNOLOGY		
Fourteenth All-Union Conference on Nuclear Spectroscopy—V. P. Rudakov	667	538
Fifth All-Union Intercollegiate Conference on Elementary Particle Theory—A. S. Bakai and A. S. Litvinenko	669	539
International Conference on Semiconductor Radiation Detectors—O. A. Matveev and B. P. Osinenko	671	540
Third International Conference on the Separation, Analysis, and Use of Stable Isotopes —V. S. Zolotarev	673	541
Second Soviet Symposium on Sources of Ionizing Radiations for Radioteletherapy —V. N. Nikeshichev	676	543
Brief Communications	680	546
BIBLIOGRAPHY		
Articles from the Periodical Literature	681	547

ATOMNAYA ÉNERGIYA
EDITORIAL BOARD

A. I. Alikhanov	A. I. Leipunskii
A. A. Bochvar	M. G. Meshcheryakov
N. A. Dollezhal'	M. D. Millionshchikov
K. E. Erglis	(<i>Editor-in-Chief</i>)
V. S. Fursov	I. I. Novikov
I. N. Golovin	V. B. Shevchenko
V. F. Kalinin	A. P. Vinogradov
N. A. Kolokol'tsov	N. A. Vlasov
(<i>Assistant Editor</i>)	(<i>Assistant Editor</i>)
A. K. Krasin	
I. F. Kvartskhava	M. V. Yakutovich
A. V. Lebedinskii	A. P. Zefirov

SOVIET ATOMIC ENERGY

A translation of **ATOMNAYA ÉNERGIYA**
A publication of the Academy of Sciences of the USSR

© 1965 CONSULTANTS BUREAU ENTERPRISES, INC.
227 West 17th Street, New York 11, N.Y.

Vol. 17, No. 1

July, 1964

CONTENTS

	P A G E	
	ENG.	RUSS.
Heavy Hydrogen and Neutron Isotopes—N. A. Vlasov and L. N. Samoilov	687	3
Average Energies of Electron and Positron β Spectra—N. S. Shimanskaya and E. G. Zaletskii	694	9
Polarized Ion Source—B. P. Ad'yasevich, V. G. Antonenko, Yu. P. Polumin, and D. E. Fomenko	703	17
Analysis of the Observed Resonance-Width Distributions of U^{233} and Pu^{239} —L. N. Usachev, V. A. Pavlinchuk, and N. S. Rabotnov	709	22
Some Data on the Spontaneous Fission of Cm^{244} —V. I. Bol'shov, L. I. Prokhorova, V. N. Okolovich, and G. N. Smirenkin	715	28
Space-Energy Distribution of Neutrons in a Homogeneous Moderator—D. A. Kozhevnikov	722	34
Transfer of Iodine From Aqueous Solutions to Saturated Vapor—M. A. Styrikovich, O. I. Martynova, K. Ya. Katkovskaya, I. Ya. Dubrovskii, and I. N. Smirnova	735	45
Investigation of the Penetration of Metal Tube Walls by Helium—I. S. Lupakov and Yu. S. Kuz'michev	740	49
Radiochemical Processes in the Radiolysis of Perfluorocarbons—V. A. Khramchenkov	744	53
LETTERS TO THE EDITOR		
Longitudinal Instability of a Charged Beam Circulating in an Accelerator or Accumulator With Finite Conductivity of the Chamber Walls—A. A. Kolomenskii	748	57
Elastic Scattering of α Particles on Boron—S. V. Starodubtsev and B. I. Khrushchev	751	59
Passage of Neutrons Through Carbon and Through an Iron-Carbon Mixture—V. K. Daruga, I. I. Lazutkin, A. N. Nikolaev, V. K. Sakharov, B. I. Sinitsyn, and S. G. Tsypin	754	60
Investigation of the Space-Energy Distribution of Neutrons From the Br-5 Reactor in an Iron-Ore Medium—V. K. Daruga, I. I. Lazutkin, A. N. Nikolaev, D. M. Pinkhasik, V. K. Sakharov, B. I. Sinitsyn, and S. G. Tsypin	757	63
Attenuation of the Flux of Fission Neutrons in Iron-Water Mixtures—V. P. Mashkovich, A. N. Nikolaev, B. I. Sinitsyn, and S. G. Tsypin	760	65
The Effect of Radioactive Irradiation on the Stability of Plastic Scintillators—V. D. Bezuglyi and L. L. Nagornaya	762	67
Separation of Labeled Compounds by Gas Chromatography—S. A. Volkov and K. I. Sakodynskii	766	70
A Simple Radiographic Technique in Fingerprint Studies—A. Ya. Gel'fman, G. L. Granovskii, and L. Ya. Kheifets	768	71

Annual Subscription: \$95

Single Issue: \$30

Single Article: \$15

1312

All rights reserved. No article contained herein may be reproduced for any purpose whatsoever without permission of the publisher. Permission may be obtained from Consultants Bureau Enterprises, Inc., 227 West 17th Street, New York City, United States of America.

CONTENTS (continued)

	P A G E	
	ENG.	RUSS.
NEWS OF SCIENCE AND ENGINEERING		
Third International Conference on Low-Temperature Physics and Engineering—R. A. Alikhanov	769	72
Applications of Mineral Sorbents in the Purification of Liquid Radioactive Slurries—V. Gromov	771	73
The Uranium Industry in the Capitalist Countries in 1963—V. D. Andreev.	775	75
Uno Scientific Consultative Committee	779	78
BIBLIOGRAPHY		
Books	780	79
Jaderna Energie, No. 5 (1964).	783	80

ATOMNAYA ÉNERGIYA
EDITORIAL BOARD

A. I. Alikhanov	A. I. Leipunskii
A. A. Bochvar	M. G. Meshcheryakov
N. A. Dollezhal'	M. D. Millionshchikov
K. E. Erglis	(<i>Editor-in-Chief</i>)
V. S. Fursov	I. I. Novikov
I. N. Golovin	V. B. Shevchenko
V. F. Kalinin	A. P. Vinogradov
N. A. Kolokol'tsov	N. A. Vlasov
(<i>Assistant Editor</i>)	(<i>Assistant Editor</i>)
A. K. Krasin	M. V. Yakutovich
I. F. Kvartskhava	A. P. Zefirov
A. V. Lebedinskii	

SOVIET ATOMIC ENERGY

A translation of **ATOMNAYA ÉNERGIYA**
A publication of the Academy of Sciences of the USSR

© 1965 CONSULTANTS BUREAU ENTERPRISES, INC.
227 West 17th Street, New York 11, N. Y.

Vol. 17, No. 2

August, 1964

CONTENTS

	P A G E	
	ENG.	RUSS.
Ohmic Heating and Electrical Conductivity of a Plasma in Strong Electric Fields		
—V. A. Suprunenko, E. A. Sukhomlin, and N. I. Reva	787	83
Apparatus for Studying the Motion of Particles in Accelerators—M. Barbier.	793	88
Determination of the Optimum Fuel Burn-up and Energy Intensity of Nuclear Fuel by the Method of Cost Calculations—Yu. I. Koryakin, V. V. Batov, and V. G. Smirnov.	800	94
Stability Regions of the Control Loop of a Cold Reactor—Pavel Štřífský.	804	97
Theoretical and Experimental Studies of the Efficiency of Absorbing Rods in a Reflected Reactor		
—N. N. Ponomarev-Stepnoi and V. I. Nosov.	810	103
Dispersion Type Absorbing Materials for Thermal Reactor Control Rods—V. I. Nosov, N. N. Ponomarev-Stepnoi, K. I. Portnoi, and E. G. Savel'yev	815	107
Propagation of Neutrons in Uranium Carbide—I. I. Bondarenko, V. I. Golubev, A. V. Zvonarev, M. N. Nikolaev, M. Yu. Orlov, and O. P. Uznadze	821	113
Some Characteristics of the Process of Oxidizing Uranium by Tervalent Iron Ions		
—Vikt. I. Spitsyn, G. M. Nesmeyanova, and A. I. Vikulov.	827	119
Cementation of Hydroxide Precipitates Containing Certain Radioactive Elements—Yu. M. Butt, V. V. Timashev, L. A. Kutsenko, I. E. Kozlova, and A. V. Gordievskii	832	124
The Effect of Solar Radiation on the Spread of Radioactive Products from Nuclear Explosions in the Atmosphere—D. L. Simonenko.	838	130
Effect of Roughness of the Ground on the γ Field above a Region Contaminated by Radioactive Fallout—Yu. A. Izraél'.	845	137
Conductivity of a Turbulent Plasma in the Magnetohydrodynamic Approximation		
—V. M. Eleonskii and Yu. Ya. Polyak.	849	141
Some Reactions in Zinc Due to 30 MeV Protons—T. N. Mikhaleva	851	142
Optimized Shutdown Sequence for a Nuclear Reactor—Yu. P. Petrov.	853	144
Investigation of Fast-Neutron Penetration Through Sodium—V. K. Daruga, A. N. Nikolaev, D. S. Pinkhasik, B. I. Sinitsyn, and S. G. Tsypin.	855	145
How to Choose the Parameters of Planar Emitters in Radiation Processors—F. A. Makhliis	857	147
A Liquid-Type Scintillation Counter for the Investigation of Biological Specimens		
—V. N. Podymakhin and É. G. Toropygina.	860	149
SCIENCE AND ENGINEERING NEWS		
At the All-Union Conference on Solid State Theory—V. Agranovich.	863	152
Radiation Chemistry Conference—N. Spoloso.	866	153

Annual Subscription: \$95

Single Issue: \$30

Single Article: \$15

1314

All rights reserved. No article contained herein may be reproduced for any purpose whatsoever without permission of the publisher. Permission may be obtained from Consultants Bureau Enterprises, Inc., 227 West 17th Street, New York City, United States of America.

CONTENTS (continued)

	P A G E	
	ENG.	RUSS.
Progress in the Processing and Disposal of Radioactive Wastes—B. S. Kolychev.	868	154
BIBLIOGRAPHY		
New Books.	872	157

ATOMNAYA ÉNERGIYA
EDITORIAL BOARD

A. I. Alikhanov	A. I. Leipunskii
A. A. Bochvar	M. G. Meshcheryakov
N. A. Dollezhal'	M. D. Millionshchikov
K. E. Erglis	(<i>Editor-in-Chief</i>)
V. S. Fursov	I. I. Novikov
I. N. Golovin	V. B. Shevchenko
V. F. Kalinin	A. P. Vinogradov
N. A. Kolokol'tsov	N. A. Vlasov
(<i>Assistant Editor</i>)	(<i>Assistant Editor</i>)
A. K. Krasin	M. V. Yakutovich
I. F. Kvartskhava	A. P. Zefirov
A. V. Lebedinskii	

SOVIET ATOMIC ENERGY

A translation of **ATOMNAYA ÉNERGIYA**
A publication of the Academy of Sciences of the USSR

© 1965 CONSULTANTS BUREAU ENTERPRISES, INC.
227 West 17th Street, New York 11, N. Y.

Vol. 17, No. 3

September, 1964

CONTENTS

	P A G E	
	ENG.	RUSS.
New Progress for the Peaceful Use of the Atom—I. D. Morokhov	879	163
Investigation of Ohmic Heating of the Plasma in the "Tokamak-3" Toroidal Assembly —L. A. Artsimovich, S. V. Mirnov, and V. S. Strelkov	886	170
Effect of a Transverse Magnetic Field on a Toroidal Discharge in a Strong Longitudinal Magnetic Field—B. M. Grigorovich and V. S. Mukhovatov	893	177
On the Mechanism of X-Ray and Neutron Radiations from High-Power Pulse Discharges —M. D. Raizer and V. N. Tsytovich	901	185
Optimum Reactor Shutdown Conditions—V. N. Artamkin, G. V. Vasenkova, I. V. Otroshchenko, and R. P. Fedorenko	906	189
Space-Energy Distribution of Thermal Neutrons in a Homogeneous Reactor—N. I. Laletin	911	193
The Effect of Flattening on Certain Thermal and Physical Characteristics of a Cylindrical Fast Reactor—V. V. Khromov, S. B. Shikhov, A. M. Kuz'min, and A. N. Shmelev	918	199
The Effect of the Intensity of Mass Exchange on Certain Parameters of the Autoclave Leaching of Uranium Ore—B. V. Nevskii, I. P. Smirnov, and S. A. Pirkovskii	921	201
Reduction—Oxidation Potential and Degree of Extraction of Uranium in Sulfuric Acid Solutions —A. P. Filippov and E. A. Kanevskii	925	205
Probe Method of Measuring the Displacement of the Current Pinch in Cylindrical and Toroidal Chambers—S. V. Mirnov	929	209
Magnetic Field with Mirror Configuration, Increasing Radially—Yu. V. Martynenko and R. I. Sobolev	932	211
Calculation of the Maximum Possible Delayed-Neutron Yields Obtainable from Certain Photonuclear Reactions—M. M. Dorosh, Ya. É. Kostyu, and V. A. Shkoda-Ul'yanov	937	215
The Penetration of Beta Particles Through a Material—K. K. Aglintsev and I. P. Kasatkin	940	217
U^{238} Fission with 26.5-MeV Alpha Particles—B. A. Bochagov, S. S. Vasil'ev, G. G. Semenchuk, and G. E. Solyakin	943	219
Measurement of the Diffusion Coefficient for RaA by Deposition from Laminar Flow —V. I. Korpusov, B. I. Ogorodnikov, and V. N. Kirichenko	945	221
Use of the Relationship between Linear Energy Transfer and Radiochemical Yield for the Dosimetry of Sources of Ionizing Radiation—M. V. Vladimirova	947	222
LETTERS TO THE EDITOR		
Relation between the Linear Attenuation Coefficient for γ Radiation from Co^{60} and the Temperature of a Metallic Absorber—V. I. Kutovoi and V. I. Stetsenko	950	224

Annual Subscription: \$95

Single Issue: \$30

Single Article: \$15

1316

All rights reserved. No article contained herein may be reproduced for any purpose whatsoever without permission of the publisher. Permission may be obtained from Consultants Bureau Enterprises, Inc., 227 West 17th Street, New York City, United States of America.

CONTENTS (continued)

	P A G E	
	ENG.	RUSS.
Graphical Method for Analyzing Radioactive Decay of Mixed Parent and Daughter Isotopes -S. G. Malakhov	952	226
SCIENCE AND ENGINEERING NEWS		
Conference Commemorating the Tenth Anniversary of the Startup of the World's First Nuclear Reactor Electric Power Station.	954	227
International Symposium on Medical Radioisotope Scanning (IAEA, Athens 1964).	957	229
Seminar on Applications of Radioisotope Techniques and Instrumentation in Industry.	960	231
French Exhibit of Measuring and Electronic Instrumentation at Moscow, May 1964	963	232
BIBLIOGRAPHY		
Papers Presented by Soviet Scientists at the Third International Conference on the Peaceful Uses of Atomic Energy (Geneva 1964).	966	235

ATOMNAYA ÉNERGIYA
EDITORIAL BOARD

A. I. Alikhanov	A. I. Leipunskii
A. A. Bochvar	M. G. Meshcheryakov
N. A. Dollezhal'	M. D. Millionshchikov
K. E. Erglis	(<i>Editor-in-Chief</i>)
V. S. Fursov	I. I. Novikov
I. N. Golovin	V. B. Shevchenko
V. F. Kalinin	A. P. Vinogradov
N. A. Kolokol'tsov	N. A. Vlasov
(<i>Assistant Editor</i>)	(<i>Assistant Editor</i>)
A. K. Krasin	M. V. Yakutovich
I. F. Kvartskhava	A. P. Zefirov
A. V. Lebedinskii	

SOVIET ATOMIC ENERGY

A translation of **ATOMNAYA ÉNERGIYA**
A publication of the Academy of Sciences of the USSR

© 1965 CONSULTANTS BUREAU ENTERPRISES, INC.
227 West 17th Street, New York 11, N. Y.

Vol. 17, No. 4

October, 1964

CONTENTS

	P A G E	
	ENG.	RUSS.
Pathways of Nuclear Power Development in the USSR—N. M. Sinev, B. B. Baturov, and V. M. Shmelev	973	243
International Cooperation and the Development of Nuclear Reactor Projects—I. D. Morokhov, V. S. Kandaritskii, and Yu. V. Arkhangel'skii	982	252
Review of Work on Research Reactors and Their Application in the USSR—V. V. Goncharov . . .	989	258
Studies on the Problem of Controlled Nuclear Synthesis and the Physics of High-Temperature Plasma in the USSR—L. A. Artsimovich	1000	269
Use of Isotopes and Radiation Sources for Research in the Physical Sciences—P. L. Gruzin	1008	278
Fundamental Technical Characteristics of the Experimental Thermonuclear System "Tokamak-3"—M. A. Gashev, G. K. Gustov, K. K. D'yachenko, E. G. Komar, I. F. Malyshev, N. A. Monoszon, A. V. Popkovich, B. K. Ratnikov, B. V. Rozhdestvenskii, N. N. Rumyantsev, G. L. Saksaganskii, F. M. Spevakova, A. M. Stolov, N. S. Strel'tsov, and A. Kh. Yavno	1017	287
Some Characteristics of a Fast Reactor with Thorium Shield—G. A. Batyrbekov, I. I. Bondarenko, Yu. F. Koleganov, M. N. Nikolayev, and O. P. Uznadze	1025	294
LETTERS TO THE EDITOR		
Theory of Diffusive Deposition of Decay Products of Inert Gases in Circular and Flat Channels— V. M. Berezhnoi and V. V. Kirichenko	1031	300
Age of Neutrons from U ²³⁵ Fission in Monoisopropyldiphenyl and in Diphenyl-Iron and Diphenyl-Aluminum Mixtures—L. N. Yurova, A. A. Polyakov, and A. A. Ignatov	1035	303
Theoretical Neutron Cross Sections of U ²³⁸ and Th ²³² Nuclei—G. I. Marchuk, V. E. Kolesov, and A. G. Dovbenko.	1038	304
Coefficient of Viscosity of N ₂ ¹⁴ - N ₂ ¹⁵ in the Temperature Range 78-300° K—N. E. Menabde	1042	307
Radioactivity of Atmosphere and Water from the Atlantic Ocean and the Black and Caspian Seas—N. N. Alfimov, N. I. Matyzov, and P. N. Yagovoi.	1044	309
Synthesis and Physical Identification of the Isotope with Mass Number 260 of Element 104— G. N. Flerov, Yu. Ts. Oganessian, Yu. V. Lobanov, V. I. Kuznetsov, V. A. Druin, V. P. Pereilygin, K. A. Gavrillov, S. P. Tret'yakova, and V. M. Plotko	1046	310
SCIENCE AND ENGINEERING NEWS		
Scientific Research Colloquium of the Moscow Engineering and Physics Institute—V. V. Frolov. .	1049	313
International Conference on Scintillation Counters for Recording and Spectrometry of Nuclear Radiations—A. Radyvanok	1052	314

Annual Subscription: \$95

Single Issue: \$30

Single Article: \$15

1318

All rights reserved. No article contained herein may be reproduced for any purpose whatsoever without permission of the publisher. Permission may be obtained from Consultants Bureau Enterprises, Inc., 227 West 17th Street, New York City, United States of America.

CONTENTS (continued)

	P A G E	
	ENG.	RUSS.
Dubna Conference on Acceleration Electronics—Yu. N. Denisov	1054	316
BIBLIOGRAPHY		
New Books	1059	319

ATOMNAYA ÉNERGIYA
EDITORIAL BOARD

A. I. Alikhanov	A. I. Leipunskii
A. A. Bochvar	M. G. Meshcheryakov
N. A. Dollezhal'	M. D. Millionshchikov
K. E. Erglis	(<i>Editor-in-Chief</i>)
V. S. Fursov	I. I. Novikov
I. N. Golovin	V. B. Shevchenko
V. F. Kalinin	A. P. Vinogradov
N. A. Kolokol'tsov	N. A. Vlasov
(<i>Assistant Editor</i>)	(<i>Assistant Editor</i>)
A. K. Krasin	M. V. Yakutovich
I. F. Kvartskhava	A. P. Zefirov
A. V. Lebedinskii	

SOVIET ATOMIC ENERGY

A translation of **ATOMNAYA ÉNERGIYA**
A publication of the Academy of Sciences of the USSR

© 1965 CONSULTANTS BUREAU ENTERPRISES, INC.
227 West 17th Street, New York 11, N. Y.

Vol. 17, No. 5

November, 1964

CONTENTS

	P A G E	
	ENG.	RUSS.
The Third International Geneva Conference—A. M. Petros'yants	1065	323
High-Temperature Reactor-Converter "Romashka"—M. D. Millionshchikov, I. G. Gverdtsiteli, A. S. Abramov, L. V. Gorlov, Yu. D. Gubanov, A. A. Efremov, V. F. Zhukov, V. E. Ivanov, V. K. Kovyrzin, E. A. Koptelov, V. G. Kosovskii, N. E. Kukharkin, R. Ya. Kucherov, S. P. Lalykin, V. I. Merkin, Yu. A. Nechaev, B. S. Pozdnyakov, N. N. Ponamarev-Stepnoi, E. N. Samarin, V. Ya. Serov, V. A. Usov, V. G. Fedin, V. V. Yakovlev, M. V. Yakutovich, V. A. Khodakov, and G. V. Kompaniets	1071	329
Development of Superheating Power Reactors of the Beloyarsk Nuclear Power Station Type —N. A. Dollezhal', I. Ya. Emel'yanov, P. I. Aleshchenkov, A. D. Zhirnov, G. A. Zvereva, N. G. Morgunov, Yu. I. Mityaev, G. D. Knyazeva, K. A. Kryukov, V. N. Smolin, L. I. Lunina, V. I. Kononov, and V. A. Petrov	1078	335
Novo-Voronezh Nuclear Power Station—In Operation—N. M. Sinev	1088	*
Sodium-Cooled Fast Reactors—A. I. Leipunskii, O. D. Kazachkovskii, I. I. Afrikantov, M. S. Pinkhasik, N. V. Krasnoyarov, and M. S. Poido	1090	345
Operating Experience with the Nuclear Propulsion Plant on the Icebreaker "Lenin" —I. I. Afrikantov, N. M. Mordvinov, P. D. Novikov, B. G. Pologikh, A. K. Sledzyuk, N. S. Khlopkin, and N. M. Tsarev	1094	349
Experience in Operating the First Nuclear Power Station as an Experimental Facility —G. N. Ushakov, L. A. Kochetkov, V. G. Konochkin, V. S. Sever'yanov, V. Ya. Kozlov, O. A. Sudnitsyn, N. T. Belinskaya, P. N. Slyusarev, and V. A. Ivanov	1105	359
Containment of Plasma in a Trap with Combined Magnetic Field—M. S. Ioffe and R. I. Sobolev.	1112	366
Calculation of Water-Moderated Water-Cooled Reactors—E. A. Garusov and Yu. V. Petrov	1121	375
The Burn-Up of Natural Uranium When it is Moved Axially in a Reactor—V. Bartosek and V. Lelek	1126	380
Column Packings Used in Isotope Separation—Yu. R. Akopov, I. G. Gverdtsiteli, V. A. Kaminskii, and G. L. Partsakhashvili	1133	384
Some Characteristics of Radiolysis Under the Influence of a Pulsed Beam of Fast Electrons —V. L. Tal'roze and V. E. Skurat	1142	393
Producing High-Purity Tantalum—O. P. Kolchin and I. K. Berlin	1150	400
LETTERS TO THE EDITOR		
Thermodynamic Calculation of the Reaction Between Sodium and Water for a Sodium-Water Type Steam Heater—N. N. Ivanovskii and F. A. Kozlov	1155	406

Annual Subscription: \$95

Single Issue: \$30

Single Article: \$15

1320

All rights reserved. No article contained herein may be reproduced for any purpose whatsoever without permission of the publisher. Permission may be obtained from Consultants Bureau Enterprises, Inc., 227 West 17th Street, New York City, United States of America.

CONTENTS (continued)

	P A G E	
	ENG.	RUSS.
The Critical Heat Fluxes in Tubes Carrying Monoisopropyldiphenyl, Heated Below the Saturation Temperature—F. F. Boganov	1159	408
Errors in the Calibration of γ -Dosimeters with a Collimated Beam—É. F. Garapov, Yu. N. Gryaznov, and G. A. Dorofeev	1162	410
SCIENCE AND ENGINEERING NEWS		
Interaction of Neutrons and Nuclei in the 1 eV—100 keV Range—L. B. Pikel'ner	1165	413
Symposium on Control Rod Physics and Control Rod Materials—I. R.	1168	414
A Symposium on Assay of Human Body Burden—Yu. V. Sivintsev	1170	415
A Polish Whole-Body Counter—Yu. V. Sivintsev	1173	417
New Device Unpacks Irradiated Targets—B. G. Chistov	1175	419
News Item	1177	420
BIBLIOGRAPHY	1178	421

*Two page insert facing page 336.

ATOMNAYA ÉNERGIYA
EDITORIAL BOARD

A. I. Alikhanov	A. I. Leipunskii
A. A. Bochvar	M. G. Meshcheryakov
N. A. Dollezhal'	M. D. Millionshchikov
K. E. Erglis	(<i>Editor-in-Chief</i>)
V. S. Fursov	I. I. Novikov
I. N. Golovin	V. B. Shevchenko
V. F. Kalinin	A. P. Vinogradov
N. A. Kolokol'tsov	N. A. Vlasov
(<i>Assistant Editor</i>)	(<i>Assistant Editor</i>)
A. K. Krasin	M. V. Yakutovich
I. F. Kvartakhava	A. P. Zefirov
A. V. Lebedinskii	

SOVIET ATOMIC ENERGY

A translation of **ATOMNAYA ÉNERGIYA**
A publication of the Academy of Sciences of the USSR

© 1966 CONSULTANTS BUREAU ENTERPRISES, INC.
227 West 17th Street, New York, N. Y. 10011

Vol. 17, No. 6

December, 1964

CONTENTS

	P A G E	
	ENG.	RUSS.
Some Ways of Development for Water-Moderated Water-Cooled Power Reactors —A. Ya. Kramerov, Yu. V. Markov, S. A. Skvortsov, V. P. Denisov, E. V. Kulikov, Yu. P. Sorokin, V. V. Stekol'nikov, A. A. Khokhlachev, V. P. Tatarnikov, and V. A. Sidorenko.	1183	427
The Organic-Cooled Organic-Moderated Nuclear Power Station "Arbus"—K. K. Polushkin, I. Ya. Emel'yanov, P. A. Delens, N. V. Zvonov, Yu. I. Aleksenko, I. I. Grozdov, S. P. Kuznetsov, A. P. Sirotkin, Yu. I. Tokarev, K. P. Lavrovskii, A. M. Brodskii, A. R. Belov, E. V. Borisyuk, V. M. Gryazev, V. D. Tetyukov, D. N. Popov, Yu. I. Koryakin, A. G. Filippov, K. V. Petrochuk, V. D. Khoroshavin, N. P. Savinov, M. N. Meshcheryakov, V. P. Pushkarev, V. A. Suroegin, P. A. Gavrilov, L. N. Podlazov, and I. N. Pogozhkin.	1197	439
TÉS-3 Compact Atomic Power Station—N. M. Sinev, A. K. Krasin, I. F. Bychkov, O. I. Blokhin, D. L. Broder, V. N. Gabrusev, Yu. V. Dudnikov, V. A. Zhil'tsov, M. A. Koptev, A. Ya. Komarov, A. P. Kotov, M. N. Lantsov, G. A. Lisochkin, G. A. Merzlikin, I. G. Morozov, Yu. I. Orekhov, Yu. A. Sergeev, P. N. Slyusarev, G. N. Ushakov, N. V. Fedorov, V. Ya. Chernyi, and V. M. Shmelev	1207	448
Physical and Operating Characteristics of the SM-2 Reactor—S. M. Feinberg, N. A. Dollezhal', E. D. Vorob'ev, V. A. Tsykanov, I. Ya. Emel'yanov, V. M. Gryazev, A. S. Kochenov, Yu. M. Bulkin, V. I. Ageenkoy, and P. G. Aver'yanov	1212	452
The PGR Pulsed Graphite Reactor—I. V. Kurchatov, S. M. Feinberg, N. A. Dollezhal', P. I. Aleshchenkov, F. S. Drozdov, I. Ya. Emel'yanov, A. D. Zhirnov, M. A. Kazachenko, G. D. Knyazeva, F. V. Kondrat'ev, V. D. Lavrenikov, N. G. Morgunov, B. V. Petunin, V. P. Smirnov, V. M. Talyzin, A. G. Filippov, I. L. Chikhladze, P. M. Chulkov, and Ya. V. Shevelev.	1224	463
Statistical Reactor Kinetics Equations—A. B. Govorkov.	1236	474
Channel Effects in Fission of Even-Even Compound Nuclei—L. N. Usachev, V. A. Pavlinchuk, and N. S. Rabotnov.	1242	479
Neutron Angular and Energy Distribution at the Boundary of Two Media—V. A. Dulin, V. G. Dvukhsherstnov, Yu. A. Kazanskii, and I. V. Shugar.	1249	486
The Neutron Background at the Surface of the Earth—G. V. Gorshkov, V. A. Zyabkin, and O. S. Tsvetkov.	1256	492
Addition of Hetero-Organic Compounds to Polystyrene—E. E. Baroni, S. F. Kilin, T. N. Lebsadze, I. M. Rozman, and V. M. Shoniya	1261	497

Annual Subscription: \$95

Single Issue: \$30

Single Article: \$15

1322

All rights reserved. No article contained herein may be reproduced for any purpose whatsoever without permission of the publisher. Permission may be obtained from Consultants Bureau Enterprises, Inc., 227 West 17th Street, New York City, United States of America.

CONTENTS (continued)

	P A G E	
	ENG.	RUSS.
In Memory of Konstantin Konstantinovich Aglintsev	1265	501
LETTERS TO THE EDITOR		
Study of the Transformations of Ruthenium Dioxide in the Presence of Chromium Oxide -M. K. Baranaev, V. G. Vereskunov, and K. P. Zakharova	1267	502
Use of the Time of Flight Method for Measuring the Range/Energy Relation for 18 to 38 MeV Helium Ions in Aluminum-N. I. Venikov and N. I. Chumakov	1269	503
Charge-Exchange of Oxygen Ions of Energy 2-13.3 MeV in Thin Alundum Films -N. I. Venikov, N. I. Chumakov, and B. I. Khoroshchavin	1271	504
Neutron Radiative Capture in Copper and Molybdenum-V. A. Tolskikov, V. E. Kolesov, A. G. Dovbenko, and Yu. Ya. Stavisskii	1272	505
Radiative Capture Cross Sections for Fast Neutrons in Iron-A. V. Malyshev, Yu. Ya. Stavisskii, and A. V. Shapar	1277	508
Use of the Monte Carlo Method for Calculating the Penetration of γ -Radiation Through Matter-L. M. Shirkin	1279	509
SCIENCE AND ENGINEERING NEWS		
Symposium on the Biological Effects of Radioisotopes	1282	512
Special-Purpose Heavy Cement with Enhanced Absorbing Power-K. S. Kutateladze and A. V. Rustambekov	1286	515
BIBLIOGRAPHY		
New Books	1288	517
Author Index, 1964	1295	
Tables of Contents	1300	

Soviet Journals Available in Cover-to-Cover Translation

ABBREVIATION	RUSSIAN TITLE	TITLE OF TRANSLATION	PUBLISHER	TRANSLATION Vol. Issue	BEGAN Year
AE	Atomnaya énergiya	Soviet Journal of Atomic Energy	Consultants Bureau	1 1	1956
Akust. zh.	Akusticheskiy zhurnal	Soviet Physics - Acoustics	American Institute of Physics	1 1	1955
Astr(om). zh(urn).	Astronomicheskii zhurnal	Soviet Astronomy - AJ	American Institute of Physics	34 1	1957
Avto(mat). svarka	Avtomaticheskaya svarka	Automatic Welding	Br. Welding Research Assn. (London)	12 1	1959
	Biofizika	Automation and Remote Control	Instrument Society of America	27 1	1956
	Byulleten' ékspierimental'noi biologii i meditsiny	Biochemistry Bulletin of Experimental Biology and Medicine	National Institutes of Health** Consultants Bureau	6 1 21 1	1961 1956
		Doklady Biologicheskoye Sekciiy (includes: Anatomy, biochemistry, biophysics, cytology, ecology, embryology, endocrinology, evolutionary morphology, genetics, histology, hydrobiology, microbiology, morphology, parasitology, physiology, zoology)	Consultants Bureau National Science Foundation*	41 1 112 1	1959 1957
		Doklady Botanicheskoye Sekciiy (includes: Botany, phytopathology, plant anatomy, plant ecology, plant embryology, plant physiology, plant morphology)	National Science Foundation*	112 1	1957
		Proceedings of the Academy of Sciences of the USSR, Section: Chemical Technology	Consultants Bureau	106 1	1956
		Proceedings of the Academy of Sciences of the USSR, Section: Chemistry	Consultants Bureau	106 1	1956
		Proceedings of the Academy of Sciences of the USSR, Section: Physical Chemistry	Consultants Bureau	112 1	1957
DAN (SSSR) Dok(lady) AN, SSSR	Doklady Akademii Nauk SSSR	Doklady Earth Sciences Sections (includes: Geochemistry, geology, geophysics, hydrogeology, lithology, mineralogy, oceanology, paleontology, permafrost, petrography)	American Geological Institute	124 1	1959
		Proceedings of the Academy of Sciences of the USSR, Section: Geochemistry of the USSR, Section: Geology	Consultants Bureau	106- 123 6	1956- 1958
		Proceedings of the Academy of Sciences of the USSR, Section: Geology	Consultants Bureau	112- 123 6	1957- 1958
		Soviet Mathematics - Doklady (includes: Aerodynamics, astronomy, crystal lography, cybernetics and control theory, electrical engineering, energetics, fluid mechanics, heat engineering, hydraulics, mathematical physics, mechanics, physics, technical physics, theory of elasticity sections)	American Mathematical Society American Institute of Physics	130 1 106 1	1960 1956
		Telecommunications			
		Entomological Review			
		Physics of Metals and Metallography			
		Soviet Physics - Solid State			
		Sechenov Physiological Journal USSR			
		Plant Physiology			
		Geodesy and Aerophotography			
		Geochemistry			
		Petroleum Geology			
		Geomagnetism and Aeronomy			
		Artificial Earth Satellites			
		Measurement Techniques			
		Electrosvyaz'			
		Entomologicheskoye obozrenie			
		Fizika metallov i metallovedenie			
		Fizika tverdogo tela			
		Fiziologicheskii zhurnal imeni I.M. Sechenov			
		Fiziologiya rastenii			
		Geodeziya i aerofototsyemka			
		Geokhimiya			
		Geologiya nefti i gaza			
		Geomagnitizm i aeronomiya			
		Iskusstvennyye sputniki zemli			
		Izmeritel'naya tekhnika			
Entom(ol). oboz(r).			Am. Inst. of Electrical Engineers	1 1	1957
FMM			National Science Foundation**	1 1	1956
FTT. Fiz. tverd) tela			Acta Metallurgica	5 1	1957
Fiziol. Zh(urn). SSSR			American Institute of Physics	1 1	1959
			National Institutes of Health**	47 1	1961
Fiziol(logiya) rast.			National Science Foundation*	4 1	1957
Geol. nefti i gaza			American Geophysical Union	1 1	1962
Izmerit. tekhn(ika)			The Geochemical Society	1 1	1956
			Petroleum Geology	2 1	1958
			American Geophysical Union	1 1	1961
			Consultants Bureau	1 1	1958
			Instrument Society of America	1 1	1958

The translation of this journal
is published in sections

Language/Code	Organization/Source	Count	Year
Izv. AN SSSR O(td), Kh(im), N(auk)	Bulletin of the Academy of Sciences of the USSR: Division of Chemical Science	16	1952
Izv. AN SSSR O(td), Tekhn), N(auk); (Metall) i top.)	Bulletin of the Academy of Sciences of the USSR: Physical Series	18	1954
Izv. AN SSSR Ser. fiz(ich).	American Geophysical Union	7	1957
Izv. AN SSSR Ser. geofiz.	American Geological Institute	23	1958
Izv. AN SSSR Ser. geol.	The Textile Institute (Manchester)	4	1960
Iz. Vyssh. Uch. Zav., Tekh. Teks. Prom. Kauch. i rez.	Palmerston Publishing Company, Inc.	18	1959
Kolloidn. zh(urn).	Coal Tar Research Assn. (Leeds, England)	1	1960
Metallov. i term.	Consultants Bureau	6	1957
Met. i top.(gorn.) Mikrobiologiya	American Institute of Physics	1	1958
OS, Opt. i spektr. Paleontol. Zh(urn)	Acta Metallurgica	26	1957
Priboiy i tekhn. eks(perimenta)	National Science Foundation*	6	1960
Prikl. matem. i mekh(an). PTE	Acta Metallurgica	6	1959
Radiotekh. Radiotekhn. i elektron(ika)	American Geological Institute	53	1958
Stek. i keram. Svaroch. proiz-vo Teor. veroyat. i prim. Tsvet. metall	Consultants Bureau	2	1952
UKh, Usp. khimi UMN Vest. mashinostroeniya Vop. onk(ol)	Taylor and Francis, Ltd. (London)	4	1959
Zav(odsk) lab(oratoriya) ZNAKh, Zh. anal(it); Khim(ii) ZHETF Zh. eksperim. i teor. fiz. Zh. fiz. khimii Zh. fiz. khimii Zh. neorg(an); khim. Zh. obschch. khim. Zh. prikl. khim. Zh. strukt(urnoi) khim. Zh. tekhn. fiz. Zh. vyssh. nervn. deyat. (im. Pavlova)	Instrument Society of America Am. Society of Mechanical Engineers National Research Council of Canada Consultants Bureau Am. Institute of Electrical Engineers Am. Institute of Electrical Engineers Iron and Steel Institute Production Engineering Research Assoc. Consultants Bureau Br. Welding Research Assn. (London) Soc. for Industrial and Applied Math. Primary Sources American Institute of Physics Chemical Society (London) Cleaver-Hume Press, Ltd. (London) Production Engineering Research Assoc. National Institutes of Health** Instrument Society of America Consultants Bureau American Institute of Physics Chemical Society (London) Chemical Society (London) Consultants Bureau Consultants Bureau Consultants Bureau American Institute of Physics Pergamon Press, Inc. National Institutes of Health**	3 22 4 16 16 19 30 13 5 1 1 33 29 15 39 7 24 28 33 4 19 23 1 26 1 11	1958 1958 1961 1961 1959 1959 1956 1959 1956 1960 1960 1959 1961 1952 1955 1959 1959 1949 1950 1960 1956 1962 1961

*Sponsoring organization. Translation published by Consultants Bureau.
**Sponsoring organization. Translation published by Scripta Technica.

SIGNIFICANCE OF ABBREVIATIONS MOST FREQUENTLY
ENCOUNTERED IN SOVIET PERIODICALS

FIAN	Phys. Inst. Acad. Sci. USSR.
GDI	Water Power Inst.
GITI	State Sci.-Tech. Press
GITTL	State Tech. and Theor. Lit. Press
GONTI	State United Sci.-Tech. Press
Gosenergoizdat	State Power Press
Goskhimizdat	State Chem. Press
GOST	All-Union State Standard
GTTI	State Tech. and Theor. Lit. Press
IL	Foreign Lit. Press
ISN (Izd. Sov. Nauk)	Soviet Science Press
Izd. AN SSSR	Acad. Sci. USSR Press
Izd. MGU	Moscow State Univ. Press
LEIZhT	Leningrad Power Inst. of Railroad Engineering
LET	Leningrad Elec. Engr. School
LETI	Leningrad Electrotechnical Inst.
LEIIZhT	Leningrad Electrical Engineering Research Inst. of Railroad Engr.
Mashgiz	State Sci.-Tech. Press for Machine Construction Lit.
MEP	Ministry of Electrical Industry
MES	Ministry of Electrical Power Plants
MESEP	Ministry of Electrical Power Plants and the Electrical Industry
MGU	Moscow State Univ.
MKhtI	Moscow Inst. Chem. Tech.
MOPI	Moscow Regional Pedagogical Inst.
MSP	Ministry of Industrial Construction
NI ZVUKSZAPIOI	Scientific Research Inst. of Sound Recording
NIKFI	Sci. Inst. of Modern Motion Picture Photography
ONTI	United Sci.-Tech. Press
OTI	Division of Technical Information
OTN	Div. Tech. Sci.
Stroiizdat	Construction Press
TOE	Association of Power Engineers
TsKTI	Central Research Inst. for Boilers and Turbines
TsNIEL	Central Scientific Research Elec. Engr. Lab.
TsNIEL-MES	Central Scientific Research Elec. Engr. Lab.-Ministry of Electric Power Plants
TsVTI	Central Office of Economic Information
UF	Ural Branch
VIESKh	All-Union Inst. of Rural Elec. Power Stations
VNIIM	All-Union Scientific Research Inst. of Metrology
VNIIZhDT	All-Union Scientific Research Inst. of Railroad Engineering
VTI	All-Union Thermotech. Inst.
VZEI	All-Union Power Correspondence Inst.

Note: Abbreviations not on this list and not explained in the translation have been transliterated, no further information about their significance being available to us. — Publisher.

RUSSIAN TO ENGLISH

Scientist-translators wanted

You can keep abreast of the latest Soviet research in your field while supplementing your **income** by translating **in your own home** on a part-time basis. In the expanding Consultants Bureau publishing program, we **guarantee a continuous flow of translation** in your specialty. If you have a native command of English, a good knowledge of Russian, and experience and academic training in a scientific discipline, you may be qualified for our program. Immediate openings are available in the following fields: physics, chemistry, engineering, biology, geology, and instrumentation. Call or write now for additional information: TRANSLATIONS EDITOR




CONSULTANTS BUREAU


227 West 17 Street, New York, N. Y. 10011 • (Area Code: 212) AL-5-0713

HANDBOOKS


HANDBOOK OF INDUSTRIAL INFRARED ANALYSIS

by Robert G. White. A practical, self-sufficient handbook in the techniques of industrial infrared analysis. The volume has been written with the intent of answering in concise, convenient terms, the thousands of questions that are posed by industrial analysts or students who intend to work in industrial laboratories. It is the single best tutorial reference to the qualitative and quantitative analysis of the multitude of materials essential to industry. 452 pages \$19.50  Plenum Press

INFRARED BAND HANDBOOK


Edited by Dr. Herman A. Szymanski. Over 8500 band positions of organic and inorganic compounds are tabulated according to wavelength of their infrared absorption spectra. Thus, by referring to the Handbook, it is possible to find compounds at any selected wavelength having at least a medium-intensity band at that wavelength. Data retrieval time is much shorter than with any other method because in most cases the wavenumbers of the listed band are reported to an accuracy of 1cm^{-1} , a great improvement over previous systems. Supplements 1 & 2 bound in one volume cover a range of 15-25 microns (a region especially important in compound identification).  Plenum Press **INFRARED BAND HANDBOOK** 496 pages \$35.00
SUPPLEMENTS 1 & 2 271 pages \$15.00


HANDBOOK OF X-RAY STRUCTURE ANALYSIS OF POLYCRYSTALLINE MATERIALS

Edited by L. I. Mirkin. In this exceptional volume, the calculated and experimentally determined constants and data essential to the production and interpretation of x-ray patterns of polycrystalline materials have been collected from the world literature and are presented in a single volume in tabular, graphic and nomographic form organized in the sequence in which the analysis is usually performed. Some tables are published here for the first time; many have been expanded especially for the English edition. 752 pages Translated from Russian \$35.00  Consultants Bureau

PLENUM PRESS HANDBOOKS OF HIGH-TEMPERATURE MATERIALS, 1 & 2

Forewords by Dr. Henry Hausner

NO. 1 — MATERIALS INDEX by Peter T. B. Shaffer. Offers data on the general, chemical, electrical, mechanical, nuclear, optical, structural, and thermal properties of approximately 520 refractory materials arranged by compound. Compounds listed include borides, carbides, nitrides, oxides, silicides, mixed oxides, mixed carbides, and elements. 782 pages \$17.50  Plenum Press

NO. 2 — PROPERTIES INDEX by G. V. Samsonov. Classifies 600 refractory compounds systematically arranged by the following properties; crystal-chemical, thermal, thermochemical, electrical, magnetic, optical, mechanical, chemical and refractory. An invaluable appendix gives the most up-to-date phase diagrams of systems in which refractory compounds are formed. Revised by the author to include work up to late 1963. Translated from Russian 430 pages \$22.50  Plenum Press



PLENUM PRESS / CONSULTANTS BUREAU
227 W. 17th St., New York, N. Y. 10011